AN EXPLORATION OF VASCULAR ADHESION PROTEIN (VAP)-1 EXPRESSION IN PRIMARY SCLEROSING CHOLANGITIS (PSC)

by

Palak Jitendrakumar Trivedi

A thesis submitted to the University of Birmingham for the degree of:

DOCTOR OF PHILOSOPHY

School of Immunity and Infection

College of Medical and Dental Sciences

University of Birmingham

June 2015

ABSTRACT

Primary sclerosing cholangitis (PSC) is an immune-mediated cholangiopathy and extra-intestinal manifestation of inflammatory bowel disease (IBD). It is hypothesised that long-lived, $\alpha4\beta7^+$ $CCR9^+$ effector memory T-cells generated within the intestine drive hepatobiliary injury in PSC, being recruited to the liver via hepatic endothelial expression of mucosal addressin cell adhesion molecule (MAdCAM)-1 and CCL25.

Previous studies (mainly murine) claim CCL25 expression and $CCR9^+$ T-cells as confined to small bowel under homeostatic and inflammatory conditions, whereas PSC is typified by colonic disease. However, I was able to illustrate that in man, a significant proportion of tissue-infiltrating T-cells do express CCR9 in colitis relative to low numbers in the absence of colonic inflammation. Moreover, CCL25 expression is not only apparent in colonic IBD but also correlates with inflammatory indices.

Vascular adhesion protein (VAP)-1 is a potent amine oxidase capable of augmenting expression of other hepatic endothelial adhesion molecules through an enzyme-dependent process. I found that hepatic VAP-1 enzyme activity is greater in PSC than other autoimmune liver diseases; mirrored by high circulating serum levels that correlate with patient clinical outcomes. I then examined the effect of several potential amine substrates on VAP-1 dependent expression of MAdCAM-1 by liver endothelium, illustrating cysteamine as the most potent – an amine that is notable for inducing colitis in mice. Targeted deletion of VAP-1 enzyme function did not confer protection against early sclerosing cholangitis in *Mdr2*$^{-/-}$ mice. However, this model does not replicate links between colitis and liver inflammation seen in clinical PSC.

This thesis is dedicated to my wife, Hetal, my son Jaidev, and to my parents Mina and Jitu, without whose support and understanding this work would not have been possible.

Acknowledgements

I would like to acknowledge the help, support and direction of my supervisors, Dr. Chris Weston and Professor David Adams; and the assistance offered to me Dr. Evaggelia Liaskou and fellow PhD candidate Joseph Tickle. I also thank Dr. Gideon Hirschfield for his mentorship over the entire course of my PhD.

Funding from the Wellcome Trust and National Institute of Health (NIHR) Birmingham Liver Biomedical Research Unit is gratefully acknowledged.

Acknowledgement is also given to the body of consultant hepatologists and specialist nurses at the Queen Elizabeth hospital (Birmingham, UK); as well as David Smith and Jani Vianio at Biotie Therapies Corp. (Turku, Finland) in relation to their help obtaining and processing human tissue samples.

Completed and pending publications arising from this thesis

Trivedi P.J., Adams D.H. Mucosal Immunity in Liver Autoimmunity: a Comprehensive Review. *J. Autoimmun. 2013 46:97 – 111*

Trivedi P.J., Weston C.J., Webb G.J., Newsome P.N., Hirschfield G.M., Adams D.H. Serum Alkaline Phosphatase in Multidrug Resistance 2 (*Mdr2*$^{-/-}$) Knockout Mice is Strain Specific. *Hepatology 2015* [Epub: ahead of print; PMID: 25930031]

Trivedi P.J., Bruns T., Ward S.T., Mai M., Schmidt C., Hirschfield G.M., Weston C.J., Adams D.H. Intestinal CCL25/CCR9 Expression is Upregulated in Colitis and Correlates with Inflammatory Burden *J. Autoimmunity* 2016 [Accepted; *In Press*]

Vascular Adhesion Protein-1 is Upregulated in Primary Sclerosing Cholangitis, Predicts Clinical Outcome, and Facilitates Hepatic Endothelial Adhesion of α4β7 T-cells [in preparation].

Oral abstracts, prizes and invited speaker presentations

VAP-1 Is Elevated in PSC, Correlates with Clinical Outcome and Exhibits Amine Oxidase Abstract Activity in a Substrate-Dependent Manner

- *European Association for Study of the Liver (EASL) International Liver Congress (ILC) 2015 – Oral abstract presentation*
- *Falk Autoimmune Liver Diseases' Symposium 2015: Abstract of Distinction*
- *EASL Monothematic Conference (Autoimmne Hepatitis) 2015 – Oral abstract presentation*

VAP-1 Activity is Elevated in PSC and Modulates α4β7-Dependent Lymphocyte Adhesion to HSEC Under Flow

- *American Association for Study of Liver Disease (AASLD) annual congress 2013 – Oral abstract presentation*
- *British Society of Gastroenterology (BSG) Annual General Meeting 2013 – Abstract of Distinction and Best Poster Prize*
- *Falk Advances in the Management of Liver Diseases Symposium 2013 – Abstract of Distinction*

Connecting Gut to Liver in Primary Sclerosing Cholangitis: Intestinal CCL25/CCR9 Expression is Upregulated in Colitis

- *Falk Autoimmune Liver Diseases' Symposium 2015 – Abstract of Distinction*
- *British Society of Gastroenterology (BSG) Annual General Meeting 2015 – Abstract of Distinction*
- *EASL Monothematic Conference (Autoimmne Hepatitis) 2015 – Oral abstract presentation*

Primary Sclerosing Cholangitis: an Autoimmune Disease Driven by the Gut

- *3rd Conference on Translational Medicine on Pathogenesis and Therapy of Immune-Mediated Diseases 2014 – Invited Speaker*

Immunopathogenesis of Primary Sclerosing Cholangitis

- *Falk Autoimmune Liver Diseases Symposium 2015 – Invited Speaker*

Contents

List of figures

List of tables

List of Abbreviations

AASLD:	American association for Study of the Liver
ABCB:	ATP-binding cassette subfamily B
AGE:	Advanced glycation end products
AICD:	Activation-induced cell death
AIH:	Autoimmune hepatitis
ALD:	Alcohol-induced liver disease
ALT:	Alanine transaminase
ALP:	Alkaline phosphatase
ANA:	Anti-nuclear antibody
ANCA:	Anti-neutrophil cytoplasmic antibody
ANOVA:	Analysis of variance
AOC:	Amine-oxidase copper containing
APC:	Antigen presenting cell
ASBT:	Apical sodium bile acid transporter
ASMA:	Anti-smooth muscle antibody
AST:	Aspartate transaminase activity
ATRA:	All-trans retinoic acid
AUROC:	Area under the receiver operator curve
BEC:	Biliary epithelial cell
BCA:	Bicinchoninic acid
BSA:	Bovine serum albumin
BSG:	British Society of Gastroenterology
CA:	Cysteamine

CAM:	Cellular adhesion molecule
CARD:	Caspase recruitment domain family member
CCA:	Cholangiocarcinoma
CCl_4:	Carbon tetrachloride
CCR:	Chemokine receptor
CD:	Cluster of differentiation
Cdx:	Caudal homeobox transcription factor
CLEVER-1:	Common lymphatic endothelial and vascular endothelial receptor-1
Col1a1:	Collagen type 1 alpha 1
ConA:	Concavalin A
CRC:	Colorectal cancer
CT:	Threshold cycle
DC:	Dendritic cell
DA:	Dopamine
DAMP:	Danger associated molecular pattern
DAO:	Diamine oxidase
DAPI:	4',6-diamidino-2-phenylindole
DR:	Ductular reaction
DSS:	Dextran sulphate sodium
DT:	Distal-to-tumour
D.T.A.C.:	Descending, transverse and ascending colon and caecum
EASL:	European Association for Study of the Liver
ECM:	Extracellular matrix
ECRIF:	Europium-coupled time-resolved fluorescence

EGR:	Early growth response protein
ELISA:	Enzyme-linked immunosorbent assay
EpCAM:	Epithelial cell adhesion molecule
ESAM:	Endothelial cell-selective adhesion molecule
ESL:	E-Selectin ligand
FAC:	Fluorescence-associated cell
FAD:	Flavine adenine dinucleotide
FasL	Fas-ligand
FBS:	Foetal bovine serum
FMO:	Fluorescence minus one
FMOC:	Fluorenylmethyloxycarbonyl chloride
FoxP3:	Forkhead box P3
FS:	Forward scatter
Ftsz:	Filamenting temperature-sensitive mutant Z
Fut:	Fucosyltransferase
GALT:	Gut-associated lymphoid tissue
GAPDH:	Glyceraldehyde 3-phosphate dehydrogenase
GPCR:	G-protein-coupled receptor
GPX:	Glutathione peroxidase
GUS:	Glucuronidase
GWAS:	Genome-wide association study
H&E:	Haematoxylin and eosin
HC:	Healthy controls
HCV:	Hepatitis C virus infection
HDAC:	Histone deacetylase

HEV:	High endothelial venules
HGF:	Hepatocyte growth factor
HLA:	Human leucocyte antigen
HR:	Hazard ratio
HRP:	Horseradish peroxidase
HPLC:	High-performance liquid chromatography
HPRT:	Hypoxanthine phosphoribosyltransferase
HS:	Human serum
HSC:	Hepatic stellate cell
HSEC:	Hepatic sinusoidal endothelial cell
IBD:	Inflammatory bowel disease
ICAM:	Intracellular cell adhesion molecule
iFABP:	Intestinal fatty acid-binding protein
Ig:	Immunoglobulin
IL:	Interleukin
ILC:	Innate lymphoid cell
IEL:	Intraepithelial lymphocyte
IP:	Immunoprecipitation
IQR:	Interquartile range
KC:	Kupffer cell
KS:	Kolmogorov-Smirnov
KW:	Kruskal-Wallis
LD:	Liver disease
LFA:	Lymphocyte function-associated antigen 1
LOX(L):	Lysyl oxidase (like)

LP:	Lamina propria
LPL:	Lamina propria lymphocytes
LPS:	Lipopolysaccharide
L-SIGN:	Liver/lymph node-specific intracellular adhesion molecules-3 grabbing non-integrin
LT:	Lymphotoxin
LYVE:	Lymphatic vessel endothelial hyaluronan receptor
MA:	Methylamine
MAdCAM:	Mucosal addressin cell adhesion molecule
MAIT:	Mucosa-associated invariant T-cell
MALT:	Mucosa-associated lymphoid tissue
MAO:	Monoamine oxidase
MCD:	Methyl choline deficient
mDC:	Myeloid dendritic cell
MdM:	Monocyte-derived macrophage
MDR:	Multidrug resistant
MDSC:	Myeloid-derived suppressor cell
MFI:	Median fluorescence intensity
MHC:	Major histocompatibility complex
MLN:	Mesenteric lymph node
MMP:	Matrix metalloproteinase
M.O.M.:	Mouse-on-mouse
MW:	Mann-Whitney
NAFLD:	Non-alcoholic fatty liver disease
NC:	Normal / Non-inflamed colon

NFκB:	Nuclear factor kappa B
NIHR:	National Institute for Health Research
NK:	Natural killer
NL:	Normal liver
NOD:	Nucleotide-binding oligomerization domain-containing protein
NSAID:	Non-steroidal anti-inflammatory drug
OR:	Odds ratio
OVA:	Ovalbumin
PAMP:	Pathogen-associated molecular pattern
PAO:	Polyamine oxidase
PBC:	Primary biliary cirrhosis
PBL:	Peripheral blood lymphocyte
PBS:	Phosphate-buffered saline
PCR:	Polymerase chain reaction
pDC:	Plasmacytoid dendritic cell
PDGF:	Platelet-derived growth factor
PF:	Portal fibroblast
PLZF:	Transcription factor promyelocytic leukaemia zinc finger protein
PRK:	Serine-threonine protein kinase
PRR:	Pathogen recognition receptor
PSC:	Primary sclerosing cholangitis
PSGL:	P-selectin glycoprotein
qRT-PCR:	Quantitative real-time PCR

QC:	Quality control
Q-Q:	Quantile-quantile
RGD:	Tripeptide sequence: Arginyl-glycyl-aspartic acid
ROC:	Receiver operator curve
RTC:	Rat tail collagen
SB:	Small bowel
ScZ:	Semicarbazide
SD:	Standard deviation
SDS:	Sodium-docecyl-sulphate
SFM:	Serum-free media
SFRS4:	Arginine/serine-rich splicing factor
SS:	Side scatter
SSAO:	Semicarbazide-sensitive amine oxidase
SIK:	Salt-inducible kinase
TBS:	Tris-buffered saline
T_c	Cytotoxic T-cell
T_{CM}	Central memory T-cell
TCR:	T-cell receptor
T_{eff}	Effector T-cell
T_{EM}	Effector memory T-cell
TGF:	Transforming growth factor
T_h	Helper T-cell
TIMP:	Tissue-inhibitor of metalloproteinase
TLR:	Toll-like receptor
TNBS:	Tri-nitrobenzene sulfonic acid

TNF:	Tumour necrosis factor
TRAIL:	TNF-related apoptosis-inducing ligand
UC:	Ulcerative colitis
VAP:	Vascular adhesion protein
VCAM:	Vascular cell adhesion molecule
VE:	Vascular endothelial
VEGF:	Vascular endothelial growth factor
VVO:	Vesicovascular organelles

1 GENERAL INTRODUCTION

1.1 Overview

In order to cope with the daily exposure to a vast array of nutrients and microbes, the mucosal immune system has evolved specific compartments to respond to pathogens whilst continuously monitoring and providing tolerance to harmless commensals and food-borne antigens [1]. Nevertheless, microbes may penetrate intestinal defence mechanisms and enter the liver via the portal circulation where further levels of immune regulation operate [1]. In light of such close integration between mucosal and hepatobiliary immune systems, it is perhaps unsurprising that the liver can be affected by immune-mediated diseases primarily those affecting the gut [1]. The strong association between primary sclerosing cholangitis (PSC) and inflammatory bowel disease (IBD) led to the hypothesis that in this condition, liver disease is driven by lymphocytes generated in the intestine, which enter the portal circulation and trigger hepatic inflammation upon reactivation. This enterohepatic pathway is likely to be facilitated by aberrant expression of adhesion molecules and chemokines which under normal conditions are restricted to either the gut or liver [1,2].

The focus of this thesis is to further interrogate mechanisms linking lymphocyte recruitment to the liver and gut in PSC/IBD, therein providing scope for new therapeutic approaches. Before reviewing tissue-specific mechanisms, the general principles of T-cell activation and differentiation, lymphocyte migration and trafficking and roles in tissue inflammation and fibrosis will be discussed.

1.2 The immune system

The immune system is made up of a coordinated network of cells, tissues and organs, which exist to identify and control invading organisms, tumours and substances with the potential to cause host damage. Structural classification is divided into central (genesis site of undeveloped/immature leucocytes e.g., thymus and red bone marrow) and peripheral lymphoid tissues (locale of antigen presentation e.g., lymph nodes, spleen and mucosa-associated lymphoid tissues). Bone marrow represents the site where cells of erythroid (erythrocytes, platelets), myeloid (neutrophils, monocytes/macrophages, basophils, eosinophils, dendritic cells) and lymphoid (B- and T-lymphocytes, natural killer cells) lineages derive. During early gestation, haematopoiesis begins in the umbilical vesicle [3] and subsequently shifts to the foetal liver, before being taken over by bone marrow and spleen. The thymus represents the location of T-lymphoid cell education and maturation wherein progenitor T-cells differentiate into $CD4^+$ or $CD8^+$ subtypes.

1.2.1 Innate and Adaptive Immune Responses

Broadly speaking, responses to pathogens can be non-specific and short-lived (innate); or targeted and antigen-specific (adaptive) with potential for immunological memory and long-lasting, protective immunity. Innate immunity refers to ‘front line’ mechanisms participating in early host defence in response to infection or tissue damage. Primary components comprise physical epithelial barriers (skin and gastrointestinal surfaces) and mucosal secretions (defensins, acidic pH exudations, lysozymes and phospholipase). Microorganisms penetrating these principal defences immediately encounter anti-microbial proteins (complement system, lactoferrins and transferrins and coagulation peptides) and phagocytic immune cells (neutrophils,

macrophages, eosinophils and natural killer (NK)-cells) bearing pattern-recognition receptors (PRR). Innate signalling pathways initiate when pathogen-associated molecular patterns (PAMPs) are recognised by host PRR [4], which although non-antigen-specific, allow host discrimination of foreign molecules from self. NK-cells are a specialised cytotoxic lymphocyte subset, which belong to the innate lymphoid cell family. In addition to bearing phagocytic properties, NK-cells can release perforin and granzymes thereby inducing apoptosis or cell lysis. Morphologically, NK-cells resemble lymphocytes but are larger, bear numerous granules and do not require major histocompatibility complex (MHC)-bound peptides to exert their effector functions.

Whereas the innate response is rapid, tissue-damage can result from a lack of antigen-specificity, and as a consequence adaptive responses have evolved to be a more precise form of host-defence. Although mobilisation is relatively gradual (days – weeks), adaptive immunity leads to 'immunological memory' so that subsequent exposure to the same antigen results in a more rapid, potent immune response [5]. Induction of the adaptive response begins following pathogen uptake and processing by antigen presenting cells (APC) the most important of which are dendritic cells (DC). This specialised phagocytic population are tissue-resident, relatively long-lived and share a common lineage with macrophages. However, their primary function is to transport associated antigens to peripheral lymphoid structures for presentation to T-lymphocytes. When an immature DC ingests pathogen it becomes activated, matures into a highly effective APC, and processes and presents antigen to prime nearby antigen-specific lymphocytes. Activated DC secrete cytokines crucial in shaping innate and adaptive immune responses, making these 'professional' APC essential

gatekeepers governing whether and how the immune system responds to the presence of infectious agents.

Both B- and T-lymphocyte subsets are capable of recognising unique antigens and react in a highly specified manner. B-cells mediate the 'humoral' component of adaptive immunity, their principal function being the production of specific antibodies. Secreted antibodies eliminate extracellular pathogens by blocking interactions with host cell entry receptors; and also through opsonisation, subsequently facilitating their recognition and ingestion by phagocytic cells. B-cells are also highly effective APC and evolve into memory cells upon activation through antigenic interaction, as well as being capable of mediating immune regulatory functions [6]. Cellular immunity is mediated by T-cells, specifically helper (T_h) $CD4^+$ lymphocytes which can stimulate B-cells, facilitate other T-cell populations to mature and proliferate, attract neutrophils and enhance macrophage activity; as well as cytotoxic $CD8^+$ (T_c) lymphocytes that directly kill pathogen-infected cells through secretion of toxic granules or activation of tumour necrosis factor (TNF) receptors. All T-cells originate from haematopoietic stem cells in the in the bone marrow but in contrast to their B-cell counterparts, first migrate to the thymus for differentiation. Therein, T-lymphocytes first experience a positive selection step, wherein cells capable of responding to potential harmful antigens presented by MHC are selected for survival; and a negative selection event in which T-cells reacting to self–peptide complexes undergo apoptosis [7]. The earliest 'thymocytes' express neither CD4 nor CD8, and classed as 'double-negative.' Subsequently, thymocytes develop as 'double-positive' precursors and finally mature to single-positive ($CD4^+$ or $CD8^+$) lymphocytes before release into peripheral tissues [8].

1.2.1.1 Activation of T-lymphocytes

Early T-cell precursors must also create a unique T-cell receptor (TCR), a heterodimer consisting of a highly variable α and β chain co-expressed with the surface glycoprotein CD3. V(D)J recombination is the mechanism of genetic recombination taking place in the early stages of TCR (and immunoglobulin) production in primary lymphoid tissue, wherein variable (V), diverse (D) and joining (J) gene segments are randomly combined to encode a large number of variant receptors providing a repertoire than can recognise many potential antigens. Each T-lymphocyte expresses clonal TCRs which identify specific antigens during physical contact with an APC, an interaction that elicits downstream T-cell activation [9]. Following development, naïve T-cells (never exposed to antigen) are carried by the blood to lymph nodes and secondary lymphoid structures where they can be activated by APCs bearing their specific antigen. Like all T-cells, they express the TCR-CD3 complex. The TCR consists of both constant and variable regions, the latter determining the antigen repertoire to which a T-cell can respond. $CD4^+$ T-cells express TCRs with affinity for antigenic peptides bound to MHC Class-II, whereas $CD8^+$ T-cells recognise MHC Class-I. MHC-II is expressed on the surface of professional APC (macrophages, B-lymphocytes and DC), whereas MHC-I is present on almost every nucleated cell of the human body under physiological conditions. Presentation of antigenic peptide bound to MHC-II allows $CD4^+$ T-lymphocytes that express specific TCRs to activate. When a T_h–cell encounters and recognises antigen, the TCR-CD3 complex binds avidly to the peptide-MHC complex on the APC surface. CD4 represents a co-receptor, which binds to a different portion of the MHC molecule. These interactions facilitate activation of intracellular kinases present on

the TCR, CD3 and CD4, and via assistance of CD45 (protein tyrosine phosphatase receptor type C) trigger major T_h cell intracellular pathways [9].

Having received the first TCR/CD3 signal, naïve T-cells will only survive and differentiate if a second independent biochemical pathway is activated; this co-stimulatory step acting as a protective measure to ensure that T-cells respond to foreign (as opposed to self) antigen. The second signal involves interaction between CD28 on the T-cell surface and either CD80 or CD86 on APC [7]. Once a naïve T-lymphocyte has both pathways activated, the biochemical changes induced by the first TCR-CD3 signal are altered, allowing the T-cell to become activated and undergo further differentiation. If not, the T cell becomes anergic and fails to differentiate further [7]. Requirement for a verification signal upon antigenic re-exposure thereafter becomes redundant. Following activation, T_h-cells secrete interleukin 2 (IL-2) and produce the alpha sub-unit of the IL-2 receptor (CD25 or IL-2R) allowing auto–paracrine mediated cellular proliferation and clonal expansion [10].

1.2.1.2 Differentiation of T-cell responses

During ontogeny and subsequent differentiation, $CD4^+$ T-cells undergo a sequence of complex and mechanistically distinct decision-making processes. These result in acquisition of effector or regulatory functions, which in turn orchestrate the outcome of an immune reaction [11,12]. The diversity of polarised T-cell responses is governed by a unique set of transcription factors as well the cytokine milieu produced by local APC as well as neighbouring leucocytes (Figure 1.1 [13]).

Effector T_h1 immune responses are pivotal in activating macrophages and B-cells, whereas IFNγ^+ IL-2^+ cells represent precursors of T_h1 memory cells; IL-2 stimulation of $CD8^+$ cells also being critical for memory $CD8^+$ T-cell generation [14]. In contrast, T_h2 lymphocytes facilitate antibody class switching in B-cells, whilst IL-10 secretion suppresses T_h1 proliferation and DC function [15]. Additional 'partner' effector cells include eosinophils, basophils and mast cells. The T_h17-effector subtype have evolved to deal with bacteria and fungal infection but also implicated in many organ-specific autoimmune diseases [16,17]. T_h17 cells can amplify responses through the induction of many inflammatory (e.g. IL-6) and chemotactic cytokines (chemokines; e.g. IL-8, or CXCL8).

Regulatory T-cells (T_{reg}) are a subset which play a critical role in maintaining self-tolerance as well as in regulating immune responses through suppression and down-regulating induction and proliferation of effector T-cells [18]. T_{reg} exert suppressive capabilities through several mechanisms some of which require cell-cell contact whereas others are exerted through production of cytokines including IL-10. TGF-β may also result in T_{reg} induction from the naive $CD4^+$ pool and is critical in regulating T-cell differentiation, homeostasis and tolerance [19,20]. T_{reg} are defined by the transcription factor forkhead box P3 (FoxP3); expression of which is required for conventional T_{reg} development through control of a genetic program specifying this cell's fate [21]. T_{reg} also express high levels of the IL-2 receptor alpha chain (CD25) but absent/low-level expression of the IL-7 receptor subunit alpha (IL7R-α or CD127) – the latter historically being representative of T-cell activation status. Additional suppressor T-cell populations have been described including FoxP3^- IL10^+ Tr1-cells,

and T_h3-helper cells critically involved in regulating mucosal immunity through secretion of TGF-β and IL-10.

Mounting evidence suggests that a degree of plasticity exists between individual T_h subsets [11], and given the appropriate cues T_h17-lymphocytes can alter their differentiation program ultimately giving rise to either pathogenic or protective cells. Akin to conventional T_{reg}, induction of phenotypic regulatory T_h17-cells ($_rT_h$17) could play a favourable role in modulating autoimmune disease [22].

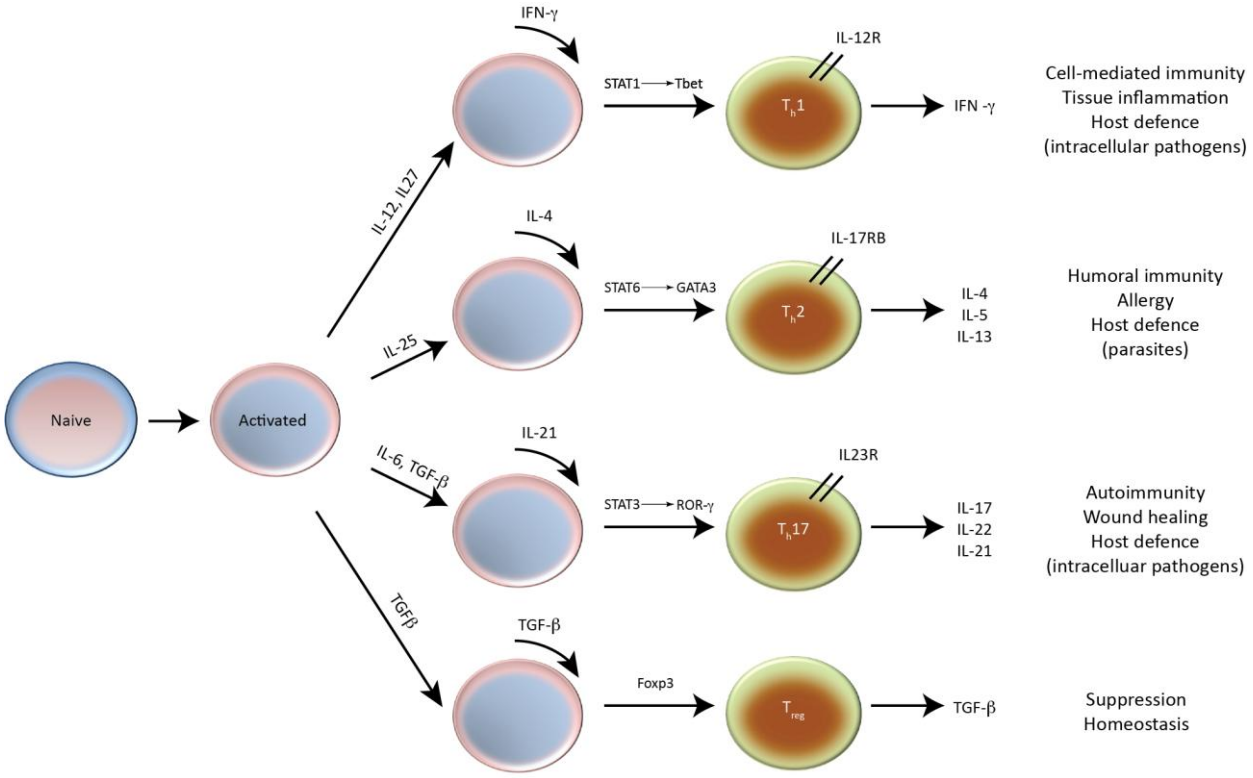

Figure 1.1: CD4$^+$ T-cell responses based on T_h-cell polarization
Upon antigen presentation by an activated APC, naïve CD4$^+$ T cells undergo several rounds of proliferation and polarise into distinct T_h cell subsets. Helper cell differentiation is mediated by unique sets of transcription factors, the expression of which is determined by soluble cytokines acting in the local microenvironment.

APC, antigen-presenting cell; Bcl6, B-cell lymphoma 6; CCR, CC chemokine receptor; CXCR, CXC receptor; FoxP3, Forkhead box p3; IFN, interferon; ROR, retinoic acid-related orphan receptor; TGF, transforming growth factor; T_h, T helper; T_{reg}, regulatory.

In contrast to their $CD4^+$ helper counterparts, $CD8^+$ lymphocytes are largely committed toward becoming cytotoxic effectors (T_c), which produce IFN-γ and kill transformed or infected target cells. However, much of the complexities of $CD4^+$ helper T-cell subsets may also apply to $CD8^+$ T-cells [23]. The $CD8^+$ T-cell pool may also consist of subsets such as T_c17s which express IL-17 [24]. Moreover, $CD8^+$ T-lymphocytes that produce IL-10, express FoxP3 and possess predominantly regulatory functions have been reported (25).

Natural killer T (NKT)-cells represent a further subpopulation of T-cells, defined by simultaneous expression of TCR and the NK surface marker CD161. The commonest subtype, invariant (i)NKT-cells, differ from conventional αβ T-cells in that their TCRs are far more limited in diversity. Additionally, NKT-cells can be $CD4^+$, $CD8^+$ or double-negative. NKT-cells recognise antigens presented by the MHC-I related molecule CD1 which is specially adapted for presentation of lipid antigens. Upon activation, NKT-cells are able to rapidly produce T_h1, T_h2 and T_h17 cytokines, as well as contribute to release of cytotoxic molecules and kill infected cells through contact dependent (FAS/FASL–mediated) and perforin–dependent pathways. CD161 is also expressed by T_h17-cells [26], likely indicative of a shared phenotypic and functional T-cell lineage [27].

Gamma-delta T-cells represent a relatively infrequent subset (2–10% of all human T-cells) that possess a distinct TCR consisting of a γ and δ chain as opposed to the conventional αβ dimer. This population are found with greatest abundance in the gut mucosa within a population of intraepithelial lymphocytes (IELs) and are often double negative ($CD4^-$ $CD8^-$). Moreover, γδ T-cells do not require MHC presentation

of antigen rather recognise stress-inducible MHC class-I chain-related antigens [28], self-lipid presented antigen by CD1 [29], or small non-peptide antigens known as pyrophosphomonesters [30]. In addition to conventional type 1 T-helper functions, γδ T-cells are $CD161^{+}$ and a source of IL-17, IL-22, granzyme B, perforin, TNF-α and IFN-γ, and promote myelopoiesis and neutrophil recruitment.

1.2.1.3 Lymphocyte memory

The continuous recirculation of lymphocytes from bone marrow/thymus to secondary lymphoid organs significantly enhances the rate of successful encounter with specific antigens. Naïve, antigen inexperienced cells pass directly from the blood to secondary lymphoid tissues through specialised high endothelial venules (HEVs) into surrounding T-cell zones [31]. Naïve B-cells follow the same route but instead migrate to adjacent B-cell follicles that contain follicular DC. If lymphocytes do not encounter an antigen in the lymph nodes, they return back to the peripheral circulation via lymphatic drainage. This continuous pathway between the blood and lymph ends only when the lymphocyte encounters its specific antigen, along with a co–stimulatory molecule on the surface of APC in a peripheral lymphoid structure.

Upon activation, lymphocytes proliferate and differentiate into effector cells. Activated B-cells within the lymphoid follicles undergo clonal expansion with the majority becoming antibody–producing plasma cells, and a small remainder surviving as long–lived memory cells. Activated T-cells differentiate into either $CD4^{+}$ T_h or $CD8^{+}$ T_c subtypes, and after several days some of the effector cells leave the peripheral lymphoid organs and migrate through blood to the site of primary infection. This migration pattern is a consequence of activation, differentiation and

functional maturation of lymphocytes, and serves to re–programme expression profiles of adhesion molecules and chemokine receptors, promoting recruitment toward the tissue in which they were first primed [32,33]. A small proportion of 'antigen-experienced' T-cells can persist after exposure to a specific antigen has waned, rapidly expanding to generate large numbers of effectors upon re-exposure that serve as the host's immunological memory. These memory T-cells can be $CD4^+$ or $CD8^+$, and conventionally express a shortened isoform of CD45 (CD45RO). Human memory T-cells can be further subclassified as either effector memory (T_{EM}) or central memory (T_{CM}) cells; based on receptor expression and functional properties. T_{EM} express receptors needed for migration into inflamed tissues and exhibit immediate effector functions upon antigen re-exposure (e.g., secretion of IFN-γ and IL-4). Central memory T-cells (T_{CM}), by contrast, express homing receptors for entry into lymph-nodes (CCR7, L-selectin), and although they lack immediate effector functions, T_{CM} can proficiently stimulate DC and bear the capacity to differentiate into effector T-cells upon stimulation [34].

1.3 Leucocyte recruitment

Effective immune surveillance is dependent upon the continuous circulation of lymphocytes through tissues in the quest for antigens, in addition to local innate immune responses that detect the initial invasion of tissue by antigen. This recognition is initiated by PAMPs, released by invading microorganisms as well as damage-associated molecular patterns (DAMPs) consequential to damaged/dead-cells or in response to cellular stress [35]. In addition, activation of resident memory T-cells can trigger recruitment of leucocytes via secretion of various primary inflammatory cytokines. Leucocytes must therefore be capable of traversing multiple

tissue-vascular beds; the key interaction herein occurring with endothelial cells lining vessels (Figure 1.2). Leucocyte egress from the bloodstream occurs through specialised post-capillary HEVs that exist in most secondary lymphoid organs and via microvascular endothelium within tissue. Under pro-inflammatory circumstances HEV–like structures can also be observed in non–lymphoid tissues thus supporting unremitting leucocyte recruitment to these sites [36].

1.3.1.1 Rolling

An initial capture step is required to bring the flowing leucocyte in the blood into contact with endothelium. In most tissues this is a rolling step, although in low flow vascular beds this phase becomes less important. Molecules which initiate the rolling step of leucocyte adhesion predominantly belong to the selectin family [37]. Expression of P-selectin and E-selectin are up-regulated on inflamed endothelium, whereas L-selectin is constitutively expressed by most B- and naïve T-cells, neutrophils, monocytes and eosinophils. The broad expression of L–selectin implicates a pivotal role in the trafficking of all leucocyte lineages; however, only a subpopulation of memory T-cells and natural killer (NK)-cells are L-selectin positive. P-selectin glycoprotein-1 (PSGL-1) exerts a dominant role, interacting with all 3 selectins wherein binding facilitates secondary leucocyte capture or tethering [38,39]. Although PSGL-1 is expressed on almost all leucocytes (and some endothelial cells), it is functional only when glycosylated correctly; an action mediated by enzymes termed fucosyltransferases [40]. E-selectin also binds to glycosylated CD44 and E-selectin ligand (ESL)-1 [41]. Selectins require the hydrodynamic forces of physiological shear stress to support adhesion; rolling cells undergoing detachment when flow ceases. In the low flow environment of hepatic sinusoids, selectins play

little role in recruitment [42,43]. Here rolling is attenuated as a consequence of the low flow and narrow sinusoidal channels allowing stochastic interactions with flowing leucocytes.

Integrins can also participate in rolling by interacting with Ig superfamily ligands. Cell lines expressing the integrin α4β7 can roll on immobilised recombinant mucosal vascular addressin cell-adhesion molecule (MAdCAM)-1, and lymphocytes can also roll on immobilised vascular cell-adhesion molecule (VCAM)-1 via engagement of α4β1. Moreover rolling of human lymphocytes is enhanced when intracellular cell adhesion molecule (ICAM-1) is co-expressed with L-selectin ligands [44].

1.3.1.2 Activation and arrest

The rolling step is an inherently unstable transition state, and firm leucocyte arrest is triggered by chemokines and other chemoattractants mediating downstream binding of leucocyte integrins to immunoglobulin superfamily members such as ICAM-1 and VCAM-1 expressed by endothelial cells. Under pro-inflammatory conditions, endothelial cells become activated and up-regulate expression of adhesion molecules, chemokines and other lipid chemoattractants. Chemokines can also be generated by proteolytic cleavage in platelets, thereafter being delivered to endothelial cells via circulating microparticles or exocytosis of intracellular granules [37].

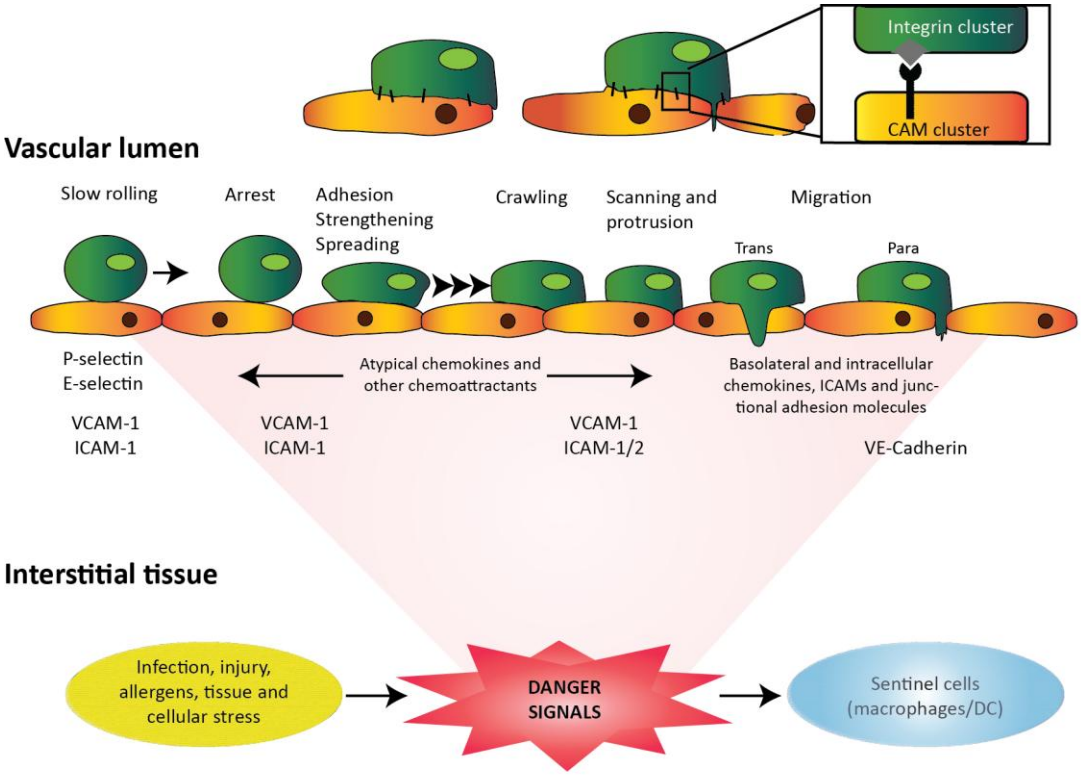

Figure 1.2: Leucocyte adhesion cascade

In response to a diverse range of pro-inflammatory triggers, released danger signals stimulate leucocytes and vascular endothelial cells to initiate a cascade of adhesion responses. Rolling on the endothelial surface facilitates initial leucocyte capture and is largely mediated by selectins and integrin/cell adhesion molecule (CAM) family members. The leucocyte starts travelling along the endothelial lining at reduced velocity, sampling the microenvironment for appropriate chemotactic signals (chemokines), either soluble or those immobilised by glycosaminoglycans on the endothelial surface. Binding of chemokines to their respective receptors on the leucocyte surface activates rapid G-protein coupled signalling pathways that trigger cytoskeletal rearrangement and integrin activation. Activated integrins subsequently undergo high affinity binding to their cognate ligands, which belong to the immunoglobulin superfamily of CAMs. This process promotes firm adhesion and allows the leucocyte to 'crawl' on the endothelial surface searching for signals to transmigrate. Thereafter, the leucocyte can pass through the basement membrane through endothelial junctions (paracellular route) or directly through the endothelial body (transcellular route).

DC, dendritic cell; ICAM, intracellular cell adhesion molecule; VCAM, vascular cell adhesion molecule; VE-cadherin, vascular endothelial cell cadherin.

1.3.1.2.1 Chemokines

Chemokines encompass a group of small (8 – 12 kDa) heparin-binding cytokines with ability to attract leucocyte subsets to specific tissue sites [45]. Virtually any cell type can express chemokines upon stimulation including activated endothelial cells, epithelial cells and leucocytes themselves. Upon secretion, chemokines become immobilised to glycosaminoglycans on the endothelial surface and extracellular matrix. This process helps leucocytes to locate chemokines as well as maintaining the latter in a multimeric form, increasing affinity for cognate chemokine receptors [46]. Immobilised chemokines can persist at higher concentrations than the 'freely diffusible' state [47]. Furthermore, different chemokines may enhance the function of one another (chemokine cooperativity [48]). Chemokines exert their functions primarily via specific G-protein-coupled receptors (GPCRs), leading to calcium flux and activation of phosphatidylinositol 3-kinase, or GTPase signalling pathways [49].

Chemokine classification can be structural, based on the position of conserved cysteine residues (Table 1.1); or functional, depending on whether chemokines are induced in response to inflammation or constitutively expressed. Inflammatory chemokines are released following stimulation by pro-inflammatory stimuli, and secreted early in response to PRR–activation from epithelium, stromal cells and immune cells [1,45]. Herein, they recruit the first line of innate immune effectors such as neutrophils, monocytes, NK-cells, NKT-cells and immature DC that bear cognate chemokine receptors. Following activation, DC prime lymphocytes, and inflammatory chemokines promote localisation of T-effectors (T_{eff}) to the site of injury. T_{reg} can be recruited in a similar manner, with the balance between effector and regulatory lymphocytes heavily influencing the outcome of the immune response. Homeostatic

chemokines are ubiquitously expressed in lymphoid and non-lymphoid structures, where they mediate physiological trafficking and positioning of cells, antigen sampling and immune surveillance. Functional distinctions can however be misleading given that chemokines previously thought to be homeostatic are often induced and up-regulated at sites of chronic inflammation [45].

1.3.1.2.2 Integrins

Integrins are heterodimeric membrane–bound glycoproteins composed of non-covalently associated α- and β-subunit chains, which collectively mediate cell-adhesion and migration through interactions with cell-adhesion molecules (CAMs) of the immunoglobulin superfamily or extracellular matrix components. Integrin chains have large, structurally complex extracellular domains containing three to four divalent cation–binding sites involved in ligand binding, a single–pass transmembrane helix, and cytoplasmic tails regulating function [50]. Chemokines are critical physiological activators of integrin-mediated adhesion and rapidly regulate their binding in a cell-specific manner through ligation of specific GPCRs and triggering complex intracellular signalling networks [51–53]. Such affinity modulation of an integrin for its ligand is recognised as a pivotal step in chemokine-induced arrest under flow, although the topology of integrin clustering may also play a role [54–56]. These mechanisms are particularly suited for controlling arrest under high-flow, shear-stress conditions, and integrin activation under physiological conditions is almost instantaneous.

Table 1.1: Chemokines/chemokine receptors in the human immune system

Chemokine receptor	Chemokine ligand	Receptor distribution
CXC subgroup		
CXCR1	CXCL6-8	Neutrophils, monocytes, mast cells
CXCR2	CXCL1-3, 5-8	Neutrophils, monocytes, mast cells
CXCR3	CXCL9-11	Helper T-cells, memory T-cells, NKT-cells
CXCR4	CXCL12	T-cells, B-cells, Macrophages, Monocytes, NKT-cells
CXCR5	CXCL13	B-cells
CXCR6	CXCL16	CD4+ T-cells, CD8+ T-cells, NK-cells
CC subgroup		
CCR1	CCL3, 5, 7, 8, CCL13-16, 23	Monocytes, memory T-cells, T_h1-cells, NK-cells
CCR2	CCL2, 7, 8, 13	Monocytes, memory T-cells, basophils, pDCs
CCR3	CCL5, 7, 11, 15, CCL16, 24, 26	Eosinophils, basophils
CCR4	CCL17, 22	T_h2 cells, T_{reg}, eosinophils, basophils, DC
CCR5	CCL3-5, 8	Monocytes, T_h1-cells, T_{reg}, DC, NK-cells
CCR6	CCL20	Memory T-cells, B-cells, T_h17, immature DC,
CCR7	CCL19, 20	Naïve T-cells, naïve B-cells, mature mDCs, T_h1, T_h2, T_{reg}
CCR8	CCL1	Monocytes, T_h2-cells, T_{reg}, NK-cells
CCR9	CCL25	DC, memory T-cells, thymocytes
CCR10	CCL27, 28	Memory T-cells, T_{reg}
CX3C and XC family		
CX3CR1	CX3CL1	Monocytes, Th1-cells, NK-cells
XCR1	XCL1-2	NK-cells

Structural distinction of chemokines and their receptors is based on the position of cysteine residues within a conserved tetracysteine motif. In CC chemokines, the first two cysteines lie adjacent to one another, whereas in CXC chemokines they are interceded by a non-conserved amino acid. These two subfamilies account for all but three of the known chemokines, the others being CX3CL1 (three intervening amino acids between the first cysteines) and XCL1 and XCL2, which lack two of four canonical cysteines. Some chemokines recognise multiple receptors whereas others only have one; conversely some receptors bind a single chemokine while others are highly promiscuous and bind several chemokine ligands (adapted (46)).

Integrins relevant to leucocyte arrest belong to β1, β2 and β7 subfamilies. β1-integrins share a common β-chain (CD29) in association with varying α subunits (CD49a or α4, CD49f or α6) and avidly bind to extracellular matrix components such as fibronectin, laminin and collagen. β2 integrins (CD18) pair with α subunits CD11a (LFA-1 or αL), CD11b (Mac-1 or αM) or CD11c (αX), and are expressed on lymphocytes (CD11a), neutrophils and monocytes (CD11a and CD11b) and DC (CD11a and CD11c). The α4β7 dimer when expressed on leucocytes mediates binding to fibronectin, VCAM-1 and most efficiently to MAdCAM-1, and is particularly associated with lymphocyte adhesion in the gut [57]; whereas αEβ7 integrin which is also constitutively expressed by intestinal intraepithelial lymphocytes mediates binding to E–cadherin. Cell-type specificity is conventionally ascribed to pre-defined patterns of integrin expression (and their ligands), in which chemokine-triggered signals regulate distinct integrin phenotypes across different leucocyte subtypes [37]. Additional diversity in leucocyte recruitment may be imparted from quantitative differences in pro-adhesive factors; for instance by the net tissue chemokine expression level or that of their receptors, and intrinsic affinity within. Collectively, such mechanisms have the capacity to regulate downstream activation of integrin-adhesion pathways [58].

1.3.1.3 Migration

Along with shear forces exerted upon an arrested leucocyte, the balance between up–regulation of ligand binding at the leading edge and down–regulation at the caudal tail maintains forward slow motility (crawling). After adhesion and crawling, leucocytes move toward endothelial cell borders looking for signals in order to complete

transendothelial migration (diapedesis). For effective migration to occur, leucocytes must not only overcome the endothelial layer of the venular wall, but also a pericyte layer underneath. Both of these cell types contribute to the generation of a non-specialised basement membrane which surrounds blood vessels. Whereas leucocyte migration through the endothelial-cell barrier can be rapid (<2–5 minutes), penetrating the endothelial-cell basement membrane takes far longer (>5–15 minutes) [37,59].

The interaction of integrins with endothelial CAMs is not only a pivotal step in leucocyte arrest, but is also able to stimulate endothelial cells in a manner that promotes transmigration. Adherent leucocytes can induce formation of 'transmigratory cups', endothelial-cell projections rich in CAMs such as ICAM-1 and VCAM-1; and cytoskeletal components like vinculin, alpha-actinin and talin-1 (60,61). Therefore interaction of a firmly arrested $\alpha L\beta 2^{+}$ leucocyte, together with expression of its cognate endothelial adhesion molecule, ICAM-1, can induce further clustering of ICAM-1 as a leucocyte approaches the endothelial cell border [60]. A similar phenomenon can be observed for other CAMs such as VCAM-1.

Multimerisation of ICAM-1 on the surface transmits signal to the endothelial cell; the most important being increased intracellular Ca^{2+} which induces cell contraction and loosening of endothelial cell junctions thereby facilitating leucocyte transit through the endothelial barrier. Loosening of the endothelial junction is further mediated by effects on vascular endothelial (VE)-cadherin phosphorylation, a molecule necessary for cell adherens junction disassembly [62]. While the leucocyte is transmigrating, there is continuous recycling of membrane components from the lateral border

recycling compartment to positions where the leucocyte is migrating, providing increased contact surface area and un-ligated molecules for leucocytes to interact with before passing through the endothelial layer [63]. In the paracellular pathway of migration, ligation of ICAM-1 by leucocyte integrin leads to translocation of ICAM-1 to actin and caveolae–rich regions. The latter represents recycling endosomes that contain ICAM-1 and are linked together forming vesico–vacuolar organelles (VVOs) which create an intracellular channel for leucocyte migration [37].

Different molecules mediate leucocyte transmigration in a stimulus-specific manner. Platelet/endothelial-cell adhesion molecule-1 (CD31) and ICAM-2 appear to mediate leucocyte transmigration in response to IL-1β but not TNF [64], although direct leucocyte activation by TNF can bypass the need for these adhesion molecules. In contrast, other adhesion molecules demonstrate leucocyte specific recruitment patterns such as endothelial cell-selective adhesion molecule (ESAM) which preferentially mediates neutrophil over T-cell transmigration [65]. Other non-conventional endothelial-cell molecules have also been implicated in leucocyte transmigration including scavenger receptors such as common lymphatic endothelial and vascular endothelial receptor-1 (CLEVER-1) and ectoenzymes such as vascular adhesion protein (VAP)-1 [66,67].

1.4 Organisation of the enteric immune system

1.4.1 Anatomy and function of the gut

The wall of the gastrointestinal tract consists of four layers (Figure 1.3). The luminal mucosa lines the surface of the digestive tract, protecting the remaining layers through secretions as well as being an absorptive interface for the end products of digestion.

The mucosa is itself composed of several sub-layers of complexity including an epithelial barrier (columnar or stratified squamous), goblet cells which secrete mucus therefore protecting the epithelium from digestion, and endocrine cells responsible for hormonal secretion. Blood and lymphatic vessels penetrate the lamina propria (LP) and provide nutrients for the epithelial layer, distribute hormones secreted by the epithelium and further absorb end products of digestion from the lumen. In addition, the LP contains mucosa–associated lymphoid tissue (MALT) and nodules of lymphatic tissue bearing lymphocytes and macrophages offering protection from bacteria and other potential food-borne pathogens. The muscularis mucosa is the outer mucosal layer, which as the name suggests is composed of a thin layer of (smooth) muscle and nerve fibres responsible for generation of local movements but also in the stomach and small intestine generates folds that further increase surface area for absorption.

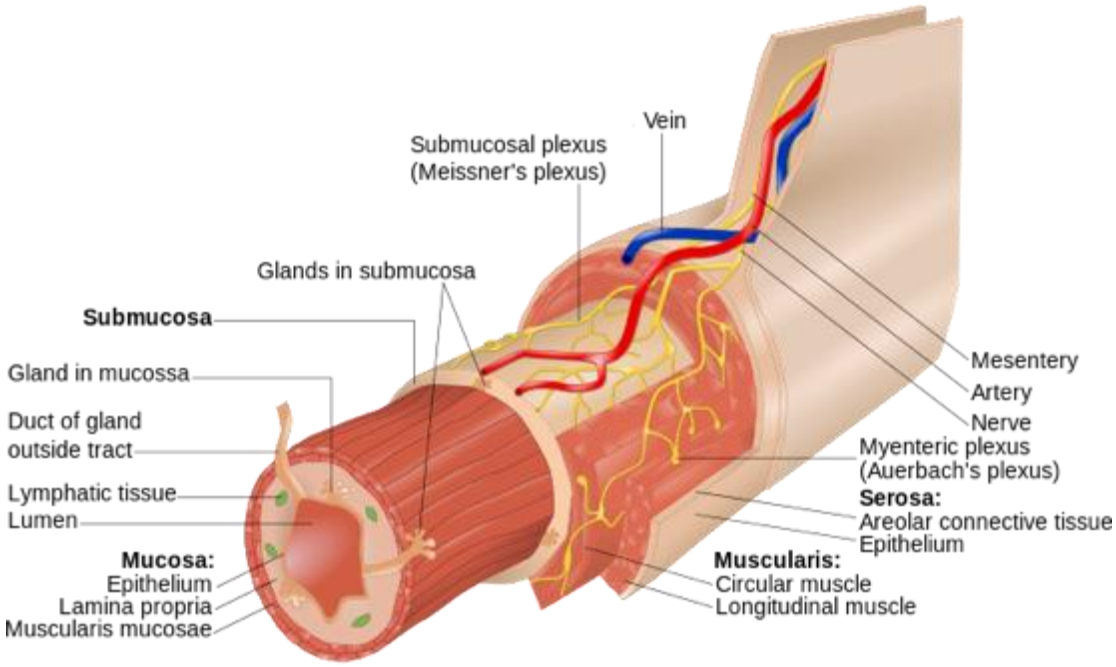

Figure 1.3: Layers of the GI tract
The gastrointestinal wall refers to a specialised series of tissue layers surrounding the lumen of the gastrointestinal tract: mucosa, submucosa, muscularis externa and serosa [68].

The submucosa contains blood vessels, lymphatics and nerves, and in the small intestine bears several distinct characteristics such as Brunner's glands (restricted to the duodenum) which secrete alkaline mucus, as well as aggregated lymphatic nodules called Peyer's patches. The muscularis externa in the mouth and pharynx consists of skeletal muscle to aid swallowing, and in the rest of the GI tract smooth muscle with associated nerve fibres responsible for peristalsis and mechanical food digestion by segmentation. The outer serosal layer is a smooth membrane that comprises a thin layer of connective tissue and an underlying epithelial layer secreting serous fluid.

1.4.2 The gut epithelial barrier

The mucus layer offers the first line of protection in the gut, and is rich in anti-bacterial substances such as alpha-defensins and immunoglobulin A (IgA), as well as a large number of commensal microbes which greatly exceed the total number of eukaryotic cells within the human body [69,70]. Invasion by pathogens is further impeded by the barrier function of the epithelial monolayer, which expresses toll-like receptors (TLR) and other PRR that recognise cellular injury or damage. This means that the mucosal epithelium is more than just a physical barrier, and activation of this "epimmunome" links barrier function to innate and adaptive immune responses [71–73]. Mucosal epithelial cells express MHC-II molecules; however, given the absence of appropriate co-stimulation, interactions with $CD4^+$ T-cells are biased toward tolerance rather than effector responses [74]. The ability of intestinal epithelial cells to secrete cytokines and chemokines in response to commensal bacteria, pathogens or injury allows them to play an active role in shaping the nature of local immune

responses and modulate sub-epithelial DC and lymphocyte positioning and activation [73]. Under normal conditions molecules that promote T_{reg} and Type-2 responses such as IL-25 dominate to maintain an anti-inflammatory environment [75]. However, in response to epithelial damage or infection, activation of nuclear factor kappa (NFk)B results in secretion of mediators including IL-1, IL-6, TNF and CCL20 which shift local differentiation toward pro-inflammatory Type-1 or Type-17 responses. Further regulation is provided through bidirectional paracrine interactions between epithelial cells and specialised subsets of tissue-associated T-cells [73]. For instance, IL-22 secreted by T_h-cells (so called T_h22 cells) has paracrine effects on the epithelium. Thus, synergistic interactions between the epithelial/stromal compartment and sub-epithelial DC and lymphocytes maintain epithelial integrity and regulate principal responses to injury or infection.

1.4.2.1 Intraepithelial compartment

The gut epithelial barrier does not completely prevent luminal antigens from entering tissue, and antigens can traverse through breaks in tight junctions, perhaps at villous tips where epithelial shedding occurs. As a result, the intestinal mucosa contains a large number of T-cells residing within the epithelium or underlying LP. Intraepithelial lymphocytes (IELs) are primarily $CD8^+$ T-cells, which include γδ and αβ subsets as well as a population of $CD8\alpha\alpha^+$ T-cells. Intestinal CD8αα T-cells are a group of $CD161^{hi}$ $CD8^+$ mucosal-associated invariant T (MAIT)-cells [76] and their development is independent of antigen presentation by MHC. In contrast, $CD4^+$ and CD8αβ T-cells localise to mucosa after MHC-restricted activation in secondary lymphoid organs, and secrete TGF-β and suppress inflammation to maintain tissue integrity [77,78]. IELs are $CCR9^+$, and under normal conditions attracted by epithelial

CCL25 to the intraepithelial compartment, where they use CD103 to bind to E-cadherin at the epithelial zonula adherens. However, in response to inflammation, recruitment pathways involving CXCR3 and other chemokine receptors may be more pertinent [79].

1.4.2.2 Lamina propria

The sub-epithelial lamina propria contains numerous antigen-presenting, CX_3CR1^+ DC which sample and process commensal and pathogenic bacteria from within the gut lumen [80]. These cells are able to receive antigen either from specialised microfold-cells (M-cells) or through dendritic processes protruding between gut epithelial cells [78,81]. DC, in particular those that express CD103, subsequently migrate to draining mesenteric lymph nodes (MLN) or Peyer's patches where they activate naïve lymphocytes [82]. Gut myeloid DC (mDCs) involved in taking up apoptotic enterocytes constantly 'traffic' to draining lymph nodes but in the absence of danger signals are not fully activated and thus maintain tolerance rather than stimulating effector responses [83]. However, following an inflammatory response to injury or extrinsic infection, specific signals drive maturation and activation of mDCs which stimulate the development of an immune response shaped by the nature of the activating stimulus [84,85]. In contrast, plasmacytoid DC (pDCs) are recruited to inflamed tissues where they secrete Type-1 interferons and promote local differentiation of immunosuppressive T_{reg} which in conjunction with non-classical regulatory cells (e.g. T_h3-cells, T_r1-cells and iNKT-cells), help control inflammation and maintain tolerogenic immune responses to food and self-antigens [86].

The outcome of immune activation in the LP is largely dependent on a balance between activation of IFN-γ-secreting $CD4^+$ T-cells, which drive inflammatory responses, and immunosuppressive regulatory cells that suppress and restrain inflammation. The importance of this interrelationship is emphasised by murine studies in which T_{reg} depletion or dysfunction leads to fulminant colitis, reversed by reconstitution with T_{reg} [87,88]. B-cell blasts also traffic to the LP where they differentiate into IgA-secreting plasma cells; and DC that contain live bacteria induce plasma cell differentiation more effectively than DC containing killed organisms [1]. It is probably for this reason that they are restricted from entering secondary lymphoid tissues, as an effort to localise the induction of immune responses and prevent carriage of bacterial organisms to other sites [1,80,89]. The outcome of the immune response is thus dictated by DC, the antigenic stimulus, and the resulting cytokine microenvironment (Figure 1.1). T_h1 responses are driven by early secretion of IL-2, whereas IL-1, IL-6, and IL-23 result in T_h17 induction. By contrast, leucocyte interactions with immature mDCs and some pDCs, or activation in the presence of IL-10 and TGF-β, preferentially leads to induction of T_{reg}.

1.4.2.3 MAIT-cells and innate lymphoid cells

MAIT-cells form a subset of non-conventional, innate-like T-cell whose TCR consists of an invariant Vα chain (iVα7.2-Jα33) combined with limited conserved Vβ chains, and are restricted to the evolutionarily conserved MHC-related molecule MR1 [90,91]. MAIT cells although detectable in peripheral blood, use CCR6 and CXCR6 to preferentially locate to the lamina propria and liver. They are phenotypically similar to NK-cells being characterised by CD161 expression and the NK-cell activating receptor NKG2D, are mostly $CD8\alpha\beta^{lo}$ (or double-negative) and display an

effector ($CD95^{hi}$ $CD62L^{lo}$ $CCR7^{-}$) memory ($CD27^{+}$ $CD45R0^{+}$ $CD45RA^{lo}$ $CD122^{+}$) phenotype [92]. Intestinal CD8αα T-cells are likely a sub-population of $CD161^{hi}$ $CD8^{+}$ mucosal-associated invariant T-cells sharing common cytokine expression, chemokine-receptor phenotype and transcriptional profiles with counterpart $CD8\alpha\beta^{+}$ T-cells [27,76]. The selective enrichment of MAIT-cells within intestine and liver suggests a close relationship with the host microbiome [93], and their rapid postnatal expansion and acquisition of memory markers is triggered by responses to colonising flora, as evidenced by murine studies in which germ-free mice have no detectable MAIT-cells until reconstituted with commensal bacteria [94].

MAIT-cells display active anti-microbial functions *in vivo* and react with MR1-expressing cells infected/co-cultured with selective bacteria and yeasts, but not viruses [95]. Recent reports suggest that vitamin B metabolites generated by unique biosynthetic pathways are ligands for MR1 [90,96]; however, it is unclear how MAIT-cells mediate anti-microbial functions and which particular cytokines are necessary for continued proliferation. It has been postulated that in the presence of an intact mucosal barrier and an absence of inflammation, MAIT-cells participate in the control of commensal flora or food-borne antigens by modulating APC function and epithelial cell homeostasis through release of IL-4 and IL-10, and secretion of anti-microbial molecules [97]. MAIT-cells also express IL-2Rβ2, IL-18Rα and IL-23R, and activation of these receptors in association with MR1-bound ligands triggers secretion of IFN-γ, TNF-α, IL-17 and granzymes, and inhibition of intracellular bacterial replication [97]. This ‘dualistic’ role coupled with their evolutionary conservation suggests a pivotal occupation in mucosal immunity. A key role of IL-23 in the pathogenesis of chronic inflammatory disorders is supported by genome-wide

association studies (GWAS) identifying components of the IL-23 pathway as susceptibility alleles for IBD, autoimmune liver disease and ankylosing spondylitis [98]. IL-23 promotes T_h17 responses but the ability to activate innate lymphoid cells (ILC) and MAIT-cells can drive T-cell-independent inflammation. ILC expressing RORγt and IL-23R accumulate in the inflamed colon, secreting IL-17 in response to IL-23 and TNF-α produced by pathogen-activated $CD103^-$ DC. This illustrates how interactions between mucosal DC and ILC can define inflammatory responses to gut microbiota [99].

1.4.3 Intestinal microbiota

Development of the human intestinal microbiome, dominated by the bacterial phyla *Firmicutes* and *Bacteroides*, and less so *Actinobacteria* and *Proteobacteria*, is established early in life [70]. Gut-resident bacteria have co-evolved with the human host and perform essential functions such as vitamin synthesis and metabolism of indigestible dietary polysaccharides. Symbiosis between commensal flora and the host promotes defence against pathogenic bacteria by out-competing for nutritional and physical niches and induces specific responses shaping local T-cell polarisation [100]. Thus, the host immune system must establish a favourable environment for this vital community yet protect against invasion or outgrowth of pathogenic species [101,102].

The gut epithelium is able to directly sense bacteria through specific PRR including TLR1–9, and nucleotide-binding oligomerisation domain-containing proteins (NOD)-1 and NOD2, although how commensal bacteria are distinguished from pathogenic strains is unknown. Mutualism is illustrated by the fact that the activation of epithelial

TLR2 or TLR9 increases gut barrier function, and mice deficient in the downstream TLR-signalling molecule MyD88 are susceptible to experimentally-induced IBD [103,104]. Disturbances in immune or epithelial homeostasis can lead to gut inflammation and in certain circumstances commensal flora may act as pathogens. For instance, stimulation of mucosal $CD4^+$ T-cells from Crohn's disease patients with their own commensal flora induces IFNγ secretion [105]. Moreover, GWAS have identified polymorphisms in NOD2 as Crohn's disease susceptibility factors [106]. Because NOD2 can regulate TLR signalling, such mutations may impair recognition of intestinal bacteria and promote secretion of pro-inflammatory cytokines in response to TLR stimulation in the gut and liver [107–111]. NOD2 is expressed in intestinal epithelial Paneth cells and NOD2-deficient mice are susceptible to intestinal infection with *Listeria monocytogenes* [112]. Further evidence to support impaired tolerance to commensal flora in IBD pathogenesis is provided by findings wherein mice subject to a congenital deletion of the tolerogenic cytokine IL-10 ($Il10^{-/-}$ mice) fail to develop intestinal inflammation under germfree conditions [113]. In addition, colonic DC expression of TLR2 and TLR4 is significantly up-regulated Crohn's disease, and these cells more commonly exhibit an activated phenotype ($CD40^+$) and enhanced production of the pro-inflammatory cytokine IL-6 [114,115].

Clinical observations support this hypothesis because Crohn's disease occurs most commonly in the terminal ileum and colon where bacterial load is the greatest and some patients improve after treatment with antibiotics. Indeed, changes in the composition of intestinal microflora are observed in human IBD [116–118], and it is conceivable that pathogenic bacteria weaken the intestinal lining resulting in translocation of commensals beyond the gut barrier and into the portal circulation.

This would facilitate entry into the liver where further levels of regulation exist to prevent uncontrolled systemic immune activation. However, if such protective mechanisms are overwhelmed then immune responses to gut bacteria could drive extraintestinal inflammation in the liver and other sites [117]. For instance, activation of TLR2 and TLR4 by PAMPs or commensal bacteria that enter the portal circulation may promote development of non-alcoholic fatty liver disease (NAFLD) [119–122]. The precise role and mechanisms of breakdown in intestinal barrier function comprising such responses remains to be defined.

1.4.3.1 Intestinal leucocyte activation and recruitment

Effective immune surveillance requires that leucocytes be recruited and positioned to specific tissue compartments and this is achieved through selective adhesion molecule and chemokine receptor expression. Under physiological conditions, CCL25 is constitutively expressed by epithelium and detected on mucosal vessels within the small bowel [123], which also expresses MAdCAM-1 [124]. This molecular combination is largely absent from other tissues in the absence of inflammation and serves as a molecular 'postal code' for recruitment of lymphocytes expressing CCR9 and α4β7. The expression of these two gut-homing receptors is selectively imprinted on lymphocytes by $CD103^+$ DC within gut-associated lymphoid tissues (GALT) such as MLN and Peyer's patches [57,82], and favoured by an environment rich in IL-7 [125].

Once primed and activated by gut DC, lymphocytes lose the ability to re-enter lymphoid tissue by down-regulating expression of CCR7 and L-selectin whilst up-regulating CCR9 and α4β7 in a process dependent on retinoic acid (Figure 1.4). The

source of retinoic acid is unclear although may derive from a pool of bile retinoids delivered to the gut by the liver [126]. High levels of retinaldehyde dehydrogenase define the preferential activity of retinoic acid in gut DC, and such enzymes are expressed at much lower levels in DC from other sites like the skin, providing a mechanism by which gut DC can compartmentalise lymphocyte recruitment [126]. Engagement of CCR9 by CCL25 results in activation of the leucocyte integrin α4β7 and facilitates stable binding to MAdCAM-1 on the endothelium of mucosal vessels [127]. In the presence of TGF-β, retinoic acid generating gut DC induce activation of gut-homing T_{reg}, and synergise with IL-6 and IL-5 to induce $CCR9^{+}$ $\alpha4\beta7^{+}$ gut homing IgA-producing B-cells [128–130]. IgA-secreting B-cells and subsets of T_{reg} also express CCR10 allowing them to engage with the mucosa through interactions with CCL28 [131], which unlike CCL25 is widely expressed on mucosal epithelium in the colon, small intestine, lung, bile ducts and exocrine glands, therefore likely embodies a common mucosal chemokine.

MAdCAM-1 and CCL25 are critically involved in the homeostatic recruitment of lamina propria lymphocytes (LPL) and although expression increases in intestinal inflammation [132], effector cell recruitment also involves other adhesion molecules including VAP-1, ICAM-1 and VCAM-1 that are induced in response to pro-inflammatory signals (Table 1.2). Moreover, LPL and IEL express CCR2, CCR5 and CXCR3 which may play a more important role during recruitment to the inflamed intestine [132,133].

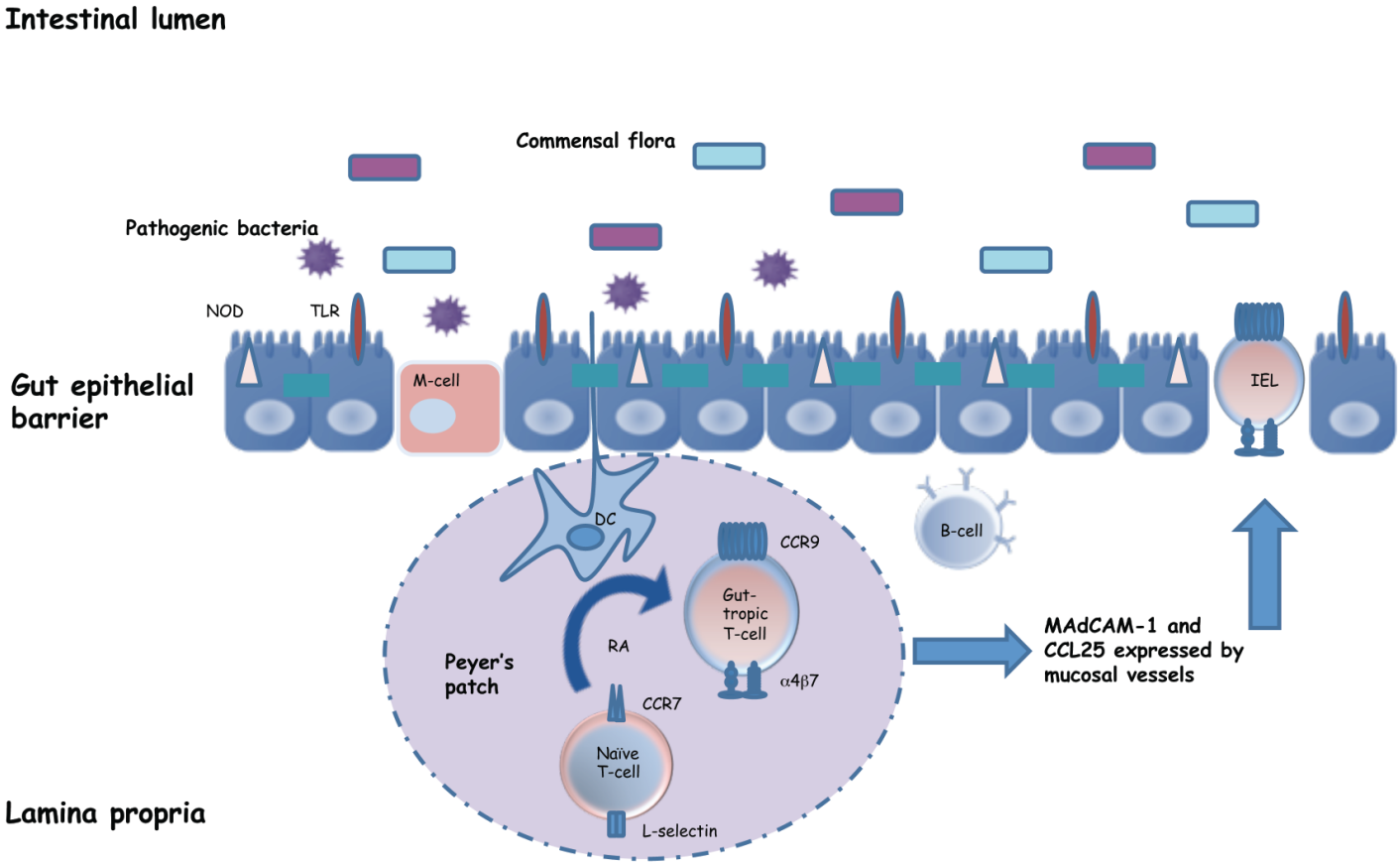

Figure 1.4: Imprinting of a gut-homing phenotype

Luminal antigens are sampled by resident DC either directly through their dendritic processes or by specialised M-cells. Antigen is then processed and transported to GALT where DC are able to interact with T-cells in order to program an immune response. DC–T-cell interactions not only activate naïve T-cells and imprint antigen recognition, but also induce a phenotype associated with gut-tropism. This process is dependent on RA generated by the DC, which drives expression of intestinal lymphocyte homing molecules α4β7 and CCR9 and allows activated T- and B-cells to respond to MAdCAM-1 and CCL25, respectively, on mucosal vessels. Although most of the recruited lymphocytes will remain in the lamina propria, a portion will migrate along a chemotactic CCL25 gradient to the intraepithelial compartment and become IEL [1].

DC, dendritic cell; M-cell, microfold cell; GALT, gut-associated lymphoid tissue; RA, retinoic acid; IEL, intraepithelial lymphocyte.

Table 1.2: Molecular determinants of leucocyte recruitment to the intestine [1]

Site	Constitutively expressed	Increased in response to inflammation
Small bowel	α4β7 – MAdCAM-1 αEβ7 – E-cadherin (intraepithelial compartment) CCR6 – CCL20 CCR9 – CCL25 CCR10 – CCL28 CXCR1 – CXCL5/6/8 CXCR2 – CXCL1/2/5/6 CXCR6 – CXCL16 CX3CR1 – CX3CL1	E-selectin P-selectin – PSGL-1 α4β7 – MAdCAM-1 VAP-1 α4β1 – VCAM-1 αLβ2 – ICAM-1 CCR2 – CCL2/7/8 CCR5 – CCL3/4/5/8 CCR9 – CCL25 CXCR3 – CXCL9/10/11 CX3CR1 – CX3CL1
Colon	α4β7 – MAdCAM-1 L-selectin* – PNAd / MAdCAM-1 CCR5 – CCL3/4/5/8 CCR6 – CCL20 CCR10 – CCL28 CX3CR1 – CX3CL1	α4β7 – MAdCAM-1 L-selectin – PNAd/MAdCAM-1 α4β1 – VCAM-1 αLβ2 – ICAM-1 VAP-1 E-selectin P-selectin – PSGL-1 CCR2–CCL2/7/8 CCR3 – CCL11 (colitis) CXCR1 – CXCL5/6/8 CXCR2 – CXCL1/2/5/6 CXCR3 – CXCL9/10/11

* L-selectin predominantly involved in recruitment of naïve T-cells

1.4.3.2 Stability of a gut-homing phenotype requires re-exposure to intestinal DC

After an antigenic insult has been cleared, most effector lymphocytes die leaving a cohort of long-lived memory cells that can rapidly expand on re-encounter with antigen. Memory T-cells and IgA-secreting plasma cells imparted with gut tropism provide long-term protection against gut pathogens indicating a degree of stability of the intestinal-homing phenotype, possibly by epigenetic imprinting at the time of activation [2]. However, this requires continual re-encounter with intestinal DC because T-cells can be re-programmed following encounter with DC from different tissues [134]. For instance, reactivation of gut memory T-cells by skin-derived DC decreases CCR9 and $\alpha_4\beta_7$-integrin expression whilst increasing expression of surface markers which promote homing to cutaneous sites, such as cutaneous lymphocyte

antigen [134]. Plasticity may reside in a subset of central memory T-cells which are $CCR7^+$ thereby retaining an ability to migrate through lymph nodes and encounter DC from other tissues, in contrast to $CCR7^-$ effector memory T-cells which retain tissue tropism.

1.5 CCR9 and CCL25

CCR9 is encoded on chromosome 3 in humans (chr. 9 in mice) and preferentially expressed by thymocytes and gut-tropic lymphocytes. In addition to being a marker for intestinal lymphocyte homing (small bowel), CCR9 is required for entry of double-negative T-cell progenitors into the thymus and consequently as they develop to double-positive cells and migrate to CCL25-rich medullary regions [135]. Gut-tropic $CD4^+$ and $CD8^+$ lymphocytes express CCR9 together with α4β7, and selectively traffic to the small intestine under normal and TNFα-stimulated conditions [136]. Interactions with CCL25 can also induce CD103 expression and positioning of CD8αα lymphocytes to the intraepithelial compartment. The importance of CCR9 expression is highlighted by observations wherein lymphocytes derived from knockout mice are hampered in their ability to enter the gut as studied in competitive homing experiments [137]. However, *Ccr9*$^{-/-}$ mice exhibit a mild phenotype under basal conditions with relatively minimal reduction in numbers of γδ IELs [138]. In fact, GALT-activated $CD4^+$ T-cells can enter the intestine through CCR9-dependent and independent mechanisms, suggesting that CCR9 expression is not an absolute prerequisite for lymphocyte homing to the small bowel, in stark contrast to β7 integrin [139].

The only known ligand for CCR9 is CCL25, expression of which is largely restricted to thymic and small bowel epithelium, although under specific pro-inflammatory conditions it can be detected in the liver and lung [127,140,141]. The CCL25 gene is located on chromosome 19 in humans (chr. 8 in mice) although mechanistic insights into its transcriptional regulation remain speculative. Overexpression of early growth response protein (EGR)-1 and caudal-related homeobox transcription factor (CDX) have been reported to increase CCL25 transcription and protein expression in endothelial cells, whereas effects of conventional inflammatory stimuli such as TNF-α remain controversial [132,136].

1.6 CCL25/CCR9 interactions in IBD

$CCR9^+$ IEL and LPL exhibit chemotaxis to CCL25 in a dose-dependent manner when studied *in vitro* [142]. There is a gradient of CCL25 expression in the small bowel, with highest tissue levels detected proximally in the duodenum and lowest in the ileum [137], implying a degree of compartmentalisation at least in murine studies. Furthermore, there appears to be a variable dependence on CCL25/CCR9-mediated recruitment in the LP in contrast to intestinal epithelium [79,142]. Regardless, patients with small-intestinal inflammation have increased numbers of peripheral blood $CCR9^+$ T-cells [143], and $CCR9^+$ T-cells isolated from MLN of patients with Crohn's disease have a more activated phenotype, producing significantly more IFN-γ and IL-17 than lymphocytes extracted from normal MLN [144]. In stark contrast, several research groups demonstrate a paucity of $CCR9^+$ lymphocytes and a distinct absence of CCL25 expression in the normal human colon at the transcriptional and protein level [123,142,143], and the CCR9-CCL25 axis is proposed to distinguish small from large bowel specific lymphocyte recruitment [142].

In a SAMP1/YitFc model of murine ileitis (developed through selective breeding), a significantly greater proportion of $CD4^+$ and $CD8^+$ lymphocytes were $CCR9^+$ compared with wild-types (~20% and 60% vs. 5% and 40%, respectively), and affected mice exhibited increased epithelial CCL25 expression indicated by enzyme-linked immunosorbent assays (ELISA), correlating with the severity of inflammatory injury [145]. Neutralising antibodies to CCL25 have been shown to reduce adhesion of adoptively transferred intestinal LPL and IEL to small intestinal post capillary venules [136], and histological indices of early intestinal inflammation are reduced following administration of antibodies targeting the CCR9-CCL25 axis in murine models of small-intestinal IBD [145]. However, targeted deletion of CCR9 has been shown to exacerbate ileitis in animal models [146,147], and in a TNFΔARE model of ileal Crohn's, deficiency of $CD4^+CD25^+FoxP3^+$ and $CD8^+CD103^+$ T_{reg} were observed within the LP and MLN of *Ccr9*$^{-/-}$ mice [146], and inflammation developed unperturbed in the context of CCL25 deficiency [148].

There are several plausible explanations for these divergent reports. Imprinting of CCR9 is retinoic acid dependent, and in the presence of TGF-β determines the induction of FoxP3. TGF-β also promotes expression of CD103 [149], and Wermers *et al*. report high concordant expression of CCR9, FoxP3 and CD103 in mice, suggesting that their respective generation might be coupled within inductive compartments [146]. Indeed, T_{reg} preferentially express CCR9 when compared to effector counterparts in the TNFΔARE model, and the $CD8^+CCR9^+$ subset was also shown to be suppressive through inhibition of proliferation of $CD4^+$ T-cells *in vitro*. More concerning, CCL25-CCR9 interactions are critical for establishing early

thymocyte colonisation and selective maturation of T-cells tolerant to self antigens [150]. Collectively, these findings imply that although congenital absence has potentially harmful consequences, targeted therapy against CCL25/CCR9 may yet be therapeutically efficacious in prevention or treatment of small bowel inflammation. Indeed, patients with small-intestinal Crohn's disease significantly improve clinical and endoscopic parameters of disease severity following treatment with the CCR9-antagonist Vercirnon (152).

1.7 Mucosal immunity in liver autoimmunity

Autoimmune hepatitis (AIH), primary biliary cirrhosis (PBC) and PSC all nestle within the umbrella term of 'autoimmune liver disease,' in which the end result is immune-mediated hepatocellular or hepatobiliary injury. All three are associated with gut inflammation; AIH and PSC in particular being linked to IBD, and PBC to coeliac disease [1]. This observation has stimulated several intriguing pathogenic concepts in which gut commensals, pathogens and intestinal antigens are all implicated in causing liver injury. T_h17 cells have also been linked to AIH, PBC and more recently PSC. Given the intestine is a key regulator of immunopathogenic T_h17 responses, this may underpin a common disease mechanism and open up novel treatment avenues based on rational targeting of immune pathways [1,22]. Moreover, the observations that long-lived mucosal memory T-cells can be recruited to the liver in response to endothelial-cell adhesion molecules and chemokines, which are normally 'gut-restricted,' could plausibly explain why these diseases are associated with site-restricted tissue distributions and pave the way for therapeutic strategies based on modulating tissue specific lymphocyte homing [1,2,152]. That particular gene-

polymorphisms exist which confer combined PSC/IBD susceptibility, underscores the fundamental role of mucosal immunogenicity [1,98].

1.7.1 Anatomy of the human liver

The liver is the largest internal organ in the human body, being morphologically divided into 4 anatomical lobes: right, left, quadrate and caudate. The vast majority (~80%) of the liver's blood supply is derived from the hepatic portal vein, a vessel that delivers deoxygenated yet nutrient-rich blood from the gastrointestinal tract. Arterial and portal venous bloods permeate the hepatic sinusoids generating a mixed arterio-venous perfusion draining into a central vein.

Ultrastructurally the intrinsic functional unit is represented by the liver lobule, a polyhedral prism limited by four to five portal triads each containing a bile duct, hepatic artery and hepatic portal vein (Figure 1.5). Within each lobule hepatocytes (epithelial cells of the liver) are arranged in layers that radiate from a central vein, interspersed by hepatic sinusoids. Up to 80% of the liver cell population consists of metabolically active hepatocytes, arranged into cell plates separated by sinusoids lined with endothelial cells. Hepatocyte cellular machinery is responsible for numerous metabolic functions, including synthesis of plasma proteins, complement, growth factors, cytokines and clotting factors, and synthesis of lipids and bile. Bile consists of bile salts, bilirubin, phospholipids (including lecithin), cholesterol and various ions. Following secretion from the liver, bile is delivered to the small bowel (duodenum) via bile ducts where it is responsible for assimilation of nutrients, in particular lipids. Another important function lies in the metabolism of amino acids, plasma proteins and vitamins, as well as glycogenesis and glycogenolysis. In addition,

the liver acts as a storage site of fat-soluble vitamins and also responsible for xenobiotic detoxification by cytochrome P450 enzymes. For these functions to be efficiently served, hepatocytes must extract nutrients, as well as waste and toxins from the blood circulating through the sinusoids.

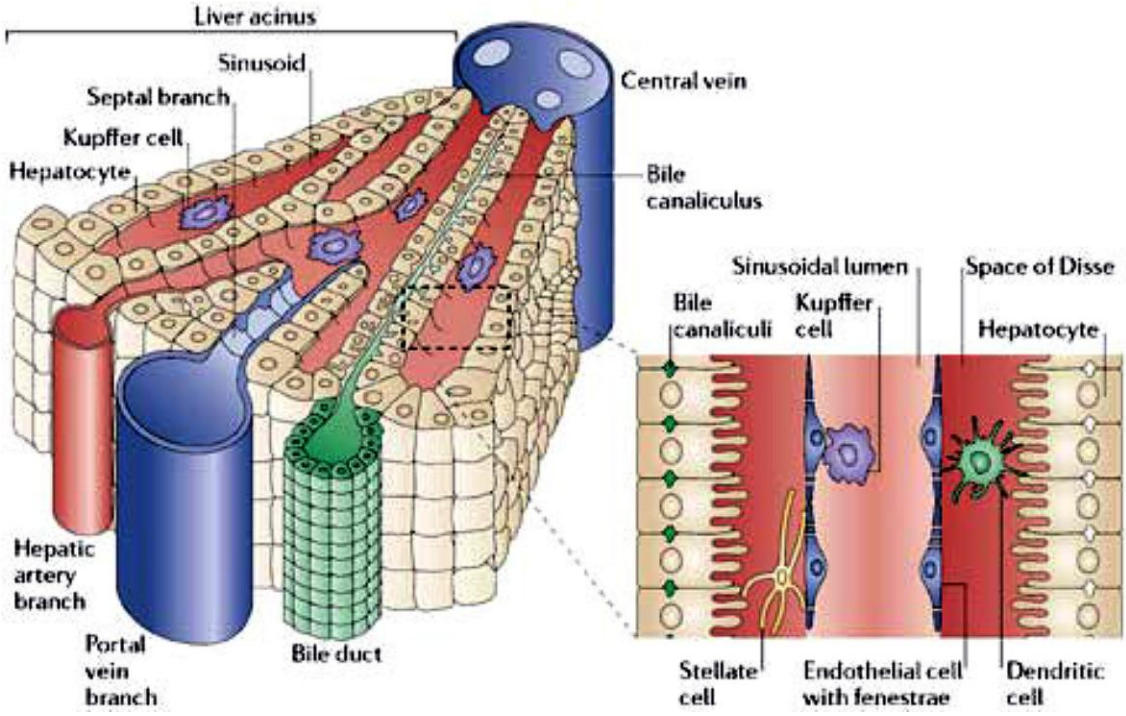

Figure 1.5: The hepatic lobule
A hepatic triad consists of three vessels, one branch of the hepatic portal vein, one branch of the hepatic artery and one bile duct. Hepatic triads are located at the corners of the polyhedral (usually hexagonal) lobules. Arterial and portal venous blood percolate through the hepatic sinusoids into the central veins that coalesce into hepatic veins and finally drain into the inferior vena cava [2].

The hepatic sinusoidal lumen is narrow and penetrated by Kupffer cells, resident macrophages that patrol the entrance of sinusoids. Kupffer cells represent the largest population of tissue-resident macrophages within the human body and their predominant localisation toward the periphery of the liver lobule permit effective phagocytosis and clearance of antigens entering via portal venous blood, as well as intimate contact with circulating immune cells [153]. Kupffer cells thus play a crucial

homeostatic role in host protection and capable of inducing both immunogenic and tolerogenic immune responses [154]. Monocyte-derived macrophages (MdM) constitute a minority of the intrahepatic macrophage population within normal liver and preferentially localise to the perivascular zone [155]. However, in response to hepatic injury macrophage populations markedly differ, with a decrease in the number of Kupffer cells during hepatic inflammation and fibrogenesis [156,157]. Conversely, MdM populations markedly increase, indicative of a pro-fibrogenic role.

The interval between hepatocytes and sinusoidal endothelial cells is known as the perisinusoidal space of Disse, and is characterised by extracellular matrix (ECM) components including collagen (type III > types I and IV), proteoglycans and fibronectin. The ECM serves as a docking point for cells, permitting intercellular communication and differentiation. Hepatic stellate cells (HSC) – precursors of tissue myofibroblasts are also located in the space of Disse. In addition to being crucial mediators of the inflammatory response, they serve as intracellular stores of vitamin A, control sinusoidal blood flow by contraction, and play a critical role in development and propagation of tissue fibrosis.

1.7.2 Enterohepatic immune system

In addition to resident Kupffer cells, hepatic sinusoids are lined by a unique fenestrated endothelium that bears intrinsic scavenging properties. The sinusoids are also patrolled by innate immune cells including NK-cells, NKT-cells and MAIT cells, which are enriched in the human liver. Thus the liver acts as a second “firewall” to prevent the spread of infection that evades immune surveillance in the gut and also as

a second line of processing to determine whether gut antigens, including nutrients, mount an immune response or are tolerated.

1.7.2.1 Biliary epithelium

The biliary and gut epithelia are contiguous mucosal components, sharing common barrier functions and mechanisms to prevent invasion by pathogens. These include IgA secretion, expression of TLR and NOD-like receptors [158], and the presence of resident epithelial associated lymphocytes and DC. Intestine-derived PAMPs such as lipopolysaccharide (LPS), lipoteichoic acids and bacterial DNA fragments can be detected in portal blood and bile, and biliary epithelial cells (BEC) actively participate in leucocyte recruitment by up-regulating adhesion molecules and secreting chemokines including CXCL8, CX3CL1 and CXCL12 in response to cytokines or TLR agonists such as endotoxin [159–162]. In particular, epithelial CXCL16 enhances the adhesion of $CXCR6^+$ liver-infiltrating lymphocytes by activating α4β1, which binds to epithelial VCAM-1 induced in response to inflammation [163]. CXCR6 expression is increased on NK, NKT and T_h1-cells in the liver, and may also localise $CD8^+$ effector cells to biliary epithelium, which mediate bile duct destruction in cholangiopathies such as PBC and PSC [162,164]. Biliary CCL28 is also up-regulated in inflammation and promotes recruitment of T_{reg} which are $CCR10^+$. As CCL28 expression is a feature of intestinal epithelium, this suggests shared signals localise T_{reg} to the gut and liver [165].

1.7.2.2 The balance of intrahepatic immunity: activation vs. tolerance

The liver's ability to promote immune tolerance is essential to prevent disproportionate immune responses to nutrients or commensals entering via the portal vein. However the liver needs to be able to respond appropriately to pathogens and does so in most cases including hepatitis A and hepatitis E, although pathogens such as malaria and hepatitis C, which are characterised by persistent host infection, may exploit the liver's tolerogenic properties to evade immune surveillance.

In addition to conventional DC the liver is characterised by populations of resident non-professional APC that regulate local activation of T-cells [166]. The ability of hepatic sinusoidal endothelial cells (HSEC) and hepatocytes to interact with T-cells is facilitated by the specialised structure and characteristics of liver sinusoids, including fenestrations that not only facilitate solute transport, but permit hepatocytes to extend protrusions into the sinusoidal lumen. Furthermore, the low levels of flow in the sinusoids allow lymphocytes in transit to interact with endothelial cells, as well as Kupffer cells and hepatocytes which have been shown to extend cell protrusions through the fenestrations into the sinusoidal lumen. Of note, antigen presentation by hepatocytes can lead to T-cells entering hepatocytes following which they are degraded by suicidal emperipolesis [167]. HSEC also possess the ability to take up, process and present soluble antigens and apoptotic cells from the sinusoidal blood, and can directly cross-present antigen to naive $CD8^+$ T-cells in a process that usually results in tolerance [168,169]. The contribution of HSEC to intrahepatic $CD4^+$ T-cell priming is less clear [170–172]; murine studies suggest HSEC have an ability to prime naïve T-cells with a regulatory phenotype and that such activation impart

responding cells with gut-tropism, providing another potential link between the gut and liver [173–176].

Liver-derived DC in mice and humans are also inherently tolerogenic, expressing low levels of co-stimulatory molecules required for full T-cell activation [177,178]. Liver-derived DC preferentially secrete IL-10 and are capable of inducing peripheral T_{reg} which suppress immune responses [179]. Recent studies have further illustrated that the liver microenvironment modulates the ability of bone-marrow derived APC to activate viable effector T-cells [180]. Activation of naïve T-cells in the liver induces lymphocytes to undergo apoptosis in part due to a failure of the protein Bcl-2 to counteract the pro-apoptotic effects of another protein, Bim. Such an outcome is not seen in other tissues suggesting that it is the liver microenvironment which determines this fate. One factor may be the secretion of IL-7 by hepatocytes which has been shown to regulate T-cell survival, or other cytokines such as IL-6, IL-10 or TGF-β secreted by stromal cells or Kupffer cells [156,181].

The importance of local IL-10 secretion is illustrated by studies of murine infection with the enteric pathogen *Trichinella spiralis* [182]. Wild-type animals infected orally develop gut infection and local expansion of $CD4^+$ T-cells but no hepatitis, whereas IL-10 deficient mice develop severe hepatitis mediated by $CD4^+$ T-cells activated in the gut. This illustrates that local regulatory networks in the liver are critical for protection against effector responses generated in the gut. Further evidence of the ability of the gut to regulate intrahepatic DC maturation and function comes from studies showing that intestinal commensals and bacterial products carried to the liver via portal vein regulate the threshold for DC maturation and activation in the liver

[183]. The constant exposure to bacterial products means that the liver is relatively insensitive to endotoxin, and Kupffer cells and HSEC respond by preferentially secreting immunosuppressive cytokines preventing the liver from being in a constant state of inflammation [184]. Plasmacytoid DC recruited to the liver in response to inflammation can also induce tolerance through anergy or apoptosis of antigen-specific $CD8^+$ T-cells [185]. This may be important for the elimination of antigen-specific cytotoxic T-cells as part of the process of regulating cytotoxic T-lymphocyte responses to infection.

Thus, under homeostatic conditions antigen presentation within the liver usually results in immune tolerance. However, the fate of intrahepatic immune responses is largely dependent on the local inflammatory microenvironment and the predominant site of antigen expression and lymphocyte activation. Early antigen expression within secondary lymphoid tissue can result in an effective cytotoxic T-lymphocyte response and hepatocellular injury, although when antigen is presented predominantly within the liver, $CD8^+$ T-cell tolerance is likely to ensue [168]. Chronic infection under these circumstances (e.g. HCV infection) may be difficult to overcome because of exhaustion or depletion of T_c-cells. Nevertheless, recent studies from the Bonn group have illustrated that TLR-signalling is able to transiently induce intrahepatic aggregates of myeloid cells which enable population expansion of cytotoxic T-cells [186]. Lymphocyte proliferation under these circumstances appears restricted to stimuli provided by monocyte-derived $CD11b^+$ cells. Signalling via TNF induces myeloid aggregate formation, and these dynamic structures, generated in a likely effort to overcome normal regulatory cues that normally limit T_c-cell expansion, may represent a putative avenue of therapeutic intercession in chronic hepatic infection.

1.7.2.3 Autoimmune liver disease and mucosal immune activation

The targets of autoimmune hepatobiliary injury are hepatocytes in AIH, and cholangiocytes (BEC) in PBC and PSC, although the cholangiopathies are also characterised by varying degrees of interface hepatitis, and inflammatory bile duct lesions occur in some patients with AIH [187]. The factors that initiate and perpetuate immune-mediated liver injury are poorly understood but likely to be environmental triggers on a background of genetic defects in immune regulation, which allow persistent inflammation and breakdown in self tolerance [164,188,189]. All three of the major hepatic autoimmune diseases are associated with bowel disease, most strikingly PSC with IBD.

1.7.2.3.1 T_h17 cells and T_{reg} in autoimmune liver disease

All autoimmune liver diseases are associated with an inflammatory infiltrate consisting of macrophages, B-cells and T-cells, with the latter in particular playing a central role in the underlying pathogenesis. Defects in the number and function of intrahepatic and peripheral blood T_{reg} have been demonstrated in AIH, PBC and PSC, although others argue no such deficit [25,190–193]. However, the fact that hepatitis is a common finding in both humans and mice with defective regulatory cell function suggests that they are important in maintaining tolerance to liver antigens.

T_h17-cells have been linked to PBC, AIH and PSC [16,194,195] and are abundant in the intestinal lamina propria where they are induced by commensal bacteria and provide protection against invading pathogens [196,197]. In mice, peripheral T_h17-cells secrete IL-17A which induces expression of CCL20 in the small intestine, and T_h17-cells can then be redirected to the gut via CCR6-CCL20 interactions. In humans,

CCL20 is also expressed on inflamed bile ducts suggesting that the same chemokine pathway might promote accumulation in the inflamed liver [22,198]. CD161 expression by human T-cells correlates with IL-17 secretion, and $CD161^+$ T-cells include T_h17 $CD4^+$ T cells, $CD8^+$ T_c17 cells and IL17-producing MAIT-cells [92,199]. Many of these cells express CXCR6, which is involved in recruitment and targeting to hepatocytes and BEC in the inflamed liver.

The terminal ileum produces IL-1 and IL-23 in the presence of commensal microbes and increased secretion of these cytokines is associated with the development of IBD [200,201]. 'Spill-over' of T_h17 cytokines including IL-23 into the systemic circulation has been proposed to lead to the development of immune mediated joint disease in IBD [202,203] and a similar mechanism might contribute to the hepatobiliary manifestations observed in ulcerative colitis (UC) and Crohn's disease [16]. Thus, there is evidence to implicate the gastrointestinal tract as a site for control of both T_h17 and T_c17 cells.

1.7.2.4 Lymphocyte recruitment in immune-mediated liver injury

The normal human liver contains γδ and αβ $CD4^+$ and $CD8^+$ T-cells as well as NK-cells, NKT-cells, innate lymphoid cells and MAIT cells. Most intrahepatic T-lymphocytes are primed memory cells, which traffic under homeostatic conditions to maintain immune surveillance throughout the liver [2]. It is plausible that a proportion of these memory cells are actually activated in the intestine prior to undergoing hepatic recirculation, in an effort to generate 'memory' of shared mucosal antigens encountered both in the gut and liver [1,204]. Indeed, mucosal memory T-cells

preferentially re-circulate through the liver under homeostatic conditions in a process not necessarily dependent on expression of gut-tropic homing receptors [205].

The mechanisms of lymphocyte recruitment to the liver are complex and involve specific combinations of adhesion molecules and chemokines including the atypical endothelial adhesion molecule VAP-1. However, no tissue-specific homing receptor has been reported for the liver despite the presence of important differences in phenotype and function of hepatic vascular and sinusoidal endothelium [45]. Leucocytes can enter the liver at several sites including post-capillary portal venules, although the majority undergo adhesion and transmigration in the hepatic sinusoids (Table 1.3). There is increasing evidence that lymphocyte interactions within hepatic microvasculature does not conform to the classical pathways of leucocyte adhesion [206]; the low shear environment allowing for selectin-independent recruitment with only a brief rolling step leading to firm adhesion [207]. Indeed, under homeostatic conditions portal endothelium expresses low levels of selectins, ICAM-1, ICAM-2 and VCAM-1; whereas sinusoidal endothelium constitutively expresses ICAM-1, with VCAM-1, P-selectin and E-selectin expression being minimal or undetectable [208]. Sinusoidal endothelial cells also express receptors more commonly associated with lymphatic endothelium including lymphatic vessel endothelial hyaluronan receptor (LYVE)-1, liver/lymph node-specific intracellular adhesion molecules-3 grabbing non-integrin (L-SIGN), CLEVER-1 and VAP-1 [208].

Table 1.3: Molecular determinants of leucocyte recruitment to the liver [1]

Site	Constitutive expression	Increased in response to inflammation
Portal vessels	CCR5 – CCL3/4/5	E-selectin P-selectin – PSGL-1 CX3CR1 – CX3CL1
Sinusoids	VAP-1 CLEVER-1 ICAM-1 (low levels) - αLβ2 CXCR6 – CXCL16 CXCR4 – CXCL12 CXCR3 – CXCL9/10/11 (low)	CD44 VAP-1 α4β7 – MAdCAM-1 αLβ2 – ICAM-1 α4β1 – VCAM-1 CCR9 – CCL25 CXCR3 – CXCL9/10/11 CX3CR1 – CX3CL1 CXCR4 – CXCL12
Biliary epithelium	CCR10 – CCL28	αLβ2 – ICAM-1 α4β1 – VCAM-1 CCL20 – CCR6 CXCR1 – CXCL8 CXCR4 – CXCL12 CXCR6 – CXCL16 CX3CR1 – CX3CL1

Animal models of immune-mediated hepatitis have demonstrated roles for endothelial ICAM-1 as well as inflammation induced VCAM-1, P-selectin and L-selectin and several pro-inflammatory chemokines [45,209–211], none of which are tissue-specific. However, VAP-1 is constitutively expressed on the endothelial cell surface in human liver, with little detected elsewhere in the absence of active inflammation. In the inflamed liver, VAP-1 is further up-regulated on endothelium and expressed by pericytes/stellate cells together with ICAM-1 and VCAM-1; inhibition of which can reduce inflammation in models of immune-mediated hepatitis [212–214].

Effector T-cells infiltrating the inflamed human liver express higher levels of CXCR3, CXCR6, CCR1 and CCR5 than circulating cells [45]. CXCR3 is highly expressed on T_h1, T_h17 and $CD8^+$ T-cells, and its ligands CXCL9, CXCL10 and CXCL11 (induced by IFN-γ and TNF-α) can be detected on damaged bile ducts in

PBC [215]. CXCR3 ligands recruit T_h1 and T_h17-cells via the sinusoidal endothelium, although subsequent positioning within the liver may involve other chemokines including CCL20 which localises T_h17 cells to bile ducts [198]. Plasma levels of CXCL9 and CXCL10 increase with advancing disease stage in PBC and AIH [216], and can be reduced with disease specific treatment [217].

Liver infiltrating T_{reg} express homing receptors such as CXCR3 that overlap with their effector counterparts, facilitating co-localisation in order to suppress inflammation. CXCR3 and $\alpha4\beta1$ integrins mediate the recruitment of T_{reg} via HSEC, and CCR4 ligands secreted by DC localise them to sites of chronic hepatitis [218]. Recently, CLEVER-1 was shown to preferentially induce transendothelial migration of $CD4^+$ $FoxP3^+$ T_{reg} through liver endothelial cells *in vitro,* and may provide an organ-specific signal for T_{reg} recruitment to inflamed liver [66].

1.7.3 Immune regulation in hepatic fibrosis

Hepatic fibrosis represents the gradual wound-healing response following long-standing injury, in which chronic inflammation from a variety of aetiologies results in ECM deposition, parenchymal death, angiogenesis and formation of scar tissue, with any potential for reversal decreased significantly once cirrhosis is established. Broadly speaking, accretion of 'scar-tissue matrix' results from dysregulated matrix remodelling due to an imbalance between matrix metalloproteinases (MMP) that degrade ECM components, and tissue inhibitors of metalloproteinases (TIMP). The ECM is increasingly recognised as a dynamic structure, bearing a pertinent role in regulating cell behaviour rather than simply serving as an inert 'scaffold.' Components of the ECM can mediate cell-matrix adhesion through integrin binding,

participate in cell-signal transduction, and bind soluble growth factors and regulate their distribution, activation, and presentation to cells [219].

Accumulation of myofibroblasts is a key feature of fibrosis, most deriving from activation of resident mesenchymal cells, called HSC. However, a subset of portal fibroblasts have also been proposed to mediate biliary-type fibrosis [220]. In chronic liver injury HSC become activated, up-regulate the expression of mesenchymal cell markers (αSMA and collagen-I), and trans-differentiate to myofibroblasts characterised by increased proliferation and migration, secretion of ECM proteins, enhanced contractility and release of pro-inflammatory and pro-fibrogenic mediators such as TGF-β1.

1.7.3.1 Ductular reaction in fibrosis

Proliferation of BEC occurs with varying degrees in all causes of hepatic fibrosis, and activated proliferating epithelia can release many fibrogenic growth factors including TGF-β1/2, platelet derived growth factor (PDGF) and connective tissue growth factor. This ductular reaction (DR) also contributes to the production of basement membrane proteins, which can impart branching vascular and biliary structures with the necessary structural support through induced and *de novo* formed ECM. This process can progress unperturbed in fibrotic disease. During fibrogenesis, expression of αvβ6 on activated epithelia can modify the cellular response to fibrogenic stimuli [221], through binding and activation of TGF-β precursors [222]. Activated myofibroblasts also express αv integrin, and perpetuation of myofibroblast activation results from several auto/paracrine feedback loops involving (amongst others) expression of receptors for TGF-β and PDGF [223,224]. Moreover, αvβ6 is a receptor for

fibronectin and tenascin-C [225]; essential matrix components of granulation tissue. Binding these substrates augments epithelial cell activation and proliferation through mitogen activated kinases [222]. αvβ6 integrin expression is absent in uninjured human and mouse liver but up-regulated following activation of BEC and hepatocytes with features of ductular transformation, and correlates with fibrosis stage [222]. Furthermore, studies in mice and rats have illustrated that conditional deletion of the αv subunit, or administration of antibodies targeting αvβ6, attenuate bile ductular proliferation, peribiliary collagen deposition and favourably alter the expression of pro-fibrogenic vs. fibrolytic genes [221,222,226].

1.7.3.2 Pro-fibrotic vs. pro-resolution macrophage populations

As well as being key mediators of ECM-production, HSC actively participate in the innate immune response, mediating a range of immunoregulatory effects through production of NADPH oxidases, reactive oxygen species and pro-inflammatory cytokines and chemokines including M-CSF and CCL2, CCL3, CCL4 and CCL5. HSC also express chemokine receptors CCR5, CCR7, CXCR3 and CXCR7 [154], react to bacterial components through TLR4 signalling and function as non-professional APC in the injured liver [227]. Macrophages localise in proximity to activated myofibroblasts [228,229], and evidence of a major functional role is provided by studies in which unselected depletion (rats [230]), or conditional deletion (CD11b monocytes and macrophages in mice [228]), result in attenuated numbers of HSC-derived myofibroblasts and reduced liver fibrosis. Similar effects are obtained using clodronate arbitrated deletion in parenchymal and biliary models of fibrosis [231,232].

Monocyte-derived macrophages substantially expand following tissue injury, implying that the pro-fibrogenic macrophage population derives from within [156,157]. In mice, a subgroup of iNOS-producing pro-inflammatory macrophages, arise from Gr-1^{+} (subtype Ly6C) inflammatory monocytes, which are recruited to the liver via CCR2-dependent trafficking; and represent the key pro-fibrogenic population in carbon tetrachloride (CCl_4)-induced murine fibrosis [233]. The $Ly6C^{hi}CD11b^{+}F4/80^{+}$ susbet of hepatic macrophages is the most proliferative population in this setting [157], and believed to correlate to human intrahepatic $CD16^{+}$ monocytes. Of interest, the latter represent precursors of inflammatory tissue macrophages and inflammatory DC in humans, which exhibit VAP-1–dependent migration across HSEC [234]. The crucial role of monocyte recruitment in hepatic fibrogenesis is further supported by studies in which inhibition of CCL2 (rats) or congenital absence of CCR2 (mice) abrogates macrophage infiltration and development of fibrosis [235,236].

A population of ‘restorative macrophages’ have been described, which also reside close to hepatic fibrotic scar tissue [154]. This subset is opulent in MMP [229,237] and TNF-related apoptosis-inducing ligand (TRAIL), which mediate apoptosis of myofibroblasts. Moreover, phagocytosis of apotopes is able to further induce MMP expression (positive feedback) therein potentiate the degradation of ECM components [157,238]. This population in mice are characterised as being $CD11b^{hi}F4/80^{int}Ly6C^{lo}$. That they derive from a phenotypic switch of the pro-inflammatory $Ly6C^{hi}$ subset, possibly induced by ‘apophagocytosis,’ highlights the critical importance of highly-plastic monocyte-derived macrophages in both the response to liver injury and

restitution of tissue architecture [157]. However, it is not yet apparent how imminently translatable these observations are to human disease [239,240].

1.7.3.3 Adaptive immune responses in hepatic fibrosis

The precise role of adaptive immune responses in hepatic fibrogenesis is less understood, and contributions of individual T-cell populations likely dependent on the underlying aetiological driver. Indirect evidence suggests that a skew toward T_h2 immune responses is influential in the fibrotic response. C57BL/6 mice (in which T_h1 cell responses predominate) have a weaker propensity towards fibrosis than BALB/c mice (more commonly exhibiting a T_h2-type profile). Furthermore the T_h2-associated cytokine IL-13 stimulates TGF-β1 synthesis [241], whereas antagonism of IL-13 signalling ameliorates fibrosis [242]. In contrast, IFN-γ and IL-12 are anti-fibrotic and suppress collagen deposition and inhibition of MMP activity [243]. The IL-17 receptor can be expressed on monocytes, Kupffer cells, BEC and HSC, and activation induces secretion of pro-inflammatory cytokines such as IL-1β, IL-6, TNF and TGF-β [154]. Indeed, T_h17 and T_c17 lymphocytes can directly induce type-I collagen production in HSC through activation of STAT3 [244].

Adoptive transfer experiments in mice also implicate cytotoxic T-cells in a pro-fibrogenic role, and $CD8^+$ T-cell–mediated liver fibrosis can be ameliorated by IL-10 [245]. However, in a CCl_4 model, mice deficient in $CD4^+$ or $CD8^+$ T cells demonstrated little variation in their propensity toward hepatic fibrogenesis compared with wild-type controls [246]. iNKT-cells are also activated in acute or chronic liver injury, a process thought driven by CXCR6–CXCL16 interactions, and result in secretion of IFN-γ and IL-4. Moreover, *Cxcr6*$^{-/-}$ mice have reduced macrophage

accretion and pro-inflammatory cytokine production following liver injury and are relatively protected from liver fibrosis; a phenotype reversed upon reconstitution with wild-type hepatic NKT-cells [247].

1.7.3.4 Biliary fibrosis

BEC are the primary site of injury in chronic cholangiopathies such as PSC, and as fibrosis originates in the peri-ductular region, the portal localisation of portal fibroblasts (versus the peri-sinusoidal location of HSC) would make them attractive candidates as mediators of biliary fibrosis. Portal fibroblasts (PF) undergo myofibroblastic differentiation in the chronically injured liver and akin to typical myofibroblasts express large numbers of αSMA–containing microfilament [220], as well as fibronectin, fibrillar collagen and elastin (248–251). In contrast to HSC however, PF do not store retinoids and can be identified through expression of Col5α1 [252].

Until recently, evidence regarding the relative contributions of various myofibroblast sources (and function) in fibrogenic liver disease was limited to studies of isolated cell populations, and the advent of *in vivo* cellular fate-tracing studies have significantly enhanced our understanding in this regard. In a landmark paper, Mederacke *et al*. studied several murine models of toxin-induced (CCl_4, thioacetamide), steatotic (methionine-choline-deficient diet) and biliary (bile-duct ligation, *Mdr2*$^{-/-}$) fibrosis [253], in which HSC were found exert a dominant role across all aetiologies. Indeed, HSC constituted the majority (>80%) of αSMA and ECM (collagen)-producing cells even in cholestatic liver injury, with only low-level fibrotic gene expression by the less abundant PF-like population. The authors propose

HSC as universal responders in hepatic wound repair [253], irrespective of the underlying cause of injury. A higher proportion of portal myofibroblast populations were nevertheless observed in biliary injury, and whilst PF may not contribute significantly to hepatic fibrosis their localisation adjacent to bile ducts is likely indicative of more specialised functions.

1.8 Mucosal immune activation and primary sclerosing cholangitis

Given the intimate relationship and shared antigen exposure between the gut and hepatobiliary immune systems, it is perhaps unsurprising that the liver can be affected as an extra-intestinal complication of immune-mediated disease of the bowel. PSC is a chronic inflammatory cholangiopathy resulting in fibrotic stricturing of the intrahepatic and extrahepatic bile ducts (Figure 1.6). The majority (>80%) of patients develop concomitant IBD at some point in their lifetime whereas 2.5 – 7.5% of the IBD population may develop PSC. The clinical phenotype of IBD in PSC is unique, being characterised by rectal sparing, backwash ileitis and either pancolonic involvement or predominantly right–sided disease [254]. Despite the majority having relatively quiescent intestinal inflammation, there is a ~30% lifetime risk of colonic malignancy [255], imparting need for annual colonoscopic surveillance [256,257]. No known medical therapy has consistently proven to retard disease progression, with the majority of patients requiring liver transplantation (>50%) or developing hepatobiliary malignancy (~15%) [258]. Furthermore, issues relating to risk stratification are particularly marked in PSC given the dearth of validated tools or biomarkers. In this regard there is a desperate need to track PSC immunologically more precisely over time, in order to facilitate early disease intervention.

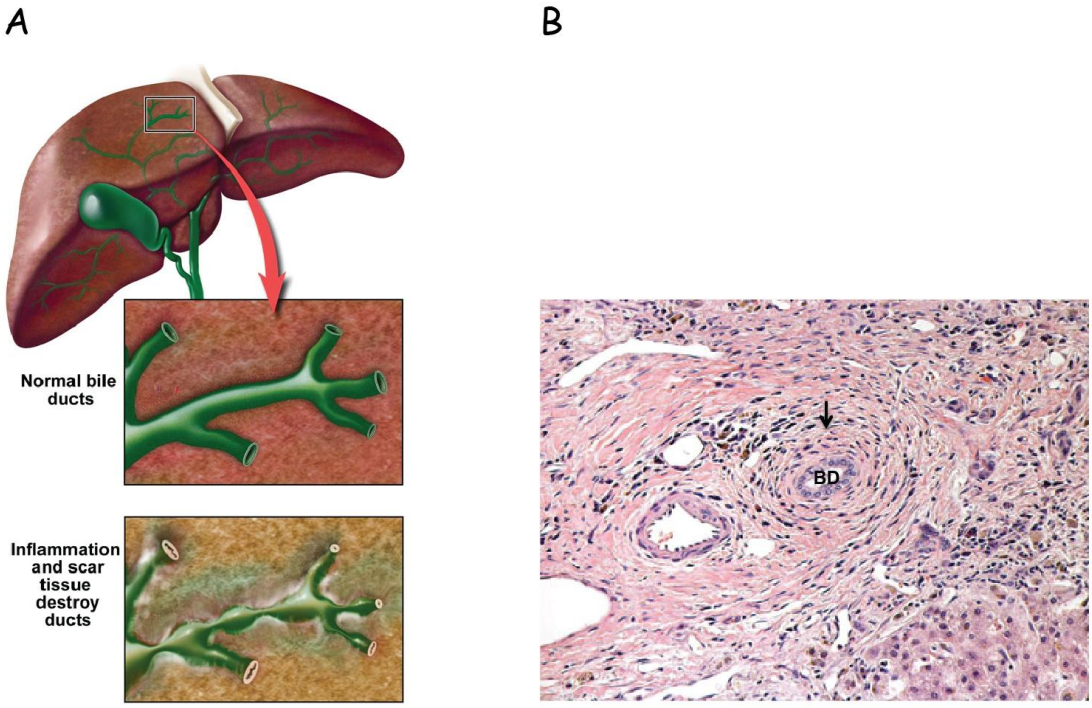

Figure 1.6: Primary sclerosing cholangitis
Morphologically, primary sclerosing cholangitis is manifest by multi-focal stricturing of the hepatobiliary tree (A) as a result of inflammation and scar tissue formation of intra- and extra-hepatic bile ducts. The classical histological lesion (B) is characterised by dense, portal inflammation and concentric peri-ductal fibrosis (black arrow) around bile ducts (BD). *Adapted from www.liver.ca*

1.8.1 The clinical impact of IBD on PSC

The presence of IBD has a significant, negative impact on the clinical course of hepatobiliary disease in PSC. Patients with IBD are reported to have reduced survival and an increased cholangiocarcinoma (CCA) risk when compared to those without bowel disease [259]. Moreover, patients who develop CCA are likely to have experienced a significantly longer prior duration of colitis [260], and in one study all who developed CCA had evidence of concurrent IBD whereas no hepatobiliary malignancy was found in the absence of intestinal inflammation [261]. Liver transplant-free survival is also curtailed in patients with IBD [261]; however, the activity of hepatobiliary disease does not necessarily parallel that of colonic inflammation. Indeed, colitis can develop many years after liver transplantation with

variable disease activity [262]. Similarly, patients can develop PSC for the first time after total colectomy for colitis.

1.8.2 Mucosal Genetics in PSC

PSC has an insidious onset making recognition of identifiable triggers difficult although the strong relationship with IBD suggests a common pathway for liver and gut inflammation centred on dysregulated mucosal immunity. The prevalence of PSC among first-degree relatives of PSC patients is increased 100-fold relative to family members of a matched control population, the former of which also carry an increased lifetime risk of developing IBD [263–266]. The strongest genetic associations in PSC lay within the human leucocyte antigen (HLA) region (chromosome 6) that encode all MHC molecules, although mostly differ from those that predispose to IBD. However, several non-HLA genetic associations that relate to mucosal immunity are intricately shared between IBD and PSC [267]:

a) The importance of IL-2/IL-2Rα polymorphisms is supported by the fact that mice lacking IL-2Rα develop a T-cell mediated cholangitis together with colitis [268]. Moreover, liver-derived lymphocytes from PSC patients show reduced expression of the IL-2-receptor and an impaired proliferative response (264).
b) Caspase-recruitment domain (CARD)-9 is an important downstream mediator of signalling from NOD2 and TLR, and genetic associations suggest a link between defective intestinal mucosal microbial handling and the development of PSC [270].
c) Macrophage-stimulating (MST)-1 is one of the strongest non-HLA associations in PSC and also linked with UC and CD. MST-1 is expressed by biliary epithelium and involved in regulating innate immune responses to bacterial ligands, and also plays a role in lymphocyte trafficking in lymphoid tissues by modulating integrin-

mediated adhesion [271–273]. MST-1 variants could therefore signify an important overlapping susceptibility locus for PSC and intestinal inflammation. Glutathione peroxidase (GPX)-1 is an anti-oxidant enzyme located close to MST-1, and GPX polymorphisms may also confer increased disease susceptibility [265], for *Gpx1/2*$^{-/-}$ mice develop ileocolitis with an increased frequency of colonic malignancy (269).

d) Variants in *Fut-2* encoding the enzyme galactoside 2-alpha-l-fucosyltransferase-2, alter recognition and binding of various pathogens to carbohydrate receptors on the epithelial mucosal surface, and associated with changes in the commensal phyla characterised by elevated *firmicutes* and reduced *proteobacteria* [275]. This is akin to changes found in *Fut-2* mutations associated with Crohn's colitis, linking defective immune responses to the microbiota in PSC [275–277].

e) Salt-inducible kinase (SIK)-2 influences expression of IL-10 in macrophages and the leucocyte transcription factor Nur77 [278]. The IL-10 gene is an established susceptibility factor for early onset colitis [279], and exposing *Il10*$^{-/-}$ mice to a diet high in saturated fat has been shown to induce specific changes in the bile acid pool, consequential alteration in the gut microbiome and increased susceptibility to IBD [280]. A role for histone deacetylase (HDAC)-7 – a gene implicated in the negative selection of T-cells in the thymus [278] and development of immune tolerance – is supported by a genetic association at 19q13, where the most associated polymorphism is located within an intron encoding serine/threonine protein kinase (PRK)-D2. When T-cell receptors of thymocytes are engaged, PRKD2 phosphorylates HDAC7 resulting in loss of gene regulatory functions, apoptosis and negative selection of immature T-cells. This negative selection takes

place owing to a loss of HDAC7-mediated repression of Nur77 (regulated by SIK2) linking multiple new PSC loci to a common pathway [1,278].

1.8.3 Bacterial translocation, mucosal antigens and molecular mimicry

Under normal circumstances gut commensals and pathogens are confined to the gut by mesenteric lymph nodes [89]. However in the context of colonic inflammation and a 'leaky' mucosa, bacteria can enter the portal circulation, thereby the liver, leading to local immune activation which could initiate or potentiate inflammation in PSC. Although frank portal bacteraemia is rare in PSC, bacterial products can be detected in the portal vein; and despite a blunted response of the liver to endotoxin, Kupffer cells and HSEC can be activated by bacterial TLR ligands. A recent study in mice illustrates how changes in the gut microbiota as a consequence of defective inflammasome pathways and IL-18 can trigger the development of liver inflammation [119]. Herein, inflammation was driven by hepatic TNFα activation as a consequence of TLR4 and TLR9 agonists in the portal circulation. Thus, defective pathogen sensing as a consequence of genetic polymorphisms might alter the gut microbiota leading to hepatic inflammation in liver diseases associated with IBD. This is supported by murine models in which alterations in the intestinal bacterial population, or direct infusion of bacterial antigens into the portal circulation, leads to pericholangitis and hepatic inflammation. Moreover, peripheral blood lymphocytes in PSC manifest significantly higher frequencies of T_h17-cells on pathogen stimulation compared to other cholestatic liver diseases [16]. CARD9 and REL gene polymorphisms are thus of particular interest given their role in T_h17 differentiation and transduction of TLR-signalling.

Patients with PSC have a particularly high prevalence of circulating anti-*Sacchromyces cerevisiae* antibodies even in the absence of advanced disease and irrespective of IBD phenotype [281]. Moreover, it has recently been found that the pANCA isolated from PSC patients is reactive against the microbial cell division protein FtsZ present in virtually every bacteria of the intestinal microflora [282]. Some identified autoantibodies also bind to BEC and induce TLR4 and TLR9 expression, activation of which results in the secretion of pro-inflammatory cytokines and chemokines [283,284].

Further support of the PSC-microbiota hypothesis is lent by observations wherein patients manifest a leucocyte differential with increased neutrophils, even in the absence of signs or symptoms of overt cholangitis, which could suggest circulation of endotoxins or immune-reactive molecules. Moreover, antibiotics targeting the intestinal microbiome may improve surrogate biochemical endpoints [285]. More sophisticated analysis of intestinal permeability and the intestinal and hepatobiliary microbiome may yet reveal subtle defects that have not been apparent in previous efforts [286].

1.8.4 Bile acid modifications

As already discussed, several lines of evidence implicate mucosal dysbiosis and restricted biodiversity of the intestinal microbiome as being a pivotal event in the pathogenesis of IBD. Enzymatic reactions catalysed by intestinal commensals may also be responsible for bile acid transformation, and it has been hypothesised that IBD associated dysbiosis could lead to abnormal bile acid metabolism in the gut lumen

[116]. Such a process could conceivably erase the anti-inflammatory effects of certain bile acids and thereby participate in the inflammatory loop of IBD [116].

Genetic modification of bile has been shown to induce sclerosing cholangitis and biliary fibrosis in a number of animal models of PSC. Mice with targeted disruption of the *Mdr2* (*Abcb4*) gene encoding a canalicular phospholipid flippase spontaneously develop cholangitis and periductal fibrosis mirroring some of the key features of human PSC [287]. Although *Mdr2*$^{-/-}$ mice do not develop IBD, dextran sulphate sodium (DSS)-administration provoked colitis in heterozygous *Mdr2*$^{+/-}$ mice and as a "two hit" model induced portal inflammation in animals that were otherwise free of hepatobiliary disease [288]. (Genome-wide studies have not thus far identified any significant associations with the human ortholog MDR3 and PSC; however, variants may still play an important role by altering bile composition, and by proxy aggressiveness of bile, influencing secondary responses to immune-mediated bile duct injury.

1.8.5 Aberrant homing of mucosal lymphocytes to the liver

PSC is characterised by a predominantly T-cell portal infiltrate and immune-mediated damage to bile ducts which progresses through an iterative inflammatory process to periductal and portal fibrosis and progressive ductopenia. Any model attempting to explain the development of PSC in the context of IBD needs to take into consideration that hepatobiliary disease usually runs an independent course to that of bowel inflammation. The existence of an enterohepatic immune system that allows surveillance across both liver and gut by memory T-cells capable of homing to both organs would provide a second line of protection against pathogens penetrating the

mucosal barrier. However, dysregulation of this system may allow the spread of uncontrolled inflammation from the gastrointestinal tract to the liver.

Endothelial cells in the gut and liver are phenotypically distinct, the gut mucosa being characterised by high expression of MAdCAM-1 and CCL25, whereas, at least in humans, liver endothelium expresses VAP-1 and other atypical receptors such as LYVE-1 and CLEVER-1. However, in PSC, MAdCAM-1 is also found on portal vein endothelium and CCL25 on sinusoids, and ~20% of liver-infiltrating lymphocytes express CCR9 and $\alpha4\beta7$ [127,289], implying recruitment directly from the inflamed intestine. Most liver-infiltrating $CCR9^{+}$ lymphocytes are $CD45RA^{-}$ $CCR7^{-}$ $CD11a^{hi}$ and secrete IFN-γ in keeping with a long-lived memory phenotype [127]. There is also mounting evidence that monocyte-derived macrophages express CCR9, and recruitment through the CCL25 axis is able to activate HSC and promote liver fibrosis [140].

Murine models of antigen-specific gut and hepatobiliary inflammation provide further support of the aberrant lymphocyte homing hypothesis. In the works by Seidel and Eickmeier, mice expressing the antigen ovalbumin (OVA) under control of an apical sodium bile acid transporter (ASBT) and intestinal fatty acid transporter (iFABP) develop T-cell mediated cholangitis and colitis, respectively, following adoptive transfer of OVA-specific T-cells [173,175]. Of interest, these animals illustrate well-defined gut- and liver-specific lymphocyte homing patterns dependent on CCR9 and MAdCAM-1.

One anomaly with this hypothesis is the fact that PSC usually develops in patients with colonic inflammation whereas under non-inflamed conditions CCL25 is largely confined to Peyer's patches and small bowel mucosa; however, rigorous interrogation of CCL25 expression and $CCR9^+$ leucocyte populations in the inflamed human colon has yet to be performed. Other mucosal chemokines may facilitate recruitment of these cells and both CCL28 and CXCL12 are capable of triggering α4β7-mediated adhesion of human lymphocytes to MAdCAM-1 *in vitro* [290,291]. After recruitment to the liver $\alpha4\beta7^+$ gut-derived lymphocytes may use other chemokines such as CXCL12 and CXCR6 to localise to biliary epithelium where they can destroy bile ducts. Some of the recruited $\alpha4\beta7^+$ T-cells may undergo local differentiation to express $\alpha E\beta7^+$ providing another pathway to bind biliary epithelium [289]. Lymphocytes use VAP-1 expressed on sinusoidal endothelium to enter liver tissue and the surface expression of VAP-1 on intestinal endothelium is greatly increased in IBD, suggesting that liver-derived lymphocytes may be able to enter the inflamed bowel by using VAP-1 [2,292,293].

The factors leading to aberrant expression of MAdCAM-1 and CCL25 in the PSC liver are incomp liver are incompletely understood but may involve a combination of inflammation and activation of activation of the enzymatic activity of VAP-1, which in addition to being an adhesion molecule is als molecule is also an ectoenzyme with potent amine oxidase activity. It has recently been proposed th been proposed that the products of VAP-1-mediated deamination of dietary amines can lead to the can lead to the activation NFκB in hepatic endothelial cells and in the presence of TNFα this results TNFα this results in expression of MAdCAM-1 (

Figure 1.7). Thus, in the presence of an inflamed gut, increased portal vein levels of biological amines could activate VAP-1-dependent hepatic MAdCAM-1 expression thereby promoting the recruitment of mucosal effector cells to the liver [294]. VAP-1

can catabolise a broad range of substrates, and several gut commensals and enteric pathogens such as *Bacteroides fragilis*, *Salmonella typhimurium*, *Yersinia entercolitica*, *Escherichia coli* and *Clostridium perfringens* secrete other branched chained amines which may be putative substrates [295], providing another potential link between the microbiota, mucosal immunity and the pathogenesis of PSC [1].

The ability to imprint gut tropism on naïve lymphocytes is dependent on the capacity of APC to convert retinol to all-trans-retinoic acid (ATRA) [57], which complexes with intracellular retinoid receptors to activate transcription of CCR9 and α4β7. This ability can be conferred *in vitro* by the addition of exogenous ATRA suggesting that retinoids in bile or stored in HSC might be able to endow liver APC with ability to induce a gut-homing phenotype [126]. However, Eksteen *et al*. found that human hepatic DC and HSC were unable to induce high-level α4β7 and CCR9 expression on T-cells, suggesting the ability to imprint naïve lymphocytes with gut tropism is restricted to intestinal $CD103^+$ DC [296]. This concept has recently been challenged by a murine study that demonstrated priming of naïve T-cells by antigen-presenting HSEC is able to induce the expression of α4β7 and CCR9 on $CD4^+$ T-cells in a retinoic acid dependent manner [174]. These T-cells are dominated by regulatory functions and their preferential recruitment into the gut may support local tolerance of food antigens or control intestinal inflammation [176], and partly explain the paradox of finding relatively quiescent colitis in patients with PSC/IBD.

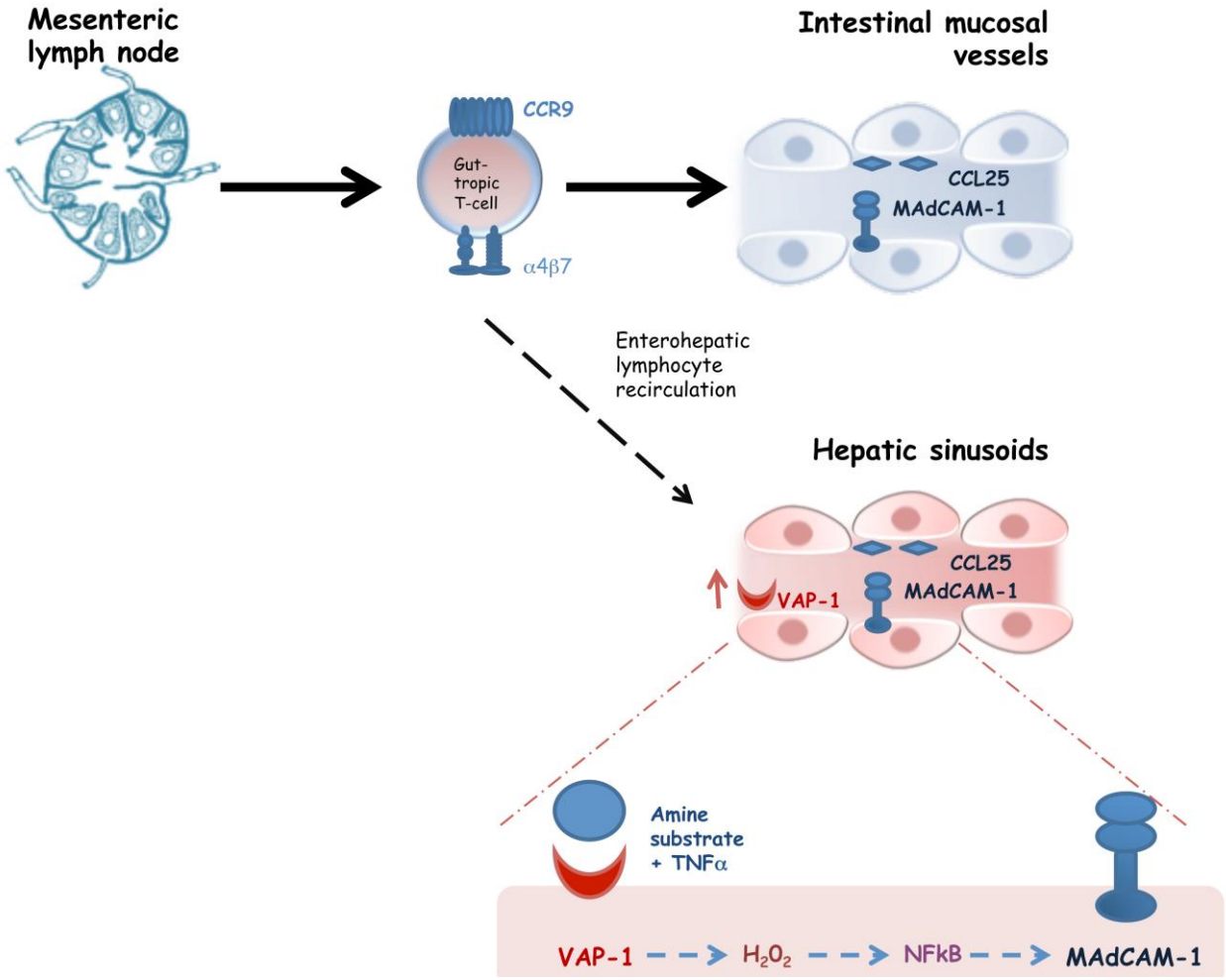

Figure 1.7: Aberrant lymphocyte homing hypothesis of PSC

Under normal physiological conditions, intestinal lymphocytes activated by gut dendritic cells imprint a gut-homing phenotype characterised by expression of the chemokine receptor CCR9 and the integrin α4β7. These receptors direct migration of activated lymphocytes back to gut tissue where their respective ligands CCL25 and MAdCAM-1 are expressed. In PSC, hepatic VAP-1 expression is up-regulated. As well as supporting endothelial adhesion directly, VAP-1 is as an amine oxidase. Methylamine and other amines present in the diet or generated by enteric bacteria can enter the liver via portal vein and act as substrates for VAP-1 leading to the generation of catabolites, which in the presence of inflammation activate NFκB-dependent expression of MAdCAM-1 on hepatic sinusoids. Hepatic CCL25 expression is also increased in PSC, resulting in the recruitment of mucosal lymphocytes activated in response to gut antigens in the setting of IBD to the liver where they contribute to inflammation and biliary destruction upon reactivation [1].

MAdCAM, mucosal addressin cell adhesion molecule; PSC, primary sclerosing cholangitis; VAP, vascular adhesion protein; IBD, inflammatory bowel disease.

1.8.5.1 Insights from other autoimmune diseases

In addition to autoimmune hepatobiliary disease, IBD is associated with cutaneous, ocular and rheumatic manifestations. Subclinical inflammation of the terminal ileum is present in up to 68% of individuals with spondyloarthropathy and associated with up-regulation of IL-23 within intestinal Paneth cells residing in the inflamed mucosa [203,297]. The consequent increased levels of circulating IL-23 act on a population of RORγt^+ $CD4^-$ $CD8^-$ T-cells resident in the inflamed joint which secrete IL-17 and IL-22 [298]. These cells express the transcription factor promyelocytic leukaemia zinc finger protein (PLZF), also expressed by MAIT-cells [97], potentially implicating a common cellular lineage. The role of MAIT-cells in maintaining mucosal immunostasis has also been illustrated in murine models of colitis [299]; and given their preferential recruitment to the human liver, their aetiopathogenic potential in PSC warrants further exploration.

1.9 Vascular adhesion protein-1: an adhesion molecule and ectoenzyme

VAP-1 was first identified as an adhesion molecule involved in leucocyte trafficking to sites of inflammation in humans [300]. Cloning and sequencing reveal homology within the semicarbazide-sensitive amine oxidase (SSAO) family [301], copper-dependent class (Table 1.4). Oxidative deamination results in the production of aldehydes, ammonia, and hydrogen peroxide (enzymatic reaction: $R\text{-}CH_2\text{-}NH_2 + O_2 + H_2O \rightarrow R\text{-}CHO + NH_3 + H_2O_2$). The catalytic site contains a modified tyrosine residue, a topaquinone, which in the presence of a copper ion is responsible for enzymatic function.

Table 1.4: Classification of amine oxidases

	FAD-containing		**Copper-containing**			
	MAO A+B	*PAO*	*DAO*	*Cell-surface*	*Soluble*	*Lysyl oxidases*
Expression	mitochondria	intracellular	intracellular	extracellular	serum	extracellular
Archetypal substrates	NA, DA, A, B-PEA, tryptophan, octopamine	spermine spermidine	cadaverine, histamine, putrescine	benzylamine, methylamine		lysine
Inhibitors	pargyline, clorgyline		semicarbazide			
Function	neurotransmission	cell growth	Histamine degeneration, cell division	amine catabolism, glucose uptake, leucocyte adhesion		formation of ECM
Cloned human SSAO						
AOC1		*AOC2*	*AOC3*			
amiloride binding protein 1 (kidney diamine oxidase)		retina amine oxidase	vascular adhesion protein 1			

Amine oxidases are broadly classified on the chemical nature of the attached cofactor. The flavin adenine dinucleotide (FAD)–containing enzymes, monoamine oxidase (MAO) A + B and polyamine oxidases (PAO) are intracellular enzymes. The other classes contain a cofactor possessing one or more carbonyl groups, most often a topaquinone and include diamine oxidases (DAO), lysyl oxidase (LOX) and plasma membrane and soluble amine oxidases. These enzymes are collectively designated semicarbazide sensitive amine oxidases (SSAO) due to their sensitivity to inhibition by semicarbazide. Four copper-dependent amine oxidase (*AOC*) genes have been identified in mammals encoding a diamine oxidase (*AOC1*), a retina-specific amine oxidase (*AOC2*), vascular adhesion protein-1 (*AOC3*) and a serum amine oxidase (*AOC4* – not shown). In some mammals, the product of the *AOC4* gene is not functional due to the presence of an internal stop codon (humans) or truncation of the coding sequence (mice, rats) [302]. NA, noradrenaline; DA, dopamine; A, adrenaline; B-PEA, β-phenylethylamine; ECM, extracellular matrix.

1.9.1 Structural overview

The transmembrane form of VAP-1 is a sialylated glycoprotein bearing a short 4 amino acid N-terminal cytoplasmic tail, single transmembrane segment and a sequence of large extracellular domains (molecular weight ~90kDa) [303] **Figure 1.8**). VAP-1 exists as a homodimer, each unit containing a copper atom, two calcium atoms and N-acetylglucosamine sugar units at two separate sites. The molecular structure is that of a 'heart-shaped' copper dependent amine oxidase (amine oxidase copper dependent; AOC) consisting of the extracellular domains D2 (residues 55-169), D3 (170-300) and D4 (301-761). D4 represents the most conserved domain, comprising many residues involved in enzyme cofactor (topaquinone) generation

and/or in the formation of the active site. Located at the C-terminal portion is the RGD motif (tri-peptide sequence Arg-Gly-Asp); a feature typical of integrin binding sites although there is currently no evidence to suggest that this motif is required for VAP-1 activity [304,305]. The domain structure of human (h)VAP-1 resembles that of other AOC family members with the exception of *Escherichia*-derived AOC which contains an additional N-terminal D1 domain [306].

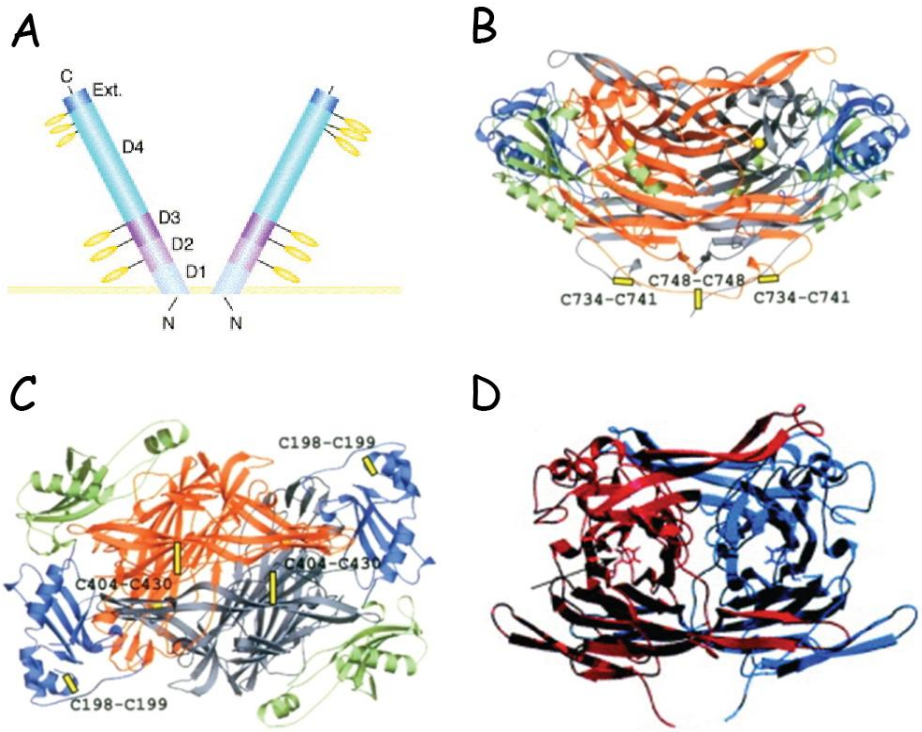

Figure 1.8: Vascular adhesion protein (VAP)-1 structure
Molecular cloning of VAP-1 has revealed a homodimeric sialoglycoprotein. The proposed four domain extracellular structure is illustrated, with sites of potential glycosylation indicated in yellow in (A) [307].

The four domains are shown as a ribbon diagram in (B) with the same structure rotated 90^{o} in (C); β-strands drawn as arrows and α-helices as spirals. The C-terminal portion of the hVAP-1 dimer is stabilised by three disulfide bridges; in each subunit Cys734 and Cys741 form an intra-subunit bond whereas Cys748 x 2 form an inter-subunit disulfide bond. Domain colouring is as follows: D2, green; D3, blue; D4 of subunit A, orange and D4 of subunit B, grey. The copper atom of the active site is shown as a yellow sphere [306].

The overall fold of domain 4 of the VAP-1 dimer is redrawn in (D), with the enzyme active site indicated by the black arrow [307].

A large proportion of protein volume is occupied by cavities including those at the dimerisation interface (C1-3), and of particular note, the active site cavities A1 and B1 (present in subunit A and subunit B, respectively). Residues from the least conserved domain (D3) as well as the most conserved (D4) protrude into the active site cavity, modifying the shape and scope for molecular interactions (the RGD site being located at the mouth of the cavity). hVAP-1 also bears many potential glycosylation sites spread across the domains which are likely to play a vital role in interactions with inflammatory cells [301,308,309].

1.9.2 Hepatic VAP-1 expression

In the human body endothelial VAP-1 is stored in cytoplasmic granules and transported to the endothelial cell surface under inflammatory conditions, being located on the membrane of HEV, lymphatic endothelium and follicular DC in lymph nodes of highly vascularised tissues. Expression becomes up-regulated under pro-inflammatory situations in the gut, synovium and kidney, where VAP-1 promotes leucocyte recruitment, and in some reports tumour development [292,310,311]. However, in the absence of inflammation cell surface VAP-1 expression is very low in non-lymphatic tissues, the one exception being liver. In man, hepatic endothelial VAP-1 expression is constitutively at a high level, and in some chronic inflammatory liver diseases such as PSC, lymphoid follicles develop in close association with portal tracts and contain $CD34^{+}$ $VAP\text{-}1^{+}$ neovessels with HEV-like morphology [289]. VAP-1 is also up-regulated on neovessels in septal areas and portal tracts in chronic hepatitis, implicating involvement in the organisation and development of such structures. VAP-1 has been shown to mediate adhesion and transendothelial migration in several experimental models of liver inflammation [212,213,312,313], and

facilitates recruitment of multiple leucocyte subsets including $CD4^+$ helper T-lymphocytes, cytotoxic $CD8^+$ T-cells, as well as granulocytes and monocytes [312].

The identity of the VAP-1 ligand remains elusive. Siglec-10 has been put forward following screening of a phage display library [314], wherein VAP-1 would enzymatically deaminate an arginine residue present on a surface exposed loop. Although Siglec-10 is highly expressed on the surface of B- and NK-cells, only low levels are detected on monocytes with a virtual absence on granulocytes, suggesting the presence of additional/alternative ligands. Siglec-9 has also been proposed as a putative ligand because expression on granulocytes facilitates VAP-1 mediated endothelial adhesion; a property partially dependent on SSAO enzyme activity and the presence of arginine residues [315]. The unusual choice of arginine in preference to conventional primary amine substrates, coupled with divergent species-specific Siglec sequences (mouse orthologues of Siglecs-9 and -10 do not bear arginine residues) indicate that further efforts are required to elucidate the ligand for VAP-1 [67].

1.9.2.1 Leucocyte recruitment

The presence of an RGD motif in the C-terminal portion of the human protein was historically thought to be a prerequisite for adhesion. However, as eluded to earlier, variants in which the aspartate residue is substituted with alanine exhibit comparable binding properties, suggesting the RGD-motif is not an absolute requirement [314]. VAP-1 has the potential to interact with leucocytes via carbohydrate moieties present on the apical surface [308]; however primary amines presented by leucocyte surface proteins (e.g. N-terminus of a protein, amino-sugars) may also bind to the active site

of VAP-1, resulting in transient covalent crosslinking of the leucocyte and endothelial cell [307]. These interactions may involve a common ligand, or require stepwise binding of soluble/cell-bound factors [316].

Despite high constitutive expression of hVAP-1 in the liver, only low hepatic levels are detectable in mice compared to the more prominent expression observed in murine adipocytes [317–319]. Indeed, the hepatic parenchyma is largely negative for VAP-1 in healthy mice when examined either by immunohistochemistry, western blotting or at the transcriptional level. This contrasts with the relatively strong staining seen in human liver tissue. An ability to mediate hepatic lymphocyte recruitment has nevertheless been supported by several *in vivo* studies. *Aoc3* knockout mice develop normally and have no overt phenotype, but exhibit a reduced capacity to support leucocyte adhesion on inflamed vascular endothelium associated with decreased transmigration into sites of inflammation [320]. Studies from the Kubes lab in Calgary suggest that VAP-1 is able to selectively recruit T_h2 $CD4^+$ T-cells in a concanavalin A (ConA)-induced model of hepatitis [212], in which mice demonstrate significantly reduced lymphocytic infiltration and markers of hepatic inflammation (serum ALT) upon VAP-1 inhibition or genetic deletion, but not inhibition of enzymatic activity [213]. Furthermore, Weston *et al*. have shown that although there is little difference between wild-type and *Aoc3*$^{-/-}$ mice in the uninjured state, following chronic CCl_4–induced hepatic inflammation knockout animals show a marked reduction in the numbers of liver-infiltrating $CD8^+$ T-cells, $CD4^+$ T-cells, B-cells, NK-cells and NKT-cells, with significantly fewer inflammatory foci observed histologically [214]. Of interest, similar changes in infiltrate were observed in mice bearing a mutated form of VAP-1 in which a single amino acid substitution renders

VAP-1 enzymatically inactive, which in part supports a role of SSAO activity in leucocyte recruitment.

Function blocking antibodies and enzyme inhibitors both appear to reduce leucocyte binding to VAP-1 by approximately 50% *in vitro*, with little or no additive effect when administered concurrently [214,316]. There are also reports of attenuating leucocyte infiltration *in vivo*, albeit with differential impact on individual subsets: in mice, antibody-blockade has been shown to reduce the migration of $CD8^+$ T-cells into tumour sites with little effect on leucocytes of myeloid lineage; whereas inhibition of amine oxidase activity significantly mitigated the infiltration of Gr-1^+ CD11b^+ myeloid cells, with no impact on $CD8^+$ T-cell recruitment [311]. The effects of small molecule inhibitors and antibody blockade on recruitment of T_{reg} and immunosuppressive monocyte populations appear less consistent. Studies by Marttila-Ichihara *et al*. suggest that inhibition via either mechanism did not alter homing of these cell populations in a murine non-liver tumour model [311]. However, VAP-1-blockade was recently shown to synergistically enhance the effects of CLEVER-1 inhibition on T_{reg} transendothelial migration across human HSEC *in vitro* [66].

In addition to its role as a primary adhesion molecule, VAP-1–mediated deamination gives rise to H_2O_2, a major reactive oxygen species that can cause cell damage in addition to serving as a potent signalling molecule. The liver sinusoidal bed is continually exposed to amines via the gut, and provision of such substrates can result in H_2O_2 release, enhance NFκB activation and up-regulate expression of chemokines and adhesion molecules [294,321]. Lalor *et al*. illustrated that provision of benzylamine promotes the expression of CXCL8, E-selectin, ICAM-1 and VCAM-1

on HSEC. Similarly, provision of the physiological substrate methylamine has recently been shown to up-regulate MAdCAM-1 in vitro and in vivo. Taken together these findings indicate how enzymatic functions of VAP-1 further modulate the ability of HSEC to recruit leucocytes under flow.

1.9.2.2 Tissue fibrosis

Catabolism of the VAP-1 substrate methylamine gives rise to the formation of formaldehyde; an extremely potent inducer of protein crosslinking as well as formation of advanced glycation end products (AGE) [322,323]. VAP-1 has been implicated in matrix remodelling because its overexpression in arterial smooth muscle cells leads to elastin deposition [324]. Together with its direct and indirect roles in leucocyte recruitment, these mechanisms may contribute to persistent inflammation and the progression of tissue fibrosis. VAP-1 small molecule inhibitors have been shown to significantly abrogate the recruitment of Gr-1$^+$ CD11b$^+$ myeloid cells into tumours [310,311], which is important given that inflammatory Gr-1$^+$ monocytes have been implicated in progression of liver fibrosis [154].

In a landmark study, Weston *et al*. demonstrated increased VAP-1 expression in αSMA$^+$ cells in fibrotic septa in close association with infiltrating leucocytes [214]. Indeed, VAP-1 was detectable in cytoplasmic vesicles within HSC, and these cells were capable of *de novo* mRNA synthesis with expression being up-regulated following provision of TGF-β or PDGF-β. Moreover, in a chronic CCl_4 model, *Aoc3*$^{-/-}$ mice as well as wild-types treated with anti-VAP-1 antibody had significantly reduced hepatic fibrosis when compared with untreated wild-type mice. Expression of fibrotic genes was also reduced in mice harbouring the enzymatically-inactive variant

(described previously) suggesting that VAP-1 amine oxidase activity is a pre-requisite for tissue fibrogenesis. Of interest, epidemiological observations imply that increased consumption of caffeine (itself, a partial inhibitor of VAP-1 enzyme activity) is associated with lower rates of fibrosis progression across a variety of chronic liver diseases, including PSC [325–327]. However, hepatic fibrosis is also abrogated in murine models of liver injury following therapeutic VAP-1 antibody-blockade, an inhibitor that does not directly bind the enzyme active site or affect substrate deamination. It has thus been hypothesised that VAP-1 antibodies can limit access of endogenous, cell-associated substrates to the molecule's enzyme active site *in vivo*, which given the as yet unknown identity of the VAP-1 ligand is difficult to prove conclusively. An alternative proposal put forward by Koskinen *et al*. suggests that mediation of immune cell recruitment would require sequential enzyme dependent and independent steps; wherein blockade of either mechanism can inhibit cell recruitment [316].

1.9.2.3 Soluble VAP-1

A catalytically active, soluble form of VAP-1 (sVAP-1) can also be detected in serum and is thought to be generated by cleavage of membrane-bound protein from the surface of endothelial cells or adipocytes [328]. The mechanism mediating release into the circulation is unknown, although TNF-α-dependent release of soluble VAP-1 has been observed in murine and human adipocytes — a process inhibited by the MMP inhibitor batimastat [319,329]. sVAP-1 appears to account for most of the circulating amine oxidase activity detectable in mouse and human serum [328,330], and elevated levels have been observed in a number of diseases including diabetes mellitus, atherosclerosis and cardiovascular disease, cardiac failure and steatohepatitis

[67,214,331]; noteworthy given the increased prevalence of diabetes and cardiovascular disease in PSC [332], and consistent with observations that adipocyte VAP-1 inhibits lipolysis and promotes glucose uptake [333–335]. Increased circulating levels also correlate with the severity of liver fibrosis in patients with fatty liver disease further implicating a role of VAP-1 in hepatic fibrogenesis. The precise role of sVAP-1 however is not yet known, although a recent study has illustrated that sVAP-1 is endowed with potent chemotactic properties and could therefore mediate distal effects on leucocyte recruitment [214].

1.10 Proposal

Hypothesis (1): CCL25 and CCR9 expression are upregulated in the human colon during times of active inflammation.

Hypothesis (2): VAP-1 expression is increased in PSC, and through an increase in catalytic activity is directly responsible for upregulating expression of intraehepatic adhesion molecules that drive mucosal lymphocyte recruitment to the liver.

Hypothesis (3): Serum VAP-1 levels and activity are increased in patients with PSC and correlate with fibroinflammatory burden of liver disease

Hypothesis (4): An absence of VAP-1 enzyme activity is able to ameliorate or mitigate sclerosing cholangitis development *in vivo.*

Specific aims:

Aim (1): Determine expression of CCL25 and CCR9 in the inflamed human colon.

Aim (2): Compare and contrast intrahepatic VAP-1 expression in PSC versus other chronic autoimmune liver diseases, and evaluate the functional consequences of enzyme activity in terms of endothelial MAdCAM-1 expression and $\alpha 4\beta 7$-dependent leucocyte interactions.

Aim (3): Quantify circulating serum VAP-1 levels and enzyme activity in patients with PSC, correlating values with clinical characteristics.

Aim (4): Evaluate the therapeutic potential of VAP-1 enzyme inhibition in a murine model of sclerosing cholangitis.

2 Materials and Methods

2.1 Human tissue

All blood and tissues were acquired through the Queen Elizabeth Hospital Liver and Gastroenterology Unit (Birmingham, UK) unless otherwise specified. Peripheral blood was obtained prospectively from patients with PSC, PBC and AIH attending the autoimmune liver disease clinic, as well as individuals with IBD alone and healthy volunteers without evidence of liver disease. Human liver tissue was acquired from explanted organs removed at time of surgery; specifically, those affected by chronic end-stage disease. Control (unaffected) specimens were obtained from normal donor livers surplus to transplantation requirements, or the 'distal-to-tumour (DT)' aspect as part of hepatic resections in patients with secondary hepatocellular cancer. Colonic tissue was acquired via mucosal biopsies taken during patient colonoscopy (provided kindly by collaborators at University Hospital, Jena), as well as colonic resection specimens from patients with treatment-refractory colitis or non-IBD associated colonic cancer.

All human tissue and blood samples were collected with local research ethics committee approval and informed patient consent.

2.1.1 Cell culture

2.1.1.1 Generic solutions and plastics

Human serum and foetal bovine serum (FBS) were obtained from Life Technologies. Penicillin, streptomycin and glutamine (PSG) were purchased from Sigma-Alrich.

TrypLE Express (1x) containing stable Trypsin-like enzyme with Phenol Red was acquired from Invitrogen. Unless otherwise specified, phosphate buffered saline (PBS) was prepared from tablets (Oxoid, UK) according to manufacturer's instructions.

Sterile 5, 10 and 20 mL pastettes, 75 cm^2 culture flasks, 48-well and 96-well plates, 15 mL and 50 mL tubes and 1.5 mL cryovials were all purchased from Corning Costar Incorporated, UK. 20 mL plastic tubes and 5 mL bijous were acquired from Ramboldi, Wheaton, UK. Sterile plastic gloves used daily were from Premier Nitric, UK. All tissue culture was carried out in a class II microflow safety cabinet. At all times aseptic technique was followed by swabbing the cabinets with industrial methylated spirit (IMS; Adams Healthcare, UK) before and after use.

2.1.1.2 Culture and passage conditions

Cells were cultured on tissue culture plastic in appropriate media (as indicated; Table 2.1) and maintained at 37^oC in a humidified, 5% CO_2 incubator. Where indicated tissue culture plastic was pre-coated with rat-tail collagen (RTC) to promote cellular adhesion. Briefly, 4 mL RTC (diluted in PBS to a working dilution of 220 µg/mL; Sigma-Aldrich, UK) was aliquoted into a 75 cm^2 flask, and following gentle agitation (~30 seconds), aspirated and discarded. The flasks were left to dry overnight (microflow chamber, ambient temperature) and rinsed (PBS) prior to use.

Cell viability and growth were monitored using an inverted phase contrast microscope (Olympus IX50). Adherent cells become flattened and form spindle-projections when attached to the growth surface. In contrast, cells that remain in suspension retained a

rounded, symmetrical appearance. All cultures were examined daily by observing cell morphology, the colour of medium and density of suspension.

Table 2.1: Cell media

	Base media	**Supplementation**	**Growth factors**
Complete lymphocyte media	RPMI-1640[*]	10% FBS 1% PSG	N/A
Complete HSEC media	Basal endothelial, serum-free media (SFM)[*]	10% Human serum (HS)[#] 1% PSG	VEGF (10 ng/mL) [§] HGF (10 ng/mL) [§]
3T3 culture media	DMEM[*]	10% FBS 1% PSG	
Adipogenic media [$]			
Differentiation	Induction media	10% FBS 1% PSG	SingleQuots PT3102B `
Maintenance	Maintenance media	10% FBS 1% PSG	SingleQuots PT3102A ``

[*] Life Technologies
[#] Heat-inactivated – 56^{o}C for 30 minutes
[§] Vascular endothelial growth factor (VEGF) and hepatocyte growth factor (HGF) obtained from Peprotech, UK
[$] Lonza, UK
` Contains: recombinant human insulin, L-glutamine, MCGS, dexamethasone, indomethacin, 3-isobuty-l-methyl-xanthine (IBMX), GA-1000; 1 vial added to 170 mL media.
`` Contains: recombinant human insulin, L-glutamine, MCGS, GA-1000; 1 vial added to 170 mL media.

Adherent cells were passaged using an appropriate volume of TrypLE (4 mL in a 75 cm^2 culture flask). Specifically, old media was discarded and adherent cells washed with PBS before adding warm (37^{o}C) TrypLE. The flask was then agitated gently by hand to enable cellular detachment. Once detachment was complete, sterile PBS was added to the suspension, and the final mixture collected and centrifuged at 600 x *g* for 5 minutes. The cell pellet was then re–suspended in appropriate media before re-seeding for further culture. Non–adherent cells were passaged without trypsinization by centrifugation of the suspension at 600 x *g* for 5 min. The cell pellet was re–

suspended in appropriate media and cells re–seeded in new culture flasks. Viability was always assessed using Trypan–blue (Life Technologies) exclusion and cells counted using a haematocytometer (MerckMillipore, UK) prior to re–seeding/downstream application.

2.1.1.3 Freezing and storing cells

For long-term maintenance, cells were preserved in liquid nitrogen. After pelleting, cells were resuspended at a density of 10^6/mL in freezing media (95% FBS+5% DMSO (Sigma-Aldrich, UK)). Cells were then transferred to cryovials and placed in a MrFrost freezing container (Wessington Cryogenics, UK) for a minimum of 24 hours at –80^{o}C to permit gradual cooling and prevent crystal formation within the cytoplasm. The next day, cells were transferred to liquid nitrogen for long-term preservation. When required, cells were removed from storage, thawed and washed in media and centrifuged to remove cellular debris. Cells were counted and viability assessed using Trypan blue exclusion followed by resuspension in appropriate media. A minimum of 10 days in culture was given prior to utilising thawed cells for downstream experiments.

2.1.2 Isolation of specific cell populations

2.1.2.1 Peripheral blood lymphocytes

Peripheral venous blood was collected into EDTA coated tubes, and the mononuclear fraction isolated by density gradient centrifugation over Lympholyte-H, (VH Bio, UK) according to manufacturer's instructions. Cells were counted and resuspended in the appropriate media at the appropriate density (application-dependent).

2.1.2.2 Colon-infiltrating lymphocytes

Mechanical digestion of retrieved tissue samples was performed using C-tubes (Miltenyi Biotec, UK) and a GentleMACs dissociator (Miltenyi) in preference to enzymatic digestion to reduce loss of cell-surface epitopes. Digested tissue was then passed through a 70 µm cell strainer (BD Biosciences, UK) and the filtrate layered atop a discontinuous gradient comprising 70% and 30% Percoll (GE Healthcare, UK) in a 1:1:1 ratio. Following brake-free centrifugation (600 x *g*, 25 minutes) the mononuclear cell band was aspirated, resuspended in PBS, washed x 2 and cell pellet resuspended appropriately for downstream application.

2.1.2.3 Hepatic sinusoidal endothelial cells

Human HSEC were isolated from liver tissue as previously described [312]. Approximately 30 g of whole liver tissue was finely diced and enzymatically digested using 5 mL 0.2% collagenase type 1A (Sigma) for 20 – 40 minutes, and then filtered in an excess of sterile PBS. The cell suspension was further washed by centrifugation in PBS (x4) and purified over density centrifugation (33/77% Percoll) at 550 x *g* for 30 minutes. Cells were removed at the interface of the gradient media, washed in PBS then subjected to a negative selection step; specifically incubation with mouse anti-EpCAM (clone HEA125, Progen Biotechnic, Germany; 50µg/mL) for 30 minutes at 37^{o}C). Thereafter, cells were incubated with secondary antibody conjugated to magnetic beads (goat anti-mouse Dynabeads, Life Technologies; 10 µl/prep.) for 30 minutes at 4^{o}C, and bead-labelled cells (indicative of BEC) removed by magnetic selection. The remaining cells were incubated with anti-CD31 antibody directly conjugated to Dynabeads (10 µg/mL; 30 min at 4^{o}C). CD31^{+} cells were then extracted from the cell mixture by positive magnetic selection, resuspended in complete HSEC

media (Table 2.1) and cultured at 37°C in RTC coated flasks until confluent (~1.5 x 10^6 cells/flask), prior to further passage.

2.1.3 Culture of human cell lines

JY cells, an Epstein-Barr virus-immortalised B-cell lymphoblastoid line, engineered to constitutively express α4β7-integrin [336] were available in house (originally provided by Dr. N. Pullen, Pfizer, USA). Cells were cultured in complete lymphocyte media (Table 2.1) and maintained in a humidified atmosphere (5% CO_2, 37°C).

2.1.4 Serum extraction

Peripheral blood was collected into uncoated clinical grade collection tubes and left to stand for a minimum of 30 minutes (max. 180 minutes) to allow clotting. Thereafter, blood tubes underwent centrifugation (1500 x *g*; 10 minutes) prior to retrieval of serum supernatant. Each sample was divided into 50 – 100 µl aliquots prior to storage at –80°C in order to minimise subsequent freeze-thaw cycles.

2.2 Cell phenotyping with flow cytometry

Phenotypic analysis of leucocyte subsets was performed using multi-colour flow cytometry. Following extraction from tissue or isolation from peripheral blood, lymphocyte cell pellets were resuspended in flow cytometry MACS buffer (PBS + 2% FBS + 2 mM EDTA) at a density of 10^6/mL. 100 µl of cell suspension was then incubated with appropriate fluorochrome-labelled antibodies or isotype-matched controls for 30 minutes at 4°C protected from light (Table 2.2). All cell labelling was performed in 5 mL polypropylene round-bottomed Falcon tubes (BD Biosciences).

Consequently, cell-antibody cocktails were washed with PBS and resuspended in 500 μL MACS buffer prior to analysis (CyAn ADP 3-laser, 9-colour flow cytometer; Beckman Coulter Inc, USA). Unlabelled cells were used to define appropriate forward- and side-scatter voltages/gain and single-colour antibody labelling conducted prior to multiple in order to perform colour compensation. Data analysis was performed using Summit software v.4.3 (Dako, USA).

When analysing colon- or liver-infiltrating leucocyte populations, the entire cell-suspension was first labelled with a viability marker (Near-IR, live/dead-fixable dye, Life Technologies), by co-incubating a 1/1000 dilution of the dye with the cells at ambient temperature and protected from light for 15 minutes, followed by washing the cells in PBS and subsequently resuspending in MACS buffer prior to labelling with antibodies of interest.

Table 2.2: Antibodies used for flow cytometry (human tissue)

Conjugated antibodies (supplier)	**Isotype (clone)**	**Stock Conc.**	**Working vol. (µl / 10^5 cells)**
Mouse anti-CD3 PE-Cy7 (BioLegend)	IgG1 (SK7)	0.2 mg/mL	5
Mouse anti-CD4 V500 (BD Horizon)	IgG1 (RPA-T4)	0.2 mg/mL	5
Mouse anti-CD4 FITC (BD Horizon)	IgG1 (RPA-T4)	0.2 mg/mL	10
Mouse anti-CD8 PE-CF594 (BD Horizon)	IgG1 (RPA-T8)	0.2 mg/mL	5
Mouse anti-CD127 PerCPCy 5.5 (BD Pharmingen)	IgG1 (HIL-7R-M21)	0.2 mg/mL	5
Mouse anti-CD127 FITC (BD Pharmingen)	IgG1 (HIL-7R-M21)	0.2 mg/mL	10
Mouse anti-CD127 APC (eBioscience)	IgG1 (eBioRDR5)	0.2 mg/mL	5
Mouse anti-CD25 Pac. Blue (BD Pharmingen)	IgG1 (M-A251)	0.2 mg/mL	5
Mouse anti-α4 integrin APC (BD Biosciences)	IgG1 (9F10)	0.2 mg/mL	2
Rat anti-β7 integrin PE (BD Pharmingen)	IgG2a (FIB504)	0.2 mg/mL	10
Mouse anti-CCR9 AF 488 (BD Pharmingen)	IgG2a (112509)	0.2 mg/mL	5
Mouse anti-CCR9 AF 647 (BD Pharmingen)	IgG2a (112509)	0.2 mg/mL	5
Isotype-matched control (IMC)			
Mouse PE-Cy7 (BD Pharmingen)	IgG1 (MOPC-21)	0.2 mg/mL	5
Mouse V500 (BD Horizon)	IgG1 (X40)	0.2 mg/mL	5
Mouse FITC (BD Horizon)	IgG1 (X40)	0.2 mg/mL	10
Mouse PE-CF594 (BD Horizon)	IgG1 (X40)	0.2 mg/mL	5
Mouse PerCPCy 5.5 (BD Pharmingen)	IgG1 (MOPC-21)	0.2 mg/mL	5
Mouse Pac. Blue (BD Pharmingen)	IgG1 (MOPC-21)	0.2 mg/mL	5
Mouse APC (BD Pharmingen)	IgG1 (MOPC-21)	0.2 mg/mL	5
Rat PE (BD Pharmingen)	IgG2a (R35-95)	0.2 mg/mL	10
Mouse AF 488 (BD Pharmingen)	IgG2a (G155-178)	0.2 mg/mL	5
Mouse AF 647 (BD Pharmingen)	IgG2a (G155-178)	0.2 mg/mL	5

2.3 Polymerase chain reaction (PCR)

2.3.1 RNA extraction and cDNA synthesis.

Extraction of total RNA was performed from snap-frozen tissue samples (~30 mg) following mechanical digestion (GentleMACs M-tubes; program RNA 01_01) and purification using the QIAGEN RNeasy mini-kit (QIAGEN, Germany) as per the manufacturer's instructions. All samples were treated with DNAse I (RNase-free DNase set, QIAGEN) during the extraction process. RNA concentration (ng/μL) and purity were then measured using a Nanophotometer (Geneflow, UK). Absorbance ratios of 260/280 at 1.8 – 2.0 were taken as acceptable 'purity.' RNA was stored in aliquots of 1 – 3 μg to minimise repeated freeze/thaw cycles. cDNA was synthesised using the iScript synthesis kit (Bio-Rad, USA) according to manufacturer's instructions. No-template (RNA-free) and no reverse-transcriptase (no-RT) samples were prepared in parallel as negative controls for downstream application.

2.3.2 Conventional PCR and agarose gel electrophoresis

The presence of *CCL25* mRNA in human colon and small bowel was first investigated by conventional PCR (Table 2.3). Intron spanning primers were selected and amplicons of ~230 bp visualised on a 1.5% (w/v) agarose gel (diluted in Bionic buffer, Sigma) stained with SYBR DNA gel stain (Life Technologies). Hyperladder IV (Invitrogen) was used as an amplicon length marker.

Table 2.3: Conventional PCR reaction primer sequences/constituents

Primers	**Human CCL25**		
Forward	5' – GCCTGCTGCGATATTCTACC – 3'		
Reverse	5' – TACTGCTGCTGATGGGATTG – 3'		
Exact amplicon length: 227 bp			
Reagent	**Vol. per-reaction (µL)**	**Stock conc.**	**Source**
Master Mix kit	10	5 U/µL	QIAGEN
Coral dye PCR buffer	2	5 U/µL	QIAGEN
Forward primer	1	0.25 pmol/µL	Alta Bioscience, UK
Reverse primer	1	0.25 pmol/µL	Alta Bioscience, UK
cDNA	2	N/A*	N/A
Nuclease-free water	4	N/A*	QIAGEN
Cycle (35 cycles run)	**Temperature (^{o}C)**	**Time (min)**	
	95	02:00	
Denaturation	95	01:00	
Annealing	60	01:00	
Extension	72	01:00	
	72	05:00	

***** RNA concentration of 50µg/mL prior to cDNA synthesis step (1 µg /20 µL)
N/A Not applicable

2.3.3 Quantitative real-time PCR (qRT-PCR)

For analysis of relative expression of human and murine mRNA of interest, VIC- and FAM-labelled Taqman probes were used according to manufacturers instructions and qRT-PCR performed with cDNA using specific primers and cycling conditions (Table 2.4). LightCycler 480 96-Multiwell plates (Roche Life Science, UK) were used with the LightCycler® 480 II (Roche).

2.3.3.1 Relative quantification of mRNA expression in human colonic tissue

Relative quantification real-time PCR was performed on each sample in duplicate or triplicate (as indicated). The level of colonic mRNA expression was compared against an internal control to which the threshold cycle (CT) values of target genes were normalised using the LightCycler device software (E-analysis method; software version 1.5.0.39).

2.3.3.2 Absolute quantification in human liver

Human liver VAP-1 (*AOC3*) mRNA expression was also assessed by qRT-PCR. Given the absence of a single, known housekeeping gene that exhibits stability across all aetiologies and between varying stages of human liver injury [337,338], levels of expression were determined by absolute quantification of samples run in triplicate. In this regard, the number of copies of VAP-1 mRNA in matched amounts of starting total RNA from each tissue sample was determined from a calibration curve of known dilutions of a linearised plasmid encoding the VAP-1 gene ranging from 10 copies/μL – 10^5 copies/μL as described by Weston *et al*. [214].

Table 2.4: Primers/probes, assay mixes and consumables – qRT-PCR (human)*

Target	**Primer/Probe assay ID**	**Source**
CCL25	Hs00608373_m1	Life Technologies
CCR9	Hs01890924_s1	
TNFα	Hs01113624_g1	
AOC3	Hs00186647_m1	
GUS-β	Hs00939627_m1	
Reaction mixture and consumables		
Reagent	**Volume (µl)**	**Source**
TaqMan Master mix	10	Life Technologies
Probe/primer	1	Life Technologies
cDNA (from 50 µg/mL RNA)	2	N/A
Nuclease-free water	7	QIAGEN
LightCycler® 480 Multiwell Plate 96	N/A	Roche

*Cycling conditions: 95°C for 10 seconds, 59°C for 30 seconds and 72°C for 1 second.

2.4 Western blotting

2.4.1 Preparation of protein lysates

The presence of CCL25 protein in intestinal samples was analysed by western blotting, using small bowel and recombinant human CCL25 (R&D systems, UK) as positive controls. Human small bowel and colonic tissue blocks (70 – 100 mg) were placed in M-tubes (Miltenyi) and homogenised in ice-cold lysis buffer (10 mL CellLytic MT Buffer (Sigma) with 2 tablets PhospSTOP, 2 tablets cOmplete Mini protease inhibitor, 10 µL of 5 U/mL DNase (Roche); 20 µl buffer per-mg tissue) using the GentleMACs (program Protein 01_01). Thereafter, samples were centrifuged at 3000 x *g* for 3 minutes to maximise recovery from the C-tubes, mixed to form a uniform homogenate and subsequently transferred to a new micro-

centrifuge tube. The lysates were then agitated for 1 hour at 4^{o}C before a further centrifugation step (21200g, 10 minutes). Supernatants were aliquoted and stored at -80^{o}C till needed.

Protein concentrations were determined using the bicinchoninic acid (BCA) assay (Pierce, Thermo Scientific, UK) according to manufacturer's instructions and utilising bovine serum albumin (BSA, Sigma) diluted in lysis buffer as a protein concentration standard.

2.4.2 Sodium dodecyl sulphate polyacrylamide gel electrophoresis (SDS-PAGE)

Protein samples were separated by electrophoresis through acrylamide gels using the Bio-Rad Mini Trans Blot Cell System. Initially, glass plates were assembled (1.5 cm thickness), resolving and stacking gels prepared (Table 2.5), sequentially poured into the glass space and left to set. Solubilised protein samples prepared in cell lysis buffer at standardised concentrations (2 mg/mL; 20 µl) were diluted in 5x loading buffer (Table 2.5; 5 µL) and boiled (100^{o}C, 10 minutes). The mixture was set aside to cool and centrifuged before gel loading. Simultaneously, the gel apparatus was assembled and 1x electrophoresis buffer poured onto the tank ensuring full cover of the electrodes. 20 µL of each protein sample was slowly loaded into wells preformed in the stacking gel, in addition to pre–stained molecular weight markers (Page ruler, Pierce, 10 µL). Electrophoresis was performed at 200 V for 30 minutes, or until the dye front reached the bottom of the gel.

2.4.3 Western blot transfer

Resolved proteins were transferred onto Hybond–ECL nitrocellulose membrane (Amersham Biosciences, UK) and directly immersed into transfer buffer in order to prime the membrane for protein binding. Pre-soaked membranes were placed on top of the gel, sandwiched between filter papers and sponges; which were also pre–immersed in transfer buffer and the assembly placed into transfer buffer apparatus, positioned within the transfer tank containing an ice pack. Transfer buffer was added into the tank and a current of 100 V applied for 1 hour. Efficient transfer was evident from the appearance of rainbow markers on the membrane and impression of protein staining with Ponceau S solution [0.1% Ponceau S (w/v) in 5% acetic acid (v/v)] for 5 minutes followed by rinsing (water) to visualise successfully transferred protein.

Table 2.5: Reagents used for western blotting

Reagents (supplier)						
Trizma base (Sigma)		Degassed acrylamide (30% acrylamide/methylene bisacrylamide – 37.5:1) (Bio-Rad Laboratories, UK)				
NaCl (Sigma)		Ammonium persulfate, APS – 10% w/v (Sigma)				
Glycine (Sigma)		N,N,N$^{'}$,N$^{'}$ – tetra-methyl-ethylene-diamine, TEMED (Sigma)				
Sodium dodecyl sulfate (Sigma)		β-mercaptoethanol, β-ME (Sigma)				
Methanol (Fisher Scientific, UK)		Bromophenol blue (Sigma)				
Tween20 (Sigma)		Glycerol (Sigma)				
Buffers						
Resolving (R)	1.5 M Trizma base (*pH* 8.8; adjusted with HCl)					
Stacking (S)	0.5 M Trizma base (*pH* 6.8; adjusted with HCl)					
Loading	200 mM Trizma Base *pH* 6.8 + 20% glycerol, 10% SDS 0.05% bromophenol blue, 10 mM β-ME					
Electrophoresis (10x)	30.3 g Trizma base + 144g glycine + 10g SDS (to 1 L with dH_2O)					
Transfer	6 g Trizma base + 28.8 g glycine + 400 mL methanol + 1g SDS (to 2 L with dH_2O)					
Blocking	PBS + 0.02% Tween20 + 5% non-fat milk					
Gels[*]						
	Buffer	*Degassed acrylamide*	*10% SDS*	*10% APS*[#]	*TEMED*[#]	*dH_2O*
Resolving (12%)	2.5 mL	3.3 mL	0.1 mL	0.06 mL	0.06 mL	3.3 mL
Stacking (5%)	1.25 mL	1.7 mL	0.1 mL	0.06 mL	0.06 mL	6.8 mL

[*] Quantity equivalent to x1 gel at 1.5cm thickness.

[#] APS and TEMED were added just prior to pouring of gels into the glass spaces, as the oxygen free radicals released from the reaction between APS and the tertiary amine TEMED are responsible for the polymerisation of bis-acrylamide.

2.4.4 Membrane development

Following protein transfer, membranes were blocked for at least 2 hours at RT in PBS containing 0.1% Tween20 (PBS-T) supplemented with 10% (w/v) non–fat dry milk (Marvel, UK) with continuous agitation. The blocking buffer was subsequently removed and membranes probed overnight at 4^{o}C with primary detection antibody raised against human CCL25 (mouse anti-human monoclonal IgG1 – clone 52529, used at 0.2μg/mL; R&D systems) diluted in fresh blocking buffer. After several washes in PBS–T, membranes were incubated with peroxidase–conjugated secondary antibody (goat anti-mouse horseradish peroxidase (HRP), used at 1/4000; Dako) diluted in blocking buffer for 1 hour at ambient temperature. After several washes with PBS–T, the blots were incubated with enhanced chemiluminescence reagent (ECL-plus; Amersham Pharmacia Biotech, UK). Enhanced chemiluminescence detection film (Amersham Biosciences) was exposed to the membrane and developed using a Kodak X–Omat 1000 processor. Semi-quantitative assessment of protein expression (relative to housekeeping targets) was performed using ImageJ software (v.1.6 NIH, USA) wherein band density was calculated using built in gel image analysis functions. Given the adoption of immunoprecipitation steps (see below), membranes were not stripped.

2.4.4.1 Immunoprecipitation

As chemokines in biological samples are often found at very low levels and subject to multimerisation [339], a prior immunoprecipitation step (IP) was incorporated to enrich and purify protein lysates where needed. Briefly, 20 μL (0.6 mg) of protein G Dynabeads® (Life Technologies) were aliquoted in a microcentrifuge tube, transferred

to a separation magnet and the supernatant discarded. Capture antibody (1 μg goat polyclonal IgG anti-human CCL25; R&D systems) was diluted in 200 μL PBS-T and then incubated with the beads (continuous rotation; 10 minutes ambient temperature); following which 100 μL sample lysate at a known concentration (2 mg/mL) was added, and the lysate-antibody-bead complex was mixed with gentle pipetting. The complex was then incubated with continuous rotation for 1 hour (ambient temperature). Thereafter, the mixture was transferred to a magnet and the non-bound cleared lysate aspirated and kept for later analysis of housekeeping protein (anti β-actin, 1 μg/mL; Sigma) and as a negative internal control of primary target. The remaining sample was washed gently with PBS x 3, then beads, antibody and target proteins were dissociated by heating at 70^{o}C for 20 minutes, and subsequently resuspended in sample buffer prior to analysis by western blotting as indicated in section 2.4.2.

2.4.5 Quantification of CCL25 protein

Intestinal CCL25 expression was quantified using a human CCL25 enzyme-linked immunosorbent assay (ELISA) approved for use in tissue lysates (Cusabio, 2BScientific, UK). Tissue-protein lysates were obtained as described in section 2.4.1. Samples and internal standards were loaded in triplicate, and the assay run according to manufacturer's instructions. The threshold for detection was 25 – 1600 pg/mL.

2.5 Soluble VAP-1 measurements

2.5.1 Patient characteristics and data collection

All individuals with an established diagnosis of autoimmune liver disease or IBD under clinical follow-up from 2011 to 2014 were considered eligible for sampling. A standardised electronic record form was created and clinical data collected prospectively. Individual clinical and laboratory characteristics pertained to patient age, gender, severity of liver disease (pre-cirrhotic, cirrhotic compensated, cirrhotic decompensated), history of ascending cholangitis, IBD status (presence or absence thereof, distribution of inflammation, disease activity and severity), autoantibody status (anti-nuclear antibodies, ANA; anti-smooth muscle antibodies, ASMA; perinuclear anti-neutrophil cytoplasmic antibodies, pANCA), concomitant mediations at time of sampling (immunosuppression, immunomodulators, UDCA, antibiotics) and laboratory indices (serum alanine transaminase (ALT), aspartate transaminase (AST), alkaline phosphatase (ALP), bilirubin, albumin and platelets).

Individual patient follow-up constituted a clinic review every 12 months in the absence of cirrhosis, and at 6-monthly intervals for patients with evidence of advanced disease. Study follow-up was until patient transplantation or death.

2.5.2 Determining soluble VAP-1 levels

Circulating VAP-1 levels in human serum were measured using a time-resolved immunofluorometric assay developed by BioTie Therapies Corp., Finland. The assay procedure (carried out by BioTie Therapies) is provided in Table 2.6 and Table 2.7. In sum, a biotin-conjugated mouse IgG2a monoclonal anti-VAP-1 capture antibody

(TK8-14, BioTie Therapies) was immobilised onto a streptavidin-coated microwell plate in which serum samples at known dilution were added. Bound sVAP-1 was then detected with a europium-coupled mouse IgG2a anti-VAP-1 tracer capture antibody (TK8-18, BioTie Therapies). Levels were then measured by time-resolved fluorescence at 615nm (Victor^3 multi-label counter, PerkinElmer) by comparing to a reference sample (positive control) of highly purified human sVAP-1 (Biovian, Finland). The assay calibration ranged from 1.5 – 1500ng/mL and linearity (R^2) of calibration curves 0.997 – 1.000. Two replicates of calibration standard, controls and test samples were run per-plate. A minimum of one quality control (QC) sample was run on each plate and at least two series of controls per sample batch.

Fluorescence signal counts of calibration standards were plotted against nominal concentrations using data analysis software (Table 2.6). A nonlinear, weighted (1/x) 4-parameter logistic model (**Equation 2-1**) was used to fit the calibration curve. The concentration of sVAP-1 in test samples was calculated from the fluorescence signal counts using the appropriate calibration curve.

Equation 2-1: The four parametric fit (sigmoidal function) regression model:

y = a + (d - a) / (1 + (x / c) ^b) , weighting 1/x,

[c is the centre point (ED50), d is the upper limit, a is the lower limit, b is the relative slope around c].

Table 2.6: sVAP-1 ELISA reagents and preparation

Reagents	
Wash solution	DELFIA wash concentrate (PerkinElmer, USA)
Sample buffer	DELFIA assay buffer (PerkinElmer)
Enhancement solution	DELFIA enhancement solution (PerkinElmer)
Capture antibody	Biotinylated anti-VAP-1 antibody, TK8-14 (BioTie)*
Tracer antibody	Europium coupled anti-VAP-1 antibody, TK8-18 (BioTie)*
Positive control	Purified soluble human sVAP-1 (Biovian)
Instruments and materials	
Victor^3-1420-012- microplate reader + WorkOut 2.5 software (PerkinElmer)	
1296-026 DELFIA Plate washer (PerkinElmer)	
1296-003 DELFIA Plate shaker (PerkinElmer)	
1296-041 DELFIA Plate Dispenser (PerkinElmer)	
4009-0010 DELFIA Streptavidin 96-well plates (PerkinElmer)	
Preparation	
Wash solution	DELFIA wash concentrate diluted 1:25 in ddH_2O.
Sample dilution	Study samples diluted 1:10
Calibration standards	sVAP-1 reference material + sample buffer
QC samples	4.5 ng/mL (low), 50 ng/mL (medium) and 1200 ng/mL (high)
Capture antibody	Diluted in sample buffer (3 μg/mL) and sterile filtered
Tracer antibody	Diluted in sample buffer (2 μg/mL) and sterile filtered

* Mouse anti-human IgG2a

Table 2.7: sVAP-1 ELISA protocol

10 μL calibration standards, QC samples and test serum (diluted) added per well
50 μL biotin-europium antibody solution added immediately to each well.
Plate sealed with tape and incubated on plate shaker (2 hours, ambient temperature)
Plate washed x 4 with wash solution
200 μL DELFIA enhancement solution added to each well and incubated on plate shaker (min. 5 minutes – max. 60 minutes, ambient temperature)
Time-resolved fluorescence measured at 615 nm

2.5.3 Quantifying SSAO activity

VAP-1 mediated deamination results in the production of H_2O_2, the rate of production of which was used as a surrogate for assessing SSAO activity.

2.5.3.1 Sample preparation – method 1

Serum samples (10 μL) were aliquoted in quadruplicate into a 96-well flat-bottomed plate, to which benzylamine 1 mM (per-well) was added as an artificial substrate of VAP-1 enzyme activity. In order to inhibit contributions to the reaction by other circulating amine oxidases, inhibitors of MAO-A (100 μM Clorgyline; Sigma) and MAO-B (100 μM Pargyline; Sigma) were included in the admixture, and the total volume was brought up to 100 μl with sterile PBS.

2.5.3.2 Sample preparation – method 2

Unlabelled capture antibody (TK8-18) was diluted to a final concentration of 5 μg/mL in carbonate coating buffer (Table 2.8) and 100 μL was added to each well of a high-affinity protein-binding ELISA microwell plate (Nunc-Immuno Maxisorp, Sigma) and sealed and incubated overnight (4^{o}C). The next day, plates were brought up to room temperature and unbound antibody removed before washing the plate (x3) with wash buffer. 200 μL blocking solution was then added to each well and the microwell plate was incubated at ambient temperature. After 8 hours, excess blocking solution was removed and the plate was washed (x3) before adding 100 μL serum (test samples) per-well in quadruplicate (Figure 2.1) and incubating overnight (4^{o}C). Non-

antibody-bound sample was then removed and the plate washed (x3). Thereafter, 100 μL amine solution was added (1 mM benzylamine per-well, prepared in PBS).

2.5.3.3 Detection system

To be certain that all H_2O_2 detected was dependent on SSAO activity, substrate + VAP-1 inhibitor (250 μM semicarbazide; Sigma) treated samples were run in parallel with every run (Figure 2.1). Finally, standard concentrations of H_2O_2 (0.2 – 3.0 μM) were prepared and loaded into the plate. Amplex UltraRed Reagent was exploited as a stoichiometric fluorogenic substrate for HRP in order to quantify rate of H_2O_2 production. Dulbecco's PBS (100 μL) containing 20 mM Amplex UltraRed Reagent and 2 U HRP was added to each sample or standard as appropriate. Kinetic readings per-sample were obtained via rate of change of fluorescence as measured by a Synergy HT Multi-Mode Microplate reader (BioTek) according to protocol (Table 2.8) and enzyme activity calculated from the slope of the standard curve.

Table 2.8: SSAO assay constituents

Reagents	**Supplier**
Dulbecco's PBS*	Sigma
Benzylamine	
Semicarbazide	
Clorgyline	
Pargyline	
Horseradish peroxidase	
Amplex-UltraRed	Life Technologies
Buffers	
Coating buffer	8.4 g $NaHCO_3$ + 3.56 g Na_2CO_3 + ddH_2O (to 1 L, *p*H 9.5)
Wash buffer	PBS + 0.05% Tween20
Blocking solution	PBS + 1% BSA
Sample and standard diluent	Dulbecco's PBS + 0.2% Triton X-100
Kinetic reading protocol	
Excitation: 530nm (slit 25)	
Emission: 590nm (slit 35)	
Sensitivity: 20	
Shaking intensity 3; duration 2, before reading	
Kinetic reading: 10 readings/well; followed over 1 hour	

* Dulbecco's PBS (Sigma) used as opposed to tablet-prepared PBS (e.g. Oxoid) given the latter's tendency to affect the detection system

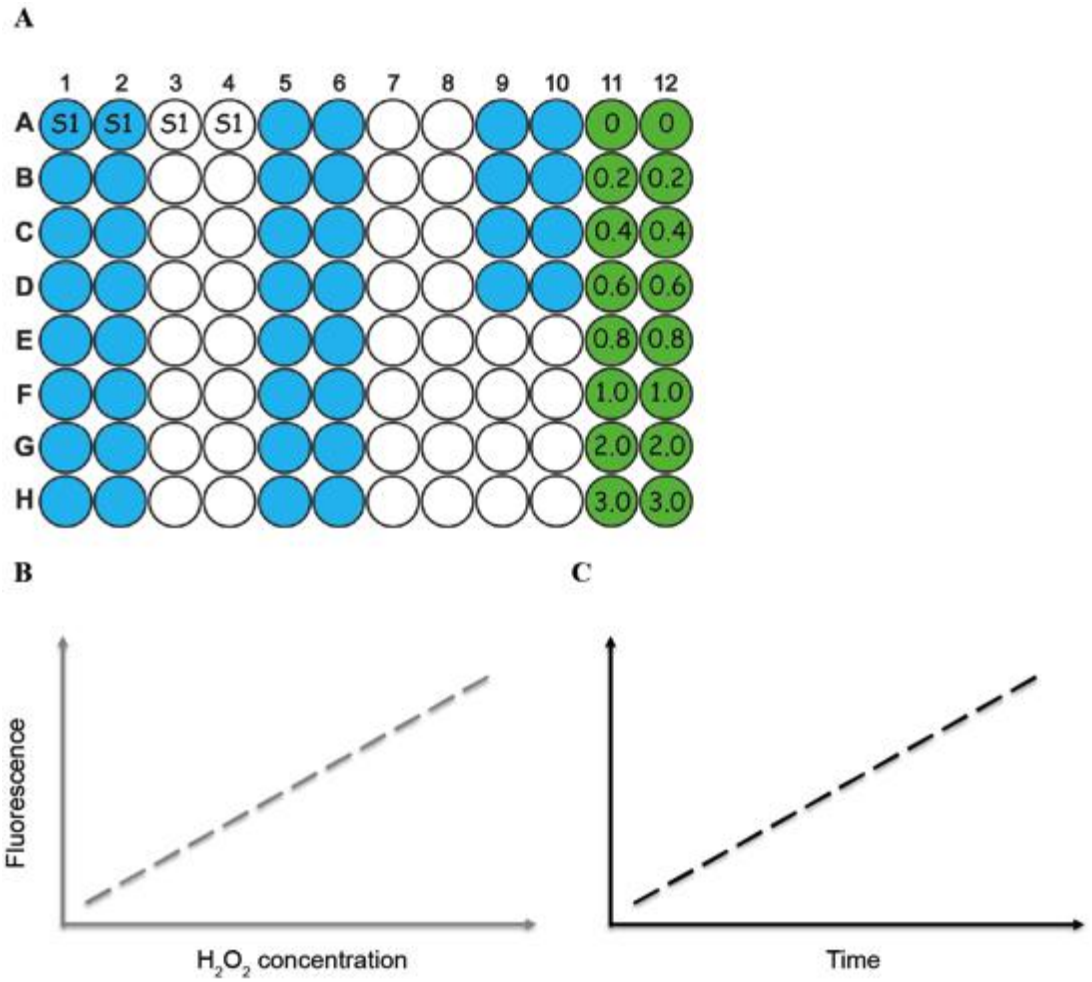

Figure 2.1: Layout and calculations in the SSAO enzyme assay
Patient samples (e.g. S1) were loaded in quadruplicate (A) with two wells containing substrate only (blue) and the remainder containing semicarbazide (white). The calibration standards (green) contained increasing μM concentrations of H_2O_2 and a standard curve generated plotting fluorescence versus known H_2O_2 concentration at a single point in time (B). For every sample pair, the mean change in fluorescence over time (C) was converted to a rate of H_2O_2 produced; the value from semicarbazide-treated samples subtracted from that of substrate only to give a true reading of SSAO activity.

2.6 Immunohistochemical staining

Single colour chromogenic staining and dual colour immunofluorescence were used to visualise protein in tissue. At time of explant tissue processing, fresh liver or colon samples were cut into 1 cm^3 cubes and either 'snap frozen' in liquid nitrogen (stored at –80^oC until time of application) or immersed in formal saline (4%; maximum 48 hours) as preparation for paraffin embedding.

2.6.1 Frozen tissue

Snap frozen tissue was embedded in TissueTek mount (Sakura, Netherlands) and 5 μm-thick sections cut using a Bright OTF cryostat (A-M systems, USA). Sections were then mounted on glass microscope slides (BDH, UK) coated in 0.01% Poly-L-Lysine. Once mounted, sections were fixed in acetone (Thermo Fisher Scientific, UK), wrapped in foil and stored at - 20^{o}C until use. Prior to staining, all slides were warmed to room temperature and bathed in acetone for 5 minutes.

2.6.2 Paraffin embedded tissue

5 μm sections were cut from formalin-fixed paraffin embedded (FFPE) tissue blocks. Sections were deparaffinised and rehydrated by passing through fresh xylene (Leica, GmBH, Germany) and graded alcohols before undergoing heat-inactivated (slides immersed in pre-heated EDTA buffer – 0.37 g EDTA in 1 L distilled water (pH 6.0 – 10.0) + 0.05% Tween20 and microwaving for 15 minutes) or proteinase K (Dako, UK) epitope retrieval.

2.6.3 Chromogenic staining

A wax pen (Dako) was used to draw around sections prior to staining. Targeted monoclonal antibodies and isotype-matched controls (IMC) used for immunohistochemical staining are summarised in Table 2.9. All incubation steps were conducted inside a humidified slide tray and at ambient temperature unless otherwise specified. First, sections were rehydrated in staining buffer (PBS + 0.1% Tween20) for 5 minutes. Endogenous peroxidase activity was then quenched (0.3% H_2O_2 in methanol, 5 minutes), followed by a subsequent buffer wash step (5 minutes). Sections were ‘blocked’ with 2.5% horse serum (ImmPRESS kit, Vector labs, UK)

for 20 minutes, following which primary antibody was added at the appropriate concentration (diluted in staining buffer + horse serum) and left to incubate overnight (4^{o}C) or 30 – 60 minutes (room temperature) depending on antibody.

Next, slides were washed with staining buffer (x2) and incubated for 1 hour (room temperature) with the appropriate secondary antibody (ImmPRESS secondary, Vector labs, 2 – 4 drops of ready mixture per-section). Slides were then washed in staining buffer (5 minutes x 2) before addition of chromogenic detection agent as per manufacturers' instructions. The detection system was left *in situ* until desired staining intensity developed (<30 minutes), washed and slides fixed in mountant (DPX, Vector labs – unless otherwise specified) before being left to dry. Images were analysed on a Zeiss Axioscope microscope in conjunction with Axiovision software (Carl Zeiss, UK). Occasionally, sections were counterstained with Mayer's haematoxylin (~1 minute) and rinsed in tap water to allow blueing of cell nuclei prior to fixing in mountant.

Assessment of staining was performed qualitatively via light microscopy and quantitatively using ImageJ software.

2.6.4 Confocal immunofluorescence

Sections were incubated with PBS + 0.3% Triton X-100 (Sigma) for 5 minutes at ambient temperature and thereafter in 10% goat serum (diluted in PBS + 0.1% Triton) for 10 minutes. Subsequently, primary antibody (Table 2.9) or IMC diluted in staining buffer (PBS/Triton) were incubated with tissue sections at the appropriate concentration (overnight, 4^{o}C). Sections were washed (staining buffer x 2) followed

by addition of fluorescently tagged secondary antibodies (Table 2.10) (pre-centrifuged at 14,000 x *g* to remove particulate matter, freshly diluted in staining buffer), incubated for 1 hour at room temperature. After another 3 wash steps, sections were mounted with ProLong Gold Anti-fade containing the nuclear stain 4', 6-diamidino-2-phenylindole (DAPI, Life Technologies) and kept at 4^{o}C protected from light until ready for visualisation. All sections were imaged by confocal microscopy on an LSM 510 microscope equipped with 63 x 1.32 objective. Images were acquired and analysed by LSM software. This was also used to create profiles of fluorescent intensity and enable graphical demonstration of overlapping fluorescent signals to confirm co-localisation.

Table 2.9: Primary antibodies for immunohistochemistry (human tissue)

Antibody (supplier)	Isotype (clone)	Stock conc.	Working dilution
Mouse anti-VAP-1 (BioTie)	IgG2a (TK8-14)	1 mg/mL	1/500
Mouse anti-VAP-1 (Hycult Biotech)	IgG1 (174-5)	0.1 mg/mL	1/200
Mouse anti-EpCAM (Progen)	IgG1 (HEA125)	0.05 mg/mL	1/10
Mouse anti-CD31 (eBioscience)	IgG1 (WM59)	0.5 mg/mL	1/400
Mouse anti-MAdCAM-1 (Serotec)	1gG1 (314G8)	1 mg/mL	1/500
Mouse anti-αSMA (Sigma)	IgG2a (1A4)	2 mg/mL	1/400
Mouse anti-CCL25 (Peprotech)	IgG1 (1.2_4G1-1G4-1C9)	1 mg/mL	1/50 – 1/200
Mouse anti-CCL25 (R&D systems)	IgG1 (52529)	0.5 mg/mL	1/50 – 1/200
Goat anti-CCL25 (R&D systems)	Polyclonal (Cat. # AF334)	0.2 mg/mL	1/25 – 1/100
IMC			
Mouse (Dako)	IgG1 (DAK-GO1)	0.1 mg/mL	*Assay dependent*
Mouse (Dako)	IgG2a (DAK-GO5)	0.1 mg/mL	*Assay dependent*
Goat (R&D systems)	Polyclonal (Cat. # AB-108-C)	1 mg/mL	*Assay dependent*

Table 2.10: Secondary antibodies for immunofluorescence (human liver)

Antibody (supplier)	Target isotype	Stock conc.	Working dilution
Goat anti-mouse AF488 (Dako)	IgG1	100 μg/mL	1/500
Goat anti-mouse AF546 (Dako)	IgG2a	100 μg/mL	1/500

2.7 Tissue-specific SSAO activity

Liver and colon tissue protein lysates (60 – 100 mg) were prepared essentially as indicated in section 2.4.1, with the exception of Dulbecco's PBS containing 0.2% Triton X-100 being used as the lysis buffer in order to preserve amine oxidase activity in tissue [320]. Protein lysate concentration was determined as described previously and samples were subsequently aliquoted and stored at –80^{o}C until required. Prior to commencing the assay, samples were thawed and concentration standardised to 2 mg/mL. 100 µl of protein lysate was used per well and quantification of SSAO activity conducted as previously described (please see section 2.5.3).

2.8 Evaluating substrate-dependent variations in enzyme kinetics

Putative substrates of human VAP-1 were selected based on inclusion in the human metabolome database version 2.5 (http://www.hmdb.ca) and with reference to [Shen et al. 2012]; specifically cysteamine, methylamine, dopamine, ethylamine and phenethylamine (Sigma). Comparisons were drawn with kinetic rates observed using benzylamine as an internal standard. A 96-well flat-bottomed plate was loaded with 50 ng recombinant (r)VAP-1 in 100 µL Dulbecco's PBS. Increasing concentrations of test substrate were supplemented to test wells (three technical repeats) and H_2O_2 standards were added in parallel as described previously (Figure 2.1). Enzyme activity was quantified using the Amplex-Red Ultra detection system and kinetic parameters estimated by Michaelis-Menten kinetics (please see Figure 2.2; Equation 2-2).

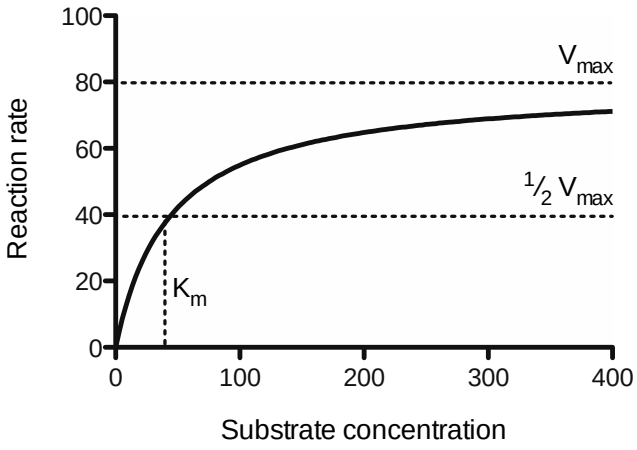

Equation 2-2:

$v' = V_{max}[S]/K_m + [S]$.

Wherein: $V_{max} = k_{cat}[E]_o$

Figure 2.2: Michaelis-Menten kinetic modelling

Substrate kinetic profiles were calculated as indicated by Equation 2-2; wherein The reaction rate increases with increasing substrate concentration, asymptotically approaching its maximum rate V_{max}, attained when all enzyme is bound to substrate.

[V_{max} represents the maximum rate achieved by the enzyme system at saturating substrate concentrations; K_m (Michaelis constant) the substrate concentration at which the reaction rate is half of V_{max}; S is the concentration of substrate; and v' the reaction rate. k_{cat}, the turnover number, is the maximum number of substrate molecules converted to product per enzyme molecule per second; and $[E]_o$ the enzyme concentration].

2.8.1 Determining amine concentrations in human serum

2.8.1.1 High-performance liquid chromatography (HPLC)

Methylamine in human serum was quantified using fluorometric reverse-phase HPLC, using 9-fluorenylmethoxycarbonyl-chloride (FMOC, Table 2.11) as a derivatising reagent [340]. Serum samples (100 – 500 µL) were homogenised in 1 mL 5% acetic acid solution by gentle pipetting. 100 µL of the resultant admixture was added to 600 µL borate buffer (0.2 M, *p*H 10.4) containing 3 mL acetonitrile in a

glass test tube and vortexed to precipitate proteins. After full speed centrifugation (15,000 x *g*, 10 minutes), FMOC reagent (150 μg in 100 μL acetonitrile) was added to the supernatant. Methylamine standards at known concentration were also prepared in acidified 50% acetonitrile, and blank samples of serum and supernatant (no FMOC) in a similar manner.

Acetonitrile underwent evaporation by flow of air (room temperature) using a fish-pump and glass pastette with extraction of the resultant aqueous phase in 3.5 mL hexane. The hexane extract (containing methylamine) was dried under a flow of air at ambient conditions, and the residue dissolved in 250 μL of acetonitrile solution (40% v/v). The mixture was transferred to a microfuge tube, centrifuged at full speed (and 100 μL of the resultant supernatant interrogated by analytical HPLC at a rate of 1 sample/hour (Shimadzu HPLC system; Japan). Fluorescence of the derivatised product was detected at an emission wavelength of 630nm and an excitation wavelength of 254nm.

Table 2.11: HPLC assay constituents

Reagents	**Supplier**
Acetic acid	Sigma
Methylamine	
Acetonitrile	
Borate buffer (sodium tetraborate + boric acid)	
FMOC chloride	
Hexane	
Glass pipettes	Corning Costar
Zebron B-5 HPLC column (Kinetic C18 column, 5 U, 250 x 4.6 mm)	Phenomenex

2.8.1.2 SSAO deamination of serum-derived endogenous amine substrates

In order to assess the putative contribution of VAP-1 substrates present in patient sera, a modified variation of the SSAO activity assay was conducted. In brief, a 96-well flat-bottomed plate was loaded with 50µl patient sera/well (± 250 µM semicarbazide) in quadruplicate as indicated in Figure 2.1 without any exogenous substrate. In order to inhibit other circulating amine oxidases that may contribute to H_2O_2 production, inhibitors of MAO-A (100 µM clorgyline) and MAO-B (100 µM pargyline) were added to the serum samples and the final volume made to 100µl with Dulbecco's PBS. The Amplex-Red Ultra detection system was subsequently employed to measure the evolution of H_2O_2 as described previously.

2.9 Monitoring HSEC viability post amine exposure

Prolonged, real-time image capture of HSEC was performed using a Cell-IQ system (CMTechnologies, Finland). A 24-well plate was coated with RTC (prepared as described previously) and left to dry overnight in a class II microflow cabinet. Pre-isolated HSEC, grown to confluence in a 75cm^2 flask were trypsinised, washed (PBS), pelleted and resuspended at 0.05 x 10^6 cells/mL in complete HSEC media (see section 2.1.2.3). The RTC-coated plate was washed with PBS, and 1 mL cell suspension was then loaded into each well and left to adhere overnight at 37^{o}C/5 % CO_2. Once confluent, the supernatant of each well was removed and substituted with media containing amines of interest ± TNFα (20 ng/mL, Peprotech, UK) at increasing concentrations (Table 2.12).

The inter-well spaces were filled with 1 mL sterile PBS (to maintain humidity) and the plate sealed with Cell-IQ well-plate lids (pre-warmed to 37^{o}C) and black electrical tape. These specialised lids facilitate efficient sterile gas exchange (5% CO_2 in air), and permit phase-contrast imaging of cells within the plate. The sealed plates were then inserted into the Cell-IQ, and output/input connectors and filter attached. The Cell-IQ software was set to record cell images every 5 minutes for 24 hours at 4 different positions per-well (temperature set to 37^{o}C). Thereafter, images were analysed offline to assess cell viability (Analyzer software, CMTechnologies).

Table 2.12: Substrates tested in HSEC viability assay

Amine	**Concentration range tested**
Benzylamine	20-640 μM
Cysteamine	5-400 μM
Dopamine	12.5-400 μM
Ethylamine	100-4000 μM
Methylamine	50-2000 μM
Phenethylamine	100-4000 μM

2.10 Flow-based adhesion assays

2.10.1 Microslide preparation

Flow-adhesion assays were conducted to assess the functional consequences of amine exposure and VAP-1 inhibition on HSEC-mediated lymphocyte recruitment. Six channel, flow-chamber Ibidi microslides (Figure 2.3) were RTC-coated and left to dry for a minimum of 4 hours, followed by 1 wash with endothelial SFM and 2 washes of PBS. Pre-isolated HSEC, grown to confluence in a 75 cm^2 flask were trypsinised,

washed (PBS), pelleted and resuspended at 1.5 x 10^6 cells/mL in complete HSEC media (section 2.1.2.3). Cell suspension (60µL) was injected into each slide channel and cells left to adhere (humidified incubator, 37°C, 5% CO_2) on a slide rack. After 2 hours, a media change was conducted and cells incubated under humidified conditions overnight. The following day, HSEC were stimulated with TNFα (20 ng/mL; Peprotech) ± amine substrate supplemented HSEC media for four hours to induce MAdCAM-1 expression [294]. In order to minimise the effect of bovine VAP-1, low serum endothelial media (2% FBS; no HGF/VEGF) was used during this step.

2.10.2 Preparing the JY-cell line

The JY cell line expressing α4β7 integrin was cultured in lymphocyte media and maintained in suspension (~1-1.5 x10^6 cells) in 75 cm^2 flasks. Prior to the flow-based adhesion assay, JY cells were centrifuged at 600x *g* for 5 minutes. The pellet was resuspended in 1 mL RPMI + 10% FBS and a small aliquot removed for viability assessment and quantification by Trypan blue exclusion. After counting, the remaining cells were pelleted and resuspended at 1 – 2 x 10^6 cells/mL in basal endothelial media (serum free) containing 0.1% BSA.

A

B

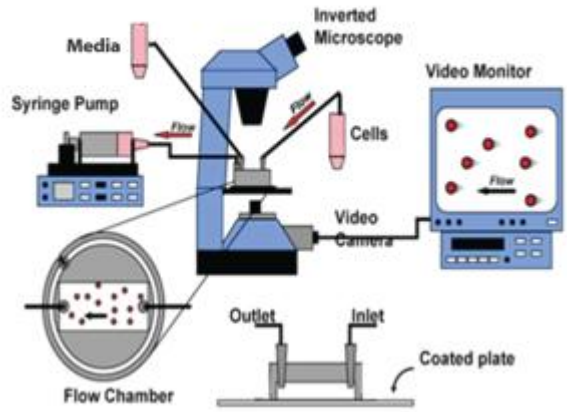

Figure 2.3: Flow adhesion assay

The flow-adhesion assay setup consists of a 6-lane microslide (Ibidi, Germany) (A) placed directly on the microscope stage. A transparent chamber (not shown) is mounted on an inverted microscope and maintained at 37°C. Ports connect silicone tubing from one side of the microslide ports (outlet) to a syringe pump set to a specific withdrawal rate (B). An electronic solenoid valve allows switching between two syringe barrels containing either cells or media with no dead space. Silicone tubing from the valve connects to ports on the other side of the slide (inlet). An external monitor connected to a DVD-recorder was attached to the microscope in order to facilitate live image capture and offline analysis [341].

2.10.3 Preparation of FAC-sorted peripheral blood lymphocytes (PBL)

To obtain purified cell populations of interest, antibody-labelled (Table 2.2) peripheral blood lymphocytes were sorted using a MoFlo XDP High-Speed Cell Sorter (Beckman Coulter Inc.) in purity mode. Sorted lymphocytes were incubated overnight in a 48-well culture plate (Corning Costar) in lymphocyte media to allow their surface markers to recycle. The following day, cells were centrifuged, pelleted, and viability confirmed before being resuspended to 10^6 cells/mL in basal endothelial media (serum free) containing 0.1% BSA.

2.10.4 Evaluation of anti-VAP-1 antibody and enzyme inhibitors

In order to test the functional significance of VAP-1 blockade on α4β7/MAdCAM-1 dependent lymphocyte adhesion, the enzyme inhibitor semicarbazide (250 μM; a concentration previously demonstrated to effectively induce enzyme inhibition yet preserve cellular viability [312]), and the anti-VAP-1 antibody TK8-14 (10 μg/mL) were employed. In brief, enzyme inhibitor or antibody was added to HSEC at the same time as TNFα and methylamine stimulation and HSEC were washed following 1 hour incubation. This was followed by 3 further hours of stimulation with TNFα and substrate and a further wash with media (x2) prior to running the assay.

2.10.5 The assay

Prior to initiating the experiment, the flow assay chamber was warmed to 37°C. A 50 mL glass syringe was prefilled with 10 mL sterile distilled water and attached to silicone tubing and a syringe pump. The withdrawal rate of the pump was adjusted to

mimic that of low shear within the sinusoids of the human liver (0.05 Pa). The barrels of two 5 mL syringes were attached to in-flow ports of the flow-chamber electronic solenoid valve using silicone tubing. Another piece of tubing was attached to the out-flow valve, which permits alternation between cell free wash buffer (serum-free, basal endothelial media + 0.1% (v/v) BSA) contained in one syringe barrel and lymphocyte suspension within the other.

After treatment of the endothelial monolayer, the microslide was washed and fresh, ultra-low serum (0.5% FBS) media provided to each channel. Microslides were then placed on the stage of a thermostatically controlled video-microscope within the flow chamber. The silicone tubing from the syringe pump was connected to one port of a chosen microslide channel via a microslide adaptor, and silicone tubing from the outflow valve to the opposite port in a similar manner. JY or FAC-sorted cells were perfused over the endothelial monolayers at a constant shear stress for 5 minutes, then wash buffer was perfused over for 3 minutes and lymphocyte adhesion subsequently recorded to DVD over a 2 minute period. Adherent lymphocytes captured via molecular interactions with functionally expressed adhesion molecules by stimulated HSEC were visualised by phase contrast microscopy (x10 magnification).

2.10.6 Analysis

A minimum of 10 fields per-treatment condition were viewed offline for analysis. Total adhesion (and subsequent migration) were determined by counting all visible adherent and migrated cells in a number of fields of known dimension, then converted to give a value of adhesion/mm^2, normalised according to the number of cells

perfused (Equation 2-3). Adhesion and migration are expressed as cells/mm^2/10^6 cells perfused, unless otherwise indicated.

Equation 2-3: Quantifying proportion of cells undergoing adhesion

$A' = a' / (f \times b \times s) \times (1/c)$

[A' represents the normalised adherent cell number, a' the average number of adherent cells per-field, f being the flow rate (mL/min), b indicative of flow bolus (mL), s signifying the surface area (mm^2), and c the cell density (10^6)].

2.11 Cell-based ELISA

The expression of adhesion molecules on primary cell cultures was investigated by ELISA of cultured HSEC. Cells were cultured and stimulated as described in section 2.10.1 before being fixed in 100% ice-cold methanol (Fisher Scientific) for 5 minutes and subsequently washed with PBS. Thereafter, cells were incubated with 2% normal goat serum (Sigma) for 45 minutes at room temperature (continuous shaking) to reduce non-specific antibody binding. The wells were washed twice with wash buffer (PBS + 0.1% BSA), following which primary antibody (Table 2.13) or IMC diluted in PBS were added and incubated with the cells for 45 minutes with continuous shaking. Following two further washes, cells were incubated with a relevant secondary antibody conjugated to HRP (diluted in PBS) for 45 minutes. Cells were then washed a further three times before development of the peroxidase enzyme conjugate using an OPD-based substrate (1,2-phenylenediamine dihydrochloride in tablet form; Dako) in accordance with manufacturer's instructions. Colour development was allowed to continue for up to 10 minutes before being stopped by addition of 0.5 M sulphuric acid (H_2SO_4; Fisher Scientific). Absorbance at 490nm was measured on an automated plate reader. Background absorbance was corrected by subtracting absorbance values

of an IMC antibody (Dako) and mean absorbance values calculated from readings of three technical repeats.

Table 2.13: Antibodies used in HSEC-ELISA

Antibody (supplier)	**Isotype (clone)**	**Final concentration**
Mouse anti-ICAM-1 (R&D systems)	IgG1 (14C11)	5µg/mL
Mouse anti-VCAM-1 (R&D systems)	IgG1 (HAE-2Z)	5µg/mL
Mouse anti-CD31 (eBioscience)	IgG1 (WM59)	5µg/mL
Mouse anti-MAdCAM-1 (AbD Serotec, UK)	IgG1 (314G8)	5µg/mL
VE-Cadherin (Novus Biologicals)	IgG1 (MM0012-8A03)	5µg/mL
Goat anti-mouse HRP 2^{o} (Dako)	IgG (polyclonal) (Cat.# P0447)	1/5000 dilution
IMC (supplier)		
Mouse-IMC (R&D systems)	IgG1 (11711)	5µg/mL

2.12 Mouse tissue

2.12.1 Animal Husbandry

Mdr2$^{-/-}$ C57BL/6 mouse embryos (gifted from Professor Lohse; Austria) were transferred into the uterus of wild-type C57BL/6 females and stock derived from generation three (and beyond) offspring. For phenotyping, exclusively homozygotes were used so genotyping was not deemed necessary at this stage. *Aoc3* point mutation knock-in mice lacking VAP-1 enzyme activity – were backcrossed onto a C57BL/6 genetic background by genOway and supplied by a contract breeder (Charles River). Henceforth, this strain will be referred to as *Ssao*$^{-/-}$. Mutant allele mice were crossed with *Mdr2*$^{-/-}$ strains in order to establish *Mdr2*$^{-/-}$ *Ssao*$^{-/-}$ animals. Identification of homozygote double knockouts was conducted by qRT-PCR-based screening (Transnetyx, USA).

All animals were housed in accordance with established care protocols at the University of Birmingham, and subject to ethical approval in accordance with the UK Animals (Scientific Procedures) Act of 1986.

2.12.2 Organ retrieval and preparation

Longitudinal phenotypic assessment was performed on mice at 5–6, 11–12 and 22–24 weeks (males and females). Blood samples were withdrawn by cardiac puncture during isofluorane anaesthesia, and mice consequently sacrificed by cervical dislocation. Previous investigators have reported that significant morphological, physiological, and structural differences exist between individual liver lobes affected with cholangiopathic injury, including the degree of ductular reaction, size of bile ducts and degree of fibrosis [342]. In this regard, a recent consensus statement has proposed a standardised work-up for mouse liver tissue. This technique was adapted and modified to permit quantification of liver-infiltrating leucocyte populations (flow cytometry) as well as assessment of intrahepatic VAP-1 enzyme activity (Figure 2.4).

2.12.3 Extraction of lymphocytes from mouse liver and flow cytometry

The appropriate liver lobe was homogenised (C-tube, GentleMACs) and the resultant suspension diluted to a minimum volume of 50 mL with RPMI. The entire cell suspension was passed through a cell strainer (70 μm) and centrifuged at 3000 x *g* (3 minutes). The sample was washed in media (x2) and resuspended in MACS buffer prior to cell labelling (Table 2.14) and flow cytometric analysis (detailed in section 2.2).

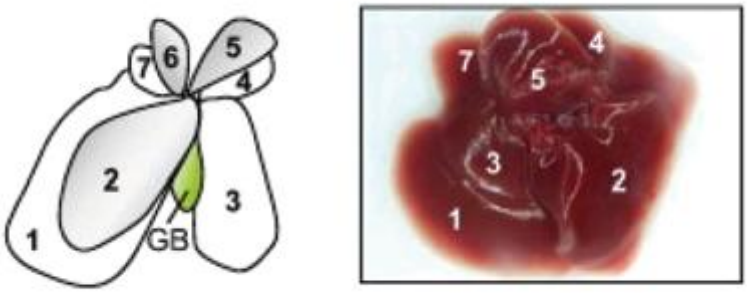

Figure 2.4: Mouse liver preparation and processing
Liver lobes are numbered consecutively according to size from 1-7. Lobe 1 was divided further into 2 segments (1a and 1b; snap frozen and formalin fixation, respectively). Lobe 2 was placed in RPMI and processed for flow cytometry and 3 (attached to the gallbladder, GB) snap frozen for hydroxyproline assays. The remainder were snap frozen and kept for protein (lobes 4 and 5) and RNA (lobes 6 and 7) extraction [342]. VAP-1 enzyme activity was assessed using protein lysates derived from the appropriate lobes.

Table 2.14: Antibodies for flow cytometry (mouse tissue)

Antibody (supplier)	Isotype (clone)	Stock conc.	Working vol. (μL / 10^5 cells)
Rat anti-CD45 PerCPCy5.5 (BioLegend®)	IgG2b (30-F11)	0.2 mg/mL	5
Rat anti-CD45 BV510 (BioLegend®)	IgG2b (30-F11)	0.06 mg/mL	10
Rat anti-CD45 PE (BioLegend®)	IgG2b (30-F11)	0.2 mg/mL	5
Rat anti-CD45 APC (BioLegend®)	IgG2b (30-F11)	0.2 mg/mL	2
Rat anti-CD45 PB (BioLegend®)	IgG2b (30-F11)	0.5 mg/mL	5
Rat anti-CD45 FITC (BioLegend®)	IgG2b (30-F11)	0.5 mg/mL	5
Rat anti-CD3 BV510 (BioLegend®)	IgG2b (17A2)	0.1 mg/mL	5
Rat anti-CD4 PE (BD Bioscience)	IgG2a (RM4-5)	0.2 mg/mL	5
Rat anti-CD8a APC (BD Bioscience)	IgG2a (53-6-7)	0.2 mg/mL	2
Rat anti-CD19 Pac. Blue (BioLegend®)	IgG2a (6D5)	0.5 mg/mL	5
Rat anti-CD49b FITC (BD Bioscience)	IgM (DX5)	0.5 mg/mL	5
Rat anti CD11b FITC (BD Bioscience)	IgG2b (M1/70)	0.5 mg/mL	5
Rat anti-F4/80 APC (eBioscience)	IgG2a (BM8)	0.2 mg/mL	2
Rat anti-Gr1 PE (BD Pharmingen)	IgG2b (RB6-8C5)	0.2 mg/mL	5
IMC			
Rat-PerCPCy5.5 (BioLegend®)	IgG2b (RTK4530)	0.2 mg/mL	5
Rat-BV510 (BioLegend®)	IgG2b (RTK4530)	0.05 mg/mL	10
Rat-PE (BD Bioscience)	IgG2a (R35-95)	0.2 mg/mL	5
Rat-APC (BD Pharmingen)	IgG2a (RTK2758)	0.2 mg/mL	2
Rat-Pac. Blue (BioLegend®)	IgG2a (eB149)	0.5 mg/mL	5
Rat-FITC (BD Bioscience)	IgM (R4-22)	0.5 mg/mL	5
Rat-FITC (eBioscience)	IgG2b (eB149/10H5)	0.5 mg/mL	5

2.12.4 Immunohistochemistry

Staining protocols were common to that used in section 2.6.3 unless otherwise stated. Primary antibodies are listed in Table 2.15.

Table 2.15: Antibodies for immunohistochemistry (mouse tissue)

Antibody (supplier)	Isotype (clone)	Stock	Working dilution
Rat anti-CD45 (eBioscience, UK)	IgG2b (30-F11)	0.5 mg/mL	1/400
Rabbit anti-CK19 (Abcam, UK)	IgG (polyclonal)	0.2 mg/mL	1/100
Mouse anti-αSMA (Sigma)	IgG2a (1A4)	2 mg/mL	1/400
IMC			
Rat IMC (AbD Serotec)	IgG2b (MCA1125)	1 mg/mL	1/800
Rabbit IMC (Abcam)	IgG (polyclonal)	0.2 mg/mL	1/100
Mouse IMC (eBioscience)	IgG2a (20102)	0.5 mg/mL	1/100

2.12.4.1 Mouse-on-mouse staining

Immunodetection of αSMA in mouse was performed on frozen sections of 0.7 μm thickness using the Vector mouse-on-mouse (M.O.M) kit as per manufacturer's instructions (M.OM Elite Peroxidase Kit, Vector labs, UK). Novared (Vector labs) was utilised as a chromogen. Briefly, endogenous peroxidase activity was blocked and sections washed in Tris-buffered saline (TBS) before undergoing an avidin/biotin blocking step (Vector). Sections were further blocked for 1 hour in working solution of M.O.M mouse Ig blocking reagent, then washed and incubated with M.O.M diluent for 5 minutes. Excess diluent was then decanted and sections incubated with primary antibody for 60 minutes. Thereafter working solution of M.O.M biotinylated anti-mouse IgG reagent (10 μL stock; 2.5 mL M.O.M diluent) was incubated with slides

for 10 minutes, the slides were then washed and exposed to Vectastain Elite ABC reagent for 5 minutes. Sections were then washed prior to addition of peroxidase substrate solution (Novared – Vector labs). Finally, samples were washed and fixed in mountant (DPX). Quantitative analysis of staining was performed using ImageJ software.

2.12.4.2 Sirius red staining

Snap frozen or deparaffinised liver sections were rinsed in distilled water and covered in 0.5% phosphomolybolic acid (Sigma) for 5 minutes. Slides were then placed into a rocking glass bath containing 0.1% Sirius Red (Direct Red 80 in saturated picric acid – 1.3% aqueous solution; Sigma) for 30 minutes. Thereafter, sections were dipped sequentially in 0.1 M HCl, distilled water, graded alcohols and clearene, before mounting in DPX. Occasionally, a haematoxylin counterstain step was employed prior to dehydration. Quantitative analysis of staining was performed using ImageJ software.

2.12.5 Hydroxyproline assay

Liver tissue (50 – 100 mg) was manually homogenised in 1 mL ddH_2O. Thereafter, 125µl 50% tricholoroacetic acid (Sigma) was added and samples incubated on ice for 30 minutes. Samples were subsequently centrifuged for 5 minutes (15000 x *g*) in order to precipitate protein following which 500 µL 6 N HCl (Sigma) was added to the pellet. Samples were transferred to 12 x 100 mm borosilicate glass tubes (Corning) and heated overnight to 120^{o}C (oven). Acid was then allowed to evaporate over 48 hours (70 – 80^{o}C) before resuspending the precipitate in 500 µL distilled

water and vortexing. Samples were filtered and 50 μL transferred to another glass tube. Volumes were made up to 1000 μL with distilled water + 500μl chloramine T (Table 2.16) and samples incubated at room temperature for 20 minutes. Subsequently, 500 μL Ehrlich's solution was added to the samples, the admixture vortexed and then incubated at 65^{o}C for 15 minutes. Samples were cooled (left to stand for 10 minutes) to room temperature and 200 μL of each sample transferred to a 96-well flat-bottomed plate. The optical density of each sample was read at 561nm versus hydroxyproline standards (trans-4-Hydroxy-L-proline (Sigma) prepared in 0.001N HCl in ddH_2O and reacted with Erlich's solution as described above). All samples and standards were run in triplicate and normalised to starting weight.

Table 2.16: Hydroxyproline assay constituents (Sigma)

Chloramine-T solution
1) Buffer • 25 g citric acid monohydrate • 6.0 mL glacial acetic acid • 60 g sodium acetate trihydrate • 17 g sodium chloride Dissolved in water and brought up to 500 mL; thereafter added to 100 mL water containing 150 mL n-propanol (*p*H 6.0) 2) 1.75 g chloramine-T (sodium N-chloro-p-toluenesulfonamide) dissolved in 10 mL water, 10 mL n-propanol and 80 mL buffer.
Ehrlich solution (p-dimethylaminobenzaldehyde perchloric acid)
7.5 g *p*-dimethylaminobenzaldehyde dissolved in 30 mL n-propanol in 50 mL flask, added to 13 mL 60% perchloric acid slowly and made up to 50 mL with n-propanol (stored in dark).

2.12.6 qRT-PCR in mouse liver

Quantitative PCR was performed on cDNA prepared as described in section 2.3.1. Probes and primers tested are listed in Table 2.17 and were purchased from Taqman®.

Table 2.17: Primers/probes – qRT-PCR (mouse)

	Primer/Probe assay ID
αSMA (*Acta2*)	Mm01546133_m1
Col1α1 (*Col1a1*)	Mm00483387_m1
VAP-1 (*Aoc3*)	Mm00839624_m1
18S (*Rn18s*)	Mm04277571_s1

2.12.7 Murine hepatic SSAO activity

Murine intrahepatic VAP-1 enzyme activity was quantified using the Amplex-Red assay, method 2 (section 2.5.3.2). Different anti-mouse VAP-1 antibodies at several concentrations were tested with regard to protein capture capability (Table 2.18).

As a positive control for murine VAP-1 enzyme activity, a 3T3 murine pre-adipocyte cell line was purchased from Sigma and differentiated toward adipocytes [295]. In brief, cells were grown to confluence in an RTC-coated 75 cm^2 culture flask (DMEM/10% FBS/1% PSG), following which media was discarded and replaced with one inducing adipogenic differentiation (Table 2.1). Induction medium was substituted after 2 days with maintenance medium; changes of the latter occurring every 48 hours. Cells were inspected daily for morphology change and once

differentiation into adipocytes was apparent (typically 10 days), cells were lysed and protein extraction performed as described previously (section 2.7).

Table 2.18: Murine anti-VAP-1 antibodies under investigation

Antibody (supplier)	Isotype (clone)	Concentration range tested
Rat anti-AOC3 (University of Turku, Finland)	IgG1 (7-106)	5–100 μg/mL
Rabbit anti-AOC3 (University of Turku, Finland)	IgG (polyclonal)	5-100 μg/mL
Rat anti-AOC3 (BioTie)	IgG1 (BTT1004)	5-100 μg/mL
Goat anti-AOC3 (Everest Biotech, USA)	IgG (polyclonal)	5-100 μg/mL

2.13 Graphical representation and statistical analysis

The distribution of continuous variables was assessed via the Kolmogorov-Smirnov method. Non-parametric data are presented using the median and interquartile range (IQR) unless otherwise specified. The Mann-Whitney (MW) test was conducted when comparing between two independent groups, and analysis of variance through Kruskal-Wallis (KW) test and Bonferroni-Dunn post-hoc correction for multiple-groups. Statistically significant differences between related groups were tested using the Wilcoxon-signed rank test or paired t-test (as indicated) for paired data, with post-hoc Bonferroni-Dunn correction (>2 groups). Non-parametric measures of statistical dependence between two continuous variables were conducted using Spearman's rank correlation coefficient.

2.14 Population statistics and survival impact

In longitudinal follow-up studies the primary endpoint was defined as liver transplantation or death; patients without a clinical event in this regard being censored

at time of last clinic follow up. The impact of continuous variables on clinical endpoints was evaluated by receiver operator (ROC) curve analysis, and where indicated an optimal cut-point for downstream polychotomisation selected therein. Univariate and multivariable Cox proportional hazards models were also fit in order to assess the impact of individual covariates on the instantaneous rate of events, with time-to-event analysis also being ascertained through Kaplan-Meier estimates. All analyses and graphical representations were conducted using Prism v.5.0 (GraphPad Inc, USA) or SPSSv.21 (IBM, USA).

3 Results I: CCL25 and CCR9 expression in the human colon

3.1 Introduction

The expression pattern of adhesion molecules, chemokine receptors and their respective ligands determine which cell types are recruited to tissues under homeostasis and at times of inflammation. Expression of CCL25 is constitutive in the small bowel where it mediates recruitment and positioning of $CCR9^+$ lymphocytes within the intraepithelial compartment and lamina propria [142]. Intestinal CCL25 expression is up-regulated under pro-inflammatory conditions, and an increased frequency of peripheral blood $CCR9^+$ lymphocytes can also be detected in patients with active small intestinal Crohn's disease [343].

The vast majority of patients with PSC have coexisting IBD [254] and it has been hypothesised that aberrant endothelial expression of CCL25 on peri-portal sinusoids facilitates recruitment of gut-primed $CCR9^+$ lymphocytes bearing an effector memory phenotype; which, upon exposure to an as yet unidentified trigger can reactivate and initiate a pro-inflammatory response, driving hepatobiliary inflammation [127]. Despite the distribution of intestinal involvement in PSC being predominantly colonic, activity of the CCR9-CCL25 axis within the gut mucosa is largely restricted to the small bowel, with little expression being detected in the human or murine large bowel [142,145,148,343,344]. However, previous analyses of intestinal $CCR9^+$ lymphocyte populations have largely focussed on the murine setting [345], and the few in human studies were either performed on cells extracted from MLN and left in culture [343], lymphocytes extracted from non-inflamed colon (NC), or peripheral

blood of patients with colitis [142]. Moreover, reports of CCL25 expression are heavily reliant on semi-quantative measures and direct visualisation with immunohistochemistry and *in situ* hybridisation (ISH), again utilising non-inflamed human colonic tissue as study material [123,142]. As such, there is a dearth of studies directed at elucidating chemokine-chemokine receptor expression in human patients with active colitis.

This chapter provides evidence for the selective enrichment of intestinal $CCR9^{+}$ T-cells in colitis when compared to tissue-infiltrating lymphocytes obtained from NC. Moreover, a systematic approach analysing CCL25 expression across varying degrees of colonic inflammatory activity is presented.

3.2 Findings

3.2.1 CCR9 expression by tissue-infiltrating lymphocytes in small vs. large bowel

As a positive control for studying CCR9 expression, intestinal lymphocytes were isolated from the most distal portion of small bowel (terminal ileum), obtained from patients undergoing surgical resection for refractory colitis (pan-colectomy; n=3) or right-sided colon cancer (subtotal colectomy; n=2). Tissue-infiltrating leucocytes were isolated as described in Chapter 2. The frequency of CCR9+ lymphocytes was examined by flow cytometry, in which the total lymphocyte population cloud was subject to gating on the live CD3+ population of cells, and subsequently gated on expression of co-receptors. In this regard, a similar proportion of small bowel derived CD4+ and CD8+ T-cells were CCR9 positive (mean 62.4%, standard deviation (SD) ± 19.7% vs. 68.2 ± 12.4%, respectively; p = n.s., MW-test). Fluorescence minus one

(FMO) controls were used in 2/5 experiments to determine the specificity of the staining for CCR9 (Figure 3.1).

Next, intestinal lymphocytes were isolated from the colonic resection specimens of patients undergoing surgery for non-IBD associated cancer (n=5; n=3 from descending colon/rectum and n=2 from ascending), and the distal-to-tumour segment exploited for studying lymphocyte populations in the absence of colonic inflammation (confirmed by a histopathologist with expertise in IBD). In contrast to the terminal ileum, only a small number of tissue-infiltrating $CD4^+$ and $CD8^+$ T-cells were observed to express CCR9 in non-inflamed colon (mean 5.7 ± 0.5% vs. 4.9 ± 2.4%, respectively; p = n.s, MW-test, Figure 3.2).

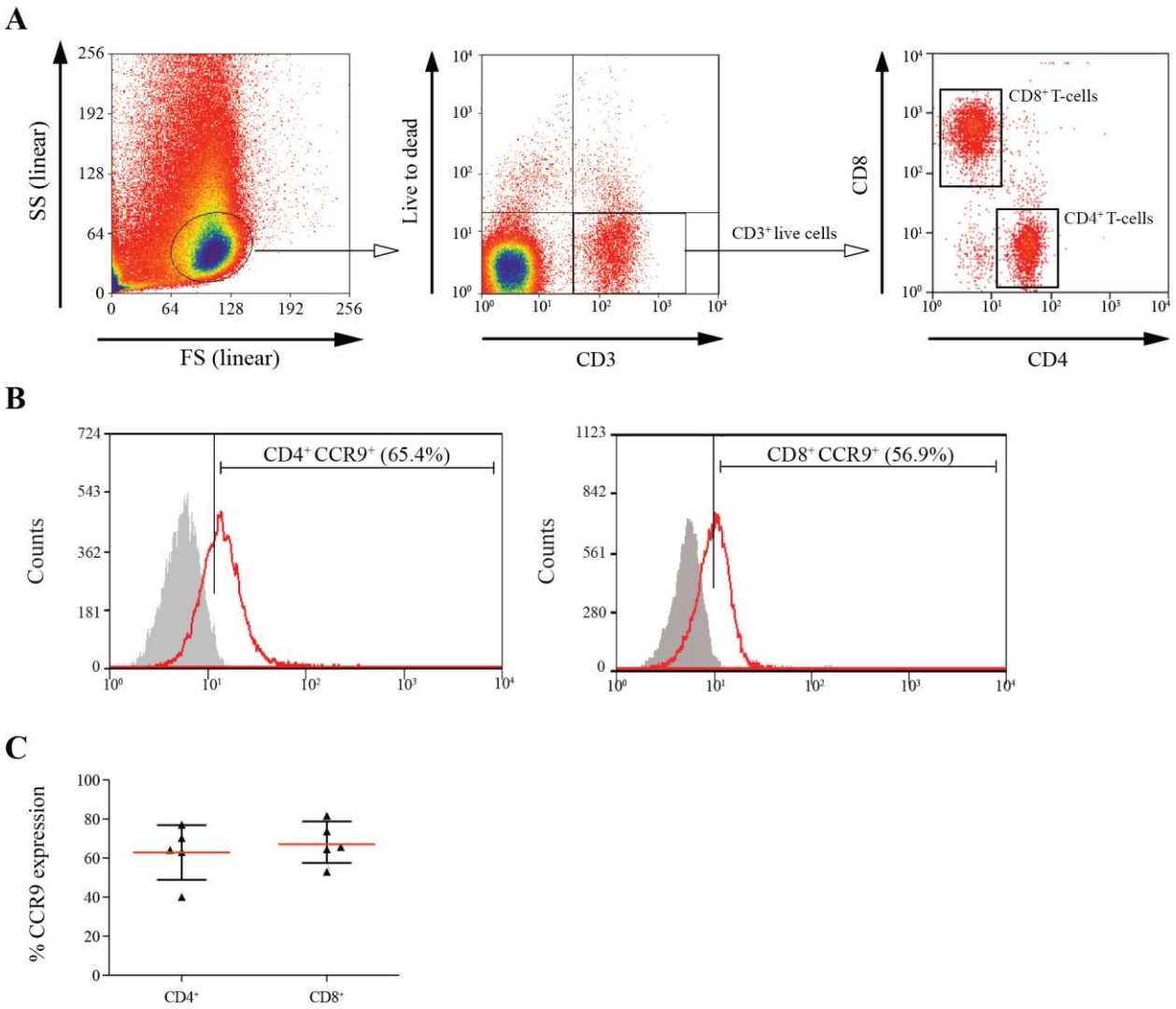

Figure 3.1: CCR9 expression on lymphocytes isolated from small bowel

The standard flow cytometry gating strategy to identify tissue-infiltrating lymphocyte populations is illustrated in (A): forward and side light scatter (FS and SS, respectively) and cell surface expression of CD3 with absence of dead cell staining defined live lymphocytes. Of this population, T-lymphocytes were sub-divided into $CD4^+$ and $CD8^+$ cell populations. Over 50% of terminal ileum/small bowel (SB) $CD4^+$ and $CD8^+$ T-cells expressed CCR9, as illustrated by the representative flow cytometry plots in (B). A summary figure of percentage populations from 5 independent samples is shown in (C), with data presented as mean $\pm$ SD.

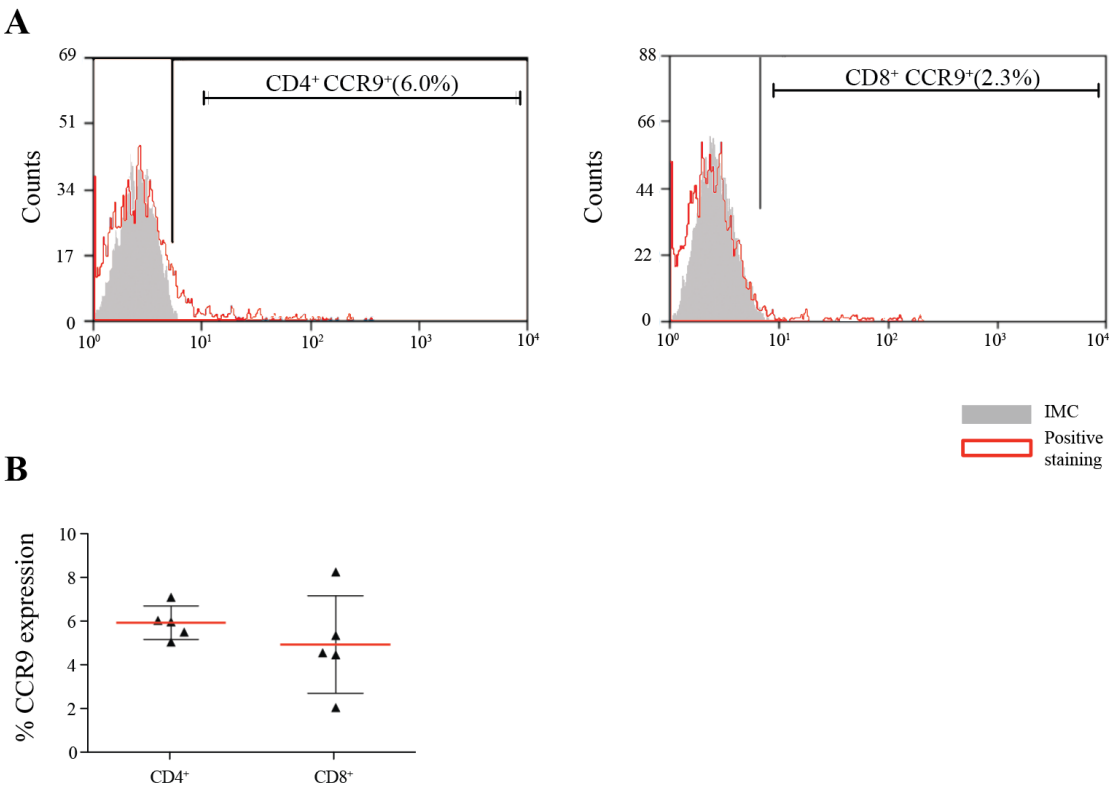

Figure 3.2: CCR9 expression on lymphocytes from non-inflamed large bowel
$CD3^+$ $CD4^+$ and $CD3^+$ $CD8^+$ T-cells isolated from non-inflamed large bowel expressed low levels of CCR9. Representative flow cytometry plots shown in (A); and summary of percentage positive cells from 5 indpendent samples shown in (B). Data presented as mean $\pm$ SD.

3.2.2 T-cells express CCR9 in active colitis

The next step was to determine whether $CCR9^+$ T-cells are present in the colon under pro-inflammatory conditions. In a similar manner to that described above, resected tissue was excised from individuals with active ulcerative colitis refractory to medical therapy undergoing pan-colonic resection (n=6). The frequency of $CD4^+$ T-cells expressing CCR9 in colitis (92.6 ± 4.1%) was higher than that reported under the non-inflamed circumstance (Figure 3.3; $p<0.001$, MW-test). The proportion of $CD8^+$ T-cells expressing CCR9 was also greater in patients with UC than NC (34.3 ± 3.8%; $p = 0.013$, MW-test).

Conventionally, the distribution of inflammation in UC begins in the rectum, spreading proximally in a continuous manner [346]. Microscopic inflammation may not be apparent on initial inspection leading me to examine the lymphocytic infiltrate in resected segments of colon reported as being quiescent by the receiving pathologist, but that which harbours active colitis histologically (on antecedent colonoscopy). In a limited number of patients manifesting such a phenotype (n=3), the proportion of $CD4^+$ and $CD8^+$ T-cells expressing CCR9 was more variable (69.8 ± 22.6% and 17.5 ± 7.2%, respectively) reflecting the varying degrees of underlying inflammatory activity (Figure 3.4).

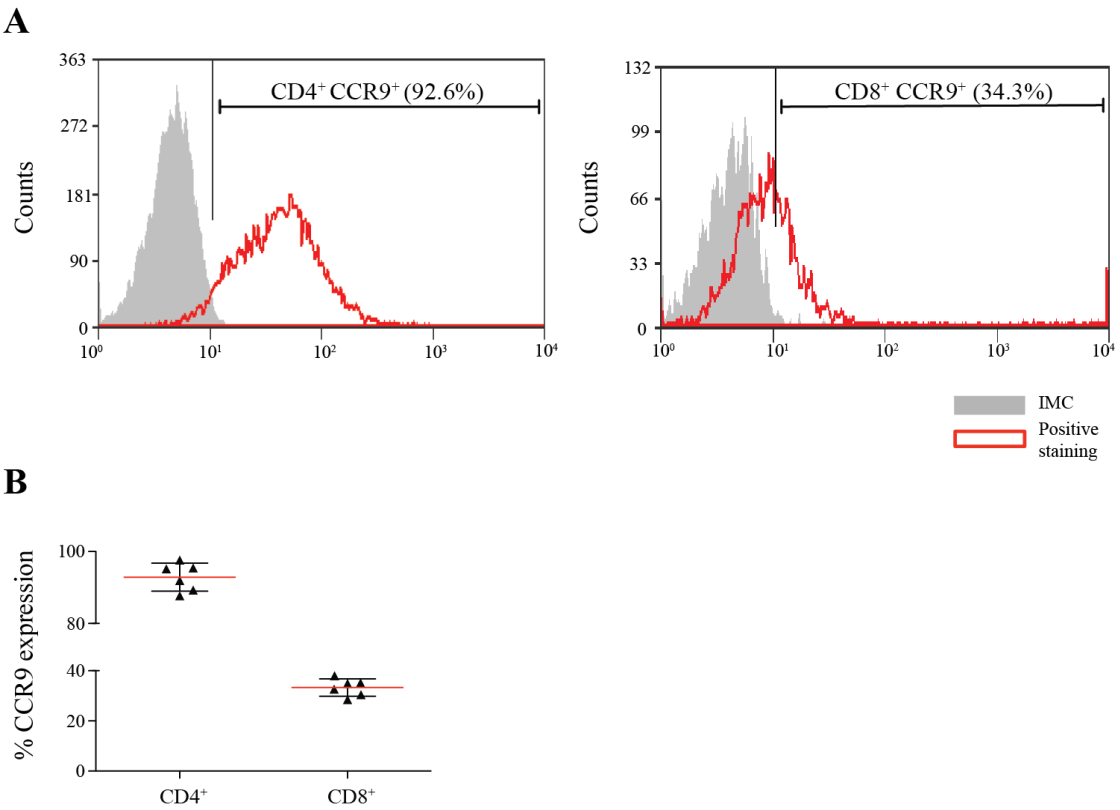

Figure 3.3: Intestinal CCR9 expression on lymphocytes in active ulcerative colitis
Representative flow cytometry data plots (of n=6) of CCR9 expression by isolation $CD4^+$ and $CD8^+$ lymphocytes (gated on live cells) (A). Summary of percentage positive cells from independent experiments shown in (B). Data presented as mean ± SD.

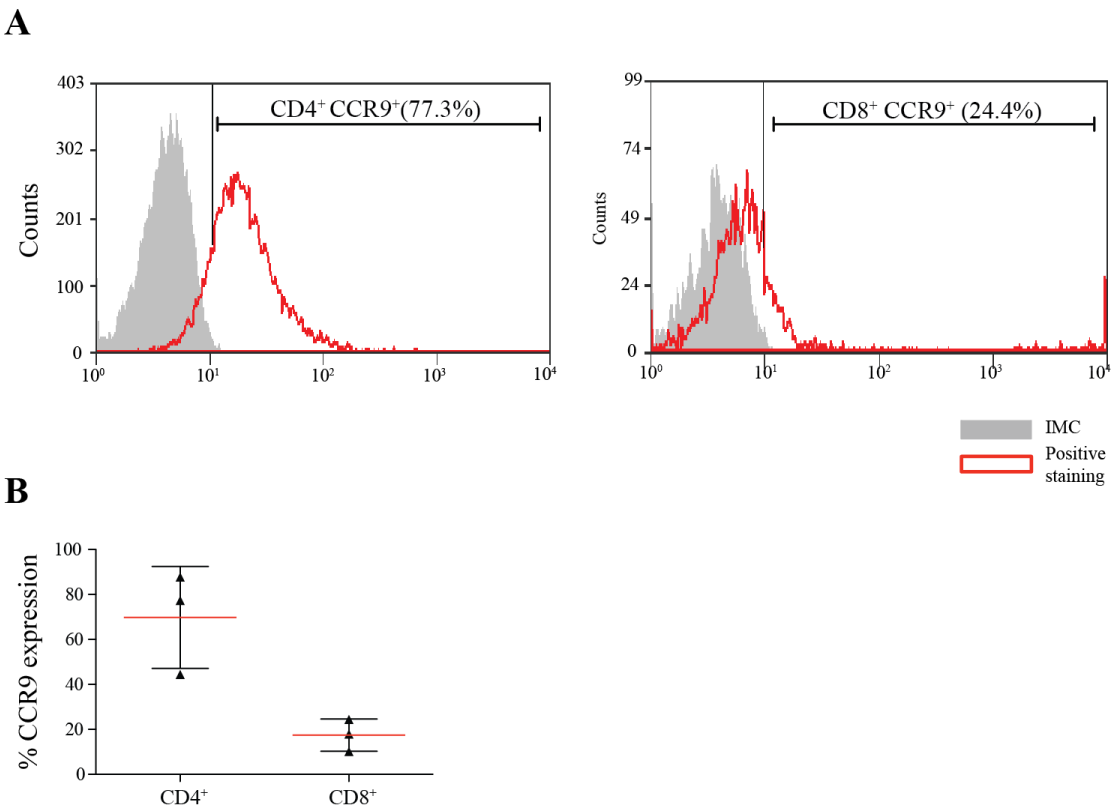

Figure 3.4: Lymphocytic CCR9 expression in macroscopically quiescent colitis
Representative flow cytometry data plots (of n=3) of CCR9 expression by isolation $CD3^+$ $CD4^+$ and $CD3^+$ $CD8^+$ lymphocytes (gated on live cells) infiltrating the colon in areas with evidence of microscopic inflammation only (A). Summary of percentage positive cells from independent experiments shown in (B). Data presented as mean ± SD.

3.2.2.1 Greater numbers of CCR9$^+$ T-cells infiltrate inflamed vs. non-inflamed colon

The proportion of $CD4^+$ and $CD8^+$ T-cells expressing CCR9 was compared between small bowel, macroscopically active colitis, colitis with evidence of microscopic inflammation only and non-inflamed colon. Significant differences identified via the previous statistical tests were adjusted for multiple comparisons using the Bonferroni method (Figure 3.5). There were significantly fewer $CD4^+$ and $CD8^+$ T-cells expressing CCR9 in NC colon versus small bowel. Moreover, a significantly greater proportion of colonic $CD4^+$ and $CD8^+$ $CCR9^+$ T-cells were present in patients with

UC compared to NC. There was a trend towards a greater proportion of $CD8^+$ T-cells expressing CCR9 in UC versus NC although this failed to reach statistical significance on post-hoc testing.

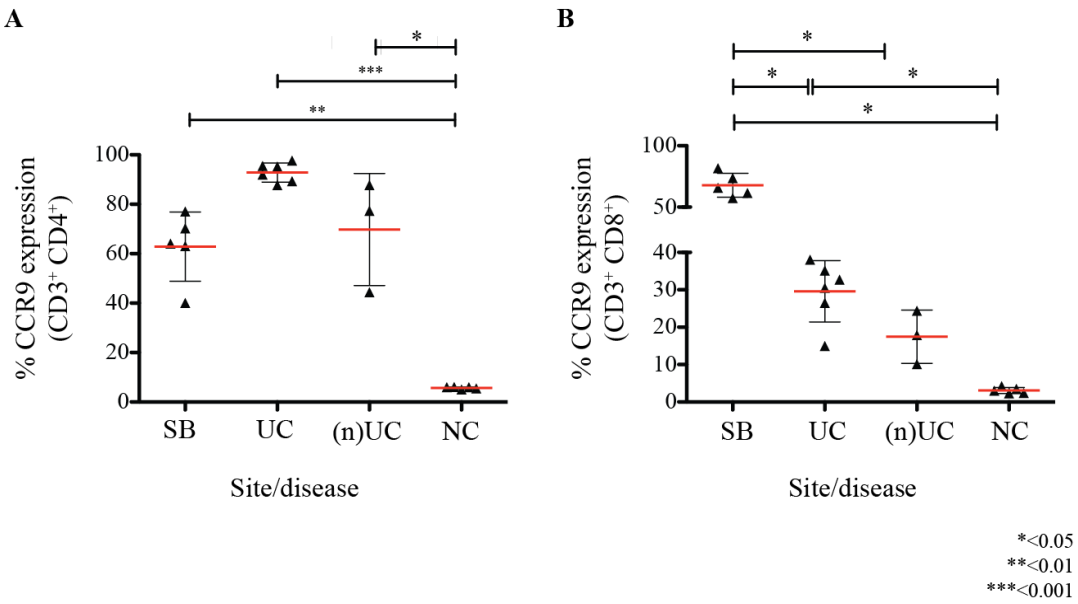

Figure 3.5: CCR9 expression in the intestine

Frequencies of tissue-infiltrating lymphocytes expressing $CCR9^+$ across the terminal ileum / small bowel (SB; n=5) and colon in patients with macroscopically active ulcerative colitis (UC; n=6), macroscopically quiescent colitis but with evidence of active inflammation microscopically ((n)UC; n=3), and those with non-inflamed colons as determined both macro- and microscopically (NC; n=5) are illustrated. Proportions represent the percentage of total $CD3^+$ $CD4^+$ $CCR9^+$ (A) and $CD3^+$ $CD8^+$ $CCR9^+$ (B) cells. Data presented as mean $\pm$ SD. Capped lines and asterisks indicate statistically comparisons between groups (*p* values) as per KW-test and Bonferroni-Dunn post-hoc correction.

The majority of $CD4^+$ $CCR9^+$ T-cells were $CD127^+$, with little or no expression of CD25. Collectively, these findings suggest that effector $CCR9^+$ lymphocytes, but not regulatory T-cells (T_{reg}), infiltrate the inflamed colon (Figure 3.6).

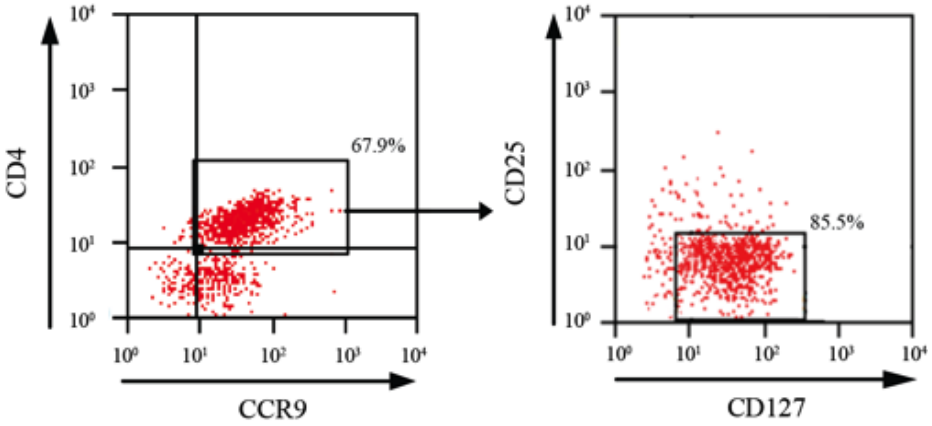

Figure 3.6: Phenotype of $CCR9^+$ T-cells
Gated $CD3^+$ $CD4^+$ $CCR9^+$ T-cells in colitis were predominantly CD127-positive in keeping with an effector phenotype.

3.2.2.2 CCR9$^+$T-cells infiltrate the inflamed colon in Crohn's disease

In contrast to UC, patients with Crohn's colitis can harbour discontinuous segments of disease, with areas of active inflammation interspersed with those that are truly quiescent (macroscopically and microscopically); so called 'skip lesions' [347]. In this regard samples from patients with Crohn's colitis (n=2) undergoing resection for an inflammatory colonic stricture were evaluated. In both the cases, two pieces from the area of active inflammatory stricturing were studied, together with the neighbouring segments of quiescent disease either side, analysed as a composite sample. Approximately 90% of CD4$^+$ and 30% of CD8$^+$ T-cells infiltrating inflamed colon in an inflammatory stricture were CCR9 positive, as opposed to ~20% and ~3%, respectively in areas of quiescent inflammation (Figure 3.7).

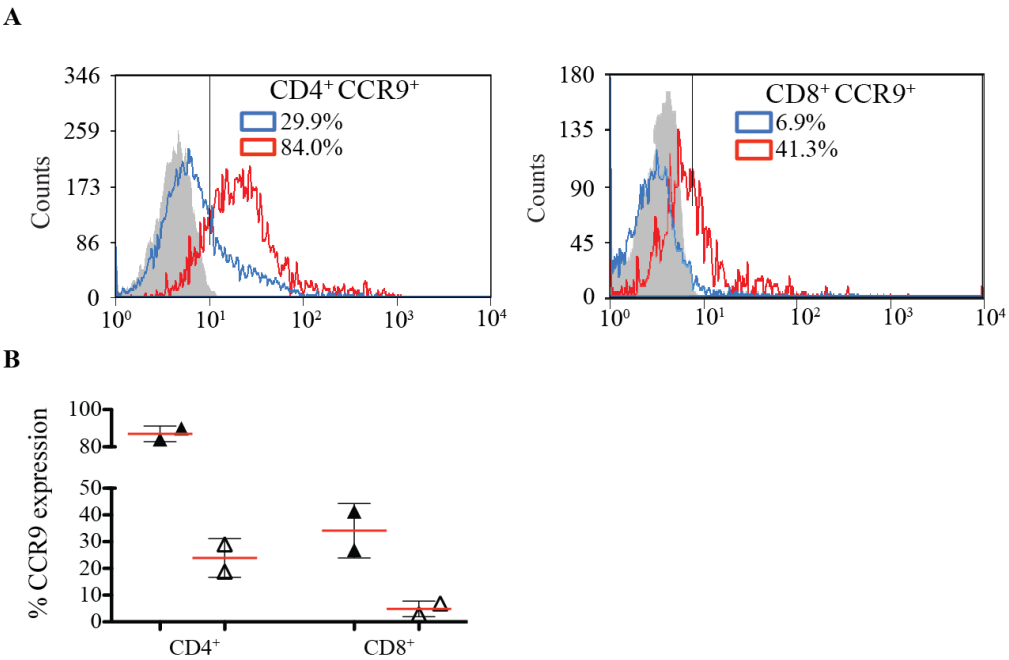

Figure 3.7: CCR9$^+$ expression in colonic Crohn's disease
Data presented for CCR9 expression on colon-infiltrating lymphocytes in quiescent vs. active Crohn's colitis segments from the same patient (A). FMO controls are indicated by the grey histograms (areas of inflammatory stricturing), and positively stained cells by the red histograms. Blue histograms indicate positively stained cell populations in paired samples of colon, without evidence of active colitis. Summary data for percentage CCR9 expression on colon-infiltrating T-cells from the two patients undergoing surgical resection for Crohn's colitis are presented in (B), wherein black triangles represent areas of active inflammatory stricturing, and white triangles neighbouring areas of quiescent disease.

3.2.3 CCL25 gene expression in normal versus inflamed colon

Having identified that an increased proportion of tissue-infiltrating T-cells express CCR9 in colitis relative to non-inflamed large bowel, I proceeded to ascertain whether its cognate ligand, CCL25, is also detectable within colon.

3.2.3.1 Qualitative PCR

Whole tissue total RNA extraction was performed from samples of NC (n=10), UC resection specimens (n=10) and small bowel (n=3). Following a reverse transcriptase step and targeted PCR with exon-exon junction spanning primers, agarose gel-electrophoresis demonstrated cDNA products at the expected size for *CCL25* in small bowel but not NC samples. Moreover, bands were detectable in samples of large bowel obtained from patients with refractory UC (Figure 3.).

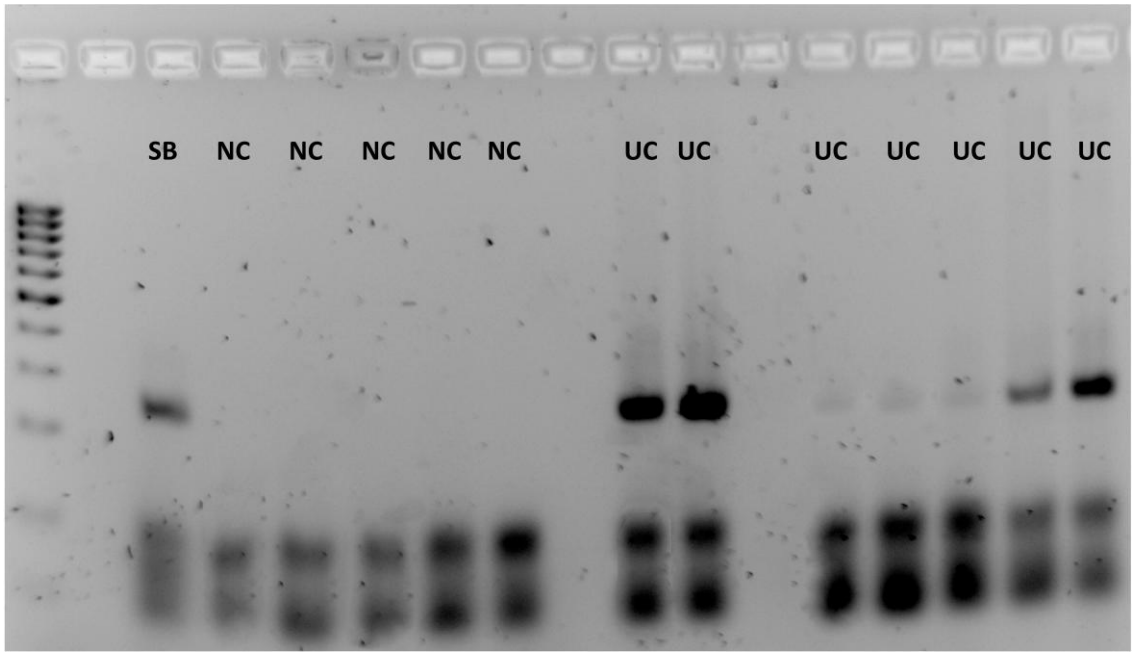

Figure 3.8: Detection of *CCL25* gene expression in the human intestine
Semi-quantative PCR was performed by a standard protocol. A representative agarose gel following PCR and cDNA electrophoresis of samples, obtained from normal/non-inflamed human colon (NC) and ulcerative colitis refractory to medical therapy (UC). Terminal ileum / small bowel (SB) was exploited as a qualitative positive control for *CCL25* gene expression. Colonic samples from UC illustrate strongly positive signals at the expected amplicon size for the *CCL25* gene (227bp) comparable to those seen in SB, with a relative absence in NC specimens.

3.2.3.2 Quantitative real-time PCR

While semi-qualitative PCR assessment of gene-expression demonstrated the absence/presence of *CCL25* in tissue samples conventional end point analysis was not sensitive enough to differentiate expression levels between samples. I used qRT-PCR as a more robust method of evaluating transcription particularly given the apparent low levels of *CCL25* expressed in normal colon shown in Figure 3.9. Moreover, qRT-PCR permits accurate quantification of target gene expression relative to housekeeping; an aspect not accurately performed through semi-quantitative methods.

3.2.3.2.1 Selection of reference genes

The MIQE guidelines advocate that when performing qRT-PCR normalisation against a single reference gene is not acceptable unless evidence is provided for its invariant expression [348]. As such, absolute quantification of two commonly applied housekeeping genes – *18S* and *GUSβ* – was compared between NC and UC samples Their choice for study was largely based on previously published literature in the IBD and colorectal cancer field [349–351]. Although no significant differences in expression between NC and UC were identified for either gene (MW test), 18S exhibited a wider range of crossing point (Cp) variation between samples (Figure 3.9). In contrast, the median Cp value of *GUSβ* was largely conserved in colonic tissue and therefore was selected as housekeeping gene of choice.

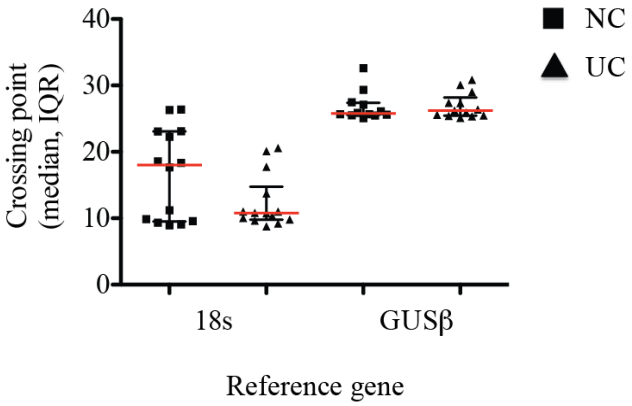

Figure 3.9: Assessment of reference genes in human colon
Absolute quantification (crossing point) of reference genes across distinct non-inflamed colon (NC, squares) and ulcerative colitis (UC, triangles) samples. Both 18S and GUSβ illustrate conservation between NC (n=14) and UC (n=14) although the degree of variability was much less with the latter.

3.2.3.2.2 Relative expression of chemokine expression

Differences in *CCL25* gene expression were analysed in triplicate relative to *GUSB* using exon-exon junction spanning primers. Median delta (Δ□ □Cp across all colitis specimens was $9.6\varepsilon^{-4}$ ($2.0\varepsilon^{-4}$ – 3.2ε-3) and all amplification curves appeared below 40 cycles. No amplicons were detected in any of the NC samples, despite a stepwise increase of starting cDNA quantity from 50 to 150ng. The duration of experiment was thereafter increased from 45 to 55 cycles without successful amplicon detection in NC specimens, and it was therefore deemed that *CCL25* was not present these samples. In this context, calculation as fold *CCL25* expression (relative to NC control samples for instance) was not possible. Therefore all results are henceforth calculated and presented as ΔCp relative to *GUSβ.*

3.2.3.2.3 CCL25 gene expression by colonic site

After identifying CCL25 in patients with colitis (please see 3.2.3.2.2 above), I investigated variation with regard to site of tissue sampling, treatment regimen,

patient age or gender. Regarding the former, most surgical resection specimens interrogated in the above analysis were provided *en bloc* and therefore it was not possible to differentiate colonic tissue by site. Moreover, all surgical resections were conducted for UC refractory to medical therapy, and such patients had been exposed to immunosuppression. This led me to study mucosal biopsies from 37 patients with an established diagnosis of UC undergoing flexible sigmoidoscopy or colonoscopy as part of routine standard of care. Individual patient characteristics for this cohort are provided in Table 3.1. Even with this approach, there were relatively few specimens from the descending colon, transverse colon, ascending colon and caecum, therefore the latter 4 compartments were grouped and analysed together (D.T.A.C).

Statistical analysis revealed no significant differences in CCL25 expression levels between biopsy site (KW test), or when grouping patients by concurrent use of immunosuppression (steroids, thiopurines, calcineurin inhibitors, biological therapy). No significant correlations were observed with patient age, although women expressed slightly higher CCL25 levels than men (Figure 3.10).

Table 3.1: Characteristics of patients undergoing colonoscopic/sigmoidoscopy

Male; N (%)	22 (60)
Median age (IQR)	38yrs. (26 – 46)
Biopsy site; N (%)	
- rectum	13 (35)
- sigmoid	16 (43)
- descending colon	3 (8)
- transverse colon	1 (3)
- ascending colon	2 (5)
- caecum	2 (5)
Endoscopic mayo score; N (%)	
0	11 (30)
1	11 (30)
2	10 (27)
3	5 (14)
PSC; N (%)	3 (8)
Immunosuppression; N (%)*	21 (57)

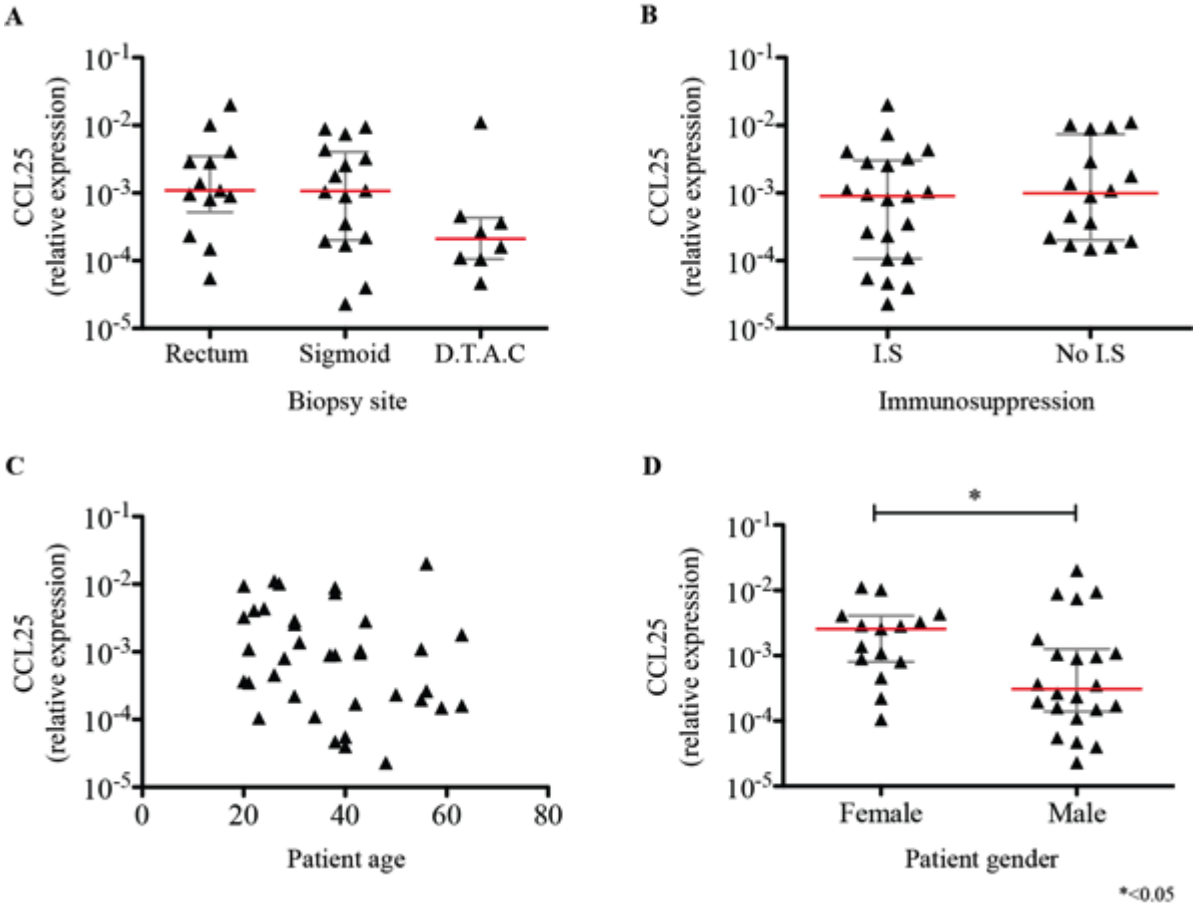

Figure 3.8: qRT-PCR of colonic *CCL25* gene expression in ulcerative colitis

CCL25 gene expression provided relative to *GUSβ*. The degree of gene transcription did not vary according to (A) biopsy site; specifically, rectum, sigmoid or colon proper (grouped as distal, transverse, ascending and caecum – D.T.A.C.); (B) exposure to immunosuppression, I.S; or (C) patient age at time of biopsy. Women were seen to express slightly higher *CCL25* levels than men (D). Asterisks indicate statistically significant differences (crude; unadjusted).

3.2.3.2.4 CCL25 gene expression and inflammatory activity.

To assess whether CCL25 expression correlated with inflammatory status I compared transcript levels with severity of disease. There are many disease activity indices in ulcerative colitis but for the purposes of this study I selected the Mayo endoscopic severity score given its widespread use and adoption as an endpoint in UC clinical trials with regard to mucosal healing [352–354].

Having demonstrated stability of *GUSβ* as a housekeeping gene in NC vs. UC samples, I proceeded to assess conservation across ordinal degrees of colitic activity (Figure 3.9). *GUSβ* demonstrated no significant variation with Mayo score (KW test *p* = n.s) and retained validity as a suitable housekeeping gene in this context.

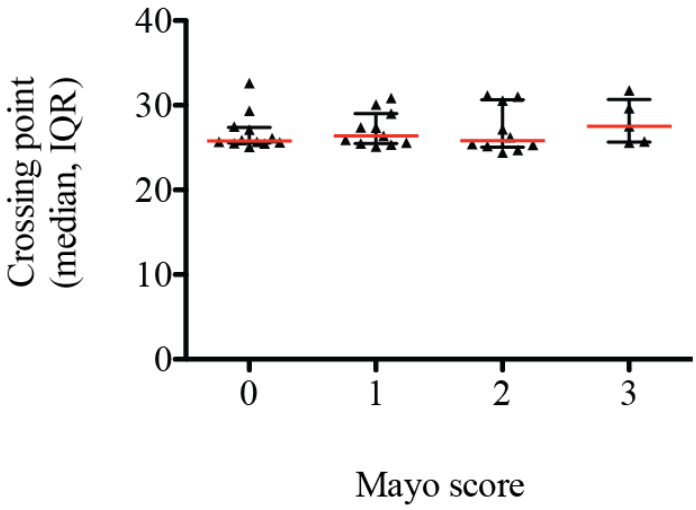

Figure 3.9: Validation of *GUSβ* as a reference gene across UC Mayo scores
Absolute quantification (crossing point) of GUSβ with colitis' according to endoscopic Mayo scores 0 (n=11), 1 (n=11), 2 (n=10) and 3 (n=5) illustrated stable conservation across disease stages.

CCL25 gene expression was examined in duplicates relative to *GUSβ*, and statistically significant associations with Mayo severity score were revealed (KW test $p = 0.0015$; Figure 3.10). Using Dunn's multiple comparison test, patients scoring Mayo 0 expressed significantly lower levels of *CCL25* than those with a score of 2 or 3 ($p < 0.01$ and < 0.05, respectively), although apparent differences between lower tiers of inflammatory activity (0 vs. 1) did not reach statistical significance. Similarly, there was a degree of overlap with respect to *CCL25* levels in those with higher Mayo score.

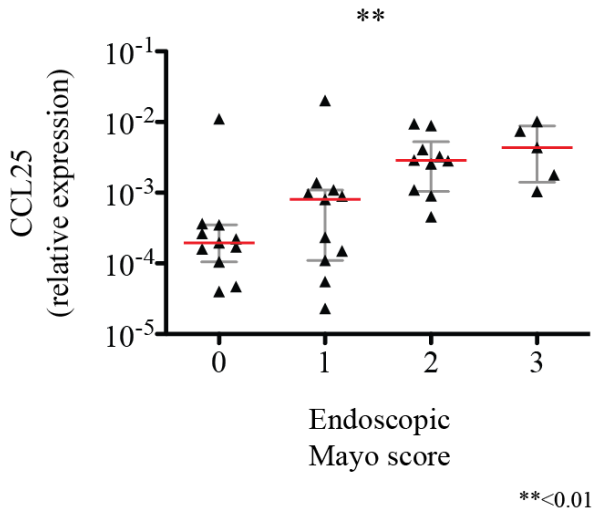

Figure 3.10: Colonic *CCL25* gene expression according to inflammatory activity
CCL25 expressed relative to *GUSβ*. Levels presented in relation to Endoscopic Mayo scoring (0 representing no inflammation and 3 severe inflammation). Capped lines and asterisks denote statistically significant results (KW test).

To obtain further information on the relationship between *CCL25* expression and disease activity in the colon, I used TNFα as an inflammatory marker, chosen in this context given associations with treatment response and disease relapse in UC [355,356] as well as the emergence as a sustainable therapeutic target in patients [353]. Statistical analysis by Spearman's rank coefficient revealed a significant and striking correlation between CCL25 and TNFα gene expression (Figure 3.11); consistent with *in vivo* models wherein increased intestinal mucosal CCL25 expression is observed following TNFα injection [136].

Given the previous association between *CCL25* expression and gender, a multiple logistic regression model was created. *CCL25* expression (independent variable) was dichotomised at the median to yield high *vs*. low values, and patient gender and endoscopic Mayo score evaluated as independent, fixed covariates. On multivariable analysis, only Mayo score retained a statistically significant association with *CCL25* expression ($p<0.0001$), indicating gender as a confounding factor and representative of female patients in our cohort bearing a larger inflammatory burden. Indeed, this model held true on substituting Mayo score with *TNFα* as a covariate.

Because we detected increased numbers of $CCR9^+$ lymphocytes in UC versus NC samples, I looked to see if there was a correlation between CCL25 and CCR9 gene expression. However, *CCR9* gene expression only appeared in late cycles (median Cp 41; IQR 39 – 43) and did not change upon increasing cDNA concentration, suggesting that receptor transcription occurs at a very low level; or that there are relatively few T-cells compared to other cell populations.

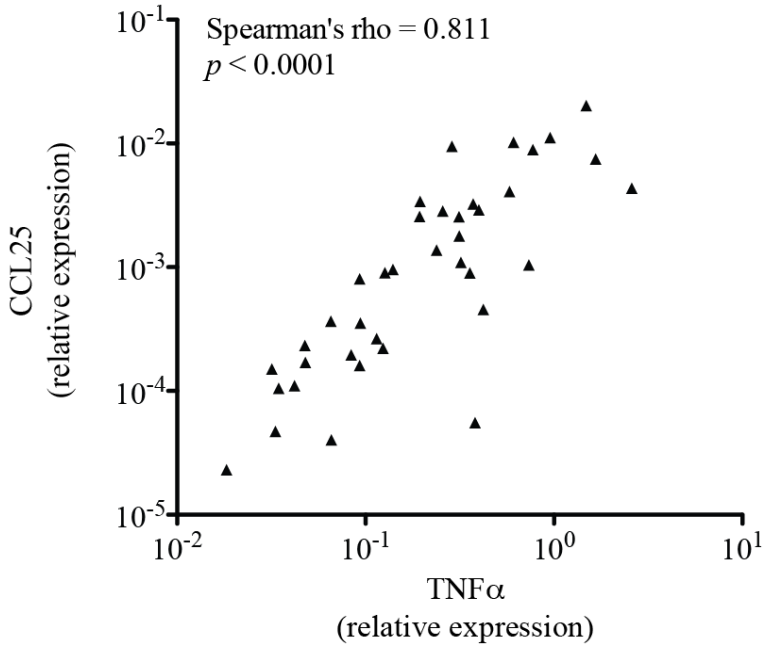

Figure 3.11: Correlation between colonic *CCL25* and *TNFα* expression in UC
Good correlation was observed between *CCL25* and *TNFα* gene expression in colitis (data expressed relative to *GUSβ*). Spearman's rank correlation coefficient was selected over Pearson's given that the scatter of *CCL25* values did not conform to a Gaussian distribution.

3.2.4 CCL25 expression at the protein level by western blotting

The presence of CCl25 gene transcripts in the colon of patients with UC may not necessarily translate to increased protein. To address this issue, protein lysates were made from the bowel resection specimens (described in Section 3.2.3.1) and CCL25 quantified using western blots. Colonic protein lysates were run in parallel to that derived from small bowel as a positive control and recombinant human CCL25 (rCCL25) (Figure 3.12).

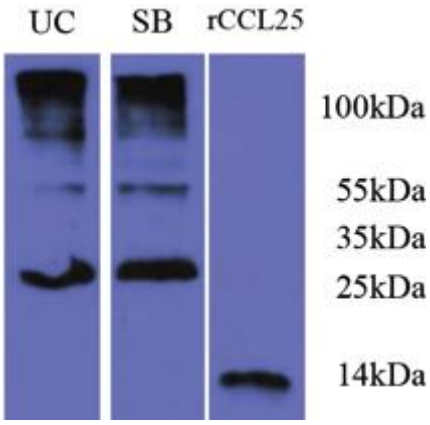

Figure 3.12: Western blot for CCL25
Representative western blot probing for CCL25 in a colonic protein lysate derived from a patient with ulcerative colitis (UC). Small bowel (SB) sample from the same patient run in parallel. Additional positive control provided by recombinant (r)CCL25. Using a standard protocol resulted in bands that can be deemed positive albeit multimeric variants of protein, but also not-specific 'smears' which precluded effective interpretation.

A notable technical issue was the degree of protein self-association, resulting in appearance of multiple bands of various sizes and 'smearing' on the film. Thus, positive protein bands could not be discerned from those that were non-specific, such as those ~100 kDa. To overcome this issue, 8 M urea was used as a chaotrope in the sample buffer to destabilise hydrophobic bonds and increased protein solubility [349,357]. However, this did not result in appearance of any bands which could be deemed specific for CCL25.

Chemokines in biological samples are often found at very low levels in tissue and their propensity to multimerise is well described [339]. Therefore a prior immunoprecipitation step was adopted in order to enrich and purify the protein from tissue lysates. The IP step used a polyclonal goat antibody raised against human CCL25 for pull-down, with mouse monoclonal anti-hCCL25 for detection. This approach resulted in successful enrichment of colitis tissue for protein at the expected size for a CCL25 dimer (~28 kDa); supported by a similar appearance using small

bowel lysates, as well as purified rCCL25 protein not subject to immunoprecipitation (Figure 3.13). An additional albeit distinct band size was also detected at ~56 kDa, possibly corresponding to a persistent tetrameric variant of human CCL25. Little expression was detected in NC and maximum film exposure time (30 minutes) was required for visualisation of even faint CCL25 signals and in some cases CCL25 was absent (2/6 NC samples). As expected, no bands were detected in the cleared lysate when probing for CCL25 (rCCL25 run simultaneously as positive control).

The total band densities (monomers + multimers per sample) were quantified relative to a housekeeping protein using ImageJ software as indicated in Chapter 2, and differences between NC and UC were tested for statistical significant (MW test). To take into account the use of immunoprecipitation to extract CCL25 prior to gel loading, unbound housekeeping protein was assessed in the matched, cleared lysate remnant. β-actin was selected as a reference based on prior evidence of stability between human large bowel specimens independent of inflammatory activity [358,359], although variation has been reported between colon and small bowel specimens. A statistically significant difference in CCL25 protein expression between UC and NC samples was evident (Figure 3.14).

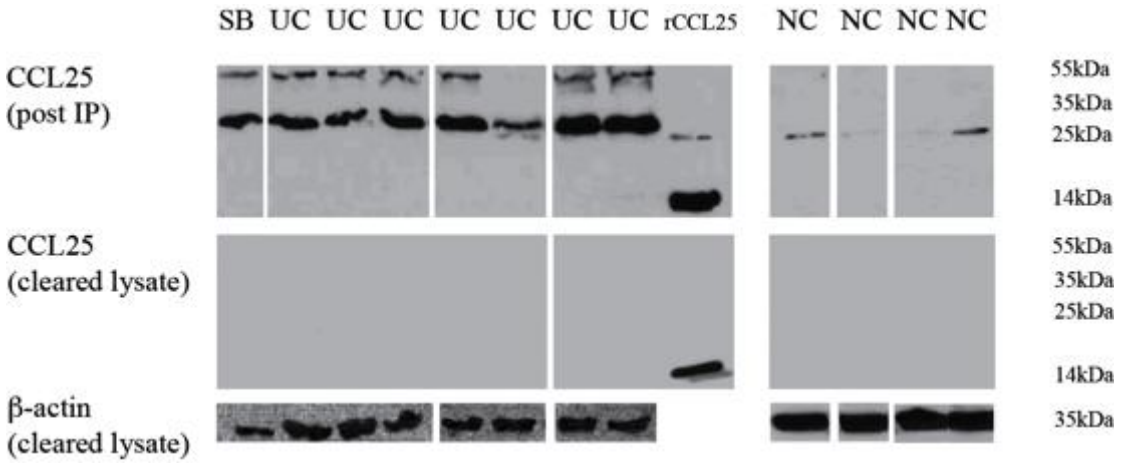

Figure 3.13: Western blots for CCL25 – post immunoprecipitation (IP)

Summary of western blots probing for CCL25 (post-IP samples and paired cleared lysates) and β-actin (cleared lysate only). rCCL25 was run with the cleared lysate as an in-run positive control. All membranes probing for CCL25 were exposed between 0.5 minutes (sufficient for SB, n=3; UC, n=7; and rCCL25, n=1) with increasing intervals up to 30 minutes (in n=4/6 NC specimens) until bands were visible. Membranes corresponding to cleared lysate in which housekeeping protein was probed were exposed for no more than 60 seconds. Breaks in the image represent where samples were run non-contiguously.

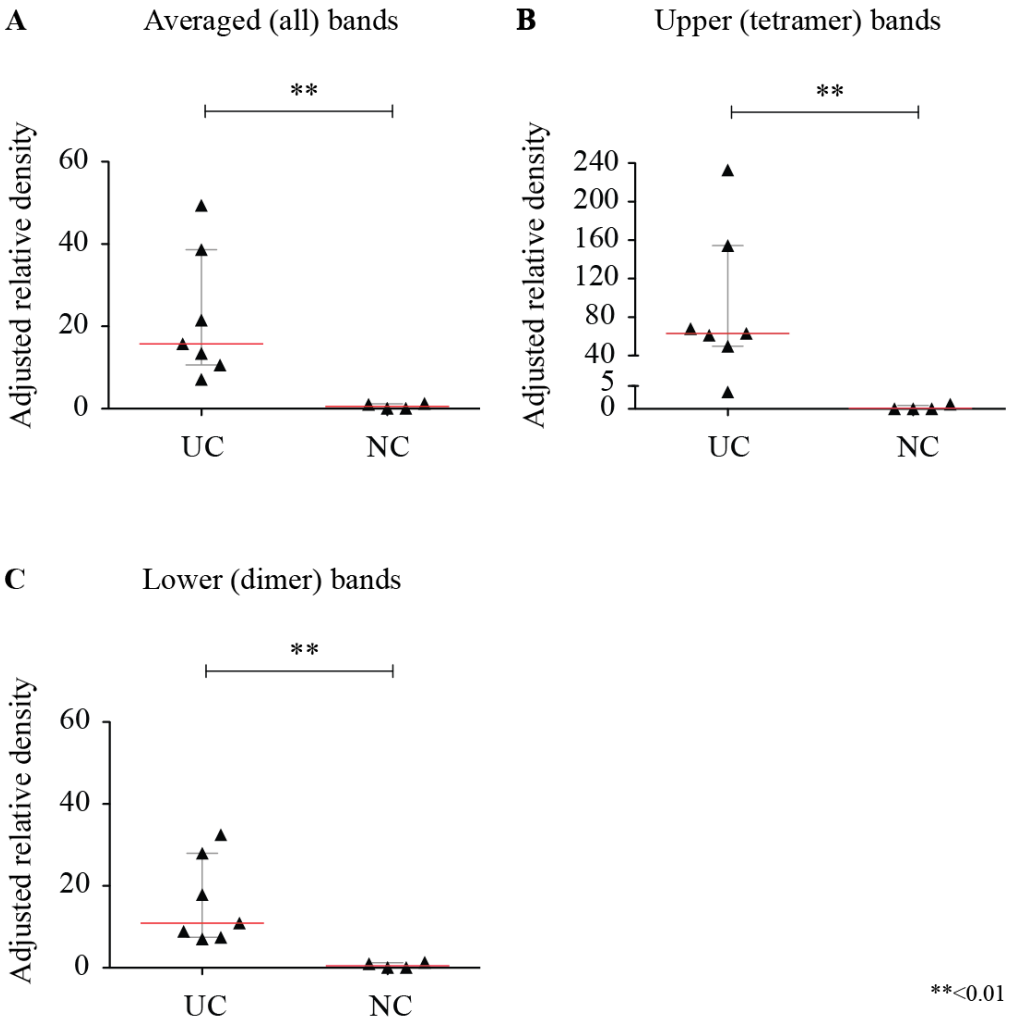

Figure 3.14: Relative CCL25 protein expression in NC and UC

Semi-quantative analysis of CCL25 protein expression by ImageJ analysis. Results presented for the sum of weighted average of all multimer bands in a given sample (A), the upper, tetrameric band only (B) and lower, dimeric bands only (C). All values are expressed relative to housekeeping protein (β-actin) and normalised to a sample of NC that demonstrated a positive CCL25 band in the dimeric position. 2/6 NC samples did not exhibit any detectable bands and were not included in the analysis. Data presented as median and IQR. Capped lines and asterisks indicate statistical significance with the MW-test.

3.2.5 Measurement of CCL25 concentration by ELISA

To confirm these findings, CCL25 concentrations were quantified using a tissue-lysate ELISA. CCL25 concentrations in tissue were significantly greater in UC than NC specimens, consistent with the findings using western blotting (Figure 3.15).

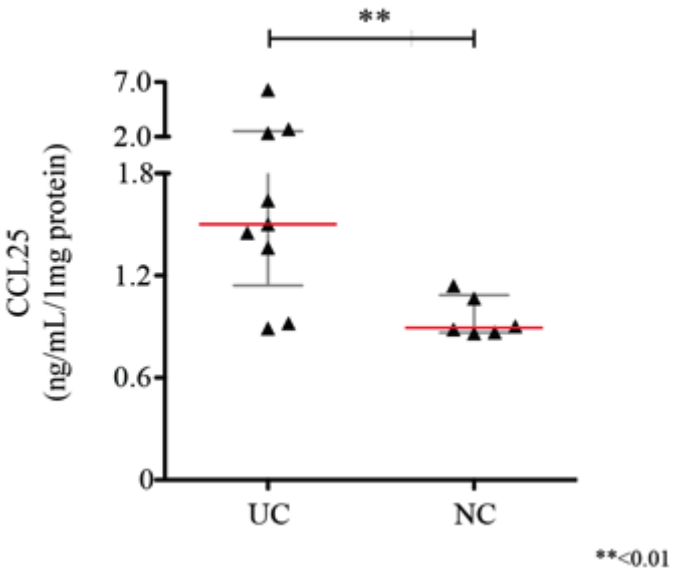

Figure 3.15: CCL25 concentration in human colon by ELISA
Quantitative measurement of CCL25 protein concentration in colonic tissue lysates pertaining to UC and NC. Plots representative of median and IQR; capped lines and asterisks indicate statistically significant differences (MW test).

3.2.6 Chemokine immunohistochemistry

Next, attempts were made to locate the protein in tissue sections using immunohistochemical staining on SB frozen tissue sections (positive control); however, no staining was observed despite antibody titration (1:25 – 1:200) of three separate antibodies (detailed in Chapter 2). As a consequence, subsequent efforts focussed on identifying CCL25 in FFPE sections, but this yielded no positive staining with either mouse monoclonal or rabbit polyclonal antibodies after standard heat–

induced epitope retrieval across a range antibody titrations and varying pH citrate buffers (*p*H 6.0, *p*H 8.0 and *p*H 10.0 tested). This was unexpected given the positive results obtained by others staining in the human liver [127]. Papadakis *et al*. have previously reported successful staining in the small bowel using antibody clone LS202 5A9 (mouse IgG1 [123,343]); however, this product has now been discontinued and is no longer available.

Further attempts were made using proteinase K antigen retrieval; however, any staining was non-specific in nature (mouse monoclonal IgG1κ, clone 1.2_4G-1G4-1C9 with no differences with control antibody of matched isotype. On reducing the antibody concentration, staining of any description was no longer apparent. A senior pathologist reviewed all stained sections. As a result of persistently negative staining in the small bowel, immunohistochemistry in colitic material was not pursued further.

3.3 Discussion

Recruitment of mucosal T-cells to the liver in response to aberrantly expressed homing signals has been proposed to drive hepatobiliary inflammation in primary sclerosing cholangitis. This is exemplified by the 'gut-homing' chemokine CCL25, which recruits intestinal $CCR9^+$ effector cells to the PSC liver. However, previous studies report CCL25 expression and $CCR9^+$ lymphocytes as being confined to the small bowel whereas PSC is typically associated with colonic inflammation.

The data presented herein illustrate enrichment of $CCR9^+$ tissue-infiltrating lymphocytes in patients with colitis relative to non-inflamed colon. This population are predominantly $CD3^+$ $CD4^+$ T-cells, bear cell surface markers indicative of an activated effector phenotype, and are manifest in the context of active microscopic inflammation in the absence of macroscopic colitis. Quantitative real time PCR was performed using genetic material of standardised concentration, measured quality, intron-spanning primers and reference genes of proven stability between non-inflamed colon and across varying degrees of inflammatory activity. Although CCR9 gene expression was not evident within whole colonic mucosa, transcription of the ligand *CCL25* was increased in UC versus NC and correlated with inflammatory burden. Associations between patient age, colonic biopsy site and medication regimen were not detected, although a greater degree of *CCL25* expression was noted in women relative to men this was lost on multivariate evaluation, being outweighed by the effect of colonic inflammatory activity. Moreover CCL25 was detectable at the protein level by western blotting; results substantiated through tissue ELISA.

3.3.1 Enrichment of CCR9$^+$ lymphocytes in colitis

The priming of intestinal lymphocytes during activation endows specific trafficking properties through imprinting of adhesion molecules and chemokine receptors, thus directing migration to specific tissues and microenvironments [344,356,360,361]. Selective induction of T-cells by DC from MLN or Peyer's patches confer CCR9 expression [57,296,362] which plays a critical role in recruitment through interactions with mucosal CCL25 [123,142,148,343]. Much evidence especially in mice suggests this applies only to SB and not to the colon. Early studies revealed CCR9 restricted to CD4$^+$ and CD8$^+$ lymphocytes infiltrating the intestine, wherein receptor expression was near universal (>90%) amongst IEL and LPL populations within the jejunum [142]. In contrast, relatively few (~25%) T-cells infiltrating the non-inflamed human colon were seen to be CCR9 positive, and a virtual absence of CCR9$^+$ T-cells was illustrated at other sites including chronic hepatitis C virus (HCV) infected liver. Moreover, only SB-derived lymphocytes were seen to undergo chemotaxis towards CCL25 in transwell migration assays [123]. In a similar vein, works from the Mt. Sinai group demonstrated that >60% of CD4$^+$ T-cells infiltrating the terminal ileum are CCR9$^+$ under homeostatic conditions although relatively fewer (~30%) CD4$^+$ CCR9$^+$ cells were detected during active Crohn's disease [343]; findings substantiated in murine models of small bowel inflammation [145]. The latter phenomenon was put down to preferential activation-induced cell death (AICD) following recruitment of CCR9$^+$ lymphocytes to the inflamed SB mucosa, and subsequent cell isolation and *in vitro* culture techniques.

Investigators in the field therefore suggest that few CCR9$^+$ lymphocytes infiltrate the colon (144,343), a hypothesis stemming from three observations: the first relates to

cultured T-cells isolated from MLN in which ~5–10% of colonic $CD3^+$ lymphocytes expressed CCR9 irrespective of inflammatory status; second, relatively fewer peripheral blood circulating $CD4^+$ T-cells expressed CCR9 in patients with colonic versus small bowel Crohn's disease; and finally, qualitative assessment through northern blotting was unable to detect CCR9 mRNA in colonic tissue. The same group report that only a small proportion of $CD3^+$ lymphocytes isolated from colonic mucosa express CCR9 [123], although only non-inflamed segments of the bowel were studied. Nevertheless, upregulation of CCR9 expression gauged by median fluorescence intensity (MFI) has been reported on subsets of $CD3^+$ T-cells and $CD14^+$ monocytes in the peripheral circulation of a small number of UC patients [363,364]. Subpopulations of IL-17^+ $CCR9^+$ γδ T-cells have also been described in extraintestinal inflammation [365], and a significant increase of circulating γδ T-cells in patients with UC (~20%) are seen to be $CCR9^+$ compared with healthy volunteers (~4% [366]).

I was able to replicate findings of prior studies with regard to $CCR9^+$ T-cell frequency in the small bowel, although proportions in the non-inflamed human colon were lower than expected. However, a selective enrichment of $CCR9^+$ lymphocytes, predominantly $CD4^+$ T-cells, was observed in the context of active colonic inflammation as gauged by flow cytometry. These observations do not contradict results of prior investigators *per se*, but rather represent an exploration of tissue-infiltrating populations obtained directly from active colitis as opposed to *in vitro* cultured MLN-derived T-cells, lymphocytes from peripheral blood or non-inflamed colon. That $CCR9^+$ lymphocytes are detectable in aspects of the colon wherein only microscopic activity was evident implies that such an infiltrate develops early in the

inflammatory response. The Samp1/YitFc model of murine ileitis mirrors this observation, wherein numbers of small bowel $CCR9^+$ T-cells infiltrate early in the disease course [145]. A detailed immunohistochemical assessment of chemokine receptors in normal versus inflamed human colon supports these findings, demonstrating overexpression of CCR9 in inflamed areas of IBD relative to NC utilising the same antibody clone exploited herein for flow cytometry [367], although cell-type expression was not reported.

Despite the detection of a $CCR9^+$ T-cell infiltrate there was little suggestion of *CCR9* mRNA expression in the inflamed colonic mucosa (examined *in toto*) as assessed using qRT-PCR. Cell-sorted populations of T-cells would be required to comprehensively evaluate chemokine receptor transcription [349]; the absence of such evaluation representing a limitation to my work. Reports from China and Sweden demonstrated increased *CCR9* gene expression in a limited number (n=10 and n=3 respectively) of colonic biopsies obtained from patients with UC suggesting that further study is commanded. The capacity to imprint CCR9 on naïve T-cells was not the focus of this project, but as previously discussed (please see Chapter 1) this function is dependent upon generation of all-trans retinoic acid (ATRA), and largely restricted to APC harbouring intrinsic RALDH activity [368]. Human colonic biopsy supernatants have been shown to induce expression of gut-homing markers β7 and CCR9 as well as CD103 on co-cultured peripheral blood-derived DC [369]. $CD103^+$ DCs can imprint gut-tropism on T-cells where they predominantly induce a tolerogenic phenotype in both mice and humans [128,370–372], undergoing relative loss in patients with active colitis [373]. APC from the inflamed colon exhibit increased production of retinoic acid [374] and an ability to imprint CCR9 on

stimulated T-lymphocytes has not been discounted [373]. A recent study by Sanders *et al*. illustrate that percentage RALDH activity as assessed by the Aldefluor assay was significantly up-regulated in both inflamed small and large bowel-derived myeloid DC, as well $CD103^+$ and $CD103^-$ DC subtypes and $CD14^+$ intestinal macrophages [374]. The capability of colon-derived APC to imprint T-cells with a gut-tropic phenotype therefore supports the existence of an intra-colonic $CCR9^+$ T-cell population in patients with active colitis.

A growing body of data suggests that substrates for RALDH activity may originate from a pool of biliary retinoids delivered by the liver [126], and that HSEC also possess capacity to imprint α4β7 and CCR9, at least in mice [174]. Murine HSEC contain functionally active RALDH1 and RALDH4 isoforms and induce a gut-tropic phenotype on $CD4^+$ T-cells to a similar degree as co-culture with MLN DC. Moreover, HSEC primed T-cells exhibit preferential recruitment to the intestine in migration studies [174]. These additional concepts of enterohepatic lymphocyte circulation, yet to be validated in humans, could plausibly explain the clinical coincidence of dual pathogenesis between gut and liver inflammation.

3.3.1.1 Phenotyping

Colon-infiltrating $CCR9^+$ T-cells were predominantly $CD4^+$ $CD127^{hi}$ $CD25^-$, and although an exhaustive assessment of cytokine profile or putative cell-surface functional markers was not conducted, this suggests an activated effector phenotype. The Mt. Sinai group report that only a few intestinal $CCR9^+$ T-cells express CD25, co-stimulatory molecules OX40 and CTLA-4 (also a cell surface marker of T_{reg}) and instead exhibit high expression of CD45RO and CD69 [144], consistent with

activated memory cells in the quiescent state. In contrast $CCR9^+$ T-cells isolated from Crohn's disease patients conform to a T_h1 and T_h17 profile [123,144] suggesting a pro-inflammatory phenotype in IBD. In the PSC liver, a long-lived population of gut-tropic memory $CCR9^+$ T-cells are also activated effector cells as evidenced by secretion of IFNγ, although in this setting $CCR9^+$ T-cells predominantly comprised a $CD8^+$ (~60%) as opposed to $CD4^+$ (35%) population [127].

3.3.2 Colonic CCL25 expression

Having identified an increased frequency of $CCR9^+$ lymphocytes in the large bowel of patients with colitis, I next investigated whether the ligand CCL25 would also be present. CCL25 is selectively expressed on murine and human small intestinal epithelial cells [142,375]; however, epithelial-expressed chemokines may diffuse to, and be presented on, vascular endothelium [144,376]. *CCL25* is highly expressed at the genetic level in small intestine, as evidenced by early studies using northern and Southern blots [361,375,377] but not the colon. However, expression studies of *CCL25* have largely examined the large bowel under non-inflammatory conditions. A parallel has been observed in murine settings, wherein *Ccl25* gene expression assessed via qRT-PCR was detected in the small bowel of wild type mice [79,345,378] as well as the Samp1/YitFc model [145]. With regard to the latter, transcription was preserved in early and chronic stages of ileitis, but absent from the large bowel despite development of a caecitis in older age groups. Similar results are reported in the $TNF\Delta^{ARE}$ model of SB Crohn's [146], $Rag2^{-/-}$ mice [147] and studies in higher order mammals such as pigs [379].

Expression of *CCL25* transcripts is evident in murine colitis induced by dextran sulphate sodium, DSS [380,381], as well as oxazolone [382]. Moreover, a paper published earlier this year reported CCL25 mRNA expression in human colitis in a small number of patients (n=10) undergoing colonoscopy [382]. Similar claims stem from the Karolinska Institute in Sweden where qRT-PCR performed in 3 colonic biopsy samples showed *CCL25* expression augmented with corticosteroid therapy [363]; however, it is unclear why only 3 specimens were examined in the latter given a starting population in excess of 50 patients. We extended these observations to show a correlation between colonic *CCL25* gene expression and inflammatory indices across a large sample size associated with detectable CCL25 protein and a $CCR9^{+}$ colon-infiltrating effector T-cell population. This is particularly pertinent given the correlation between inflammatory burden and colorectal cancer (CRC) risk in patients with colitis ± PSC, and the recent discovery of CCL25–CCR9 in meditating colonic tumour growth, invasion and metastasis [383].

Only two groups have reported direct visualisation of intestinal CCL25 protein by immunohistochemistry with "patchy" staining detected over the small intestinal crypts in close proximity to areas of lymphocyte infiltration [123,142,343]. Only one published study looked at CCL25 staining in active colonic inflammation (Crohn's colitis) [343]. The Human Protein Atlas (http://www.proteinatlas.org/ ENSG00000131142-CCL25/tissue) report positive staining in small but not large bowel; however, only normal (non-inflamed) human tissue was used to create the profile, and the reported reliability was deemed "uncertain" as only one antibody was tested. Certainly my own attempts at immunohistochemical staining (using small bowel as a positive control) with three different antibodies and varied epitope

retrieval steps did not yield any consistent staining in the positive control (SB) tissue precluding the use of immunohistochemistry in the colon. Unfortunately the previously tested antibodies claiming positive staining in the SB are no longer commercially available.

A lack of detectable CCL25 immunohistochemical staining could be due to the patchy nature of CCL25 expression in the intestine, or factors affecting chemokine presentation and cleavage from the epithelial and endothelial surface. Chemokine function is heavily governed by binding to matrix components such as glycosaminoglycans and proteoglycans on the cell surface, which may be affected *in vitro* by tissue processing, epitope retrieval, enzymatic digestion and wash steps. Endothelial cells express atypical chemokine receptors which act as molecular decoys to remove and degrade chemokines [384]. Such variation in endothelial chemokine receptor expression and cell surface glycosaminoglycan composition may explain the observed difficulties with chemokine immunohistochemistry.

Nevertheless, the western blot and ELISA data presented here clearly indicate CCL25 expression at the protein level in colitis but not in NC samples supportive of colonic CCL25 expression being associated with active inflammation. These techniques were not without obstacle, however. Clear bands on western blots were only visualised following prior immunoprecipitation. This yielded clear bands albeit of 2 – 3 distinct sizes. Reassuringly, such a pattern was observed in small bowel and with recombinant human CCL25, suggesting the staining is specific and a consequence of the presence of chemokine multimers [339]. Validation of CCL25 protein expression was provided through ELISA.

A remaining question is which cell-type produces CCL25 within the large bowel? CCL25 is secreted and expressed by small bowel epithelium; specifically the crypts of Lieberkuhn and intestinal villi [142]. However CCL25 can also be detected on the surface of certain APC [377]; and detection of protein expression on liver sinusoids in patients with PSC implies that CCL25 is either locally secreted or captured from blood and presented on the surface of endothelial cells [376]. Given the inherent difficulties with chemokine immunohistochemistry, alternative methods at visualisation in tissue may be required. *In-situ* hybridisation has been trialled by one group [142], but as with prior immunohistochemistry efforts these attempts were restricted to small bowel and non-inflamed colon, and did not reveal any positive staining in the latter.

3.3.3 Therapeutic considerations

Activation of the CCL25/CCR9 axis is responsible for many functions in the small intestine. Ligand–receptor binding fosters engagement of gut-tropic T-cells to CAMs such as VCAM-1 and MAdCAM-1 through $\alpha4\beta1$ and $\alpha4\beta7$, respectively [385,386]. Such interactions facilitate recruitment to the gut lamina propria and are pivotal in the development of gut cryptopatches. Secondary interactions result in dampening of CCR9 expression and up-regulation of CD103 on $CD8^+$ T-cells, promoting population of the intra-epithelial lymphoid compartment [345,387]. While $CD8^+$ T-cells rely on CCL25-CCR9 interactions to pass into the small bowel, entry of IgA-secreting B-cells and $CD4^+$ T-cells can occur through CCR9–CCL25 independent mechanisms [131,137].

A pathological role for the CCR9–CCL25 axis in IBD was first suggested by studies in which circulating $CCR9^+$ T-cells were detected in patients with active SB Crohn's [343], and paralleled by studies of murine IBD where expression of ligand and receptor were elevated in the context of active inflammation [145]. As previously discussed, immunoblockade of CCL25 and CCR9 in the Samp1/YitFc model tempered the induction of ileitis but with little effect on maintenance of remission, indicative of a role early in the mucosal inflammatory response. *Rag2*$^{-/-}$ mice which lack mature B- and T-lymphocytes develop spontaneous ileitis but are relatively protected from intestinal injury when crossed with a *Ccr9*$^{-/-}$ strain [147]. CCR9 expression has also been reported on T_{reg} and immunosuppressive plasmacytoid (p)DC [146,147,388,389] and upon adoptive transfer of $CD4^+$ T-cells, *Ccr9*$^{-/-}$ *Rag2*$^{-/-}$ mice develop SB intestinal inflammation, suggesting that a critical absence of non–T-cell $CCR9^+$ populations in this model is responsible for maintaining tissue tolerance, putatively $CD103^+$ $CCR9^+$ plasmacytoid DC and $CCR9^+$ T_{reg}. Furthering the argument, Wurbel *et al*. claim that CCR9–CCL25 interactions are critical for modulating protective responses against large intestinal inflammation. In acute [380] and chronic [384] models of DSS colitis, both *Ccr9*$^{-/-}$ *and Ccl25*$^{-/-}$ mice exhibited increased susceptibility to large bowel inflammation independent of T-cell colonic recruitment despite preserved T_{reg} development and function. Instead, these animals demonstrated augmented trafficking of innate immune subsets with pronounced accumulation of activate macrophages (acute model [380]) and increased $Gr\text{-}1^{hi}$ $CD11b^{hi}$ neutrophil populations infiltrating MLN and LP (chronic model [381]). Although the pDC population was unaffected in the chronic model, conventional $CD103^+$ ($CD11b^+$ and $CD11b^-$) subtypes are reduced in number following adoptive transfer of wild-type T-cells, supporting a tolerogenic role of conventional as well as

plasmacytoid DC in the murine colon. These changes were accompanied by an increase in $CD103^{-}$ $CD11b^{+}$ DC, a subset reported to increase the sensitivity of $CD4^{+}$ T-cell responses to bacterial antigens [390].

Given the pathological consequences of targeted deletion of CCR9 or CCL25 in murine models of colitis, Wurbel *et al*. raise concerns that therapeutic targeting could lead to detrimental effects in patients with IBD. Whilst congenital absence of ligand or receptor may prove harmful under specific circumstances, targeting the CCL25–CCR9 axis in the context of early, established disease could yield therapeutic benefit in patients with small and large bowel intestinal inflammation. An orally bioavailable CCR9 antagonist (CCX282-B; Chemocentryx, USA) was shown to not only inhibit chemotaxis of $CCR9^{+}$ T-cells *in vitro*, but resulted in near complete protection of intestinal injury in the $TNF\Delta^{ARE}$ model of murine ileitis [391]. Similar results were obtained in a hapten-induced colitis model, wherein a significant reduction of pro-inflammatory infiltrating iNKT-cells associated with disease improvement in mice exposed to oxazolone [382]. These results have been translated into phase-II clinical trials in which CCX282-B was well tolerated and resulted in a superior rate of remission in patients with (mixed small and large bowel) Crohn's disease at 52-weeks of therapy [151]. A recently published case report also details the successful treatment of a patient with refractory UC through CCR9 targeted leucapheresis [364] with clinical and endoscopic remission being associated with a dramatic reduction in CCR9 expression by MFI on circulating $CD3^{+}$ T-cells and $CD14^{+}$ monocytes.

Monocytes migrate into the intestinal LP via CCR2-dependent mechanisms, where they undergo differentiation into pro- and anti-inflammatory macrophages [392].

However, in T-cell mediated colitis differentiation is impaired and linked with a significant increase in pro-inflammatory subsets. Activated macrophages undergo chemotaxis along CCL25 gradients [377], and $CCR9^+$ macrophages induce acute liver inflammation in the concanavalin A model of acute hepatitis [393]. TNFα–producing $CCR9^+$ macrophages activate stellate cells during the initiation of CCl_4-induced liver injury and remain during liver fibrosis [140]; a process attenuated in the absence of CCR9. Increased tissue expression of CCR9 has also been reported in early, pre-invasive colorectal cancer [383], although this is disputed by other groups [349]. Nonetheless, colorectal cancer cells migrate in response to CCL25 chemokine gradients in transwell and Boyden chamber assays, and ligand expression is a prerequisite for metastasis in certain xenograft tumour models. This is noteworthy given the association between hepatobiliary inflammation and fibrosis, and colitis and pre-malignant potential in PSC-IBD. Extending therapeutic applications beyond small bowel disease may be effective, given the role of CCL25 and CCR9 in PSC lymphocyte recruitment, liver inflammation and fibrosis, colitis and colorectal cancer.

3.3.4 Summary

This chapter has shown CCR9 expression on the majority of colonic $CD4^+$ and a proportion of $CD8^+$ T-cells in colitis. Preliminary data suggest that these are effector T-cells, and their presence in patients with only microscopic colitic activity implies recruitment early in the inflammatory response. The cognate ligand CCL25 is overexpressed in the inflamed large bowel where expression correlates with inflammatory activity in UC patients.

4 Results II: Consequences of hepatic VAP-1 enzyme expression

4.1 Introduction

In chapter 3, data were presented showing an increased expression of CCL25 in colitis as well as an influx of $CCR9^+$ T-cells in the human colon associated with a greater inflammatory burden. The aberrant lymphocyte homing hypothesis of PSC proposes that $\alpha4\beta7^+$ $CCR9^+$ T-cells traffic from gut to liver in a process dependent upon hepatic endothelial expression of MAdCAM-1 and CCL25 [1,2,127,289,293], and that reactivation of effector memory populations bearing this phenotype drives hepatobiliary inflammation. The precise factors contributing to aberrant expression of normally 'gut-restricted' adhesion molecules in the PSC liver are incompletely understood. However, recent studies have demonstrated that deamination of certain amines catalysed by the enzymatic activity of VAP-1 can augment expression of functional CAMs on the endothelial surface in an NFκB-dependent manner [294,321]. Such amines can be derived from several sources, including foodstuffs and gut bacteria, which could traverse the 'leaky' inflamed gut in patients with colitis, entering liver via the portal circulation where they act as VAP-1 substrates.

In this chapter, tissue VAP-1 expression and enzyme activity is determined in the PSC liver and contrasted with other autoimmune liver diseases (PBC and AIH). Variations in enzyme activity with alternative substrate provision are also presented prior to addressing functional sequelae; specifically with regard to CAM expression and $\alpha4\beta7$ dependent adhesion to HSEC.

4.2 Findings

4.2.1 Hepatic VAP-1 gene expression

Gene transcription was measured using qRT-PCR on cDNA derived from human liver tissue (as described in Chapter 2). Unlike other solid organs, there is little published data on genes specific to human liver tissue which manifest stable expression (housekeeping) between aetiologies or conservation across varying degrees of inflammatory activity [337,338,394]. Therefore a calibration curve was created from known dilutions of a linearized plasmid encoding human VAP-1, in which quantification by copy number was pre-determined [214]. To ensure inter-experiment validity, near identical real-time PCR amplification efficiencies for the calibration curve as well as a sample of target cDNA were confirmed on every run prior to inter-plate comparisons.

Utilising the absolute quantification method, *VAP-1* gene expression was determined in cirrhotic, end-stage human liver diseases of parenchymal (AIH and alcoholic liver disease, ALD) and biliary (PBC and PSC) aetiology, and compared with that observed in resected non-diseased/non-cirrhotic liver (NL). The aim was to evaluate VAP-1 expression in PSC; with primary biliary cirrhosis being chosen as a comparator biliary disease and AIH and ALD as diseases characteristic of parenchymal injury. All starting mRNA concentrations were standardised and the qRT-PCR reaction performed using 100ng starting material run in triplicate wells. *VAP-1* gene expression was significantly greater in diseased versus non-diseased liver as assessed by the MW test (median 44,200 copies, IQR 29,400 – 77,925 copies vs. 22,100 copies, 3840 – 47,650 copies; $p = 0.028$). Probing differences further, the biliary diseases had more copy numbers than parenchymal injury (Figure 4.1) and

comparison of individuals revealed statistically significance differences between PSC and NL samples. Of note, there was marked spread within the different disease groups suggesting that many factors affect *VAP-1* transcription in human liver.

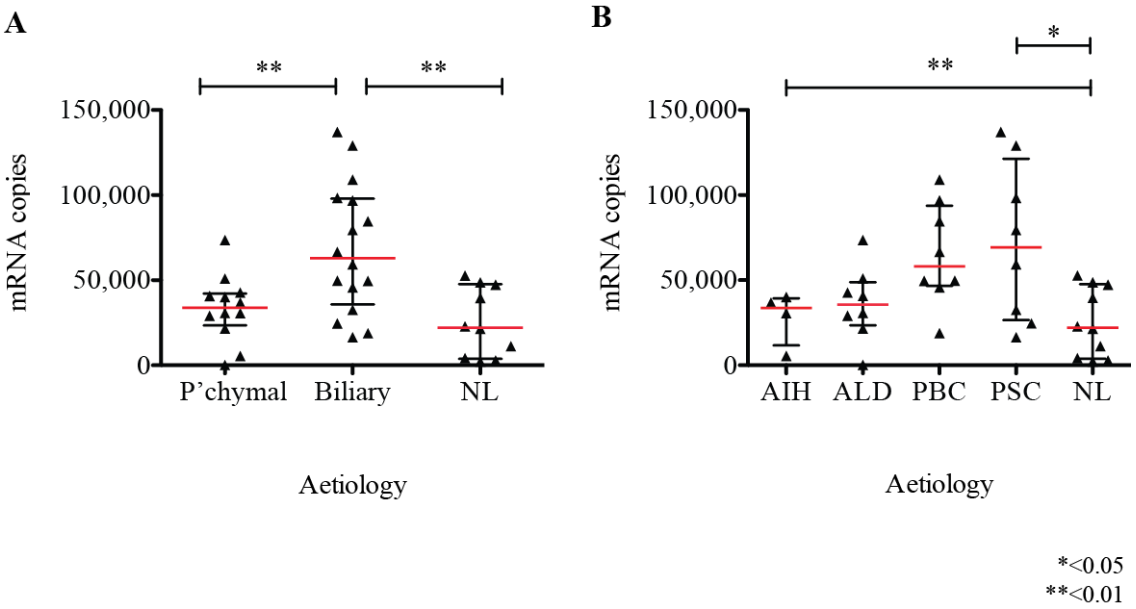

Figure 4.1: *VAP-1* gene expression in human liver

Absolute quantification of *VAP-1* gene expression in explanted liver tissue is presented. Aetiology grouped as parenchymal liver disease (median 33,750 copies, IQR 23,450 – 42,200 copies), biliary liver disease (62,900 copies, 35,800 – 97.925 copies) or non-diseased/non-cirrhotic liver (NL; 22,100 copies, 3,840 – 47,650 copies) (A); or according to individual diagnoses (B). Parenchymal diseases consist of autoimmune hepatitis (AIH: 33,700 copies, 11,715 – 39.274 copies), alcohol induced liver injury (ALD: 35,700 copies; 23,450 – 48,850 copies), and biliary diseases comprise primary biliary cirrhosis (PBC: 58,100 copies, 46,675 – 93,725 copies) and primary sclerosing cholangitis (PSC: 69.350 copies, 26,575 – 121,325 copies). Capped lines and asterisks indicative of statistical comparisons (*p* values according to KW-test and Bonferroni-Dunn post-hoc correction). In (B), the post-hoc test was conducted for PSC vs. all other aetiologies after the intitial KW-test.

4.2.2 VAP-1 immunohistochemistry

To determine whether differences in VAP-1 gene transcription between diseases were reflected at the translational level, protein expression in tissue sections was localised using immunohistochemistry. Snap-frozen tissue sections were prepared from explanted or resected human liver as detailed in Chapter 2, and stained using methods described therein.

In NL specimens, VAP-1 was largely confined to vessels and hepatic sinusoids. However, on qualitative assessment expression appeared markedly increased in all 3 autoimmune liver diseases; particularly PSC (Figure 4.2). Increased VAP-1 staining was seen in stroma and fibrotic scar tissue, as well as within neovascular structures in septa.

Colocalisation experiments using multi-colour confocal immunofluorescence were used to confirm cell-type specific VAP-1 expression in PSC liver. VAP-1 did not co-localise with biliary markers (portal bile ducts or proliferating bile ductules; Figure 4.3) but was colocalised with $CD31^{+}$ and particularly αSMA^{+}, indicative of endothelial and myofibroblast expression, respectively (Figure 4.4). Furthermore, despite the strong expression of VAP-1 and MAdCAM-1 on HSEC, these two adhesion molecules did not colocalise. VAP-1 exhibited predominantly a pericytic distribution, whereas MAdCAM-1 expression was largely restricted to a cytoplasmic pattern; as illustrated by Liaskou et al. previously [294].

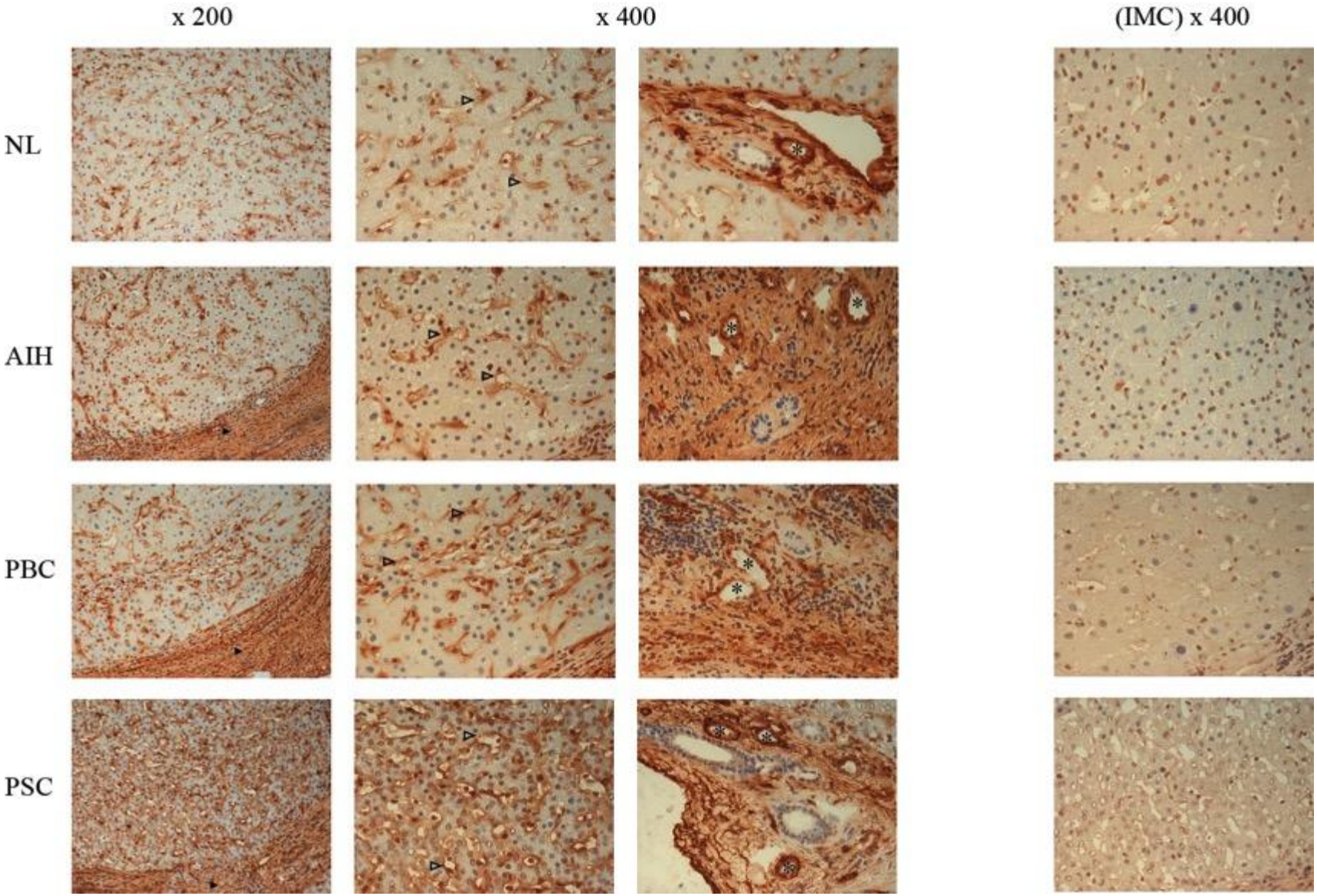

Figure 4.2: Tissue expression of VAP-1 in human liver – immunohistochemistry
Immunohistochemical staining of VAP-1 is presented for NL, AIH, PBC and PSC. ImmPACT DAB was utilised as chromogen. Filled arrowheads indicate fibrotic scar tissue. Examples of sinusoidal vessels are indicated by empty arrowheads; and intra-scar vessels by asterisks. IMC – isotype matched control.

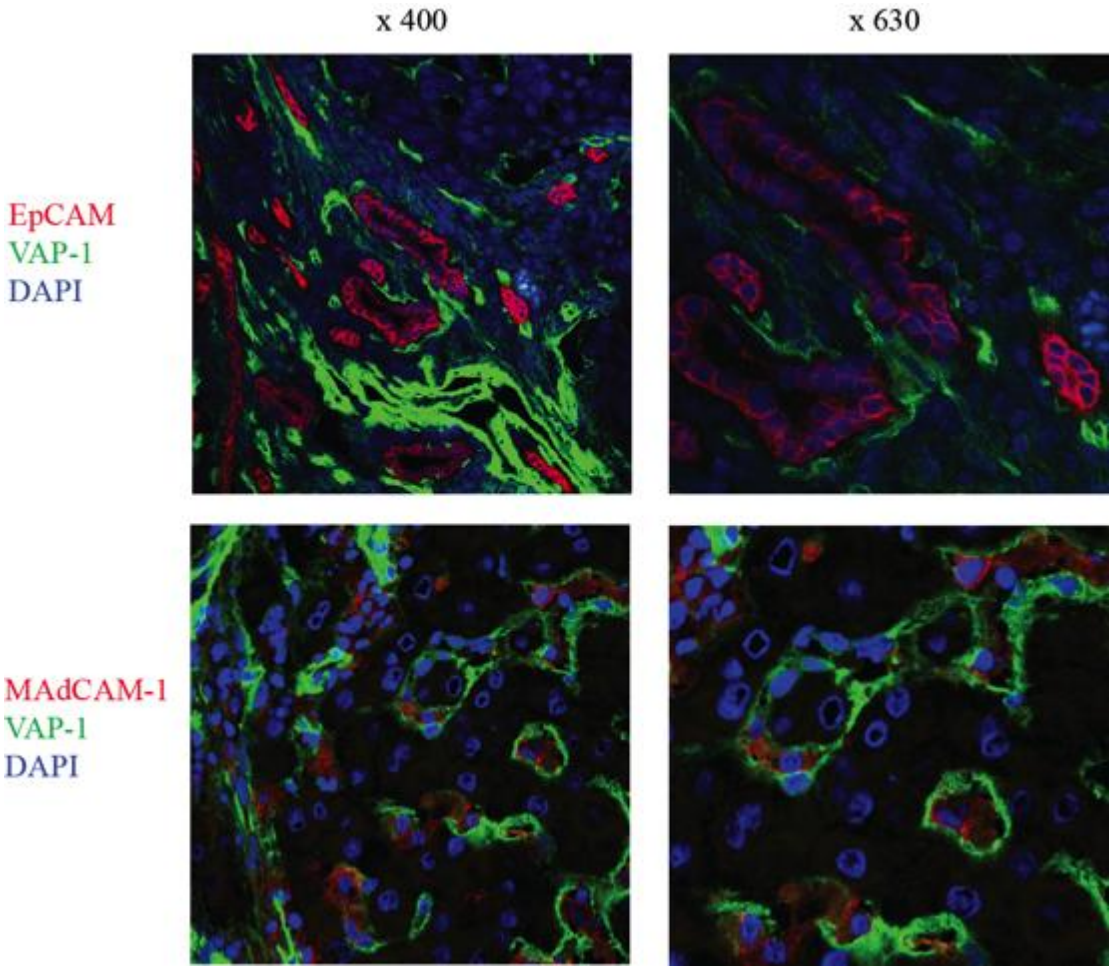

Figure 4.3: VAP-1 does not co-localise with biliary epithelium or MAdCAM-1
Co-expression of VAP-1 was investigated with the biliary epithelial marker (EpCAM) and with mucosal addressin cell adhesion molecule (MAdCAM)-1 via multi-colour confocal immunofluorescence in PSC liver.

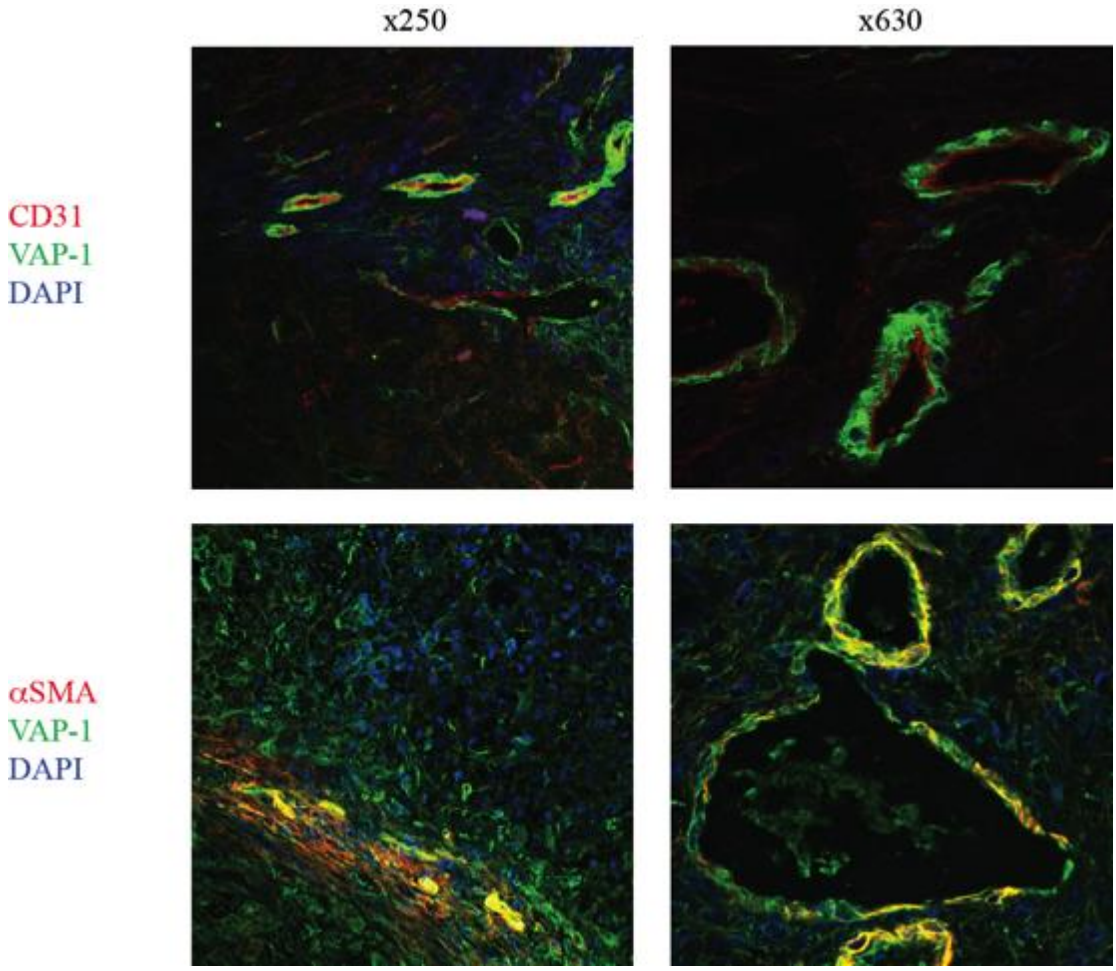

Figure 4.4: Co-localisation of VAP-1 in human liver
Multi-colour confocal immunofluorescence was conducted in order to confirm sites of VAP-1 expression in PSC liver. Cell-specific markers adopted are as follows: myofibroblasts, αSMA; endothelial cells, CD31; and nuclei staining, DAPI. VAP-1 staining was predominantly pericytic in the diseased liver: lower expression on endothelial vessels and the majority co-localisation being with αSMA positive cells.

4.2.3 Quantification of hepatic SSAO activity

Having illustrated VAP-1 expression in human liver, a comparative assessment of amine oxidase activity was performed between the three autoimmune liver diseases. Several methods have been described for quantification of amine oxidase activity; some rely on absorbance and are incompatible with measurements of activity in biological samples; whereas others require equipment not immediately attainable such as luminometers, oxygen electrodes or radiocarbon labelling of substrate [295,395]. Therefore the Amplex Red fluorescence-based method was chosen for my studies

given that it yields rapid, reproducible quantification of enzyme activity and was possible to conduct with available apparatus. This coupled reaction works on a principle wherein the rate of increase in fluorescence is directly proportional to the amount of H_2O_2 produced (detailed in Chapter 2).

The deamination of substrates by VAP-1 evolves H_2O_2, the rate of production of which was normalised to starting protein quantity in prepared liver tissue lysates and used as a surrogate for enzyme activity. Given the presence of other cellular and circulating amine oxidases in mammalian tissues, inhibitors of MAO-A and MAO-B where included in preliminary experiments. The Amplex red detection system can be subject to auto-oxidation over time, which may give rise to false-positive signals. Therefore to ensure a further level of control, parallel assays contained semicarbazide (ScZ) – a urea derivative which inhibits VAP-1 enzyme activity but not that of other amine oxidases and which gives rise to the classification of VAP-1 as an SSAO. The rate obtained from ScZ-containing wells was then subtracted from that of untreated samples to give a net/corrected value as detailed in Chapter 2. All enzyme activity values as thus presented as 'semicarbazide corrected' readings normalised to curve generated from serial dilutions of H_2O_2. Fixed concentrations of benzylamine (1 □M) and semicarbazide (250 μM) were used in all experiments unless otherwise indicated. Using this technique, statistically more VAP-1 enzyme activity was detected in PSC liver compared with PBC and AIH (Figure 4.5); in keeping with gene-expression studies.

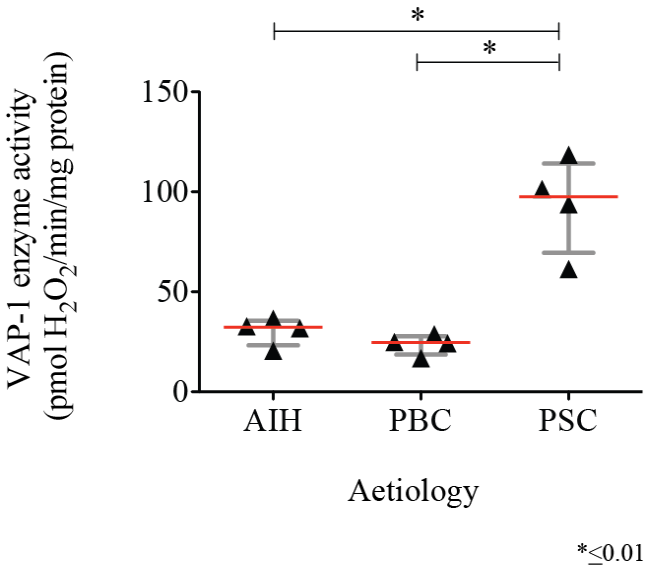

Figure 4.5: Tissue VAP-1 enzyme activity following MAO-A/MAO-B inhibition
Amine oxidase activity was determined in protein lysates extracted from explanted human liver. Values correspond to absolute amine oxidase activity in a given sample minus that of residual/background following addition of semicarbazide (VAP-1 enzyme inhibitor). Rates presented for AIH (32 pmol H_2O_2/min/mg protein, IQR 23 – 36 pmol H_2O_2/min/mg protein), PBC (25 pmol, 19 – 28pmol) and PSC (98 pmol, 70 pmol – 114 pmol). Each symbol represents one case (mean) of three technical replicates. Capped lines and asterisks indicative of statistically significant differences on post-hoc testing (KW-test with Bonferroni-Dunn post-hoc correction for multiple comparisons).

The necessary inclusion of several amine oxidase inhibitors and retained pigments from human liver may have effected the fluorometric readings And in order to overcome these potential confounders, a modification to the assay was made wherein tissue VAP-1 was first captured and immobilised from protein lysates using plate-bound VAP-1 antibody TK8-18, prior to addition of substrate and quantification of reaction rate (please see Chapter 2). This permitted exclusion of MAO-A and MAO-B inhibitors in the reaction although semicarbazide was still incorporated in parallel wells to confirm catalytic specificity, and enzyme activity results expressed as semicarbazide corrected values.

The use of this method increased the catalytic activity measurements threefold higher for each disease. This could be a consequence of improved orientation of VAP-1 for substrate binding to the active site compared with the enzyme being ‘freely’ mobile in

solution; or possible induction of conformational changes which increase enzyme activity. Nevertheless VAP-1 enzyme activity was validated as being significantly greater in PSC liver compared to lysates derived from AIH, PBC and NL specimens (Figure 4.6). As with gene expression experiments there was variability between patients in the different disease groups. Given clinical associations with IBD, VAP-1 enzyme activity was next measured in colonic protein lysates and VAP-1 enzyme activity was not significantly different in large bowel compared to PSC liver (Figure 4.6).

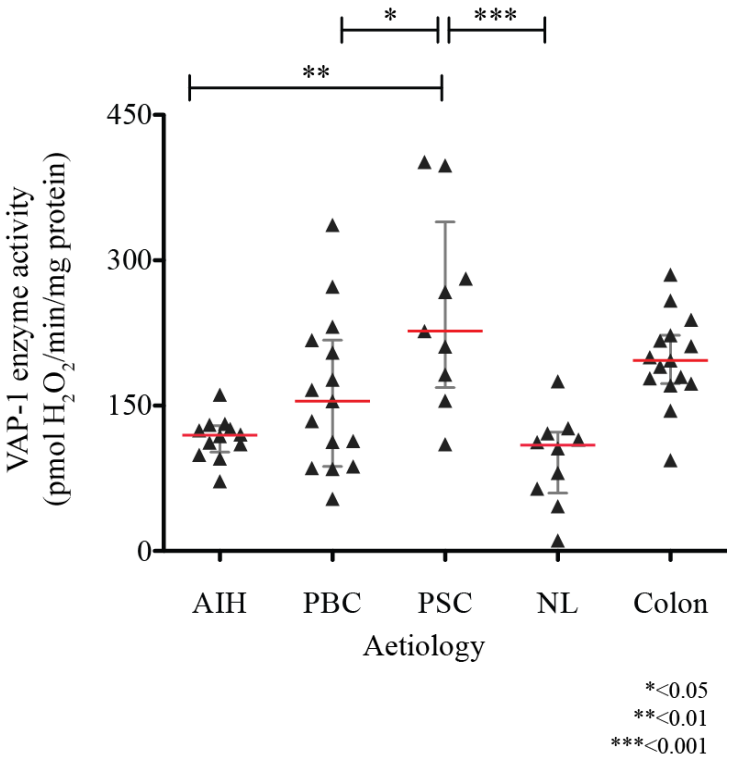

Figure 4.6: Tissue VAP-1 enzyme activity following capture and immobilisation
Enzyme activity was determined in protein lysates extracted from explanted human liver and colon following protein capture by immobilised antibody. Values correspond to absolute amine oxidase activity (in the presence of 1 mM benzylamine) in a given sample minus that of residual/background following addition of semicarbazide (250 μM). Each symbol represents one case (mean) run in technical repeats. Data presented for AIH (median 119 pmol H_2O_2/min/mg protein, IQR 102 – 129 pmol), PBC (155 pmol, 87 – 218 pmol), PSC (227 pmol, 169 – 340 pmol), NL (109 pmol, IQR 60 – 123 pmol) and colon (197 pmol, 173 – 222 pmol). Capped lines and asterisks indicative of statistically significant differences on post-hoc testing via the Bonferroni-Dunn method (KW-test, p <0.001).

4.2.4 VAP-1 enzyme activity promotes α4β7/MAdCAM-1 dependent adhesion

Having detected increased enzymatically active VAP-1 in PSC liver, I next investigated the putative functional consequences. Previous work from our group has illustrated an up-regulation of α4β7/MAdCAM-1 dependent adhesion to HSEC under flow following stimulation with TNFα, which was enhanced by provision of the VAP-1 substrate methylamine [294]. I was able to reproduce these findings in a similar flow-based adhesion assay, wherein HSEC stimulated with TNFα and methylamine (MA) supported adhesion of the $\alpha4\beta7^+$ JY (β-lymphoblastoid) cell line to a greater degree than when treated with TNFα alone (Figure 4.7), although differences were only apparent using 100μM methylamine rather than 50 μM as described by Liaskou *et al*. (detailed in Figure 4.17). No adhesion was observed when endothelium was treated with amine alone, suggesting that a pro-inflammatory environment is required for MAdCAM-1 expression on HSEC

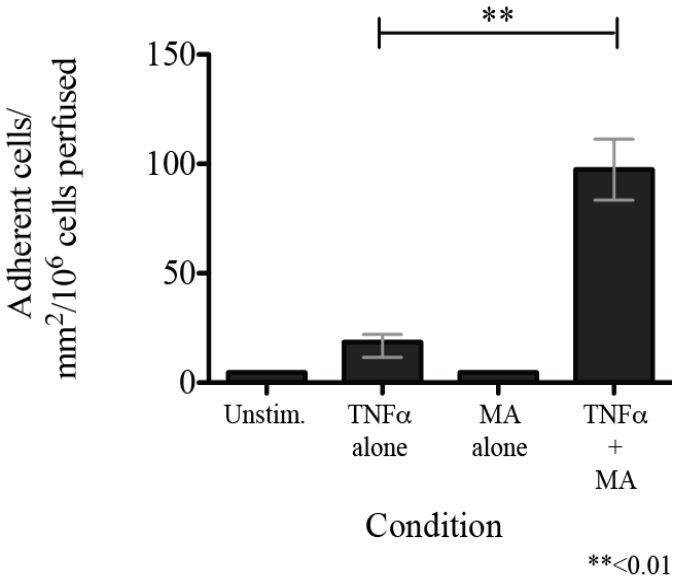

Figure 4.7: Flow adhesion assay of $\alpha4\beta7^+$ JY-cells over stimulated HSEC
α4β7-expressing JY-cells were perfused over HSEC under flow rates simulating physiological shear of human liver. The degree of lymphocyte adhesion was assessed following HSEC treatment conditions as indicated for 4 hours (TNFα, 10 ng/mL; MA 100 μM). Data representative of the mean (±SD) of 3 independent experiments using different isolates of HSEC (10 recorded fields of view in each); capped lines and asterisks indicative of statistically significant differences (Friedman matched sample test with Dunn's post-hoc correction).

To study the effects of VAP-1 inhibition on α4β7-dependent adhesion and transmigration, I obtained a purified population of $\alpha4\beta7^+$ T-cells from peripheral blood. This was necessary as transmigration of JY-cells across HSEC was not observed possibly because they are large blast cells and show defective migration responses through an endothelial cell monolayer *in vitro*. Using fluorescence-activated cell (FAC)-sorting, I was able to enrich a T-lymphocyte population to over 90% purity from peripheral blood for use in downstream flow adhesion assays (Figure 4.8).

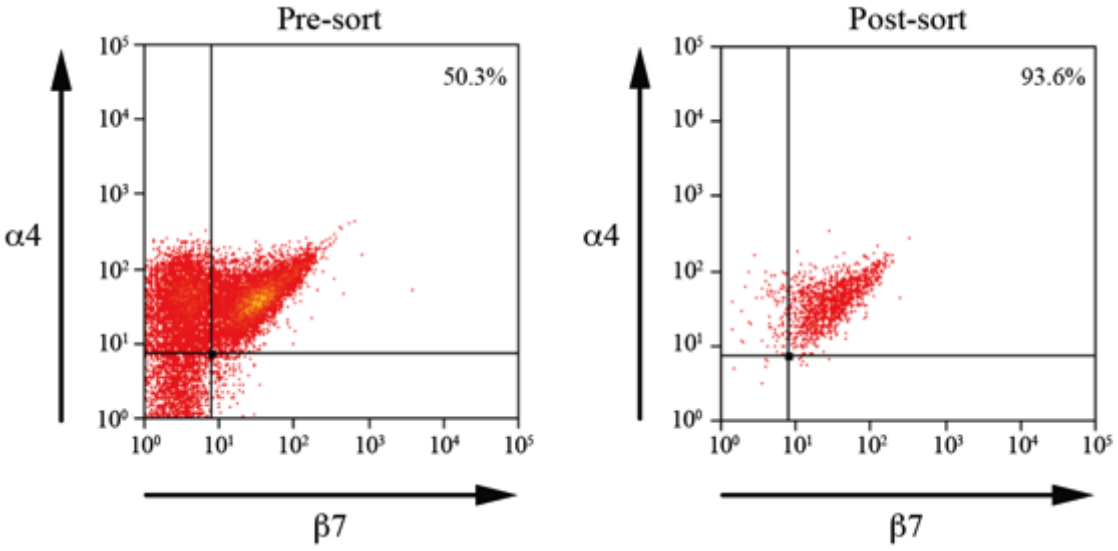

Figure 4.8: Fluorescence activated cell-sorting of $\alpha4\beta7^+$ T-cells
α4β7 positive lymphocytes were sorted from peripheral blood following gating on forward scatter (FS,) side scatter (SS), CD3+ (not shown); and subsequently α4 and β7. Post-sort purities were routinely >90%, and sorted cells maintained in RPMI +10% FBS +1% PSG for 24 hours. to allow surface receptors to recycle, prior to downstream application.

Transmigrated cells are easily distinguished from those that remain firmly adherent; the former appearing 'phase-dark' whereas the latter remain 'phase-bright.' To examine the effect of VAP-1 enzyme inhibition, semicarbazide was added at previously determined concentrations known to affect activity, whilst preserving HSEC viability (250 μM) [396]. The latter was confirmed herein through direct cell

visualisation following ScZ exposure and prior to each run of the flow adhesion assay.

Inclusion of ScZ to the HSEC media for the first hour of endothelial cell stimulation (TNFα/MA) was shown to inhibit $\alpha4\beta7^+$ T-lymphocyte adhesion by approximately 50% (Figure 4.9). ~25% reduction in adhesion was also evident using a neutralising VAP-1 antibody (TK8-14; 10 μg/mL); however, neither agent significantly affected migration. The latter suggests MAdCAM-1 is involved in adhesion but not transmigration in the lymphocyte adhesion cascade.

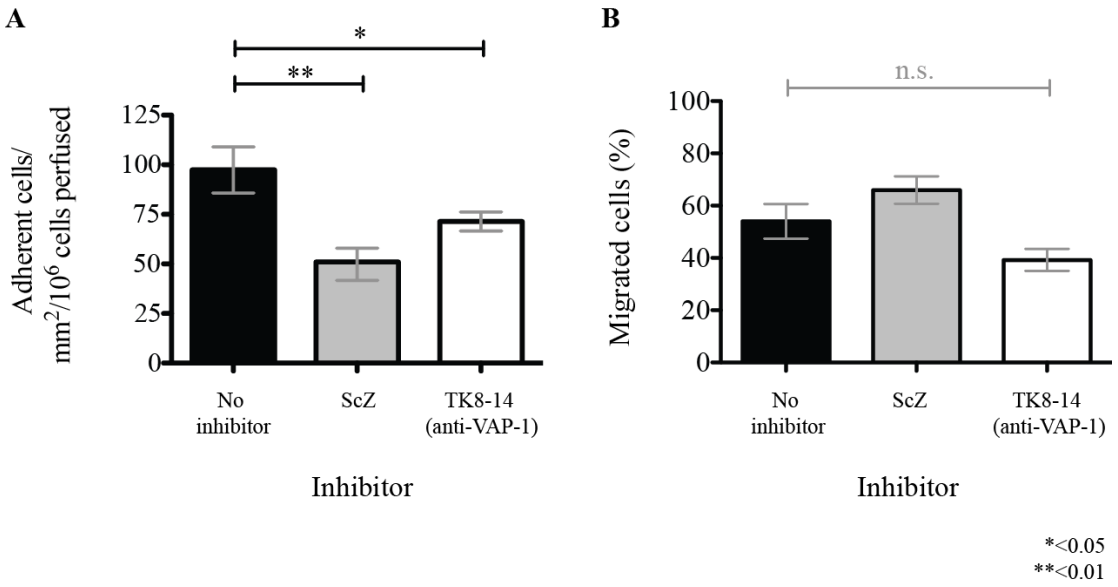

Figure 4.9: Flow adhesion assay of $\alpha4\beta7^+$ sorted cells over stimulated HSEC

$\alpha4\beta7^+$ sorted T-cells were perfused over HSEC under conditions simulating physiological shear in the human liver. The extent of lymphocyte adhesion (A) and transmigration (B) were assessed following HSEC treatment with TNFα (10 ng/mL) and methylamine (100 μM) ± inclusion of semicarbazide (250 μM) or neutralising antibody (TK8-14, 10 μg/mL). Data representative of the mean (± SD) of 3 independent experiments using different blood donors and different isolates of HSEC (10 fields of view each); capped lines indicative of statistical comparisons and asterisks highlight significant differences/*p* values between conditions (KW-test with with Dunn's post-hoc correction).

The effect of VAP-1 antibody on α4β7 T-cell adhesion was somewhat unexpected, for although this agent is a function-blocking anti-VAP-1 monoclonal antibody it is

reportedly devoid of enzyme inhibitory functions and therefore should not contribute to α4β7/MAdCAM-1-dependent attachment. The epitope on VAP-1 that is recognised by TK8-14 is not known. Therefore to confirm that binding of the antibody to VAP-1 does not impact on enzyme activity, assays were performed wherein increasing concentrations of rVAP-1 were incubated with 1 mM benzylamine and either TK8-14 (5 μg/mL, 1μg/sample) or semicarbazide (250 μM); the latter used as a positive control for 100% VAP-1 inhibition. Only a small, non-significant degree of enzyme inhibition was observed with TK8-14 – the extent of which was independent of rVAP-1 concentration (mean 17.5%; SEM 7.2%; Figure 4.10).

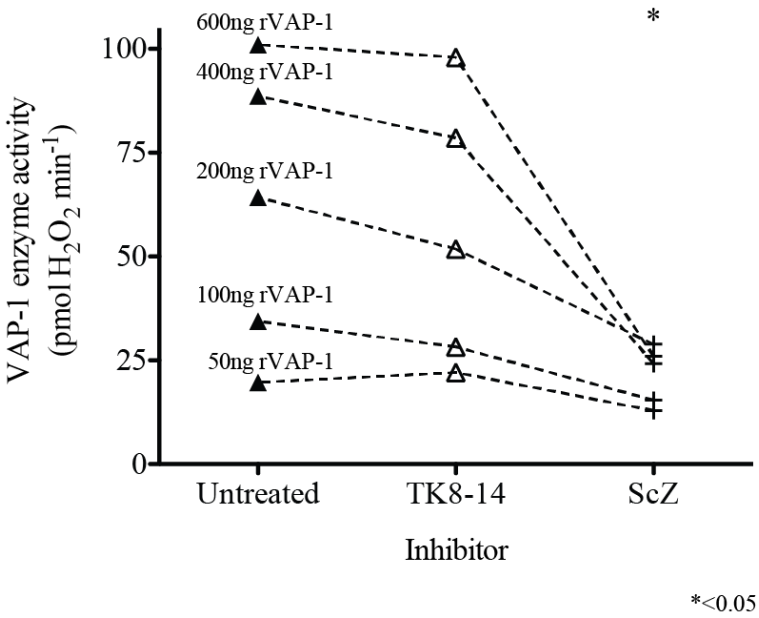

Figure 4.10: Comparison of TK8-14 vs. ScZ mediated VAP-1 enzyme inhibition
The inhibitory effect of TK8-14 (1 μg/sample) and semicarbazide (250 μM) were assessed over a range of rVAP-1 concentrations (1 mM benzylamine utilised in all wells). Asterisk indicates a significant difference in enzyme activity from the untreated state (paired t-test).

The inhibition of adhesion by anti-VAP-1 suggests that α4β7 T-cells may be able to engage directly with VAP-1 on HSEC. Although the identity of the VAP-1 ligand is not known, Siglec-9 and Siglec-10 have been shown to bind VAP-1 and act as

enzyme substrates *in vitro*. However, $CD3^+$ $\alpha4\beta7^+$ T-cells expressed very little Siglec-10 and only a small proportion expressed Siglec-9 (Figure 4.11).

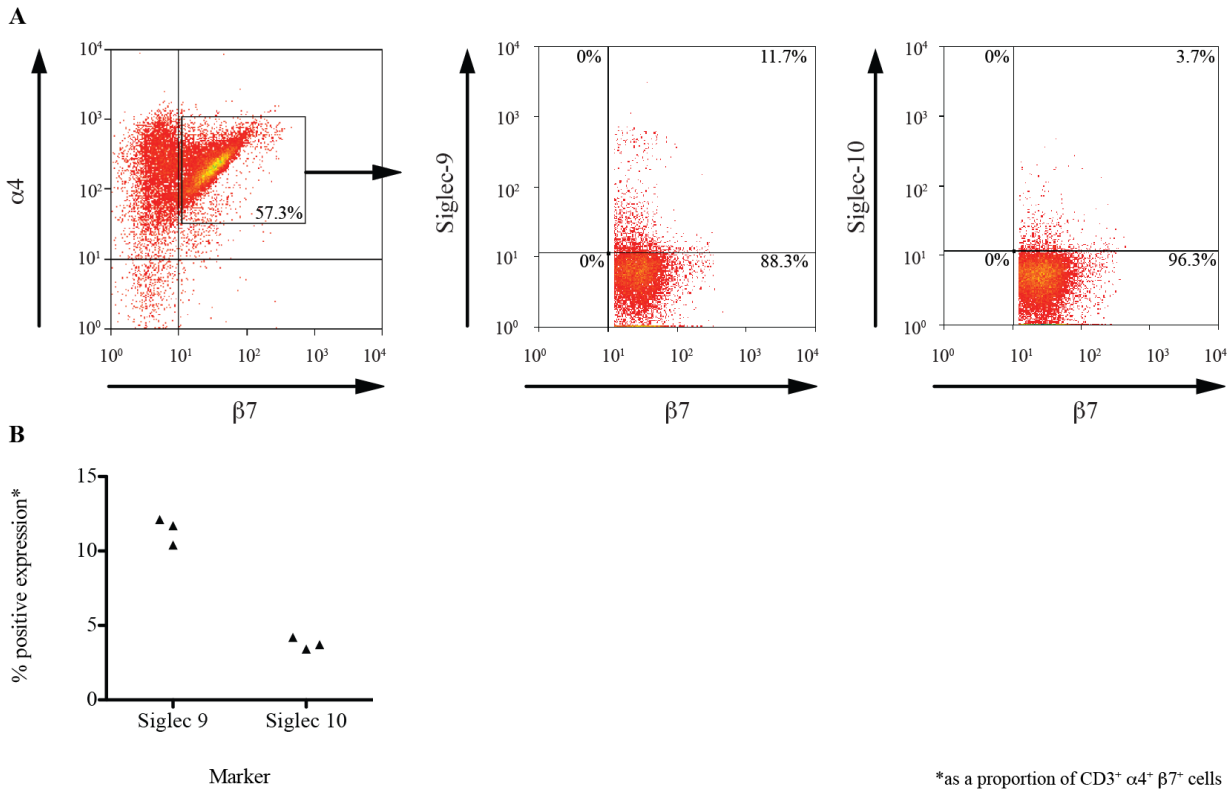

Figure 4.11: Siglec-9 and Siglec-10 expression by $CD3^+$ $\alpha4\beta7^+$ T-cells
$CD3^+$ gated, $\alpha4\beta7^+$ T-cells were analysed by flow cytometry for expression of putative VAP-1 ligands. Representative plots shown for n=3 experiments (3 different blood donors) in (A); percentage positive expression from all experiemtns summarised in (B).

4.2.5 Adhesion and transmigration of $CCR9^+$ T-cells under flow

Following the demonstration that $\alpha4\beta7^+$ T-cells adhere to stimulated HSEC under flow, I investigated whether the extent of binding was dependent upon CCR9 expression. Cell populations were obtained via FAC-sorting from peripheral blood. The $\alpha4\beta7^+$ $CCR9^+$ subset constituted a minor proportion (~3%) of the circulating $\alpha4\beta7^+$ lymphocyte population (healthy controls), therefore isolation through FAC-sorting required large volumes of whole blood from individuals undergoing

venesection (according to clinical need) in order to obtain enough cells for functional studies (Figure 4.12).

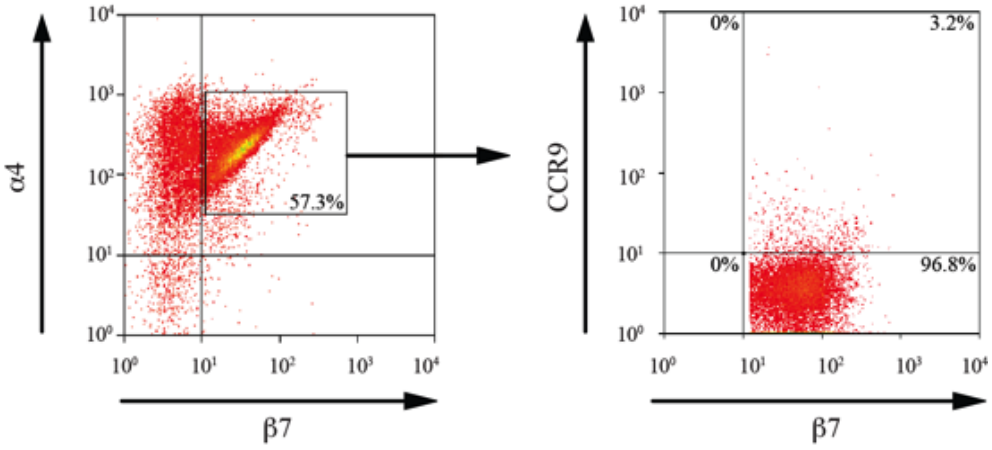

Figure 4.12: CCR9$^+$ α4β7$^+$ T-cells derived from peripheral blood
Circulating CD3$^+$ T-cells were sorted based on expression of α4β7 and CCR9.

In flow assays, α4β7$^+$ CCR9$^+$ T-cells showed a trend to greater adhesion and transmigration than their CCR9$^-$ counterparts, although the differences fell short of reaching statistical significance (p = 0.097 and p = 0.6, respectively; Figure 4.13).

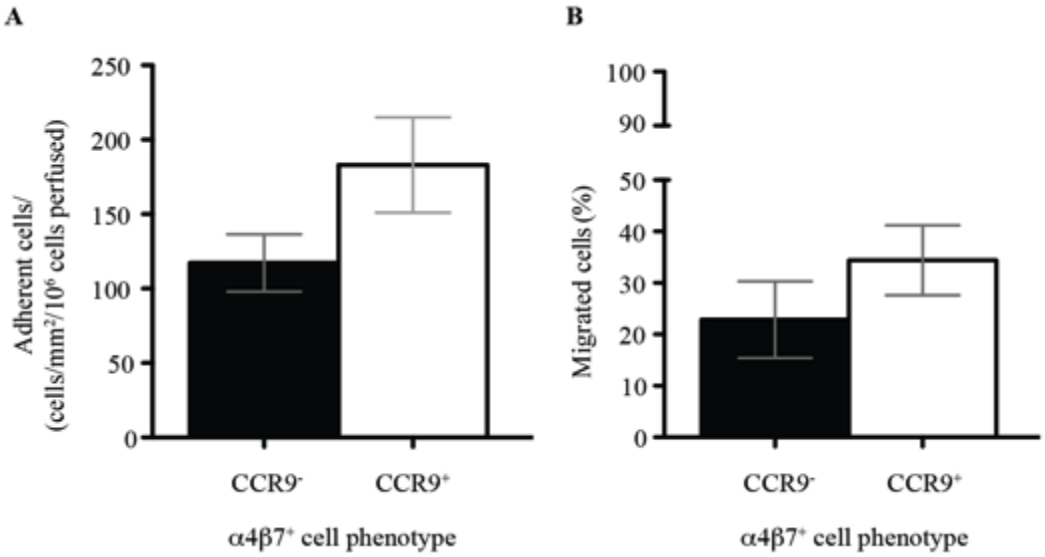

Figure 4.13: Flow adhesion assay of α4β7$^+$ sorted cells over stimulated HSEC
α4β7$^+$ T-cells were perfused over TNFα (10 ng/mL) and MA (100 μM) stimulated HSEC under conditions simulating physiological shear in the human liver. The degree of lymphocyte adhesion (A) and transmigration (B) were compared between CCR9$^+$ vs. CCR9$^-$ subtypes.

4.2.6 Enzymatic efficiency is substrate dependent

The proposal that in the presence of an inflamed gut, increased portal vein levels of methylamine activate VAP-1-dependent hepatic MAdCAM-1 expression – thereby promoting recruitment of mucosal effector cells to the liver – fuelled further investigation into alternative amine substrates that might be relevant to disease pathogenesis.

Amine substrates of human VAP-1 were selected based on their inclusion in the human metabolome database version 2.5 (http://www.hmdb.ca); specifically cysteamine, methylamine, dopamine, ethylamine and phenethylamine. The enzymatic activity of a fixed quantity of rVAP-1 (50 ng) was determined across varying substrate concentrations under atmospheric conditions (21% O_2), and comparisons drawn with kinetic rates observed using benzylamine – an archetypal VAP-1 substrate (Figure 4.14). As this series of experiments was conducted with purified rVAP-1, it was not deemed necessary to incorporate a semicarbazide step.

Following a series of dose finding studies, enzymatic efficiency as illustrated by the highest apparent k_{cat}/K_m was greatest with cysteamine; the lowest effects observed with ethylamine and phenethylamine (Table 4.1). This was of particular interest given that cysteamine is frequently adopted in experimentally induced colitis models [397–403]. It is worth noting however, that the K_m (substrate concentration at which the reaction rate is half of maximum) was greater for all amines relative to methylamine and benzylamine.

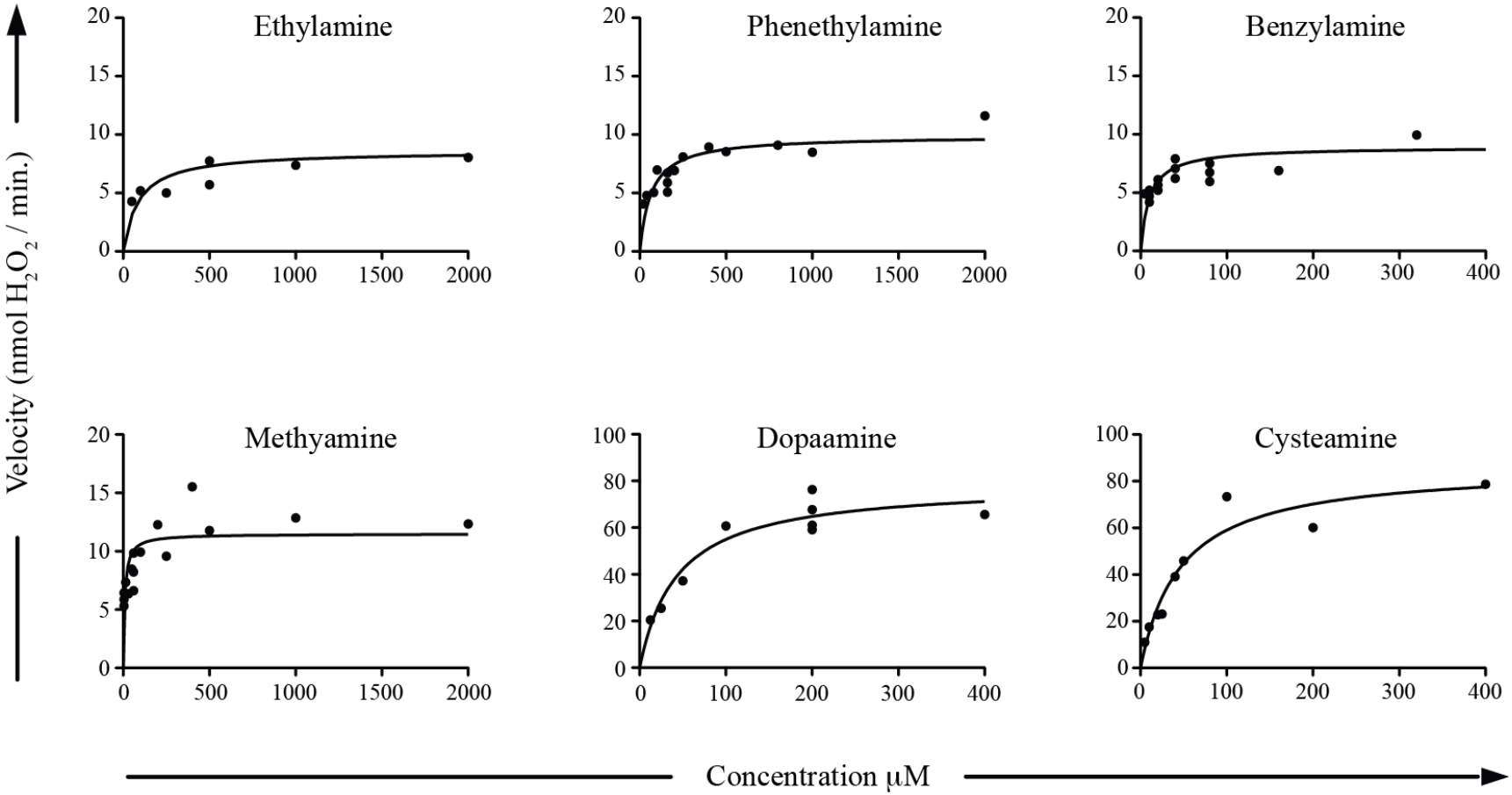

Figure 4.14: VAP-1 enzyme activity with alternating substrate provision

Non-linear fit curves illustrating VAP-1 activity across a range of substrates at varying concentrations and enzymatic rates as measured by the Amplex Red assay using 50 ng rVAP-1 as the catalyst. Each dot point represents the mean of 3 technical replicates. The kinetic constants were defined as $V_{max} = k_{cat}[E]_o$ (V_{max}, maximum rate achieved by the enzyme at saturating substrate concentrations; k_{cat}, the turnover number; and $[E]_o$, the substrate concentration).

Table 4.1: VAP-1 substrate kinetic profiling

Substrate	V_{max}	K_m (μM)	k_{cat} (s^{-1})	k_{cat}^{app}/K_m^{app}
Ethylamine	8.59 ± 0.60	88.44 ± 34.90	242.63	2.74ε+06
Phenethylamine	9.89 ± 0.69	65.69 ± 19.43	279.46	4.25ε+06
Dopamine	78.94 ± 5.97	43.70 ± 13.07	2229.94	5.10ε+07
Methylamine	11.49 ± 0.77	8.55 ± 3.45	324.58	3.80ε+07
Cysteamine	84.55 ± 13	44.52 ± 16.74	2388.42	5.36ε+07
Benzylamine	8.92 ± 0.70	9.90 ± 3.360	251.98	2.55ε+07

4.2.7 HSEC viability following amine substrate exposure

Having demonstrated the potency of cysteamine and other biogenic amines as VAP-1 substrates, I decided to assess the functional consequences of differential substrate provision to HSEC. In addition to generating H_2O_2, the enzymatic activity of VAP-1 could affect endothelial cell survival through the effects of aldehydes and ammonia, oxidative stress and glutathione depletion [397,399,402,404,405]. Therefore, I carried out viability assays in HSEC that had been incubated with increasing concentrations of the 5 amine substrates for 24 hours. Representative images of the cells after exposure to the maximum concentrations dictated by enzyme kinetic studies are illustrated in Figure 4.15. No gross morphological changes or evidence of cell death were evident for any of the treatments at the concentrations studied.

HSEC were then incubated with the 3 most potent substrates (cysteamine, dopamine, methylamine), as well as TNFα, in order to simulate treatment conditions undertaken in flow-adhesion assays. As expected, HSEC adopted a more elongated, 'spindle-shaped' conformation in response to activation by TNFα but viability was not affected (Figure 4.16).

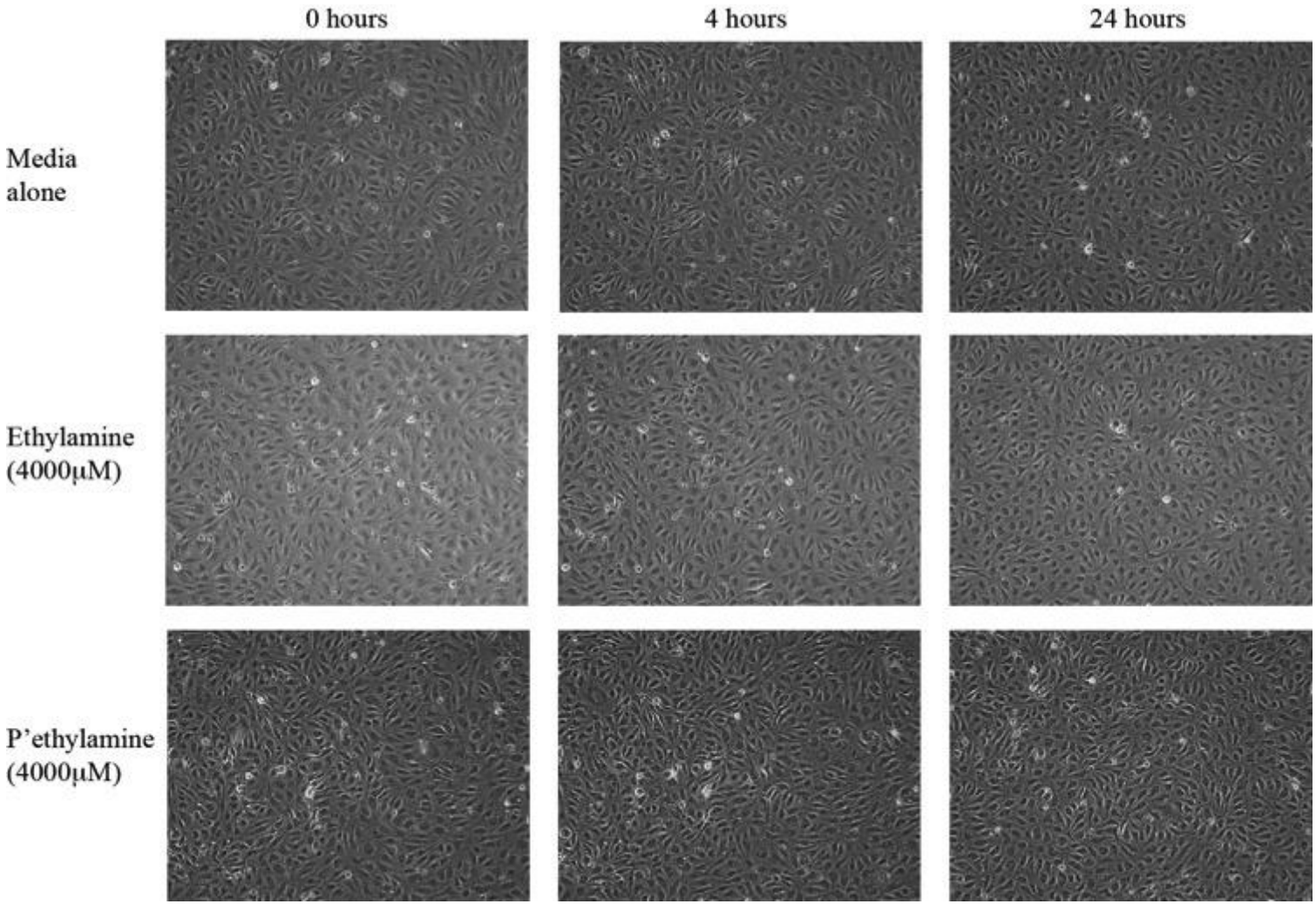
0 hours
4 hours
24 hours
Media alone
Ethylamine (4000μM)
P'ethylamine (4000μM)

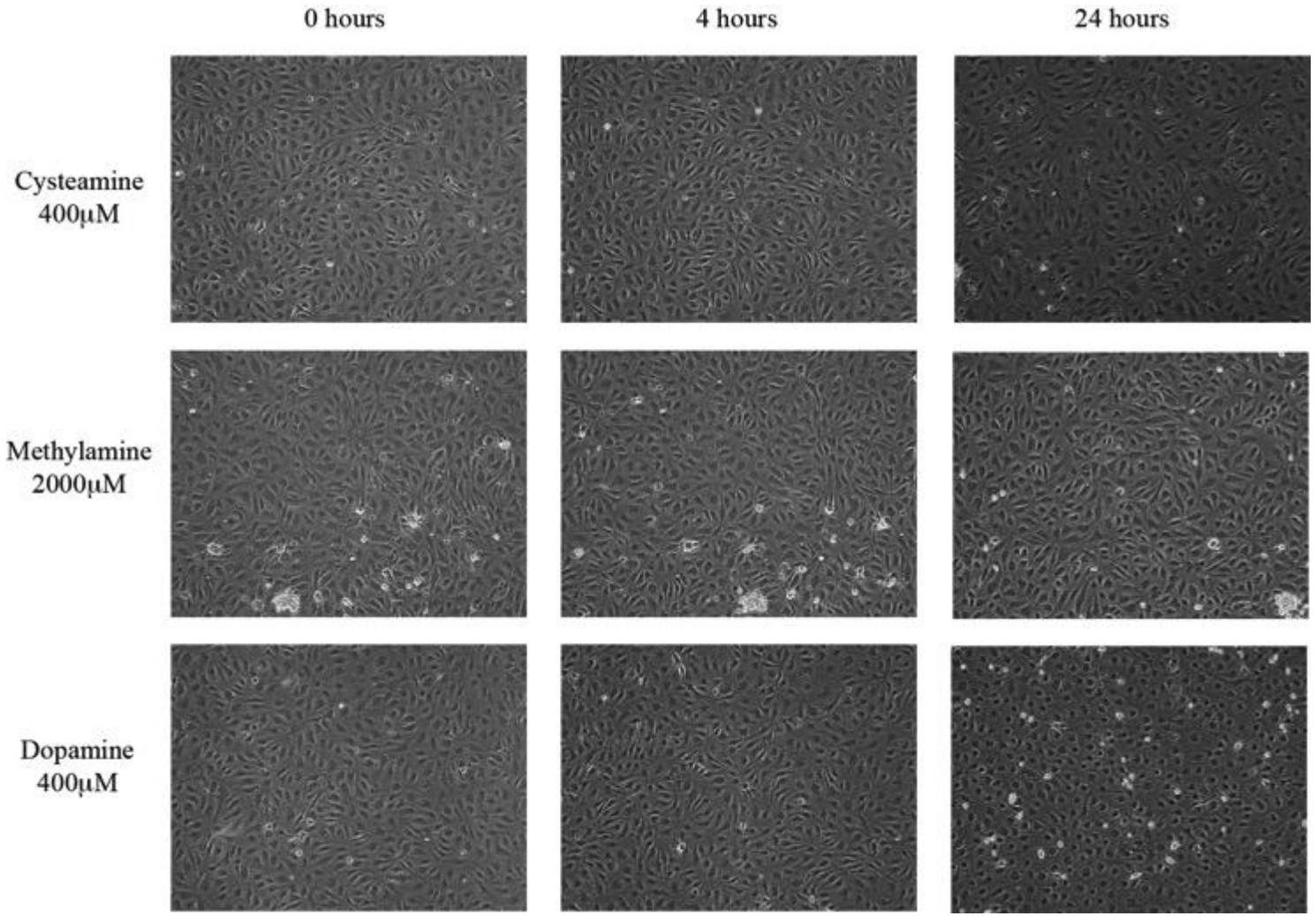

Figure 4.15: HSEC viability with variant substrate exposure
HSEC viability was monitored following exposure to several amine substrates. Representative images shown of maximum trialled concentrations at 0, 4 and 24 hours. X 10 magnification (Cell-IQ).

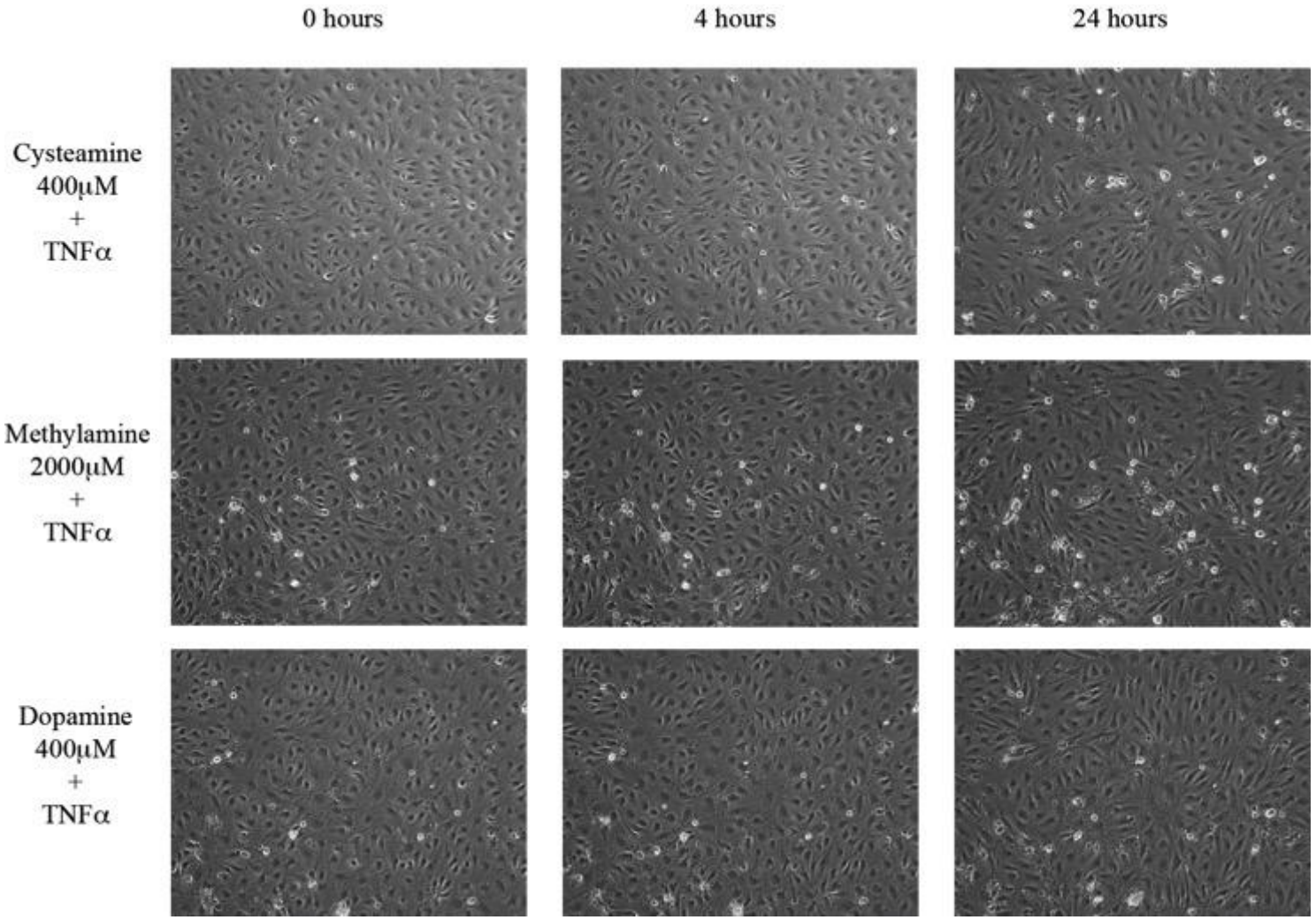

Figure 4.16: HSEC viability and morphology with variant substrate ± TNFα exposure

HSEC viability and morphology were monitored following exposure to selected substrates and TNFα at standard concentrations prior to assessment in functional assays. x 10 magnification (Cell-IQ).

4.2.8 Effects of differential substrate provision to HSEC

As cysteamine was readily deaminated by VAP-1 it was compared with methylamine in flow-based adhesion assays. HSEC were stimulated with TNFα ± methylamine or equivalent concentrations of cysteamine. Substrate concentrations were selected based on the previous studies suggesting 50 – 100 μM methylamine–treated HSEC supports lymphocyte adhesion and kinetic assays showing the rate of H_2O_2 at a plateau beyond 100 μM for both amines (see Figure 4.14). Using the JY-cells to study α4β7/MAdCAM-1 adhesion, a greater degree of attachment was observed in a dose dependent fashion with escalating amine concentrations (100 μM > 50 μM). Moreover, cysteamine treated HSEC supported α4β7–dependent adhesion to a significantly greater degree than equivalent concentrations of methylamine (Figure 4.17).

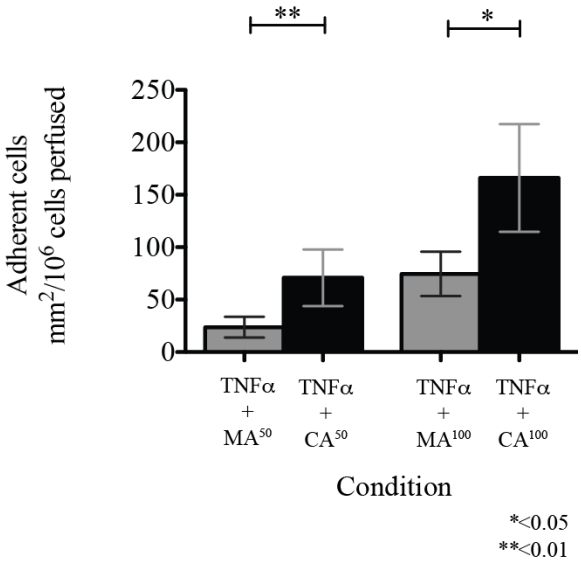

Figure 4.17: Effects of differential amine provision on α4β7 dependent adhesion
Flow adhesion assay of $\alpha4\beta7^+$ cells across HSEC stimulated with TNFα in addition to methylamine (MA) or cysteamine (CA) at 50 –100 μM. Data representative of the mean (± SD) of 3 independent experiments (10 fields of view each). Capped lines and asterisks indicative of statistically significant differences (KW-test with Bonferroni-Dunn's post-hoc correction).

4.2.9 HSEC ELISA

In addition to affecting endothelial expression of MAdCAM-1, the enzymatic activity of VAP-1 is known to up-regulate expression of other members of the immunoglobulin superfamily through NFκB activation [321]. To assess how induction of other CAMs is affected by different substrates, endothelial cells were stimulated with MA, CA or DA, and the effects on expression of MAdCAM-1, ICAM-1 and VCAM-1 compared. VE-cadherin was also included in HSEC ELISAs as this adhesion molecule is not known to be influenced by NFκB-dependent mechanisms (although VE-cadherin itself can activate NFκB [406]) and was thus deemed a suitable comparator.

HSEC were grown to confluence in a 96-well ELISA plate, and then incubated with TNFα (10 ng/mL) supplemented with methylamine, dopamine or cysteamine. Increased expression of ICAM-1, VCAM-1 and MAdCAM-1 were observed on HSEC following provision of TNFα and each of the 3 amine substrates when compared to TNFα alone (Figure 4.18). Expression of ICAM-1 and MAdCAM-1 was particularly marked using cysteamine relative to dopamine and methylamine although differences between substrates were not significantly different. However, differences in MAdCAM-1 expression were significantly greater using cysteamine + TNFα versus TNFα alone, supporting the results of enzyme kinetic studies and those of prior flow adhesion assays. As expected, no changes in VE-cadherin expression were observed following amine exposure relative to TNFα stimulation alone.

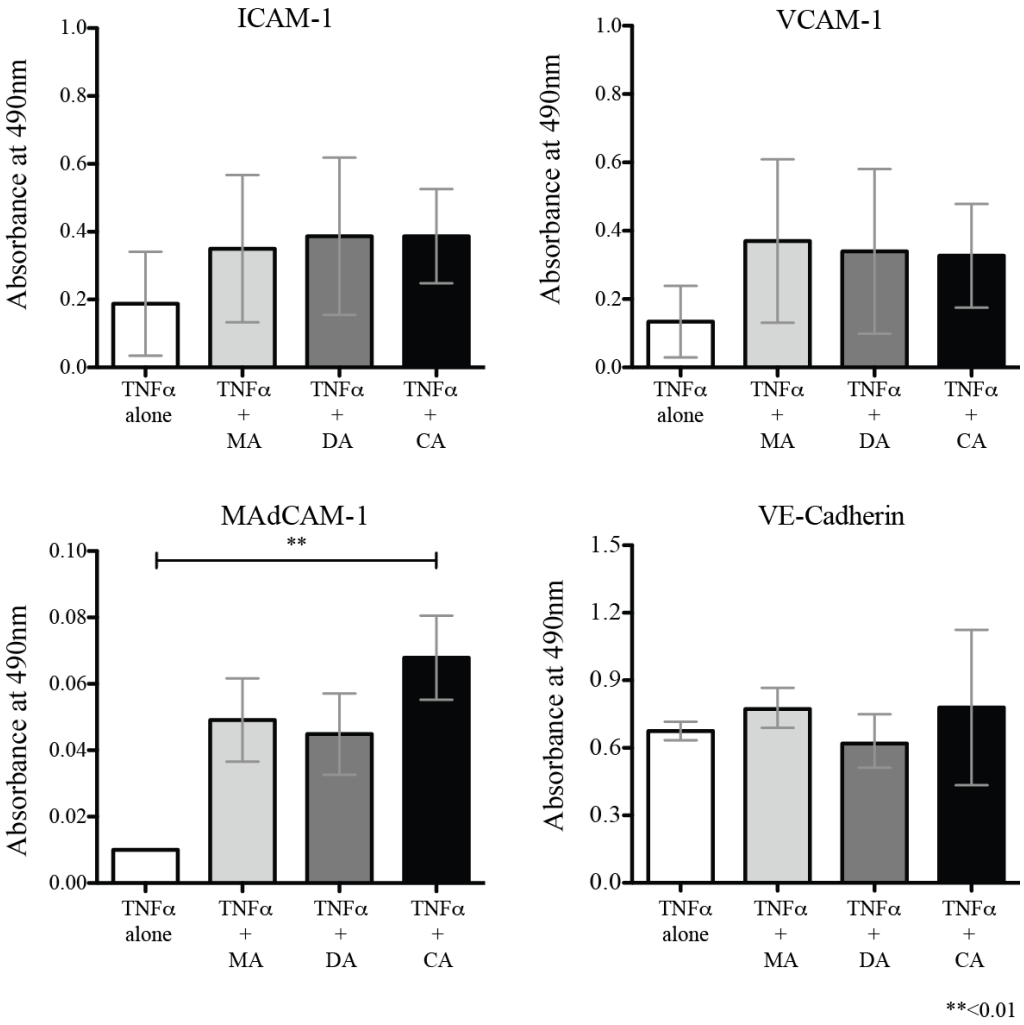

Figure 4.18: HSEC ELISA following VAP-1 susbstrate provision

HSEC evaluated for expression of cell adhesion molecules following stimulation with TNFα alone, in addition to methylamine (MA) or cysteamine (CA). Data presented as mean (± SD) with capped lines and asterisks indicative of statistically significant differences (overall KW-test; and also of TNFα and CA vs. TNFα alone).

4.3 Discussion

Vascular adhesion protein-1 is constitutively expressed in human liver and up-regulated under pro-inflammatory conditions [214]. As an adhesion molecule VAP-1 promotes hepatic inflammation and fibrosis via recruitment of B-cells, T-cells, macrophages and neutrophils; a process enhanced by enzymatic generation of aldehydes and H_2O_2. The latter is proposed to up-regulate expression of other adhesion molecules, and in autoimmune hepatobiliary diseases complicating IBD, particular attention has been drawn to the typically 'gut-restricted' molecule MAdCAM-1 and interactions with mucosal $\alpha4\beta7^+$ lymphocytes [294].

This chapter provides evidence that hepatic expression of VAP-1 and enzyme activity are elevated in PSC liver relative to AIH and PBC, and hepatic enzyme activity in the former closely resembled that of human colon; noteworthy given clinical associations with IBD. VAP-1 expression was elevated in diseased versus non-inflamed/non-cirrhotic liver with expression observed at sites of fibrotic scar tissue formation in addition to its known endothelial distribution. These findings were paralleled by an increase in measured hepatic enzyme activity. The efficiency of VAP-1 amine oxidase activity varied with different substrates; the most potent of which was cysteamine – an agent that induces colitis when applied to the colon in mice. The most consistent increase in CAM in response to cysteamine was MAdCAM-1. This is of particular interest because MAdCAM-1 does not respond as consistently to standard pro-inflammatory cytokines as ICAM-1 and VCAM-1 and it contributes to augmented $\alpha4\beta7^+$ lymphocyte adhesion under flow.

4.3.1 VAP-1 distribution in human liver

The distribution of VAP-1 in normal and diseased human liver has recently been detailed by Weston *et al*. [214]. Under homeostatic conditions, most VAP-1 is detected in endothelial cells, with staining largely restricted to vascular structures, portal vessels, central veins and sinusoids. However, in parenchymal liver disease, markedly increased staining was detected in in fibrotic septa and hepatic stroma. Confocal immunofluorescence confirmed co-localisation with myofibroblasts, implicating VAP-1 in liver fibrosis for the first time (although there is emerging evidence of a similar role in renal disease [407]).

VAP-1 expression studies in PSC liver confirmed the vascular distribution described for parenchymal liver diseases and demonstration in the hepatic scar provided further support for a role in fibrosis. However, in confocal immunofluorescence experiments there was heavy VAP-1 staining in addition to that which colocalised with αSMA and CD31. In this regard, more contemporary stromal targets discerning HSC and myofibroblasts, such as CD90 or vimentin, are needed to discriminate VAP-1 expression by cells of stromal versus non-stromal origin. The study by Weston *et al*. has shown VAP-1 co-localisation with these markers in human liver, wherein HSC associate closely with HSEC and act as pericytes, which contribute to the regulation of endothelial differentiation, function and blood flow. HSC proliferation and trans-differentiation into myofibroblasts contributes to ECM deposition during fibrogenesis, and both HSC and particularly activated myofibroblasts have recently been reported to secrete enzymatically active sVAP-1. [214]. Thus it is likely that VAP-contributes through several mechanisms to hepatic leucocyte recruitment, tissue inflammation and fibrosis in parenchymal and biliary liver diseases.

VAP-1 staining was more prominent in PSC relative to normal liver, and when compared to the other autoimmune liver diseases AIH and PBC. The histological hallmark of PSC is the fibrotic duct lesion together with a prominent ductular reaction. However, VAP-1 was not expressed by $EpCAM^{+}$ biliary epithelium. Interestingly VAP-1 did not co-localise with the adhesion molecule MAdCAM-1, which was also detected on HSEC. These findings are in keeping with reports of prior investigators that used antibodies against the same targets [214,294], and implies that despite both being ostensible vascular adhesion molecules, VAP-1 and MAdCAM-1 are either expressed by distinct areas of the hepatic endothelium or are rapidly shed into the extracellular space.

4.3.2 Hepatic VAP-1 quantification

An important goal of this chapter was to evaluate differences in expression between PSC and other autoimmune liver diseases. To do this quantitative assessment of message was done with qRT-PCR, and absolute enumeration obtained through extrapolation from a plasmid-generated calibration curve. Although commonly employed for studying variant cell populations [214], the absolute quantification approach is rarely used for assessing mRNA levels in whole tissue and the identification of a valid reference gene with low variability between aetiologies and disease stages has not yet been published. For instance, one study demonstrated little conservation of commonly tested housekeeping genes between ordinal degrees of liver injury from hepatitis, fibrosis to cirrhosis; including 18s RNA, glyceraldehyde 3-phosphate dehydrogenase (GAPDH), β-actin and arginine/serine-rich splicing factor (SFRS4)) [337]. Congiu *et al*. further report poor performance of hypoxanthine phosphoribosyltransferase-1 (HPRT1) [338], with GUS-β only slightly better

preserved across varying stages of chronic hepatitis C infection. Comparative assessments between PBC and PSC raise similar concerns, wherein ubiquitin was the only one of nine tested candidate genes illustrating consistent hepatic gene expression between aetiologies [408].

I observed high levels of *VAP-1* gene expression and enzymatic function in PSC compared with other autoimmune hepatobiliary diseases and non-inflamed/non-cirrhotic specimens. However, within any given aetiology there was a broad range of copy numbers, and not all differences between diseases amounted to statistical significance. It is probable that additional factors to disease aetiology influence VAP-1 gene expression in human liver, such as the level of inflammation or the extent of vascularisation in tissue. Nevertheless, hepatic VAP-1 gene expression was significantly greater in diseased, versus non-diseased liver specimens, providing further support for a role in propagation of hepatobiliary injury.

Perhaps more notable were the findings of in-tissue enzyme activity analysis between diseases. Aside from liver, enzymatically active VAP-1 in humans has previously been detected in adrenal glands, gallbladder, intestine, kidneys, lungs, pancreas, thyroid, spleen and adipose tissue [409]. Despite high-level constitutive expression of VAP-1 in non-inflammatory settings, enzyme activity in human liver is reportedly lower than that reported in gut or human vasculature [409]. A recent study from Finland has proposed that alternative splice variants of VAP-1 may exist with varying enzyme activity [410]. It is thus possible that a form with lesser enzyme activity is present in non-diseased liver, with up-regulation of the more active form during disease. To my knowledge, the data presented in this chapter represent the first quantification of tissue enzyme activity in liver diseases. The variation in VAP-1

amine oxidase activity within any given aetiology was quite broad and paralleled the pattern seen in gene expression studies. However, the PSC liver cohort demonstrated significantly greater enzyme activity overall, as assessed by two different techniques, compared with AIH, PBC and non-inflamed/non-cirrhotic liver.

The consequences of increased enzyme activity could include direct effects on leucocyte adhesion, and particular attention has been drawn to pro-inflammatory myeloid subsets in this regard [316]. More recently purified sVAP-1, possibly derived from activated HSC and liver myofibroblasts, has been shown to mediate enzyme-dependent chemotaxis of peripheral blood lymphocytes in migration assays [214]. I have shown that hepatic enzyme activity in PSC was comparable to that observed in the colon, suggesting a degree of conservation between mucosal sites. It is thus tempting to speculate that in the context of an increased amine substrate burden – perhaps that secreted by enteric bacteria – VAP-1 enzyme activity increases in the colon. Consequently, a 'leaky' inflamed gut in patients with colitis would allow translocation of such substrates to the portal circulation, where hepatic VAP-1 mediated deamination could increase liver inflammation. One consequence could be the 'relatively selective expression of MAdCAM-1 induced by local VAP-1 activity in hepatobiliary diseases complicating intestinal inflammation. In this context a driver of substrate provision could be inflammasome-mediated dysbiosis in patients with non-alcoholic fatty liver disease (NAFLD) or PSC [119]). Elevated hepatic VAP-1 levels can be detected in patients with NAFLD [214] and correlate with inflammatory activity and outcome, which is of interest given the reported changes in intestinal microbiome composition in obese individuals dependent upon the presence or absence of liver disease [411,412]. VAP-1 substrates are also implicated in modulating glucose transporters in isolated rodent and human adipocytes, and in *ex*

vivo human liver [333–335]. This is of particular interest given the proposed role of VAP-1 in mediating steatosis, steatohepatitis and fibrosis in NAFLD. Moreover, NAFLD and PSC not only share increased hepatic VAP-1 expression but also an increased risk of diabetes, cardiovascular disease and colonic neoplasia [332,413].

An important caveat to any technique attempting to quantify hepatic VAP-1 expression is that for absolute distinction between diseases, tissue samples should be taken from areas of liver bearing comparable vascular and stromal volume (as VAP-1 is widely distributed on vessels and fibrotic scar tissue). In reality this approach is rarely feasible and would require laser capture microdissection of precision cut tissue slices with prior immunohistochemical detailing. A further avenue to be explored is the difference in VAP-1 expression between diseases by western blotting. However, correct interpretation of the latter would similarly require sampling of comparable specimens of liver tissue between diseases. Another limitation to the studies presented in this chapter is the use of tissue from end-stage cirrhotic livers, which prevents me from commenting on whether hepatic VAP-1 expression exhibits similar differences between aetiologies in the pre-cirrhotic state. Of note, there is a distinct paucity of hepatic VAP-1 expression in acute liver failure and fulminant hepatitis [330,414], suggesting that VAP-1 is particularly up-regulated in chronic liver disease.

4.3.3 Differential substrate provision

Little is known about the pathophysiological substrates for VAP-1 amine oxidase function or whether different substrates produce different downstream consequences. Selection of substrates from the human metabolome database highlighted five amines for study with benzylamine included as a positive control and archetypal substrate.

All were evaluated in enzyme kinetic assays with data fitted to the Michaelis-Menten equation. There is debate as to whether measuring VAP-1 kinetic constants via Michaelis-Menten analysis is wholly appropriate, as some mammalian amine oxidases display non-hyperbolic behaviour [415]. Kinetic plots with rodent, porcine and other human AOC enzymes reveal a peak in initial velocity but reduced reaction rates at higher substrate concentrations. This may imply amines are binding to a second site, or more plausibly an altered form of enzyme than that which is present during initial phases of the catalytic reaction. Holt *et al*. propose that low affinity binding of cations present in buffers, to a reduced form of enzyme during the reaction could stabilise the catalyst, resulting in lower 'measured' reaction rates in the presence of higher substrate concentrations [415]. Notwithstanding the proposed effects of cations on AOC activity, it might be argued that true kinetic constants are those obtained in the absence of any competing cations which is difficult to assess given the generation of ammonium ions during the deamination reaction, and that those obtained in bench-top assays are 'apparent' values [415]. This raises questions as to what constitutes a 'true' reaction rate.

Notwithstanding these observations, the aim herein was to compare and contrast enzyme efficiency with different substrates rather than try to obtain absolute kinetic constants for each substrate. I decided to use the Amplex Red assay to detect rate of H_2O_2 production as opposed to previously described methods reliant upon oxygen consumption [295] because it allowed the assessment of amine contributions under normoxic conditions. As such, the substrate associated with highest VAP-1 enzymatic efficiency was cysteamine; noteworthy given the ability of local cysteamine to induce experimental colitis (17). A similar hierarchy of kinetic rate was however observed

(between the 6 amines chosen) when analysed under hypoxic conditions by Shen *et al*. [295].

Cysteamine production in the gut is regulated by vanin-1, an epithelial ectoenzyme belonging to the pantetheine hydrolase family that recycle pantothenic acid (vitamin B5). Vanin-1 deficient animals are relatively protected from oxidative stress injury in the gut, such as that induced by non-steroidal anti-inflammatories (NSAIDs), tri-nitrobenzene sulfonic acid (TNBS) or *Schistosoma mansoni* infection [401,402]. However, resistance to oxidative stress can be abolished and colitic injury initiated in vanin-$1^{-/-}$ mice following administration of exogenous cysteamine [401,402]. Vanin-1 polymorphisms are associated with IBD disease severity [403], and epithelial expression can promote inflammation driven carcinogenesis in murine colitis models [416]. It is thus plausible that the pro-inflammatory effects in colitis are directly attributable to an excess of cysteamine production by vanin-1.

Cysteamine belongs to the aminothiol family of compounds and is produced as a degradation product of cysteine. Amino acid metabolism differs between gastrointestinal sites, and cysteine biosynthesis by enteric flora is largely restricted to the colonic microbiome [417]. Previous studies suggest that methylamine, another potent inducer of VAP-1 enzyme activity, predominates in the proximal colon [418]; of interest given that the phenotype of IBD in PSC is predominantly a right-sided colitis. This would imply that cysteamine and methylamine not only contribute to development of colitis, but also induction of hepatic VAP-1 activity, thereby enhancing leucocyte recruitment to the liver and driving hepatobiliary inflammation. Notably, the aldehyde by-product of cysteamine deamination is 3-

mercaptopropionaldehyde [419], an agent associated with abnormal collagen cross-linking and thus a potential contributing factor in fibrogenesis.

4.3.4 Functional consequences of enzyme activity by different substrates

Increased hepatic VAP-1 expression probably drives inflammatory liver disease through increased pro-inflammatory cell recruitment and consequent hepatic fibrogenesis. In PSC a particular role has been ascribed to MAdCAM-1 in recruiting mucosal T-cells to the liver and the ability of hepatic VAP-1 enzyme activity to induce aberrant expression of MAdCAM-1 in the liver may be contribute to the role of gut lymphocytes in the hepatic manifestations of this disease. Liaskou *et al*. [294] first published data to support this hypothesis and consistent with their findings I saw, an increase in $\alpha4\beta7^{+}$ lymphocyte adhesion to TNFα stimulated HSEC which was increased further by provision of VAP-1 substrate methylamine. It is possible that amine substrates have direct toxic effects on endothelial cells [420], which could affect leucocyte adhesion and transmigration independent of VAP-1 enzyme activity. Because amines are inherently lysosomotrophic, they could interfere with receptor recycling and alter the density of surface exposed CAMs. However, if endocytic effects were predominant, they would occur independently of TNFα provision. Further support implicating a direct role for VAP-1 in this process was provided by the observation that lymphocyte adhesion was reduced by 50% by prior enzyme inhibitor treatment; near identical to that observed using targeted antibodies against MAdCAM-1 or α4β7 [294].

The residual degree of adhesion following VAP-1 enzyme inhibition may be due to the involvement of other adhesion molecules which facilitate attachment of

lymphocytes under flow including CD44, ICAM-1, VCAM-1 and CLEVER-1. That administration of an anti-VAP-1 antibody reduced adhesion by ~25% without significantly affecting enzyme function, provides support for a non-enzymatic contribution from VAP-1 as reported before. Alternatively, anti–VAP-1 treatment could have resulted in the internalisation of enzyme, reducing the availability of enzyme on the HSEC surface. Human T-cells are not known to express the putative VAP-1 ligands Siglec-9 or Siglec-10 [421], and this held true for the FAC-sorted $\alpha4^{+}\beta7^{+}$ lymphocytes used in the flow-adhesion assays. It is of course plausible that the usage of separate α4 and β7 antibodies (rather than a combined α4β7 antibody) may have resulted in a proportion of $CD3^{+}$ $\alpha E^{+}\beta7^{+}$ cells being included herein. However, these would still be T-lymphocytes, which are known to express very little Siglec-9 or Siglec-10 [67].

The identity of the VAP-1 ligands is a topic of much speculation and conjecture [67], and it is possible that gut-tropic and liver-tropic T-cells express the same as yet unknown ligand/substrate. It is worth mentioning that neither enzyme inhibition nor antibody blockade affected the relative percentage of cells undergoing transendothelial migration, supporting prior observations that MAdCAM–1/α4β7 interactions are primarily involved in the attachment and adhesion steps of the leucocyte adhesion cascade [422].

Mucosal lymphocytes expressing α4β7 and CCR9 infiltrate the PSC liver [127] [289]. In Chapter 3, data were presented indicating that a large proportion of colon-infiltrating T-cells express CCR9 in active inflammation, noteworthy given the association of PSC with colitis. In an endeavour to investigate the adhesion/transmigration of $CCR9^{+}$ T-cells to HSEC, I used flow adhesion assays to

compare peripheral blood $\alpha4\beta7^+$ T-cells FAC-sorted into $CCR9^+$ and $CCR9^-$ subsets. $CCR9^+$ T-cells constitute a minor proportion of the circulating lymphocyte pool and despite the use of $\geq$500 ml peripheral blood for cell-sorting per isolation, only 0.5 – 1.0 million $CCR9^+$ T-cells could be obtained (~4 – 6 hours FAC-sorting time). Thus it was only possible to perform 'head-to-head' comparisons between $CCR9^+$ and $CCR9^-$ subsets twice. Nevertheless, on both occasions a greater absolute number of $CCR9^+$ T-cells underwent adhesion and transmigration compared with $CCR9^-$ T-cells in the same experiment. If validated through an increased number of repeats, these findings would warrant further, detailed assessment of chemokine ligand (e.g. CCL25) expression by TNFα and amine stimulated HSEC, as well as detailing the functional profile of $\alpha4\beta7^+$ $CCR9^+$ versus $CCR9^-$ liver/colon-infiltrating T-cells.

As cysteamine was the most efficient enzyme substrate I assumed this would also be associated with the greatest efficacy in the adhesion assay. Stimulating HSEC with cysteamine induced significantly more $\alpha4\beta7^+$ lymphocyte adhesion than methylamine at identical concentrations. Moreover, ELISA confirmed induction of MAdCAM-1 on HSEC and again levels were significantly greater with cysteamine as a VAP-1 substrate. Increased expression of other IgSF members was also seen following amine supplementation to TNFα treatment. Collectively; these observations support the hypothesis that gut-derived amines can facilitate recruitment of mucosal lymphocytes to HSEC via elevated VAP-1 enzyme activity.

A notable confounding factor to interpreting any functional data, is that supplementation with serum is mandatory to ensure HSEC viability. All mammalian serum contains some VAP-1 although this may vary between species. It is thus possible that the presence of small volumes of serum could contribute non-HSEC

derived VAP-1. Nevertheless, as standardised serum concentrations are used across all experiments it is likely that the differences between conditions are due to membrane-bound protein.

4.3.5 Potential for therapeutic targeting

The evidence that enzymatically active VAP-1 is involved in the pathogenesis of PSC highlights an avenue of therapeutic interest. The availability of enzyme inhibitors with greater sensitivity and specificity than semicarbazide, as well as neutralising antibodies against VAP-1, are novel and attractive anti-inflammatory therapies in PSC.

VAP-1 knockout mice develop normally, albeit displaying aberrant lymphocyte homing to lymphoid organs *in vivo* [320]. In particular, an absolute reduction in lymphocyte populations within the gut (Peyer's patches, PP) is observed and these animals exhibit defective microbial handling and attenuated T- and B-cell responses to oral vaccination [423]. These potentially harmful effects are not observed when administering antibody or enzyme inhibitors to fully developed wild-type mice, which display intact antimicrobial activity *in vivo.* Koskinen *et al.* therefore propose that life-long absence of VAP-1 may give rise to compensatory mechanisms in development that negatively alter cellular or humoral components of the immune system involved in anti-microbial defence, not apparent in pharmacologically treated mice (49).

VAP-1 knockout mice treated with CCl_4 injection to induce liver injury, inflammation and fibrosis show a marked reduction in nearly all liver infiltrating mononuclear cell

types from as early as 2 weeks following toxin administration [214]. The influence on leucocyte recruitment early in the disease course was paralleled by a reduction in hepatitis as well as parenchymal and portal tissue fibrosis. Mice bearing a catalytically inactive form of VAP-1 (henceforth referred to as *Ssao*$^{-/-}$) fed a methionine-choline deficient (MCD) diet to induce steatohepatitis showed similar reductions in hepatic $CD4^+$ and $NK1.1^+$ T-cells (4 – 6 weeks of age) to knockout mice lacking the whole VAP-1 gene and this led to reduce fibrosis relative to wild-type counterparts [214]. This suggests that VAP-1 is an important driver of inflammation-induced fibrosis.

The effects of enzyme inhibitors and highly selective antibody blockade have been tested *in vivo.* VAP-1 expression although predominantly restricted to the liver and lymphoid tissues in healthy animals can be up-regulated on extra-hepatic sites such as the synovium and gut under non-homeostatic conditions. LJP1207 is a potent inhibitor of VAP-1 function, the administration of which in oxazolone induced colitis reduces mortality, improve body weight as well as significantly improve colonic inflammation; most likely due to reduction of T_h2 immune cell responses [424]. Such reagents have also proven useful in controlling multiple inflammatory (peritonitis, arthritis, ischemia-reperfusion injury, lung inflammation, septic shock, hepatitis, colitis, organ transplantation) and fibrotic (kidney, liver) responses inherent to several *in vivo* mouse models [212–214,309,312,407,424–429].

Antibody-treated mice are also protected from the development of liver fibrosis following or during administration of the MCD diet [214], evidenced by reduced αSMA expression and collagen deposition. This is despite the fact that the antibody used does not inhibit amine oxidase activity *in vitro* suggesting it works by a

reduction in the infiltration of NK T-cells and $CD11b^{+}F4/80^{+}$ macrophages. A direct comparison of α4 versus VAP-1 inhibition was recently performed in the concanavalin A model of hepatitis [213], wherein the latter reduced influx of $CD4^{+}$ (but not $CD8^{+}$) T-cells, attenuated early liver inflammation (reduced serum ALT at 8 hours following injury) and reduced peri-portal inflammation. The anti-VAP-1 effects on lymphocyte recruitment were predominantly restricted to T-cells bearing a T_h2 cytokine profile; whereas α4-blockade was associated with significant exacerbation of hepatitic injury through increased production of IFNγ and reduced hepatic infiltration of protective myeloid-derived suppressor cells (MDSC). Of interest, a modest (non-significant) reduction in serum ALT was also observed with SSAO inhibitor (BTT-2052), with a similar reduction in T_h2 $CD4^{+}$ T-cells infiltrating the liver [212,213]. There is little to suggest an additive effect through combining antibody and enzyme-inhibition [316], and in part this could be due to an absence of suitable *in vivo* agents which confer 100% enzyme inhibition.

4.3.6 Summary

I have shown VAP-1 expression to be increased in autoimmune hepatobiliary disease. Elevated enzyme activity was particularly marked in PSC liver, with comparable levels detected in the human colon. The amine oxidase activity of VAP-1 depends on the nature of available substrate provided; and in this regard amines generated by the inflamed human colon are likely to play a role in promoting gut-liver lymphocyte migration and hepatic fibrosis.

Given that hepatic VAP-1 enzyme activity is elevated in PSC patients, and can be modulated in a substrate dependent manner by gut-derived amines to induce

MAdCAM-1 expression on HSEC therapeutic exploration in PSC-specific models represents an avenue commanding further investigation.

5 Results III: Soluble VAP-1 in PSC

5.1 Introduction

In the previous chapter, I provided evidence for elevated hepatic VAP-1 expression and enzyme activity in diseased human liver with the strongest expression and highest levels of enzymatic activity observed in PSC. This and my finding that cysteamine, a substrate produced by the inflamed colonic epithelium and gut bacteria, was the substrate with the highest enzymatic efficiency that translated into functional sequelae supports the hypothesis that liver injury is driven by intestinal inflammation in PSC

The VAP-1 expression studies conducted in chapter 4 were confined to end-stage explanted liver tissue. This significant limitation is inevitable given that the current standard of care for PSC minimises the use of liver biopsy. VAP-1 also exists in a soluble form (sVAP-1) released from the liver possibly by cleavage from the endothelial cell surface and release by activated liver myofibroblasts [214,328,330,414]. This allowed me to investigate the clinical utility of peripheral blood sVAP-1 and enzyme activity as a biomarker in a large cohort of PSC patients at different diseases stages.

5.2 Findings

5.2.1 Serum VAP-1 assessment

5.2.1.1 Characteristics of the patient population

Peripheral blood samples were prospectively collected from a cohort of patients with an established diagnosis of PSC (n=134). Their demographic characteristics (Table

5.1) were comparable to those reported in population-based epidemiological studies [430], with a male preponderance and onset of disease in the 4th decade of life.

Over the course of the study period, 56 patients progressed to liver transplantation (n=44) or death (n=12) and these were selected as endpoints. Given the open nature of the cohort, Kaplan–Meier curves were used as a product limit estimator for evaluating endpoint function over time. This approach was taken in order to conduct time-to-endpoint analysis across inevitably different follow-up periods between patients, and is commonly adopted in large-scale population studies working with open cohorts [431,432]. Setting time zero as point of blood sampling, the median transplant-free survival obtained via Kaplan–Meier survivorship estimates was equivalent to the point at which 50% of patients experienced any clinical endpoint (39 months, IQR 32 – 46 months; Figure 5.1). This relatively short period reflects the fact that patients were attending a tertiary hepatology unit (Queen Elizabeth hospital, Birmingham), and thus a high proportion were referred only for consideration of transplantation once they had reached an advanced stage of liver disease.

Table 5.1: Characteristics of the PSC cohort

Patient age *	42yrs. (29 – 59yrs.)
Male gender	83 (62)
Ethnicity	
Caucasian	109 (81)
Black	6 (4)
Indian	6 (4)
Pakistani/Bangladeshi	8 (6)
Other/Misc.	5 (4)
Cirrhosis *	91 (70)
Decompensated	23
Ascending cholangitis §	25 (19)
w/in 2 mo. of sampling	16
Small-duct disease	3 (2)
Hepatobiliary malignancy $	8 (6)
IBD	106 (79)
Colonic IBD	106
Active IBD *	27
Colectomy (pan + subtotal)	19
Pouchitis	5
Colonic dysplasia/cancer $	9 (7)
Immunosuppression	33 (25)
Steroids	6
Anti-purinergic	7
Steroids + anti-purinergic	18
Calcineurin inhibitor	1
Anti-TNFα	1
UDCA (>6 mo) *	96 (72)
Antibiotic exposure w/in past 2 mo.	36 (27)
Laboratory parameters *	
AST	66 IU/L (34 – 100 IU/L)
ALT	61 IU/L (34 – 105 IU/L)
ALP ratio (to ULN)	2.14 (1.03 – 3.45)
Bilirubin	20 μmol/L (11 – 48 μmol/L)
Albumin	43 g/dl (38 – 45 g/dl)
Platelets	200 x 10^3 cells/mm^3 (128 – 298 x 10^3 cells/mm^3)
INR	1.1 (1.0-1.2)
Na^+	141 mmol/L (139 – 142 mmol/L)
Creatinine	72 μmol/L (58 – 82 μmol/L)
UKELD score	48 (45 – 51)
IgG	14.17 g/L (11.77 – 17.71 g/L)
ANA positive	60 (45)
ASMA positive	41 (31)
pANCA positive	50 (37) – test not performed in 26 patients

Data for categorical variables expressed as number (percentages in parenthesis). Continuous variables expressed as median (IQR in parenthesis).

* At time of sampling

§ Previously treated – not present at time of sampling.

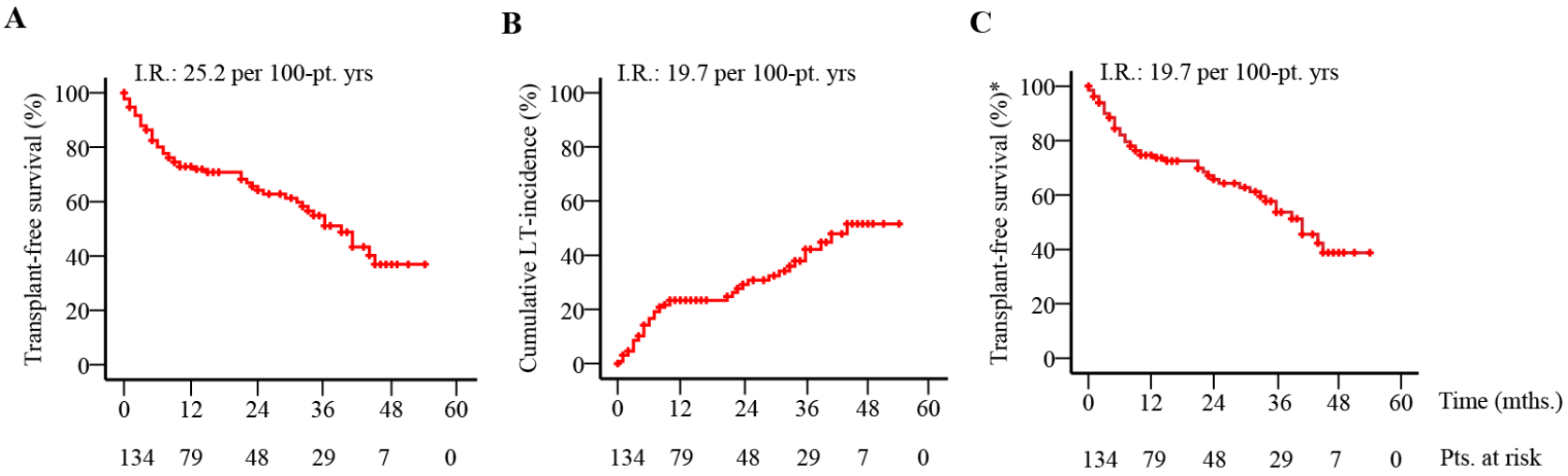

Figure 5.1: Kaplan–Meier survivorship estimates across the PSC cohort

Time to event depicted in months following blood sampling for sVAP-1 analysis. 'Patients at risk' indicate the population at given time points remaining under follow-up, free of the indicated clinical event. The objective lifetime risk was calculated as incidence rate (I.R.); specifically, the probability that a particular event would occur before a given time (overall event number divided by total patient follow-up time) and presented for each indicated measure: liver transplant or death (A), liver transplantation only (B), and liver transplantation/liver-related death (C).

The comparator groups consisted of patients with PBC (n=90), AIH (n=97), IBD without PSC (n=50) and healthy controls (HC; n=20). Observing our study populations in their entirety, notable differences were apparent with respect to patient age, gender predominance, and frequency of transplantation and mortality incidence between autoimmune diseases (Table 5.2 and Figure 5.2) consistent with the characteristics of AIH, PBC and PSC [152,433]. The significantly poorer transplant-free survival in the PSC group reflects the severity for this disease and the lack of an effective treatment to date has been shown to retard disease progression.

Table 5.2: Demographic variation across the three autoimmune liver diseases

	PSC	**PBC**	**AIH**	**IBD**	**HC**	***p* value**
Patient age, yrs. *	42 (29 – 59)	57 (49 – 66)	49 (29 – 61)	35 (26 – 54)	34 (38 – 37)	<0.0001 ^
Male gender	83 (62)	9 (10)	21 (21)	31 (62)	9 (45)	<0.0001 $
Cirrhosis	95 (71)	54 (51)	45 (46)			<0.001 $
Decompensated	28	12	4			
Clinical event §	56	16	4			<0.0001 €
LTx	44	11	0			
Death	12	5	4			

Data for categorical variables expressed as number with percentages in parenthesis. Continuous variables expressed as median (IQR).
* At time of sampling
§ During follow-up
^ Kruskal-Wallis test
$ Chi-squared test
€ Log-rank test

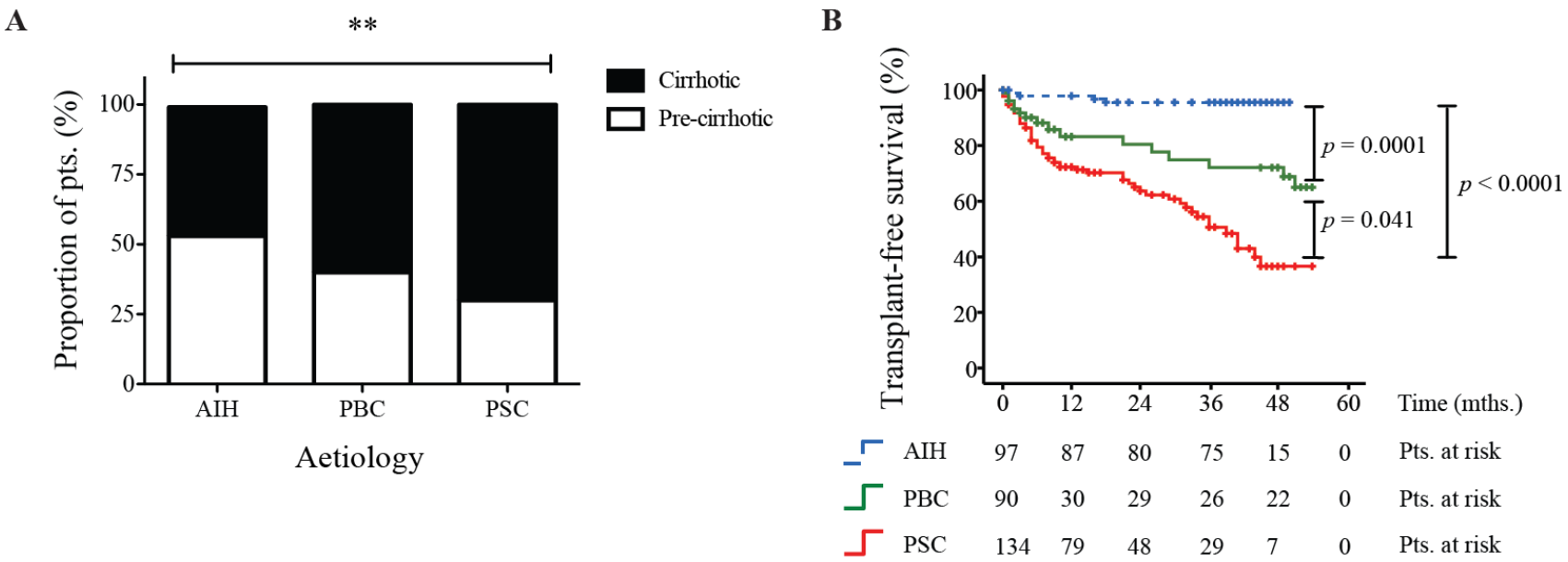

Figure 5.2: Severity and survival analysis in autoimmune liver disease

Proportions (%) of patients with evidence of cirrhosis at time of blood sampling are illustrated in (A); capped line and asterisks indicate statistically significant differences (chi-squared test). Kaplan–Meier survivorship estimates across all three autoimmune liver diseases (autoimmune hepatitis, AIH; primary biliary cirrhosis, PBC; and primary sclerosing cholangitis, PSC) are indicated in (B). Incidence rate of clinical events per-100 patient years calculated as follows: AIH 1.2; PBC, 11.7; and PSC, 25.6. Capped lines indicate significant differences (log-rank test).

5.2.1.2 Quantification of sVAP-1 levels in human serum

Serum VAP-1 levels were measured in all patients by ELISA (detailed in Chapter 2), and the most immediate observation was that the range of values in the study population did not conform to a Gaussian distribution (KS p <0.001; Figure 5.3).

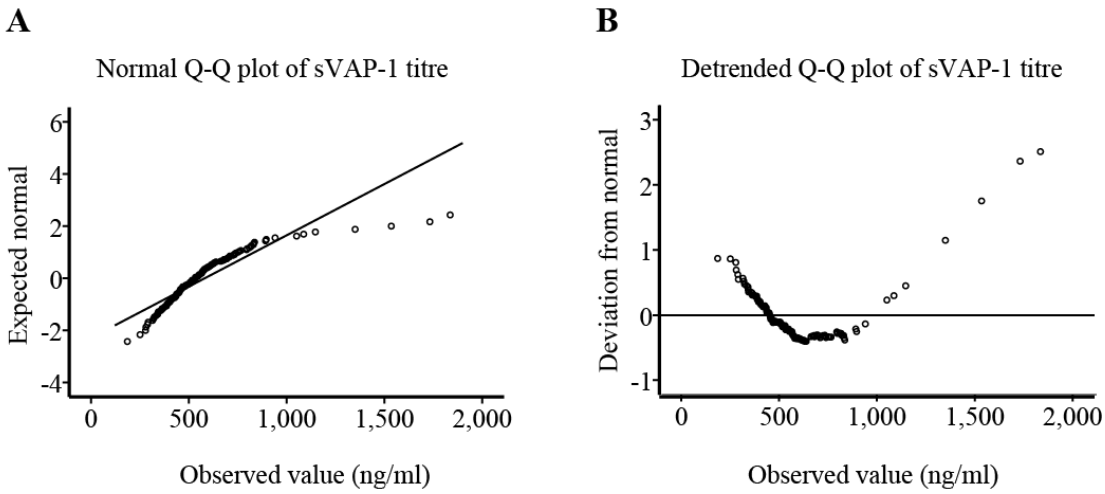

Figure 5.3: Distribution of sVAP-1 levels across the PSC study cohort
Quantile-quantile (Q-Q) plots of sVAP-1 levels indicate deviation from the expected normal distribution (diagonal) reference line (A). Extent of deviation from normal across the sample population is provided in the detrended Q-Q plot in (B).

Individuals with autoimmune liver disease (AIH, PBC and PSC) collectively demonstrated significantly higher serum sVAP-1 levels than those without evidence of liver disease (median 484 ng/mL, IQR 391 – 622 ng/mL vs. 421 ng/mL, 341 – 476 ng/mL; p <0.001; Figure 5.4a), although variation within any given aetiology was considerable (min. 156 ng/mL, max. 1836 ng/mL). When analysed by aetiology, patients with PSC had the greatest sVAP-1 levels (532 ng/mL, 432 – 668 ng/mL) compared to patients with IBD alone (413 ng/mL, 348 – 489 ng/mL), healthy controls (425 ng/mL, 336 – 466 ng/mL) and those with PBC (470 ng/mL, 374 – 653 ng/mL) or AIH (433 ng/mL. 355 – 548 ng/mL). Differences between the cholangiopathies fell short of retaining statistical significance on post-hoc testing (Figure 5.4b).

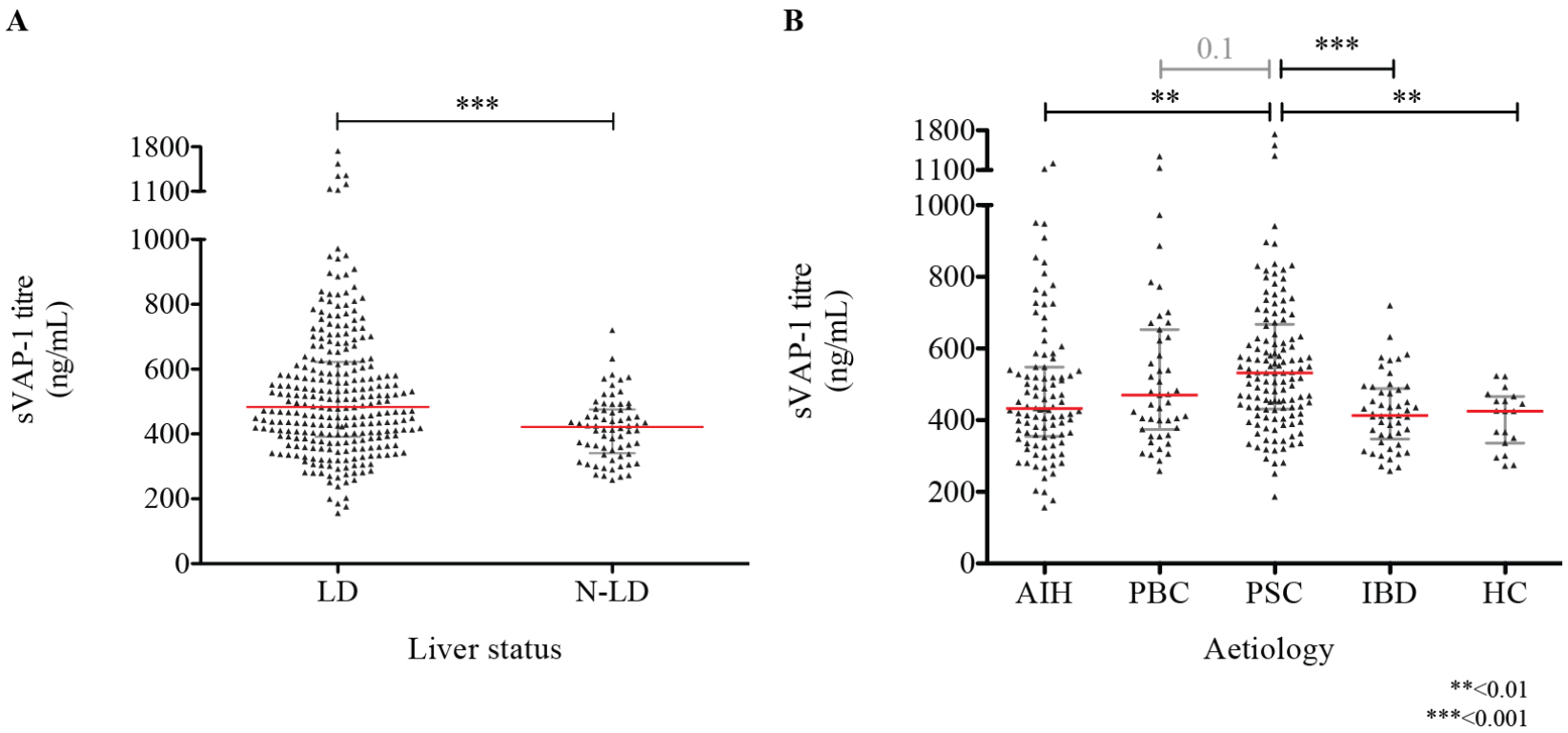

Figure 5.4: sVAP-1 quantification in human serum

sVAP-1 levels presented for patients with established liver disease (LD) and with no liver disease (N-LD) in (A). Levelss across the spectrum of autoimmune liver diseases are presented in (B); specifically AIH, PBC and PSC. Levels in those with inflammatory bowel disease without PSC (IBD) and healthy controls (HC) included for comparison. Data presented as median and IQR. Capped lines and asterisks indicate statistically significant differences on MW testing in (A) and on post hoc correction via the Bonferroni–Dunn method in (B) following the KW test (p <0.001).

5.2.2 sVAP-1 levels and clinical correlates

As the range of values varied greatly across all aetiologies I investigated whether sVAP-1 levels are associated with particular clinical characteristics. Previous studies have illustrated that sVAP-1 levels remains stable upon storage, enabling longitudinal studies to be conducted [331]. Adopting the PSC group as a derivation cohort, clinical data were collected from patient records and a correlation analysis carried out on sVAP-1 levels and the collected variables (Table 5.3). No significant associations were observed between sVAP-1 levels and IBD status, patient gender, treatment regimen with UDCA or antibiotics or immunosuppression, ascending cholangitis flares, or autoantibody positivity; nor was there any correlation with liver biochemistry, renal indices, IgG levels or UKELD score (the latter representing a medical scoring system used to allocate liver allografts in the UK).

However, indices of advanced liver disease, specifically cirrhosis and thrombocytopenia, did correlate with sVAP-1 levels; consistent with the data presented in Chapter 4 showing increased hepatic VAP-1 expression in end-stage liver disease. No significant difference in sVAP-1 levels was detectable between patients with compensated versus decompensated cirrhosis (MW test $p = 0.380$).

Given that a greater degree of PSC patients were cirrhotic relative to the PBC and AIH cohorts studied, a restricted analysis was performed exclusively in non-cirrhotic patients. Significant differences between the diseases were retained, the highest levels being observed in PSC patients (AIH: median 399 ng/mL, IQR 304 – 470 ng/mL; PBC: 411 ng/mL, 338 – 507 ng/mL; PSC: 469 ng/mL, 412 – 550 ng/mL; KW $p = 0.039$).

Table 5.3: sVAP-1 levels according to clinical covariates

Categorical associations	**sVAP-1 levels (ng/mL)**		***p* value**
Gender			
M vs. F	529 (432-627)	567 (457-698)	0.325
Disease severity *			
Pre-cirrhotic vs. cirrhotic	462 (406-547)	578 (413-736)	*0.006*
Ascending cholangitis *			
Presence vs. absence	550 (376-646)	532 (438-672)	0.350
IBD			
Presence vs. absence	532 (431-653)	542 (438-663)	0.668
Active vs. inactive	523 (387-626)	533 (443-672)	0.466
Colectomy vs. colon intact	534 (443-710)	532 (434 -651)	0.939
Immunosuppression *			
Exposure vs. absence	516 (418-621)	549 (438-663)	0.630
UDCA *			
Exposure vs. absence	534 (451-681)	457 (413-571)	0.053
Antibiotic exposure *			
Exposure vs. absence	566 (395-621)	529 (436-672)	0.600
ANA			
Positive vs. negative	517 (432-696)	551 (435-631)	0.857
ASMA			
Positive vs. negative	508 (421-627)	543 (436-676)	0.462
pANCA			
Positive vs. negative	517 (436-667)	552 (436-663)	0.794
Continuous variable correlations*	**Spearman's rho**		***p* value**
Patient age	0.194		*0.027*
AST	-0.002		0.993
ALT	-0.076		0.691
ALP ratio (to ULN)	-0.205		0.278
Bilirubin	0.217		0.250
Albumin	-0.819		0.318
Platelets	-0.585		***0.001***
INR	0.014		0.941
Na^+	0.135		0.475
Creatinine	-0.242		0.197
UKELD	0.001		0.995
IgG	0.195		0.303

Continuous data presented as median (IQR in parenthesis). Significant differences between groups are *italicised* (crude; not adjusted for multiple observations) and marked in ***bold*** (corrected for multiple comparisons via the Bonferroni-Dunn method – 24 observations, with an adjusted significance threshold of $p = 0.002$).

* At time of sampling.

5.2.3 sVAP-1 levels and clinical outcome in PSC

Having identified an association with indices of advanced disease in PSC patients, the ability of sVAP-1 to predict clinically significant endpoints was evaluated. As relatively few (<10) individuals developed hepatobiliary malignancy during follow-up, clinical endpoint analysis was restricted to liver transplantation and death. Accuracy testing of sVAP-1 was first performed by ROC-curve analysis, as the predictor under assessment (sVAP-1) is gauged on a continuous scale. Moreover, the area under the ROC curve (AUROC) method represents the most commonly adopted technique for evaluating discriminatory power of continuous variables [431,434]; with a maximum score of 1.0 indicating 100% sensitivity and specificity, and 0.5 suggesting no predictive power.

Initially, the ability of sVAP-1 to predict overall transplant-free survival was only moderate power (Figure 5.5a), with marginal improvement when restricted to predicting liver transplantation only (Figure 5.5b), or liver transplantation and liver-related death only (Figure 5.5c). A small number of individuals with PSC were listed for transplantation at time of blood sampling, which may inadvertently have led to pre-selection bias in terms of outcome prediction. The average waiting time for transplantation following listing is ~ 4 – 5 months (UK NHS Blood and Transplant; www.organdonation.nhs.uk), following satisfactory anaesthetic and surgical assessment (~1 – 2 months). In this regard, Kaplan–Meier survivorship estimates were re-calculated for only those sustaining a clinical event >6 months after blood sampling (Figure 5.6a-c). Re-examination of sVAP-1 levels by ROC-curve analysis in the remaining cohort illustrated marked improvement in predictive capacity (Figure 5.6d-f).

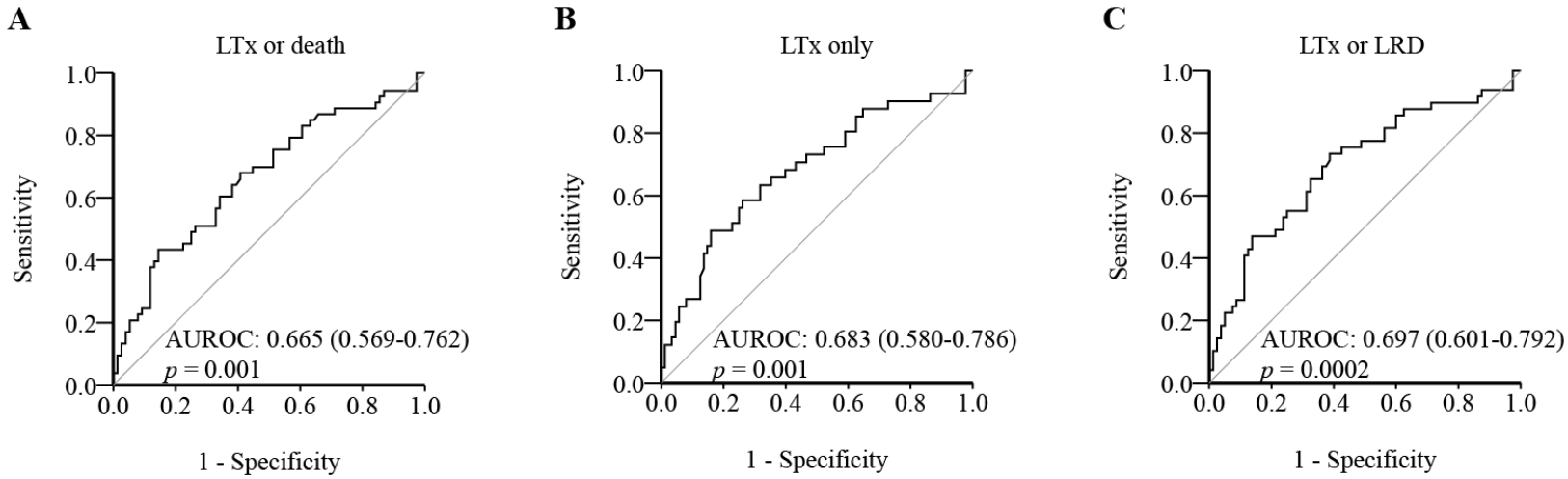

Figure 5.5: Accuracy of sVAP-1 in predicting transplant-free survival.
Receiver operator characteristic (ROC)-curve analysis of sVAP-1 levels in predicting clinical outcome; specifically, liver transplantation or death (A), liver transplantation only (B), and liver transplantation and liver-related death (C). Area under the curve (AUROC) calculated in relational to diagonal reference line and presented with 95% confidence intervals in parenthesis. Data inclusive of all PSC patients from time of sampling.

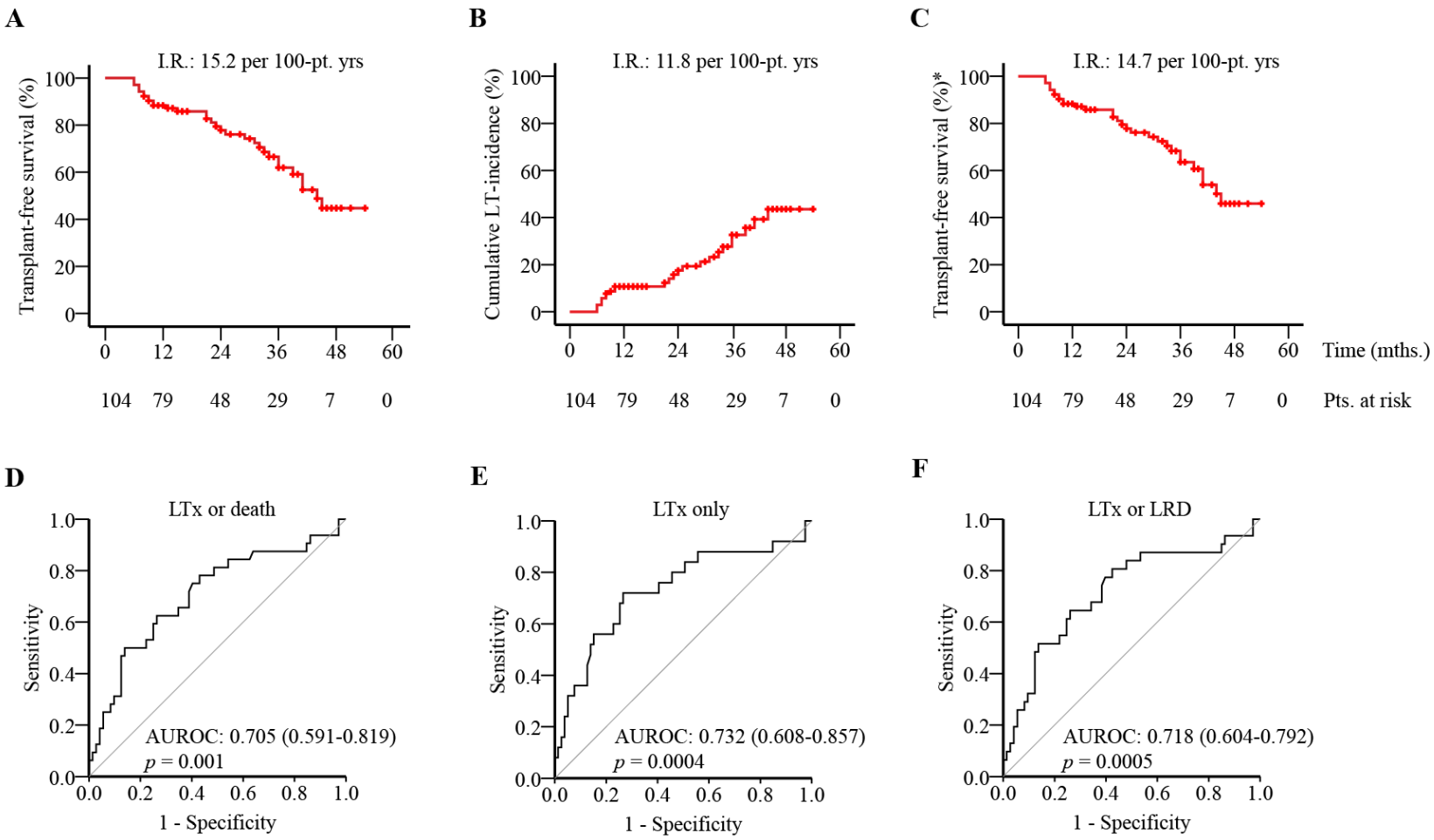

Figure 5.6: ROC and Kaplan–Meier curves following exclusion of clinical events in the first 6 months

Kaplan–Meier survivorship estimates (A – C) and ROC-curves (D – F) exclusively for those individuals in whom follow-up exceeded 6 months. Clinical endpoints are indicated as transplant–free survival (A, D), liver transplantation only (B, E) and liver transplantation/liver-related death (C, F).

ROC-curves were used to estimate a cut-off level of sVAP-1 that demonstrated maximum sensitivity and specificity with respect to outcome prediction. As the primary endpoint was overall transplant-free survival, cut-points were derived from this respective ROC-curve in which a levels of 529 ng/mL yielded sensitivity 75% and specificity of 60%. This cut-point retained predictive value for liver transplantation only (sensitivity 76%, specificity 57%) as well as liver transplantation/liver-related death (sensitivity 77%, specificity 60%). Improvement in predictive ability of liver transplantation only was obtained using a discriminatory value of 579ng/mL (sensitivity 72%, specificity 73%). This, however, did not perform as well when including mortality as an endpoint.

Dichotomising the PSC cohort based on the cut-point of 529 ng/mL, patients with an elevated sVAP-1 levels were observed to have significantly poorer clinical outcome with regard to transplant-free survival, liver transplantation alone, or liver transplant and liver related death (illustrated in Figure 5.7a – c). Similar discrimination was illustrated using 579 ng/mL as a cut-off for the transplantation alone endpoint (Figure 5.7d).

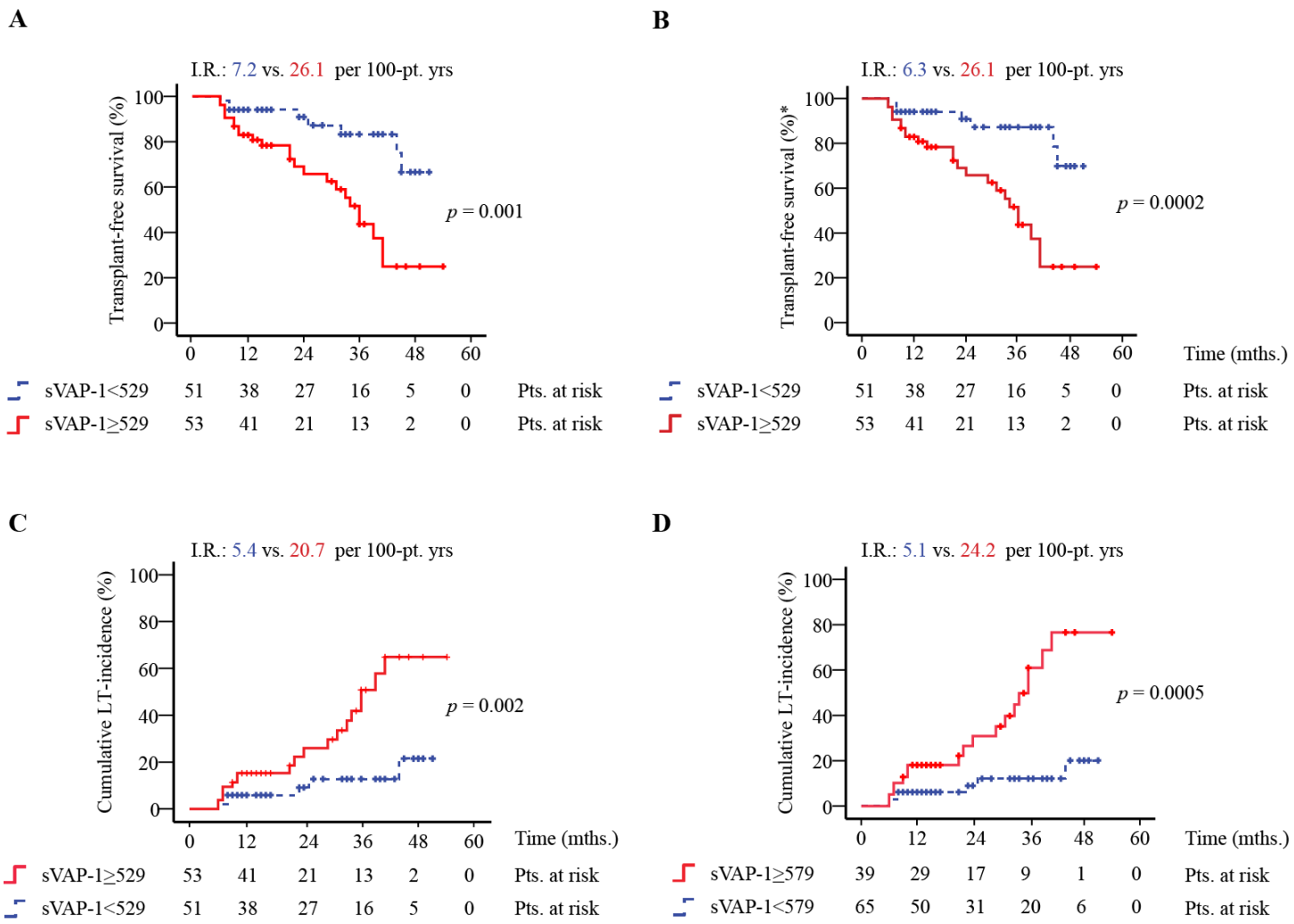

Figure 5.7: Kaplan–Meier survivorship estimates following derivation of sVAP-1 cut-points in PSC
Adopting a cut-point of 529ng/mL, a differential clinical course was observed across the PSC cohort in terms of overall transplant-free survival (A), liver transplantation and liver related death (B), and incidence of liver transplantation alone (C). Kaplan–Meier curves also provided for liver transplantation incidence using the 579ng/mL cut-point (D). Statistically significant differences in survival calculated via log-rank method.

As an additional method of analysing survival, Cox proportional hazards' models were created for the derived cut-points. Cox regression (hazards ratios, HR) involves durational modelling and possesses the ability to account for survival rates over time, being able to take full advantage of the time dimension compared to static models such as logistic regression (odds ratios, OR) that are limited in their ability to determine the likelihood of events at a singular time point.

An sVAP-1 levels >529 ng/mL was associated with significantly increased risk of progression to liver transplantation or death (Table 5.4). The resultant HR represents magnitude of risk, wherein patients with a levels >529 ng/mL have ~4 times higher risk than individuals with sVAP-1 levels below the cut-point. Performing a similar analysis for all other accrued clinical variables, the presence of thrombocytopenia, hypoalbuminaemia or the collective index of liver cirrhosis; elevated serum AST; ascending cholangitis flares ± associated antibiotic treatment, were all predictive of poorer clinical outcome in the PSC cohort.

On multivariable analysis taking a weighted account of all risk factors, statistical significance was retained for serum AST (weak predictor), cirrhosis, ascending cholangitis and serum sVAP-1 levels (Table 5.4). This suggests elevated sVAP-1 levels are an independent predictor of poor clinical outcome; however, one cannot discount potential confounding effects from the presence of cirrhosis. In an effort to resolve this issue, survival analysis was restricted to patients with pre-existing evidence of cirrhosis. Even across this pre-defined cohort, a levels >529 ng/mL significantly associated with adverse outcome (HR 2.02, 1.17 – 3.51; p = 0.012; Figure 5.8) implying independent and additive predictive utility to cirrhosis.

Table 5.4: Covariates associated with future risk of death or liver transplantation

	Univariate analysis		**Multivariable analysis (adjusted for platelet count and serum albumin)**		**Multivariable analysis (adjusted for cirrhosis)**	
	Unadjusted HR (95% CI)	***p* value**	**Adjusted HR (95% CI)**	***p* value**	**Adjusted HR (95% CI)**	***p* value**
Cirrhosis	6.02 (1.83-20.00)	0.003	N/A		7.69 (2.04-27.03)	0.002
Ascending cholangitis	2.62 (1.20-5.72)	0.016	3.40 (1.46-7.90)	0.004	4.23 (1.72-10.42)	0.002
Antibiotic exposure	1.91 (1.24-2.92)	0.003	n.s.	n.s.	n.s.	n.s.
Thrombocytopenia (per 50x 10^3 cells dec.)*	1.22 (1.02-1.42)	0.028	n.s.	n.s.	N.A	
Hypoalbuminaemia	1.21 (1.12-1.30)	<0.001	1.18 (1.08-1.28)	<0.001	N.A	
Elevated serum AST	1.01 (1.00-1.01)	0.006	1.01 (1.00-1.02)	0.003	1.02 (1.01-1.02)	<0.001
sVAP-1 (per-100ng inc.)*	1.11 (1.11-1.22)	0.002	(not included)		(not included)	
sVAP-1: ≥ 529ng/mL	3.76 (1.68-8.47)	0.001	2.70 (1.03-714)	0.043	3.85 (1.57-9.34)	0.003

* Values in parenthesis indicate that the degree of risk (indicated by HR values in the adjacent columns) varies according to magnitude change in the given variable.

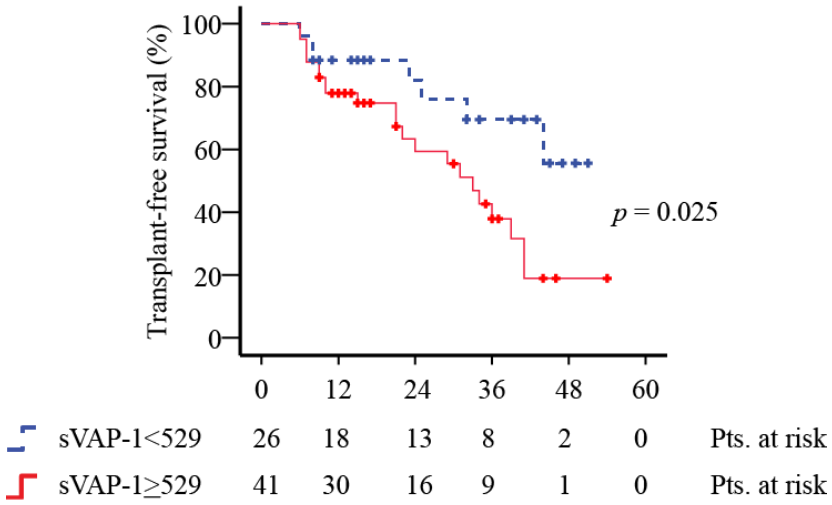

Figure 5.8: Predictive value of sVAP-1 in PSC cirrhosis
Kaplan–Meier survivorship estimate restricted to cirrhotic PSC patients. Statistically significant differences in survival calculated via the log-rank method.

5.2.4 Assessment of serum SSAO activity

In a manner similar to that described in Chapter 4 the rate of production of H_2O_2 was used as a proxy for measuring enzyme activity, and normalised to a given volume of serum. Initially enzyme activity was measured following inclusion of MAO-A and MAO-B inhibitors and presented as residual activity following semicarbazide correction (Figure 5.9). As with hepatic enzyme activity and serum sVAP-1 levels, patients with PSC exhibited greater serum enzyme activity (median 115 pmol H_2O_2/min/mL serum, IQR 101 – 188 pmol) than patients with AIH (78pmol, 51 – 125 pmol), PBC (54 pmol, 33 – 91 pmol), IBD alone (60 pmol, 39 – 73 pmol) or healthy controls (84 pmol, 78 – 106 pmol), although the distribution across any given aetiology was broad. As expected, there was a significant correlation with serum sVAP-1 levels, suggesting that VAP-1 accounted for the majority of semicarbazide

sensitive amine oxidase activity in human circulation, in keeping with current literature [214,414].

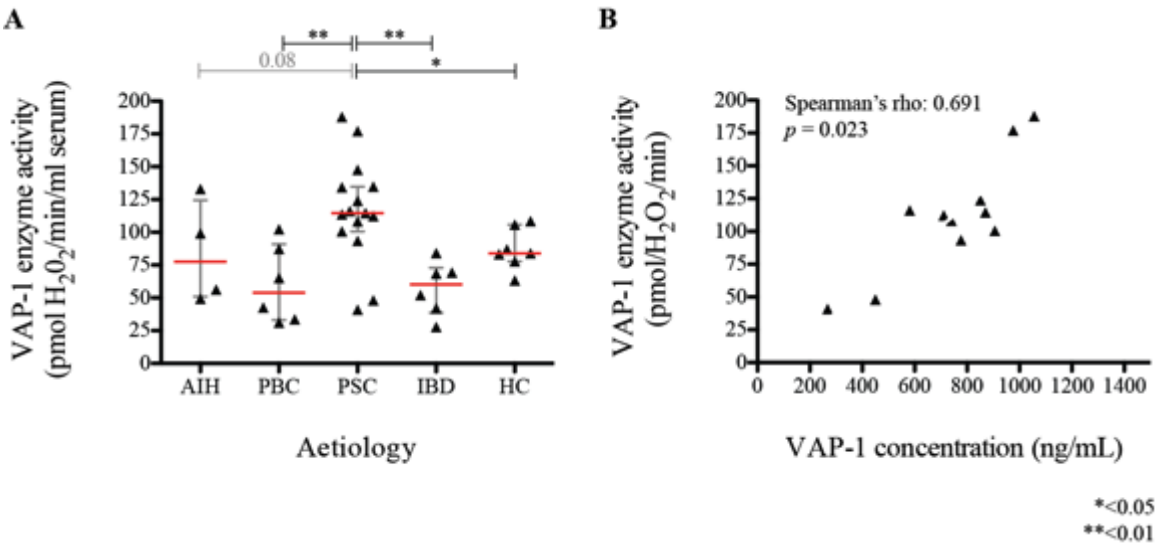

Figure 5.9: sVAP-1 enzyme activity and correlation with levels
Enzyme activity was assessed (method 1) in human serum across the 3 autoimmune liver diseases, IBD alone and healthy controls (A) – data presented as median and IQR, with capped lines and asterisks indicating statistically significant differences (KW-test and post-hoc correction via the Bonferroni-Dunn method). Correlation between enzyme activity and sVAP-1 concentration for PSC patients is provided in (B).

This preliminary series of experiments included relatively few patient samples; and as previously discussed the technique involving addition of MAO inhibitors was later substituted in favour of enzyme capture and immobilisation using high affinity binding Maxisorp plates. Using the residual of samples available following sVAP-1 ELISA, amine oxidase activity was measured in patients with PBC, PSC, and IBD alone and healthy controls. Unfortunately, serum samples from AIH patients were no longer available at this point.

Across this relatively large sample set, sVAP-1 enzyme activity displayed considerable deviation from a normal distribution (Figure 5.10). Contrary to previous results, significant differences between PSC, PBC and healthy controls were no longer evident on post-hoc testing (Figure 5.11). Patients with IBD however, continued to demonstrate persistently low sVAP-1 enzyme activity.

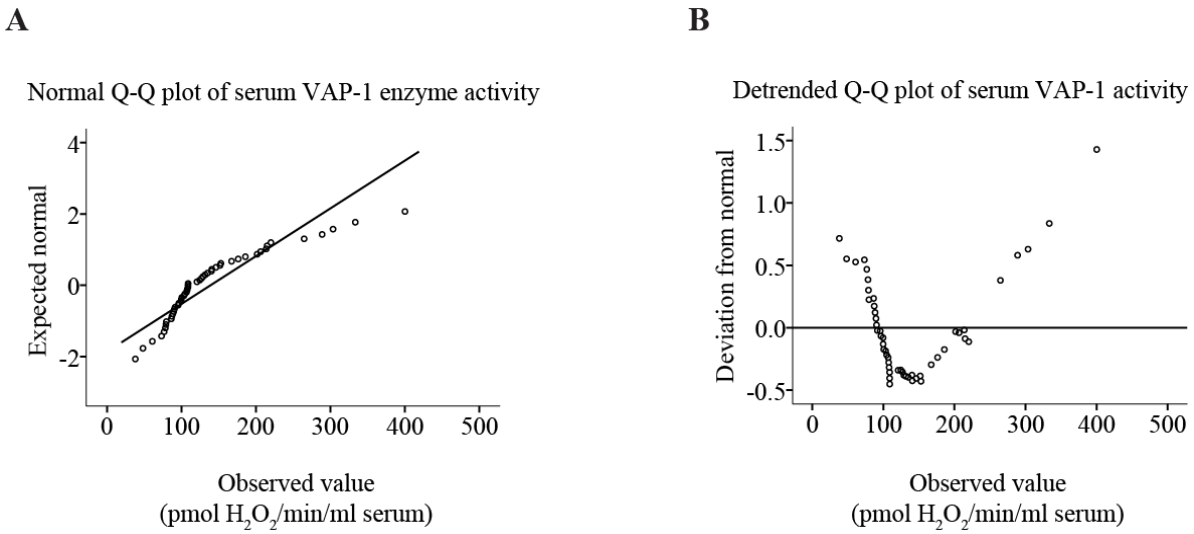

Figure 5.10: Distribution of sVAP-1 enzyme activity across the PSC study cohort
Quantile-quantile (Q-Q) plots of enzyme activity indicate deviation from the expected normal distribution (diagonal) reference line (A). Extent deviation from normal across the sample population is provided in the detrended Q-Q plot in (B).

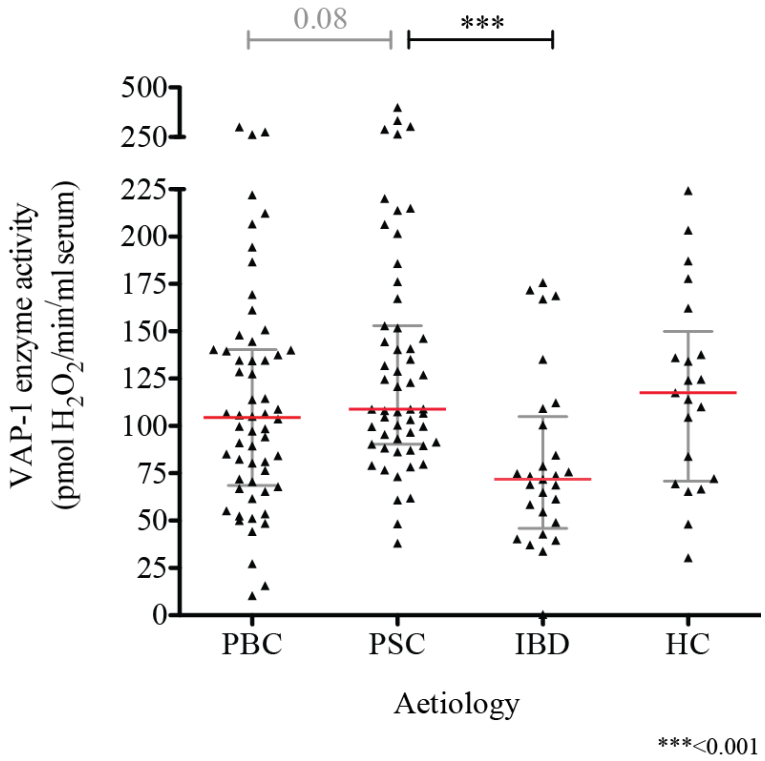

Figure 5.11: sVAP-1 enzyme activity following protein capture
sVAP-1 enzyme activity presented for patients with PBC (median 108 pmol H_2O_2/min/mL serum; IQR 69 – 140 pmol), PSC (109 pmol; 90 – 153pmol), IBD alone (72 pmol; 46 – 105 pmol) and HC (118 pmol; 71 – 150 pmol). Capped lines and asterisks indicative of statistically significant differences on post-hoc testing via Bonferroni-Dunn method (KW test p <0.001).

In the PSC cohort, there was no significant association or correlation between serum enzyme activity and any assessed clinical parameters, with the exception of patient gender (Table 5.5); noteworthy given that population studies report a male predominance of PSC. Of note, although elevated enzyme activity was observed in patients with cirrhosis relative to pre-cirrhotic individuals, these did not reach statistical significance unlike sVAP-1 levelss (MW test). Given the observed associations between sVAP-1 levels and disease stage as well as clinical outcome, survival analysis was conducted against serum enzyme activity. However, ROC-curves demonstrated poor predictive performance (AUROC 0.497, 0.274 – 0.721; p = 0.980) and such assessments were not conducted any further.

Table 5.5: sVAP-1 enzyme activity according to clinical covariates

Categorical associations	**sVAP-1 activity (pmol H_2O_2/min/mL serum)**		***p* value**
Gender			
M vs. F	131.86 (103.26-201.63)	89.96 (76.19-104.72)	*0.003*
Disease severity *			
Pre-cirrhotic vs. cirrhotic	104.64 (86.33-120.82)	133.49 (97.57-203.99)	0.062
Ascending cholangitis *			
Presence vs. absence	107.46 (96.00-149.03)	114.89 (89.64-176.25)	1.000
IBD			
Presence vs. absence	108.97 (89.01-171.18)	118.16 (106.77-140.79)	0.669
Active vs. inactive	118.25 (88.38-185.85)	108.97 (90.94-160-13)	0.804
Colectomy vs. colon intact	99.72 (93.53-131.07)	116.78 (89.64-176.25)	0.326
Immunosuppression *			
Exposure vs. absence	89.64 (87.14-131.86)	116.78 (97.57-171.77)	0.327
UDCA *			
Exposure vs. absence	108.92 (88.39-151.84)	115.68 (99.61-185.85)	0.540
Antibiotic exposure *			
Exposure vs. absence	140.79 (95.63-168.83)	108.92 (89.64-167.30)	0.649
ANA			
Positive vs. negative	101.87 (79.72-151.84)	114.89 (99.61-201.63)	0.131
ASMA			
Positive vs. negative	104.29 (88.39-130-36)	116.78 (92.93-181.04)	0.418
pANCA			
Positive vs. negative	133.49 (90.34-201.63)	106.77 (89.01-149.03)	0.523
Continuous variable correlations*	**Spearman's rho**		***p* value**
Patient age	0.073		0.463
AST	-0.103		0.326
ALT	-0.199		0.055
ALP ratio (to ULN)	-0.23		0.816
Bilirubin	0.106		0.294
Albumin	0.017		0.865
Platelets	-0.021		0.829
INR	-0.074		0.498
Na^+	-0.012		0.910
Creatinine	0.033		0.737
UKELD	0.099		0.326
IgG	-0.052		0.620

Data for categorical variables expressed as number (percentages in parenthesis). Continuous variables expressed as median (IQR in parenthesis).

* At time of sampling.

§ Previously treated – not present at time of sampling.

Unexpectedly, serum VAP-1 levels and enzyme activity no longer retained a significant correlation following assessment of the latter via the Maxisorp method (Figure 5.12).

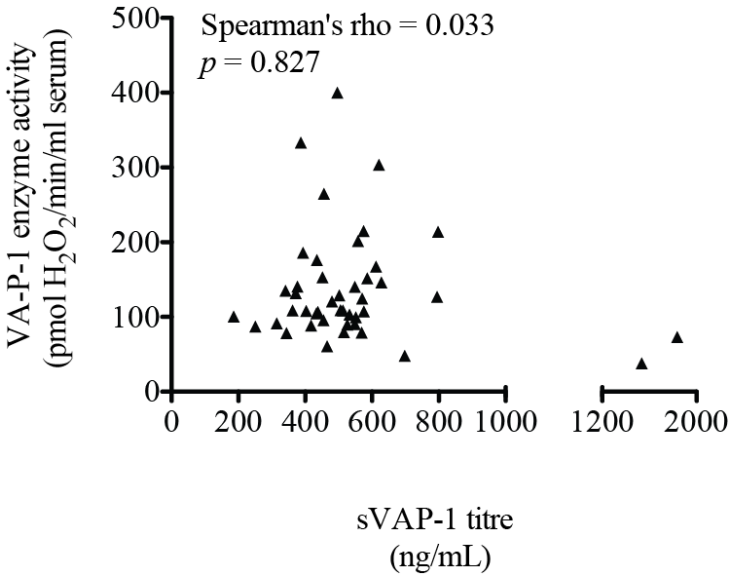

Figure 5.12: sVAP-1 enzyme activity (MaxiSorp) vs. sVAP-1 levels
Correlation between sVAP-1 enzyme activity and sVAP-1 levels in PSC serum following assessment of the former with the MaxiSorp method.

This observation could have been due to a number of factors the concentration of TK8-18 antibody (5 μg/mL; 100 μL/well = 0.5 μg/well) may not have been sufficient to capture high levelss of sVAP-1 in PSC sera. A stepwise restriction analysis based on 100ng/mL increments of sVAP-1 was conducted and compared across respective enzyme activity in the same samples. Only in the presence of sVAP-1 levels <400 ng/mL did enzyme activity correlate with circulating concenrations (Table 5.6). The number of individuals lacking paired serum sVAP-1 measurements and enzyme activity measurements is a recognised limitation, and may also have contributed to discrepancies from incomplete data. Further dose finding/optimisation steps are

therefore necessary with the Maxisorp method, incorporating incremental TK8-18 antibody concentrations to ensure maximum protein capture.

Table 5.6: Correlation between sVAP-1 levels and enzyme activity across cut-offs

Serum sVAP-1 levels	**No. of XY pairs**[§]	**Levels vs. enzyme correlation coefficient** *	***p* value** *
<400ng/mL	*10*	*0.770*	*0.013*
<500ng/mL	21	0.292	0.199
<600ng/mL	36	0.083	0.631
<700ng/mL	40	0.123	0.451
<1500ng/mL ^	45	0.175	0.517

* Spearman's rank correlation coefficient.
§ Number of cases with paired serum sVAP-1 levels and enzyme activity.

Another possibility to consider was whether the capture antibody TK8-18 exerts an inhibitory effect on enzyme activity. To test this hypothesis, recombinant VAP-1 at increasing concentrations was incubated with 5 μg TK8-18, utilising benzylamine as the archetypal substrate. Semicarbazide (250 μM) was utilised in parallel as a positive control for 100% enzyme inhibition. Only a small, non-significant degree of inhibition was seen with TK8-18 (mean 9.5%, SEM 3.7; Figure 5.13), in keeping with error of technical replicates within the assay.

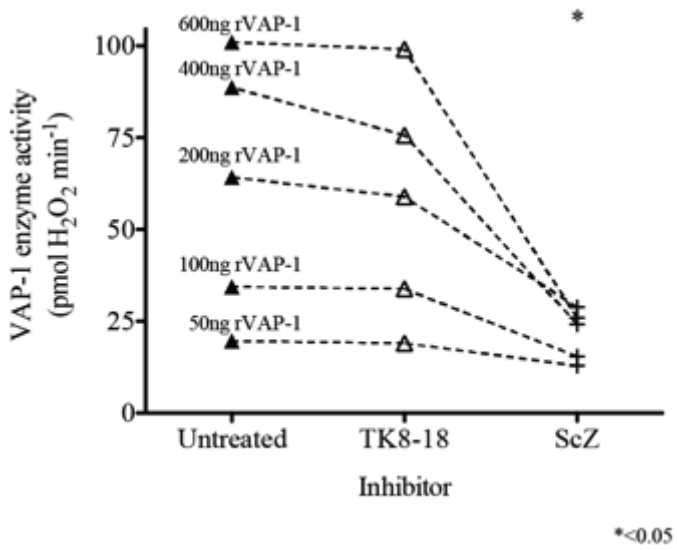

Figure 5.13: Enzyme inhibition of VAP-1 by TK8-18 vs. semicarbazide
Effects on enzyme inhibition were compared by TK8-18 and semicarbazide in the Amplex Red assay. Data points representative of the mean of 2 independent experiments (each consisting of 3 technical replicates). Asterisks denote statistically significant inhibition from untreated samples (paired t-test).

5.2.5 Detection of methylamine by HPLC

In Chapter 4 data were presented outlining the ability of different biological amines to act as substrates for VAP-1 enzyme activity. As some of these are physiological amines or produced by gut bacteria I investigated whether patients have elevated circulating levels of these substrates. Several methods of amine quantification have been described, particularly for methylamine. However, none have been deemed sufficiently sensitive or selective for use in human blood and tissues due to interference from background proteins, and more so the very low boiling point (methylamine evaporates at –6^{o}C). For the purposes of this study I adapted fluorometric HPLC using FMOC as a derivatising reagent as recently described by Xiao et al. [340].

First, known concentrations of methylamine were prepared and serial chromatograms recorded. Using this technique FMOC peaks were clearly visible in chromatograms at ~20 – 25 minutes but absent from FMOC-free samples (Figure 5.14).

Serum-free samples were spiked with increasing concentrations of methylamine in the presence or absence of FMOC; an amine peak only being manifest in samples bearing both agents. The area under each peak corresponded to the quantity of amine present within any given sample and was used to generate a standard curve (Figure 5.15a).

Unfortunately this method was not able to confidently discern methylamine concentration in serum, largely due to an excess of background noise peaks in human sera (Figure 5.15b), which may have been a consequence of the extraction procedure. Furthermore, the protocol was not deemed appropriate for high throughput use, mostly due to prolonged evaporation times (>4 hours for 2 samples) and consequently an inability to process multiple samples simultaneously. Following repeated attempts at validation, efforts to quantify methylamine using this approach were abandoned.

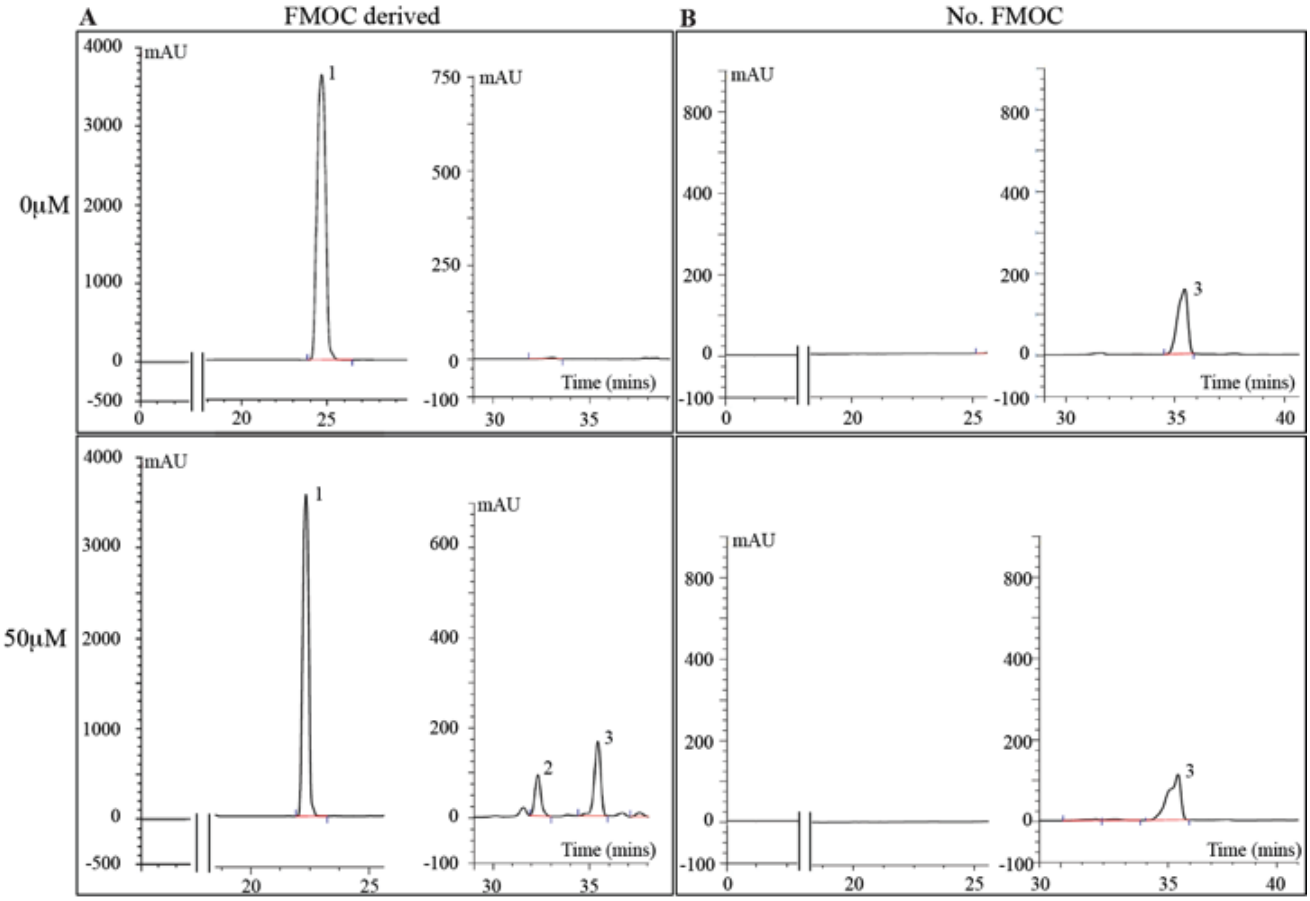

Figure 5.14: Quantification of methylamine by HPLC

Methylamine quantification was attempted using high-performance liquid chromatography (HPLC). Representative peaks presented for FMOC (derivatising agent) containing samples ± methylamine. Heights of the peaks are measured in milliabsorbance units. The corresponding peaks for FMOC (peak 1) are illustrated in the FMOC containing samples (A). The methylamine peak (peak 2) is seen in the sample containing 50μM methylamine, but not in blank (0μM) samples, or those free of FMOC (B). Non-specific signals (noise peak 3) were common, and attributed to solvents used in the procedure.

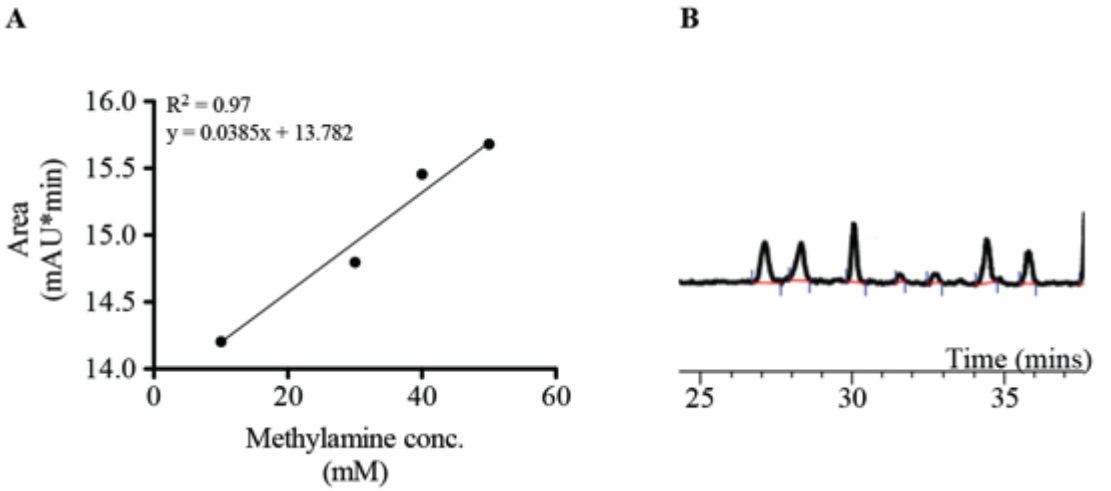

Figure 5.15: Determination of methylamine concentration in serum
Using the area under the curve (height in milliabsorbance units x duration of peak) a standard curve was created corresponding to known methylamine concentrations (A). Analysis of serum methylamine was not possible due to the presence of several possible methylamine peaks – representative specimen illustrated (B).

5.2.6 Assessing intrinsic putative substrate concentrations

As an alternative to quantifying methylamine concentration, efforts were made to indirectly measure amine substrate contributions in human serum. Adapting the Amplex red assay, serum sVAP-1 activity was measured without addition of any exogenous substrates in the presence of MAO inhibitors and in parallel to semicarbazide treatment (method 1). The rationale for doing so was that in the absence of exogenous substrate, any detectable sVAP-1 activity would be attributable to pre-existing substrates in a given sample. However, no detectable differences were illustrated between semicarbazide–treated versus semicarbazide–free samples (Figure 5.16), possibly indicating that whatever substrate was present in serum has long since evaporated, had been consumed in enzymatic reactions prior to sampling, was present at too low concentrations (< K_m) to undergo rapid catalysis, or produced quantities of H_2O_2 below sensitivity limit of the assay.

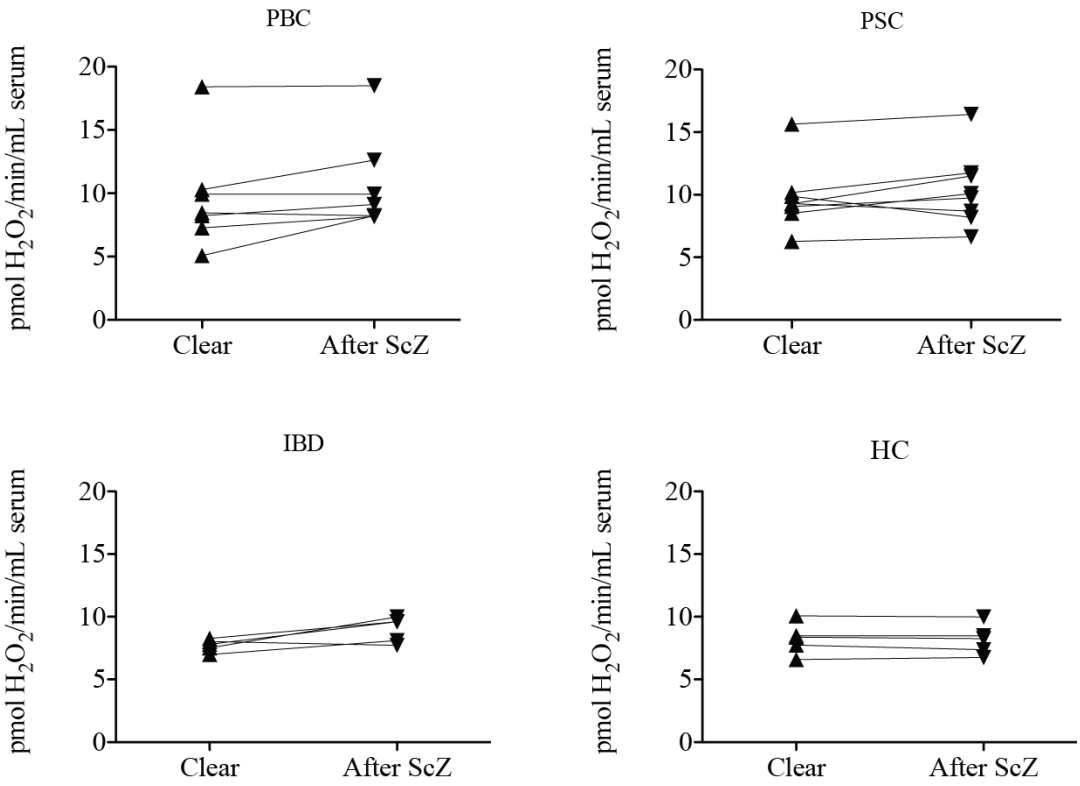

Figure 5.16: Substrate-free enzyme activity in human sera
Background serum sVAP-1 enzyme activity was assessed in the absence of exogenous substrate across autoimmune liver disease and HC samples. Amine oxidase activity attributable to sVAP-1 was determined based on differences following inclusion of semicarbazide, ScZ (VAP-1 enzyme inhibitor). Representative results shown of n=6 cases per aetiology run in triplicate.

5.3 Discussion

Herein, I demonstrate that serum sVAP-1 levels are elevated in patients with chronic autoimmune hepatobiliary disease. Serum VAP-1 levels were greatest in PSC patients and correlated with surrogate indices of cirrhosis. A notable proportion of patients in our PSC cohort were cirrhotic relative to PBC or AIH, a factor likely contributing to significantly poorer outcome. Nevertheless, when a restricted analysis was performed exclusively in non-cirrhotic patients, sVAP-1 levels were still greatest in the PSC population.

Elevated sVAP-1 concentration was a significant predictor of poor long-term outcome in PSC patients; specifically, progression to liver transplantation and early mortality – the latter likely attributable to liver-related death. Moreover, sVAP-1 retained independent predictive capacity on robust statistical testing, following adjustment of other covariates influencing clinical outcome such as liver disease severity. Moreover, sVAP-1 retained predictive capability in the cohort of individuals with evidence of cirrhosis at baseline, suggesting independent and additive predictive value in PSC patients with pre-existing cirrhotic liver disease.

In contradistinction, serum sVAP-1 enzyme activity although elevated in PSC patients relative to those with IBD alone, was not significantly greater than healthy controls; neither did it correlate with any specific clinical parameter, except gender. An assessment of circulating methylamine concentration via HPLC was also conducted, which although partly successful was not deemed practical for high throughput application.

5.3.1 Quantification of serum sVAP-1 levels in autoimmune liver disease

In Chapter 4, data were presented illustrating elevated VAP-1 gene expression and enzyme activity in chronic liver disease tissue relative to non-inflamed/non-cirrhotic liver with particularly high levels seen in patients with PSC. The liver is a major source of sVAP-1, which is proposed to enter circulation via proteolytic cleavage from the surface of endothelial cells and adipocytes [328], with additional secretion by activated liver myofibroblasts [214]. The mechanism of release however remains poorly understood although there is some evidence to implicate a metalloproteinase [319]. Soluble VAP-1 levels are also increased in patients with NAFLD independent of age and metabolic phenotype; and correlate with histological disease severity (inflammation and fibrosis) and outcome [214] using the same assays for sVAP-1 quantification as my study.

Previous studies measuring sVAP-1 in patients with autoimmune liver disease did not report higher levelss in PSC compared with AIH or PBC [414]. However, these techniques were performed on small number of retrospectively collected samples and the methodology used a chemiluminescence sandwich ELISA as opposed to europium–coupled time-resolved immunofluorescence (ECRIF) used in this chapter. Dissociation-enhanced lanthanide fluoroimmunoassays are reportedly the most sensitive and reliable immunoassay platforms, able to achieve sensitivities several orders of magnitude superior to colorimetric assays. Incorporation of lanthanide chelates like europium and time-resolved detection systems have been proposed to eliminate background interference, as lanthanide decay occurs over a prolonged time period compared to natural fluorescence [435]. Moreover, time resolution enables

fluorescence specific to europium to be quantified and proposed as conferring the highest degree of sensitivity.

Using this technique I found that sVAP-1 levelss were significantly higher in PSC patients compared to other disease groups. Given that sVAP-1 levels correlated with indices of advanced liver disease (cirrhosis as a combinatory parameter, or platelet count as an isolated covariate), a restricted analysis in non-cirrhotic individuals was performed; in which elevated sVAP-1 levels retained significant association with PSC. The low values in patients with IBD-alone is perhaps unsurprising and in keeping with the studies by Koutroubakis and Kurkijarvi who report similar serum values in UC, Crohn's disease and healthy controls [330,436] and with a recent study in colorectal cancer [437]. These findings support evidence that the source of sVAP-1 is from the liver in patients with PSC, not the gut.

Perhaps the most striking finding however, was the independent ability of sVAP-1 levels to predict clinical outcome; specifically, transplant-free survival. Several other liver disorders are associated with increased circulating levels of soluble adhesion molecules for example soluble VCAM-1 and soluble E-selectin with PBC disease stage and soluble ICAM-1 with PBC disease activity and severity of cholestasis [438–440]. More recently our group reported that in a cohort of NAFLD patients (n=144), those who subsequently died during follow-up had higher initial sVAP-1 levels than survivors [214]. Although this study was not designed for risk stratification by sVAP-1 (no survival analysis or correction of time-factor) there was suggestion of an association between higher protein levels and all-cause mortality. In a prospective cohort study over 9 years, Finnish individuals with elevated sVAP-1 levels but

without documentary evidence of liver disease had a significantly increased risk of major cardiovascular events independent of known hazard factors comprising the well-known Framingham risk score [331]. Individuals with cardiovascular risk factors often have underlying NAFLD in the absence of symptoms [441,442]; and reciprocally, morbidity and mortality in patients with NAFLD is most often attributable to cardiovascular events. [413] Of note, NAFLD patients also harbour an increased risk of colonic neoplasms, and PSC also exhibits higher rates of diabetes and cardiovascular events relative to a matched control population [254,332]. A common pathogenic link with VAP-1 cannot therefore be discounted.

Early recognition of PSC patients with a predicted poor long-term outlook would be very helpful in patient management allowing effective triage into clinical trials and early referral for transplantation and this could become an important clinical use of measuring sVAP-1 levels. The association with increased tissue expression, circulating levels and enzymatic activity of VAP-1 in PSC provides further support of a pathogenic role in PSC. Given the relatively short clinical follow-up time in the current PSC cohort, obtaining serial readings in a meaningful number of patients was not possible, and it remains to be seen whether a change in circulating levels (ΔsVAP-1 over time) corresponds to better or worse clinical outcome.

The shortened clinical follow-up time also precluded assessment of long-term transplant-free survival as a ‘hard’ end-point in our cohort. Further external validation of our results will be important although challenging given the considerable challenges to long-term prospective studies in PSC provided by the slowly progressive nature of the disease, its relative rarity and the absence of routine

histological evaluation as part of standard of care. The predictive performance would also benefit from being compared to other potential biomarkers including transient elastography [443], for which further validation is required to determine its value as a predictor of liver fibrosis and long-term outcomes in PSC.

5.3.2 Serum enzyme activity

sVAP-1 enzyme activity has been shown to closely correlate with serum protein levels [214]. In keeping with the tissue expression and circulating levels of sVAP-1, enzyme activity was significantly greater in PSC compared with other liver diseases, healthy controls and patients with IBD alone. Circulating sVAP-1 accounts for most of the amine oxidase activity detected in mouse and human serum [328,330,414]; however, the need to eliminate contributions from other circulating amine oxidases (MAO-A/MAO-B for instance) in the analysis led me to modify the Amplex Red assay (please see Chapters 2 and 4). This allowed a more accurate estimation of intra-hepatic VAP-1 enzyme activity but when applied to serum yielded results that were different from those seen using the conventional method. As such, correlations between serum protein level and enzyme activity were lost leading me to investigate why this might have occurred. Reassuringly, the capture antibody TK8-18 did not inhibit enzyme activity. The fact that a correlation between enzyme activity and serum levels were seen at the lower range of sVAP-1 values suggests further optimisation of the enzyme capture and immobilisation method is needed, perhaps using higher antibody concentrations for extracting protein. Unfortunately not all serum samples in which sVAP-1 levels was measured were available for assessment of enzyme activity and I was unable to obtain more samples from the AIH patient cohort, thus enzyme activity in this aetiology was not assessed with the new method.

Alternatively, it is possible that an SSAO variant is present in the serum that is not recognised by the TK8-18 antibody [410]. Differences between tissue and serum activity could also arise as a consequence of differences in sample processing; for instance the absence/presence of lysis buffer in the former, or perhaps stearic hindrance due to high density of VAP-1 in well-plates artificially reducing enzyme activity.

The possibility remains that serum enzyme activity may not differ between diseases, despite detectable differences in circulating protein levels. It is plausible that older methods were affected by background fluorescence on the Amplex Red fluorogen, yielding falsely elevated readings that are no longer apparent with the protein capture method. Another explanation may reside in alternatively spliced variants of VAP-1 bearing different enzyme activities [410]. This aspect has not yet been explored in gastrointestinal or liver disease, but if alternative forms of VAP-1 exist then perhaps variants with higher enzyme activity are retained in the liver during active inflammation whereas formats with lower activity have a higher turnover and cleaved into the circulation. This would not however explain the close correlation between protein levels and enzyme activity observed with previous methods of assessment.

5.3.3 Possible roles of soluble VAP-1

The physiological or pathological function of circulating sVAP-1 is unclear. Akin to the membrane-bound endothelial form, sVAP-1 is decorated with sialic acid moieties that are proposed to confer the molecule with its adhesive properties. Given the ability to induce lymphocyte chemotaxis [214], sVAP-1 may represent a compensatory

regulatory mechanism for reducing cell surface expression and tissue specific lymphocyte recruitment (negative feedback).

Alternatively, Kurkijarvi *et al*. propose that prior binding of sVAP-1 to the surface of lymphocytes confers an increase in their adhesive status, and results in overexpression and/or avidity of other cell-surface adhesion molecules (a positive feedback mechanism) [330]. The investigators created endothelial VAP-1 transfectants and observed increased lymphocyte binding following pre-incubation with sVAP-1. However, when lymphocytes were pre-incubated in sVAP-1 free conditions, adhesion was significantly attenuated. Moreover, lymphocyte binding to mock-transfected endothelial cell lines did not increase despite pre-incubation with sVAP-1. Therefore it is plausible that lymphocytes recognise endothelial adhesion molecules, expression of which depends on VAP-1 enzymatic function. This would fit with PSC patients having increased hepatic VAP-1 expression and enzyme activity and increased local expression of MAdCAM-1 and other IgSF members on the endothelial surface. Increased circulating sVAP-1 concentrations could also increased avidity and cell-binding capabilities of circulating lymphocytes, and collectively these mechanisms would facilitate increased lymphocyte-HSEC adhesion under pro-inflammatory conditions.

The role of circulating VAP-1 enzymatic activity is also unclear. Such a presence is speculated to induce a scavenging effect on circulating amines, and lead to the production of potentially cytotoxic aldehydes [414]. Generation of H_2O_2 from the deamination reaction may also contribute free radical generation in hepatobiliary disease. VAP-1 is highly expressed by adipocytes, and provision of amine substrates

has been shown to stimulate glucose uptake and inhibit lipolysis in a mechanism dependent upon H_2O_2 [334,335]. This is of particular importance given the association of both NAFLD and PSC with elevated hepatic and sVAP-1 levels, as well as increased diabetes and cardiovascular risk.

5.3.4 Quantifying serum methylamine

In Chapter 4, I showed that certain amines induce VAP-1 enzyme activity with greater efficiency and efficacy than others, with particular potency demonstrated for dopamine, cysteamine and methylamine. Based on these results, I attempted to quantify VAP-1 substrates in human tissue. Our previous studies of VAP-1 enzyme activity used methylamine to induce functional consequences *in vivo* [294] and so I focussed by investigations on this amine.

Methods for analysing methylamine in foodstuffs have been reported although none has been validated as sufficiently sensitive or selective for microanalysis in blood and human tissue. Quantitative assessment in biological samples is hampered due to volatility (melting and boiling point –93^{o}C and –6^{o}C, respectively) and hydrolipophilicity; as well as interference by complex biological constituents. A technique developed by Xiao *et al*. in which methylamine was conjugated to FMOC and analysed in a HPLC system was claimed to overcome several analytical difficulties [340]. However I was unable to replicate their success despite multiple attempts, largely due to an overwhelming contribution of background signal from various biological components. Moreover, the volatility of methylamine meant that solvent evaporation had to be undertaken cautiously over several hours per-sample, and was impractical for multiple sample processing. With later enzyme kinetic assays,

it became evident that cysteamine is the substrate associated with highest enzyme efficiency (see Chapter 4), and HPLC techniques for quantifying cysteamine from *E. coli* have recently been reported [444]. The relatively higher melting point (~95^{o}C) would theoretically provide increased stability in solution and is an opportunity yet to be explored in human sera.

An alternative approach to assess circulating substrates in PSC patients is to simply assess background amine oxidase activity in serum following MAO-A and MAO-B pre-inhibition without addition of exogenous substrate. However, no amine oxidase activity was detectable using this approach (no difference between untreated versus semicarbazide treated wells). This is probably due to the volatility of amines (e.g. methylamine) resulting in their evaporation at the benchside; or perhaps more likely that any circulating substrates would be consumed by circulating sVAP-1 amine oxidase activity prior to analysis. One possible avenue to circumvent these technical obstacles would be to precipitate all VAP-1 from serum at the time of sample collection, and then supplement rVAP-1 at a known concentration. This would mean any measured differences in enzyme activity between samples would be directly attributable to differences in endogenous substrate quantity. If successful, such an endeavour could also be applied to tissue protein lysates from human liver.

5.3.5 Summary

Soluble VAP-1 levels, were increased across the spectrum of autoimmune hepatobiliary diseases with the highest levels recorded in patients with PSC. Within each disease there was a wide range of values probably reflecting disease severity. The finding that sVAP-1 levels correlate with clinical outcome is novel and given the

dearth of reputable biomarkers in PSC of potential clinical use. However it needs to be verified by independent external validation. Putative functional consequences of increased hepatic and soluble VAP-1 have been proposed, which could plausibly enhance lymphocyte-HSEC adhesion through up-regulation of cell recruitment pathways normally restricted to the gut.

6 Results IV: VAP-1 enzyme inhibition *in vivo*

6.1 Introduction

The previous chapters show that intrahepatic VAP-1 expression and enzyme activity are up-regulated in PSC, the functional consequences of which may contribute to increased lymphocyte recruitment. That enzyme activity is substrate specific, possibly influenced by the delivery via the portal vein of amines from the gut, provides further support to the hypothesis that the intestine has a pivotal role in driving hepatobiliary inflammation in PSC. Moreover, elevated circulating sVAP-1 levels are detected in PSC probably arising from the injured liver, and predict clinical outcome.

Therapeutic targeting of VAP-1, through its adhesion molecule properties and enzyme activity, may not only reduce pro-inflammatory lymphocyte recruitment to the liver directly thereby reducing inflammation and fibrosis, but may also attenuate the expression of other cell adhesion molecules implicated in PSC disease pathogenesis. This led me to determine whether we could establish a murine model of PSC and use it to confirm the role of VAP-1 in disease pathogenesis. This would also provide a preclinical model in which to test the potential of inhibiting VAP-1 therapeutically in PSC. In this regard, a mouse model of sclerosing cholangitis (*Mdr2*$^{-/-}$) was established in-house and crossed with mice bearing a mutated variant of VAP-1 in which VAP-1 distribution in tissue is normal but due to a single amino acid mutation the molecule has no amine oxidase activity. I refer to these animals as *Ssao* KO or *Ssao*$^{-/-}$ mice [214,320]). The resultant *Mdr2*$^{-/-}$*Ssao*$^{-/-}$ mice were carefully phenotyped through assessment of the inflammatory infiltrate, biliary injury and severity of liver

fibrosis. The notable challenge of assessing VAP-1 enzyme activity in mice is also discussed in this chapter.

6.2 Findings

6.2.1 Characterisation of the *Mdr2*$^{-/-}$ mouse

Several animal models of PSC have been developed, although none recapitulate all features of the human condition [445]. The most widely studied model as evidenced by literature search is the *Mdr2* knockout mouse [342,446]. The lack of MDR impairs handling of several factors including non-micellar bound bile, resulting in a toxic injury and inflammatory response leading to histological features of a sclerosing cholangitis. However the model does not recapitulate all the features of PSC and in particular is not associated with colitis [447]. Most previous studies with *Mdr2*$^{-/-}$ mice have been conducted on an FVB/N background. Given our intent to establish a cross with the *Ssao*$^{-/-}$ strain (C57BL/6), mice bearing a targeted deletion of the MDR2 biliary transporter on the same background strain were obtained (a kind gift from Prof. Lohse; Hamburg, Germany), and phenotyped in house to establish a baseline. Due to project license limitations, it was not possible to yield comparative results against C57BL/6 wild-type mice (free of any liver injury) as a negative control.

6.2.1.1 Inflammatory liver injury

The suitability of various serum tests to monitor cholestasis and hepatobiliary inflammation has been a topic of debate [448]. Whilst serum ALP is often applied to stratify biliary disease in the clinical setting [449] and may accurately reflect cholestasis in certain mouse models [448], there is emerging evidence that most ALP

in mice on a C57BL/6 background is not derived from the liver or gut [450]. FVB/N *Mdr2*$^{-/-}$ mice exhibit a steady elevation in serum ALT and ALP levels in line with development of histological cholangitis, levels plateauing beyond six weeks of age. Matched C57BL/6 *Mdr2*$^{-/-}$ mice however, illustrate the highest ALP levels early in life at a time when bone growth is most prominent, with a sharp decline toward normal values as they grow older (Figure 6.1) [451]. Given these observations, serum ALT rather than ALP, was chosen as a biochemical surrogate of liver inflammation [452].

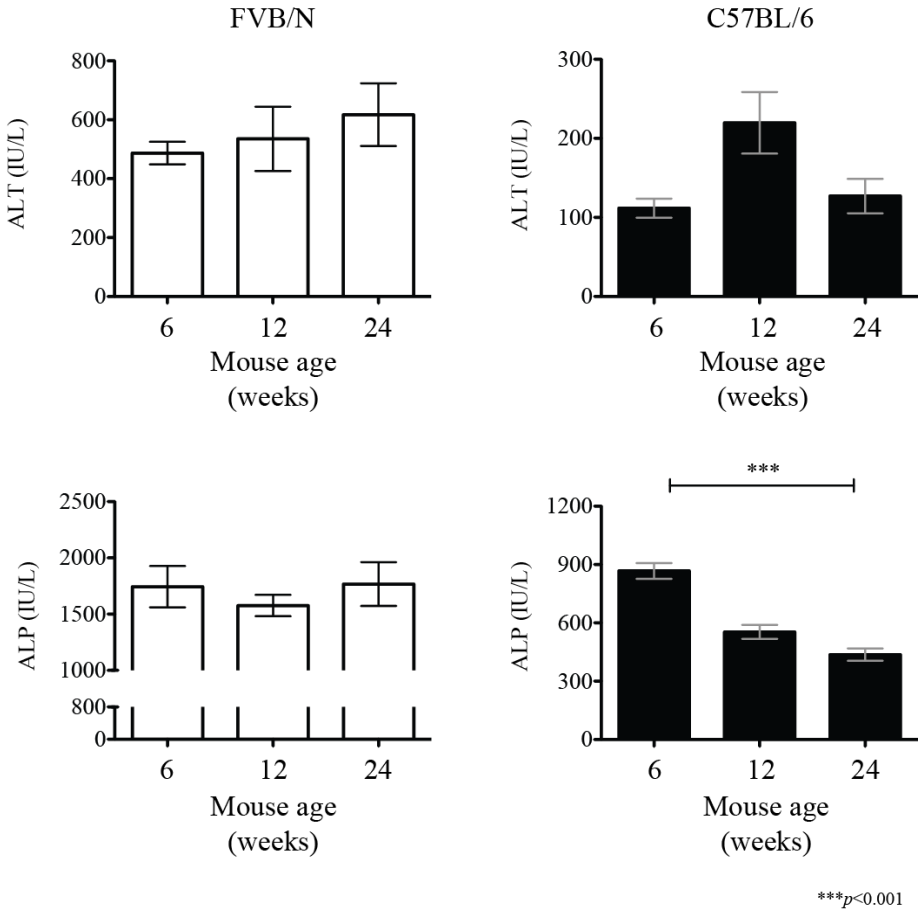

Figure 6.1: Liver biochemistry in the *Mdr2*$^{-/-}$ model according to age
Serum ALT and ALP were measured in FVB/N (open bars) and C57Bl/6 (filled bars) *Mdr2* null mice of different ages (4 – 11 mice per group). Whilst a stable elevation in serum liver-derived enzymes is evident in FVB/N mice from as early as 6 weeks of age, ALP in C57Bl/6 strains exhibit a sharp decline in older mice (at a time when bone growth has completed. Male and female mice used. Data presented as median and IQR; asterisks indicative of statistically significant differences (p<0.001; Kruskal–Wallis test) [451].

Mdr2$^{-/-}$ C57BL/6 mice exhibited marked elevation in serum ALT as early as 6 weeks old, with no significant differences between the genders (Figure 6.2). Biochemical indices of liver injury worsened with age and were worse in females.

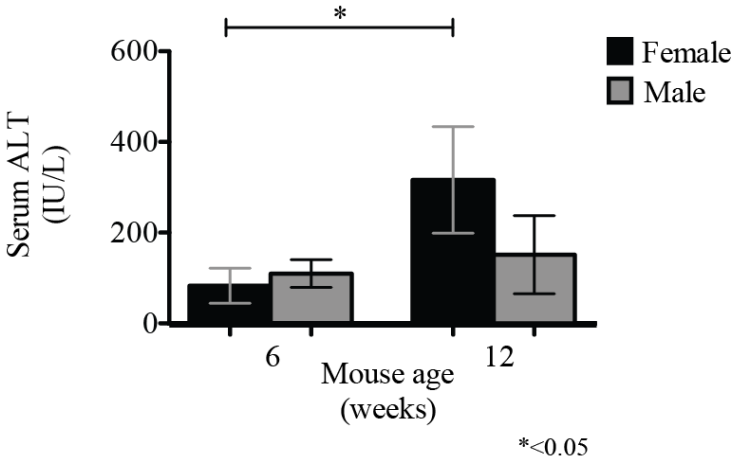

Figure 6.2: Liver biochemistry in the *Mdr2*$^{-/-}$ model according to gender
Serum ALT in the *Mdr2* knockout model (C57Bl6 background) according to age and gender. Data presented as mean ± SD. Capped lines and asterisks indicate statistically significant differences between age groups (MW-test). Data from uninjured wild-type (C57BL/6) mice in other studies suggest that normal serum ALT is in the order of 30 – 40 IU/L, although the assays chosen varies widely between reports.

Immunohistichemical staining for CD45 and H and E staining were used to evaluate inflammation. Hepatobiliary inflammation was most prominent in the portal/peri-portal region from early life (Figure 6.3). In keeping with results of biochemistry, progressive liver injury was observed in older age groups (Figure 6.4 and Figure 6.5).

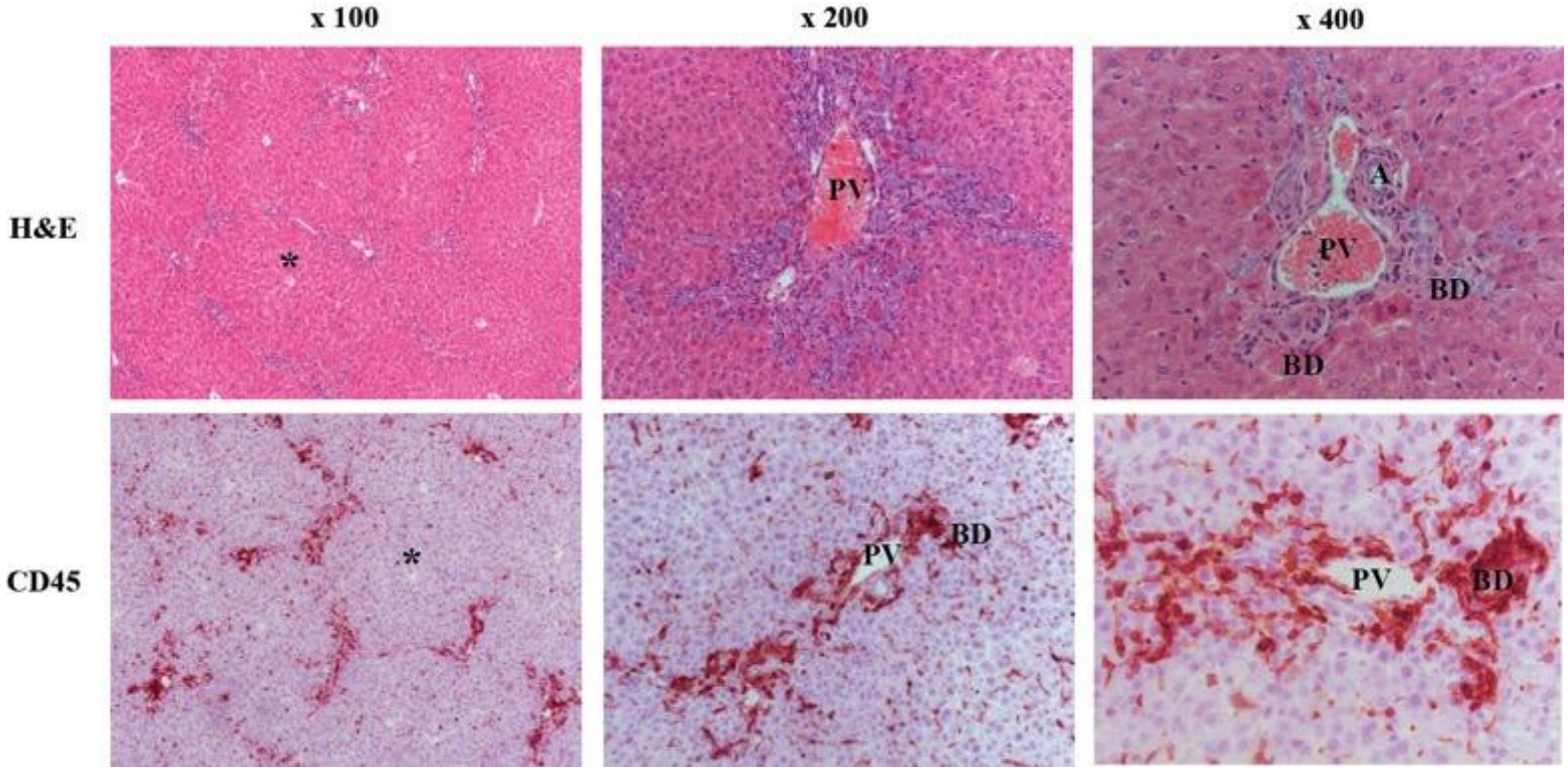

Figure 6.3: Hepatobiliary inflammation in *Mdr2*$^{-/-}$ mice

Haematoxylin and eosin (H&E) and CD45 (leucocyte marker) histochemical staining at increasing magnification. Representative images shown for female mice at ~6 weeks of age, and illustrate inflammatory infiltration of the portal region, particularly noticeable around the bile ducts. Structural denotation as follows: asterisks (adjacent to) central veins; portal vein, PV; bile ducts, BD; arteriole, A.

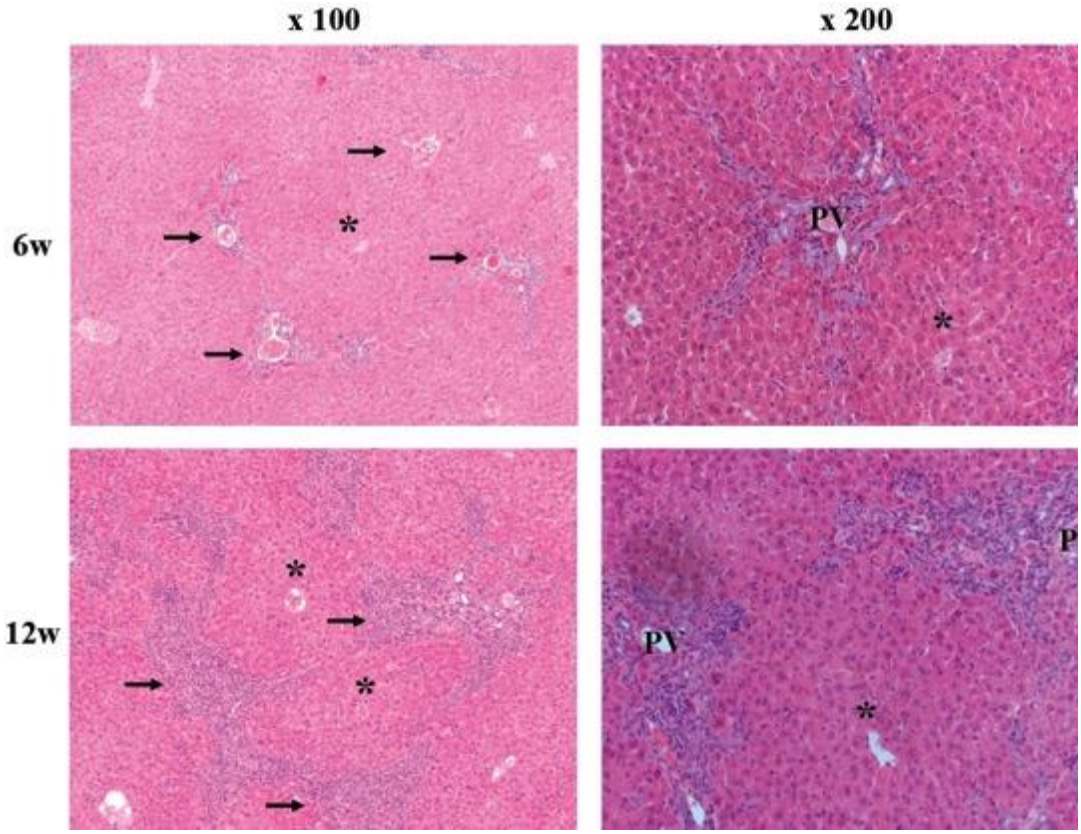

Figure 6.4: H&E staining with increasing age in *Mdr2*$^{-/-}$ mice
Histochemical staining in *Mdr2*$^{-/-}$ mice is presented for animals at 6 weeks and 12 weeks of age. Progressively worse inflammation of the portal tracts is noted with increasing age. Structural denotation as follows: asterisks (adjacent to) central veins; arrows, portal triads; PV, portal veins.

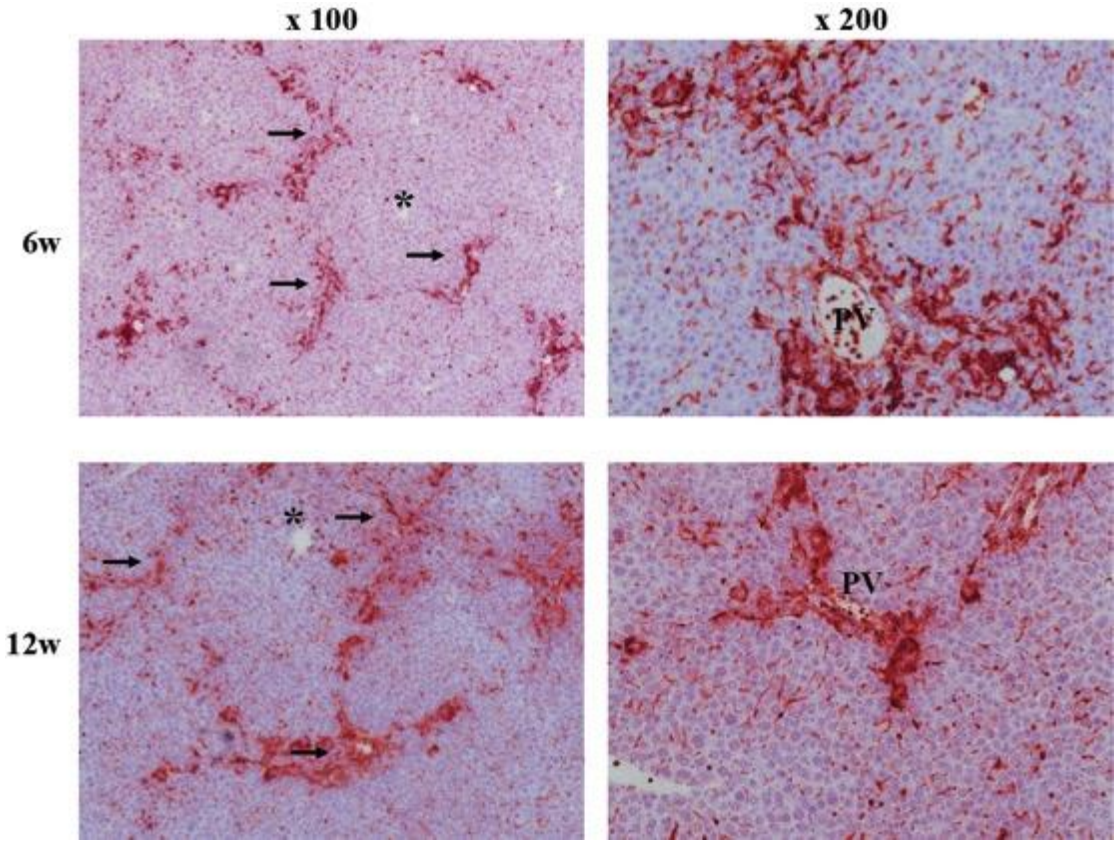

Figure 6.5: CD45^{+} leucocyte infiltration with increasing age in *Mdr2*$^{-/-}$ mice
CD45 immunohistochemical staining in *Mdr2*$^{-/-}$ mice at 6 weeks and 12 weeks of age. Histochemical staining in *Mdr2*$^{-/-}$ mice is presented for animals at 6 weeks and 12 weeks of age. Progressively worse inflammatory injury is noted with increasing age, and particularly marked in the portal regions. Structural denotation as follows: asterisks (adjacent to) central veins; arrows, portal triads; PV, portal veins.

For quantification of inflammation, digital image analysis (ImageJ) was used to assess CD45 staining (Figure 6.6). All analysis was performed on the same day with results expressed in terms of pixel count above a set threshold, and as a percentage of total viewed area (x200 and x400 magnification as indicated in Figure 6.6). For any given slide (2 slides per mouse liver), 10 independent areas were selected at random and the mean pixel densitometry calculated.

The $CD45^+$ infiltrate increased at 12 weeks of age, although differences did not reach statistical significance (MW-test), even when analysed according to distribution of inflammatory injury (portal vs. lobular).

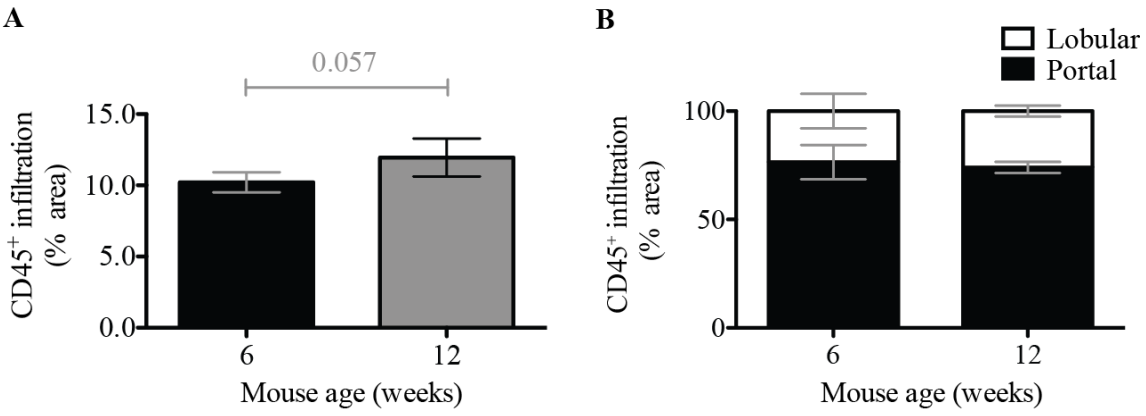

Figure 6.6: Quantification of $CD45^+$ leucocyte infiltration
Quantitative assessment of CD45 infiltration by ImageJ analysis according to *Mdr2*$^{-/-}$ mouse age (females only). Data provided by percentage surface area at x200 magnification (A), and x400 magnification specifically assessed in portal and lobular areas (B). 10 fields of view visualised per mouse liver section/slide (4 – 5 mice in each group). Data presented as mean ± SD, and capped lines indicative of comparisons approaching statistical significance on MW-test.

Higher magnification views showed conspicuous bile duct lesions, although inflammation was more evident at the 6-week time-point (CD45 staining) as opposed to older age groups (Figure 6.7).

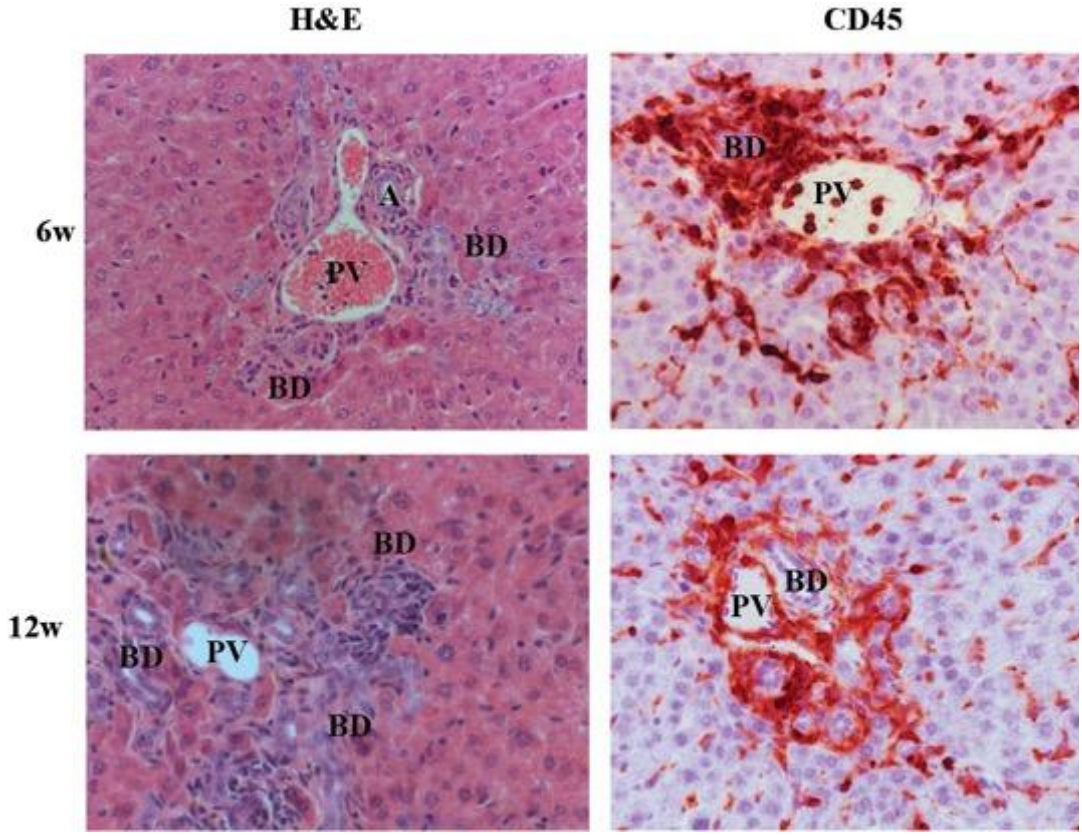

Figure 6.7: Biliary injury in the *Mdr2*$^{-/-}$ model with increasing age.
H&E and CD45 histochemical staining in 6-week and 12-week-old mice show dense portal infiltrates and bile duct inflammatory lesions (x400 magnification). Structural denotation as follows: hepatic arteriole, A; portal veins, PV; bile ducts, BD

CD45 is a pan-leucocyte marker, and for deeper phenotypic evaluation of liver-infiltrating cell populations flow cytometric analysis was conducted. There are several techniques for extraction of liver-infiltrating leucocytes; most of which rely on density gradient centrifugation. Given familiarity with Lympholyte-H in the purification of human peripheral blood lymphocyte populations, I chose to use Lympholyte-M. Despite good lymphocyte yields the yield of myeloid-lineage cell-types was poor; confirming that Lympholyte should only be used for studying lymphoid sub-types. I next tested a discontinuous Percoll gradient which had been used successfully to extract infiltrating leucocytes from human colon (detailed in Chapter 2 and Chapter 3). Unfortunately, this was associated with contamination by

parenchymal cell populations (probable hepatocytes, stellate cells, etc.) and was therefore not considered further.

Good lymphoid and myeloid cell yields from mouse liver have been reported using Optiprep [214,453]. Although providing the 'cleanest' of all gradients tried so far as well as respectable leucocyte populations, several additional problems were encountered with this method; particularly the infrequency with which a leucocyte band was visible at the interface (<50% of attempts).

Given the intermittent success, I proceeded to identify cell populations without the use of a gradient to purify cells. Mouse liver cell suspensions were labelled immediately following cell strainer filtration and wash steps (detailed in Chapter 2), and at time of analysis all leucocytes were gated based on viability and expression of CD45. This resulted in percentage yields comparable to those obtained with Optiprep.

There are several ways in which to quantify the liver-infiltrating leucocyte population. The most common are either absolute cell counts using counting beads and normalising readings to liver weight; or alternatively to express cell phenotypes of interest as a percentage of the total infiltrating CD45 population. Given that I did not use gradient centrifugation, its was deemed inappropriate to use the counting bead method due to a high likelihood of obtaining erroneous readings (e.g. from beads binding to cell debris). Therefore I adopted the latter approach. At 6 weeks, the T-cell population comprised predominantly $CD3^+$ $CD4^+$ cells, with lesser contribution from $CD3^+$ $CD8^+$ subsets (Figure 6.8); similar to that observed for mice on an FVB/N background [452] by 12 weeks the situation was reversed, with a predominantly $CD8^+$

T-cell infiltrate. This is noteworthy given that $CD8^+$ T-cells have been implicated as key mediators of bile duct destruction in autoimmune cholangitis models [454]. However, the majority of infiltrating leucocytes were CD19+ in keeping with reports that ~50% of the infiltrating lymphocytes in liver fibrosis models utilising C57BL/6 mice are B-cells [246]. The remaining lymphocyte population was composed of NK-cells as identified by CD49b expression [455], which were present with slightly increased frequency in male mice at older age groups. Myeloid cells were detected by expression of CD11b and included equal contributions of $F4/80^+$ macrophages, and pro-inflammatory ($Gr1^+$) vs. anti-inflammatory ($Gr1^-$) monocyte subsets. No significant differences were observed between genders or age groups of *Mdr2*$^{-/-}$ mice.

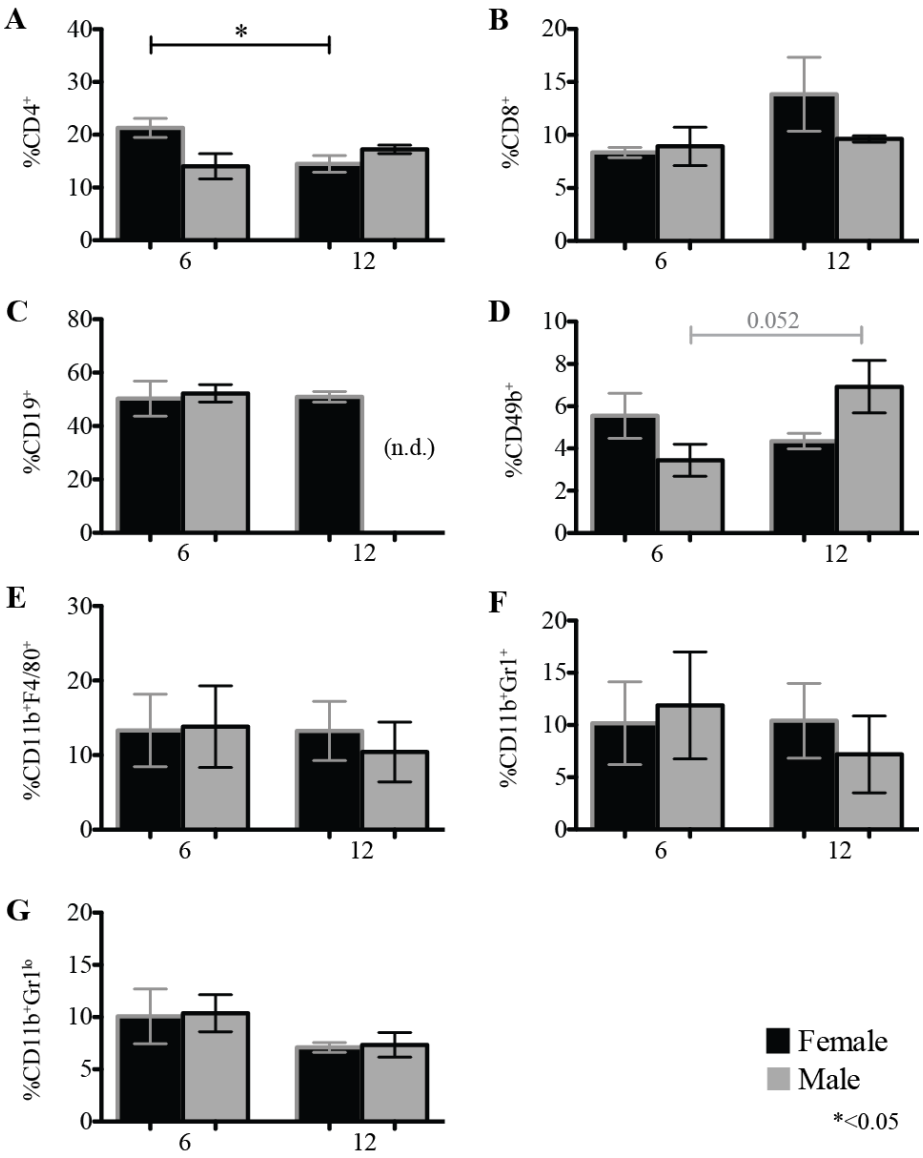

Figure 6.8: Phenotyping of the inflammatory infiltrate in *Mdr2*$^{-/-}$ mice

Flow cytometric analysis of infiltrating CD45^{+} leucocytes in the *Mdr2*$^{-/-}$ model according to mouse age and gender. Liver infiltrating lymphocytes were characterised as follows: CD3^{+} CD4^{+} T-cells (A); CD3^{+} CD8^{+} T-cells (B); B-cells (not performed for male mice aged 12 weeks – C) and NK-cells (D). Myeloid lineage cells were defined as CD11b^{+}F4/80^{+} macrophages (E); and putative myeloid-derived suppressor cells, CD11b^{+}Gr1^{+} (F). Data expressed as mean ± SD. Capped lines and asterisk indicative of statistically significant differences.

6.2.1.2 Liver fibrosis

Assessment of liver fibrosis at the transcriptional level was carried out using alpha-smooth muscle actin (αSMA) and collagen 1α1 (Col1α1) as markers of activated HSC. It has been reported that hepatobiliary injury and cholangitis in the *Mdr2*$^{-/-}$ model are more pronounced in female mice relative to males [456], although the latter display increased predisposition toward hepatocellular carcinoma [457]. Thus, all future experiments were conducted exclusively in female animals unless otherwise specified.

Gene expression of αSMA and Col1α1 was studied in 6-week and 12-week old mice by qRT-PCR using 18sRNA as a reference gene [458]. The absence of wild-type controls precluded strict analysis via the ΔΔCT method relative to an uninjured control, and results are expressed relative to reference gene only. As such, mice in younger age groups demonstrated a greater degree of αSMA and Col1α1 gene expression than their aged counterparts, suggesting greater transcription of fibrotic markers in early life (Figure 6.9).

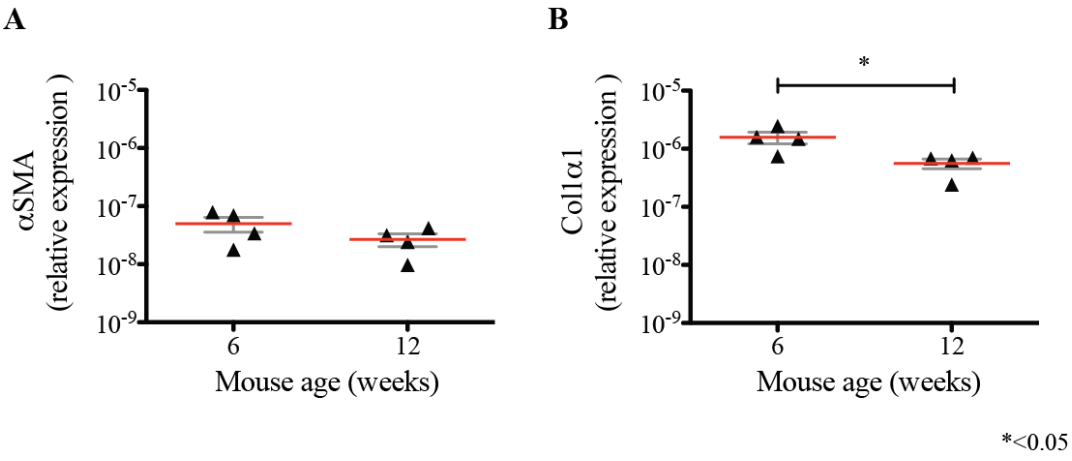

Figure 6.9: Transcription of fibrosis related genes in the *Mdr2*$^{-/-}$ model by age
Expression of αSMA (A) and Col1α1 (B) at the mRNA level in female mice at 6-weeks and 12-weeks of age. Data presented as mean ± SD. Capped lines and asterisk indicate statistically significant differences (MW-test).

Immunohistochemistry revealed a significantly increased stainig for aSMA by quantitative digital image analysis in 6-week versus 12-week old mice (Figure 6.10) confirming early HSC and myofibroblast activation. However, the immunostaining of αSMA was highly variable and was reduced on stored samples: Figure 6.11 illustrates the same mouse section stained for αSMA using identical conditions >6 months apart with notably different staining intensity. This may indicate that for future comparisons, all sections should be stained simultaneously.

Validation of fibrosis was assessed using (Picro)Sirius red staining (Figure 6.10). This allows for direct collagen staining and is widely used in both clinical and research settings [459]. Fibrotic septa and even cirrhotic nodules were seen in younger mice and increased with age, indicating the progressive nature of liver fibrosis in the *Mdr2*$^{-/-}$ model.

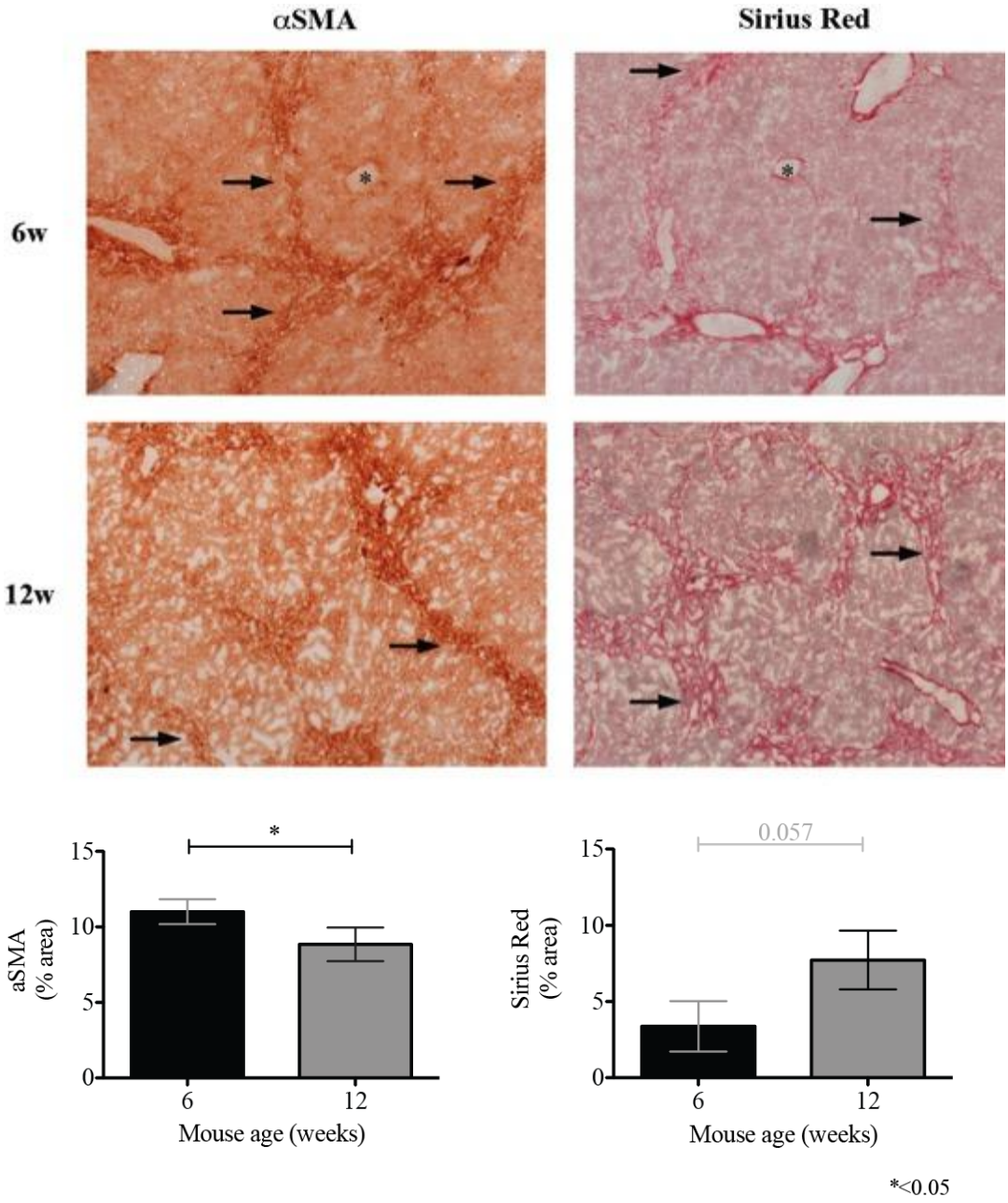

Figure 6.10: Liver fibrosis in the *Mdr2*$^{-/-}$ model with increasing age

Alpha smooth muscle actin (αSMA) and (Picro)Sirius red staining in 6-week and 12-week-old female mice. Asterisks indicate central veins; arrows indicate fibrotic septae (x100 magnification). Quantification of fibrotic injury performed via ImageJ analysis is shown in the lower panel. Mean ± SD are presented for 4 – 5 mice per group.10 fields of view obtained for each mouse taken at x200 magnification. Capped lines and asterisks indicative of statistically significant differences (MW-test).

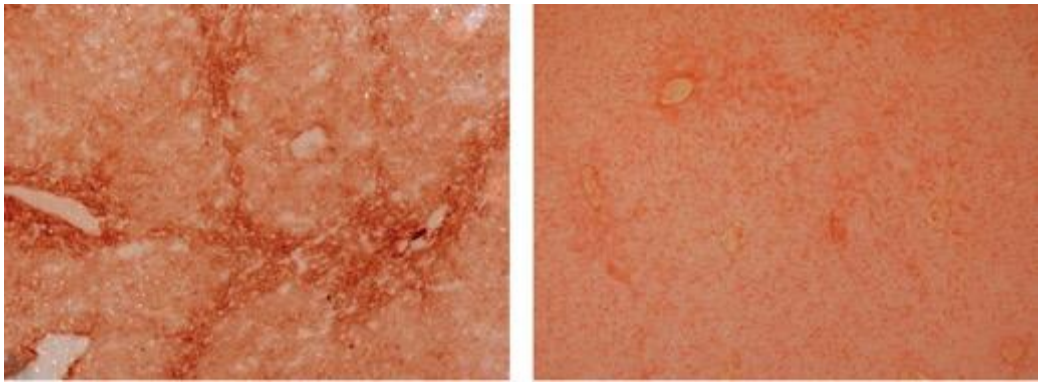

Figure 6.11: Variability in αSMA immunohistochemistry
Section of mouse liver (6-week old female Mdr2$^{-/-}$ mouse) wherein immunohistochemical staining was performed 3 months apart with the same antibody batch (x100 magnification).

Another commonly used technique for determining the degree of liver fibrosis is the hepatic hydroxyproline assay [342] which measures the hydroxylation product of proline, a major component of collagen. Indeed, hepatic hydroxyproline content was significantly greater in mice aged 12 weeks than 6-week old animals (Figure 6.12).

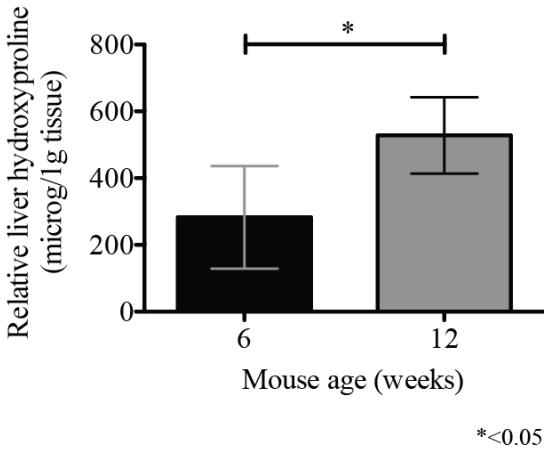

Figure 6.12: Hepatic hydroxyproline assessment in *Mdr2*$^{-/-}$ mice by age
Liver fibrosis quantified by hydroxyproline content. Data indicative of 4 – 5 mice per group; box and whiskers depict mean ± SD. Capped lines and asterisks indicate statistically significant differences (MW-test).

6.2.2 Assessment of murine VAP-1 enzyme activity

As alterations in the enzyme activity of VAP-1 were observed in human chronic liver disease, I investigated the catalytic capacity of the protein in the murine cholangiopathy model. However, little VAP-1 is detected in murine liver by qRT-PCR, northern and western blots; with minimal staining on immunohistochemistry [67,313,317,318,460]. Nevertheless, congenital deletion or therapeutic targeting of VAP-1 is associated with attenuation of hepatobiliary inflammation and tissue fibrosis in certain mouse models [212–214]; suggesting a pivotal role for VAP-1 in leucocyte recruitment and fibrosis in the mouse liver.

Intra-hepatic VAP-1 enzyme activity was assessed using a modification of the protein capture and immobilisation method described in Chapter 4. Both mice and humans express high levels of enzymatically active VAP-1 in white adipose tissue [460]. Therefore a positive control for murine VAP-1 enzyme activity was generated via adipocyte differentiation of the fibroblast 3T3 cell lineage. Differentiated adipocytes were distinguished by the presence of vacuoles and lipid droplets (Figure 6.13).

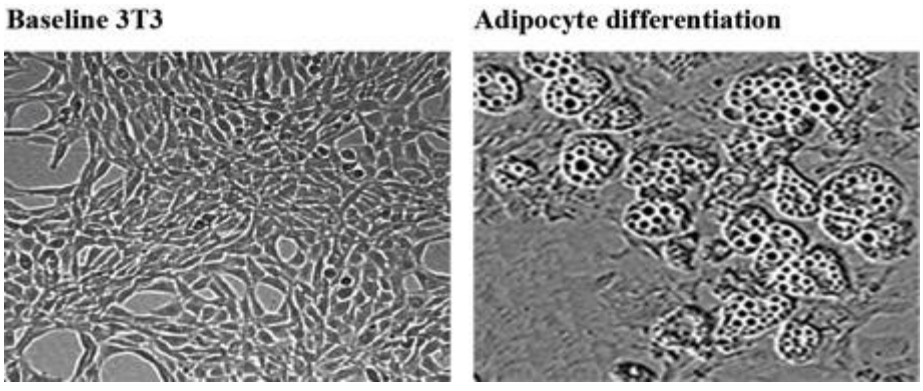

Figure 6.13: Adipocyte differentiation of 3T3 cells
The murine 3T3 fibroblast cell line was differentiated into adipocytes (x 250 magnification).

A series of anti-VAP-1 antibodies were tested for their ability to capture murine VAP-1 from lysates of adipocyte differentiated 3T3 cells. Antibodies were selected based on their availability, and quality of immunohistochemical staining [214]. A dose titration was performed, and the resultant enzyme activities from the highest trialled concentration of each antibody (20 mg/mL) are illustrated in Figure 6.14a. Protein captured by antibody clone 7-106 had the greatest enzyme activity with little/no inhibitory effects at elevated concentrations (Figure 6.14b).

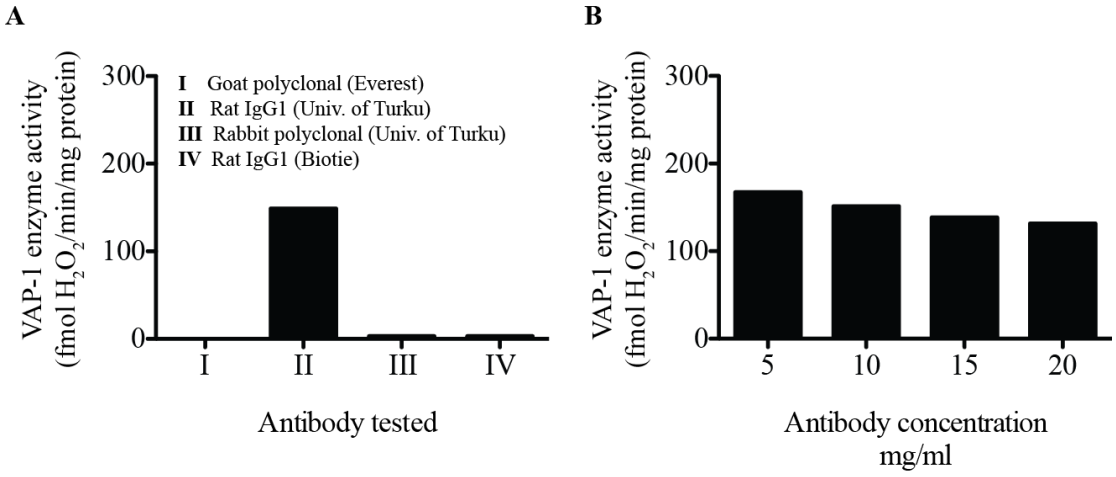

Figure 6.14: Establishing a technique to assay murine VAP-1 enzyme activity
Four different murine antibodies were tested in their ability to capture VAP-1 from murine cells and then subject to the Amplex® red assay (A). Antibody 7-106 (number II from panel A) was deemed the most potent (i.e., captured the greatest quantity of enzymatically active protein), and exhibited slight variation across concentrations (B). Histogram bars represent the mean from 3 technical replicates per condition.

Mice bearing a point mutation in which VAP-1 is devoid of all enzyme activity, but otherwise functionally competent (*Ssao*$^{-/-}$), have recently been described [214]. *Mdr2*$^{-/-}$ x *Ssao*$^{-/-}$ mice were generated through a breeding program established in-house and confirmation of genotype was obtained via qRT-PCR (Transnetyx, USA). At time of writing, only 4 mice with confirmed *Mdr2*$^{-/-}$ *Ssao*$^{-/-}$ genotype (aged 6 weeks; all female) were available for study.

To confirm absence of hepatic VAP-1 enzyme activity in double knockouts, the Amplex red assay using 7-106 as capture antibody was performed on murine liver tissue protein lysates (Figure 6.15). This confirmed there was no enzyme activity in the liver of *Mdr2*$^{-/-}$ *Ssao*$^{-/-}$ mice. Enzyme activity was detected in *Mdr2*$^{-/-}$ animals although itis worth noting that murine hepatic VAP-1 enzyme activity is several orders of magnitude lower than that observed in human liver (fmol vs. pmol. range).

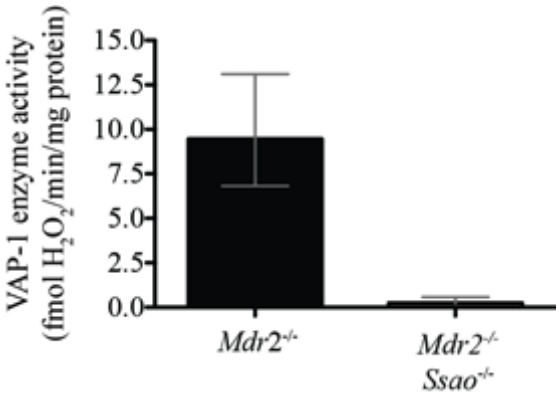

Figure 6.15: Hepatic VAP-1 enzyme activity in single and double knockouts
Amplex red assay was performed on liver protein lysates prepared from *Mdr2*$^{-/-}$ and *Mdr2*$^{-/-}$ *Ssao*$^{-/-}$ mice; no enzymatic activity was observed in *the latter*. Data representative of semicarbazide corrected values (mean ± SD) derived from 4 mice per group (aged 6 weeks; all female); 3 technical repeats per animal.

6.2.3 Phenotyping of *Mdr2 Ssao* double knockouts

In contrast to age and sex-matched *Mdr2*$^{-/-}$ mice, double knockouts demonstrated significant elevations in serum ALT levels (Figure 6.16). As mentioned previously, comparisons with wild-types was not possible, but levels were >10 times than in uninjured animals or *Ssao*$^{-/-}$ mice in previous studies [214].

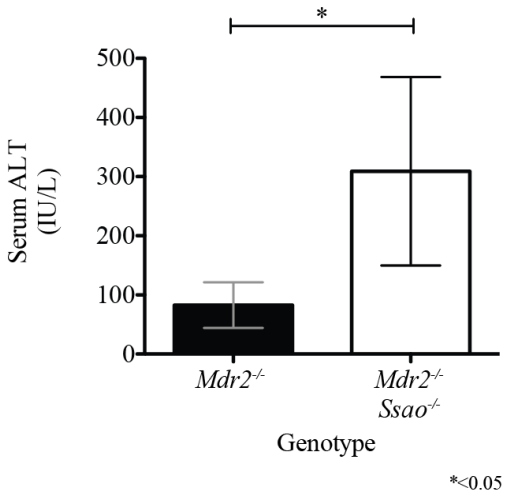

Figure 6.16: Serum ALT in single vs. double knockouts
Biochemistry measured in *Mdr2*$^{-/-}$ vs. *Mdr2*$^{-/-}$ *Ssao*$^{-/-}$ mice (all female; 6 weeks of age). Data represented as mean ± SD. Capped lines and asterisks indicative of statistically significant differences (MW-test).

Mdr2$^{-/-}$ *Ssao*$^{-/-}$ mice displayed dense septal leucocytic infiltrates associated with severe parenchymal and portal inflammation and early bridging fibrosis between portal tracts (Figure 6.17) (Figure 6.18). Differences in total immunohistochemical CD45^{+} staining between single and double knockouts did not however reach statistical significance (MW-test).

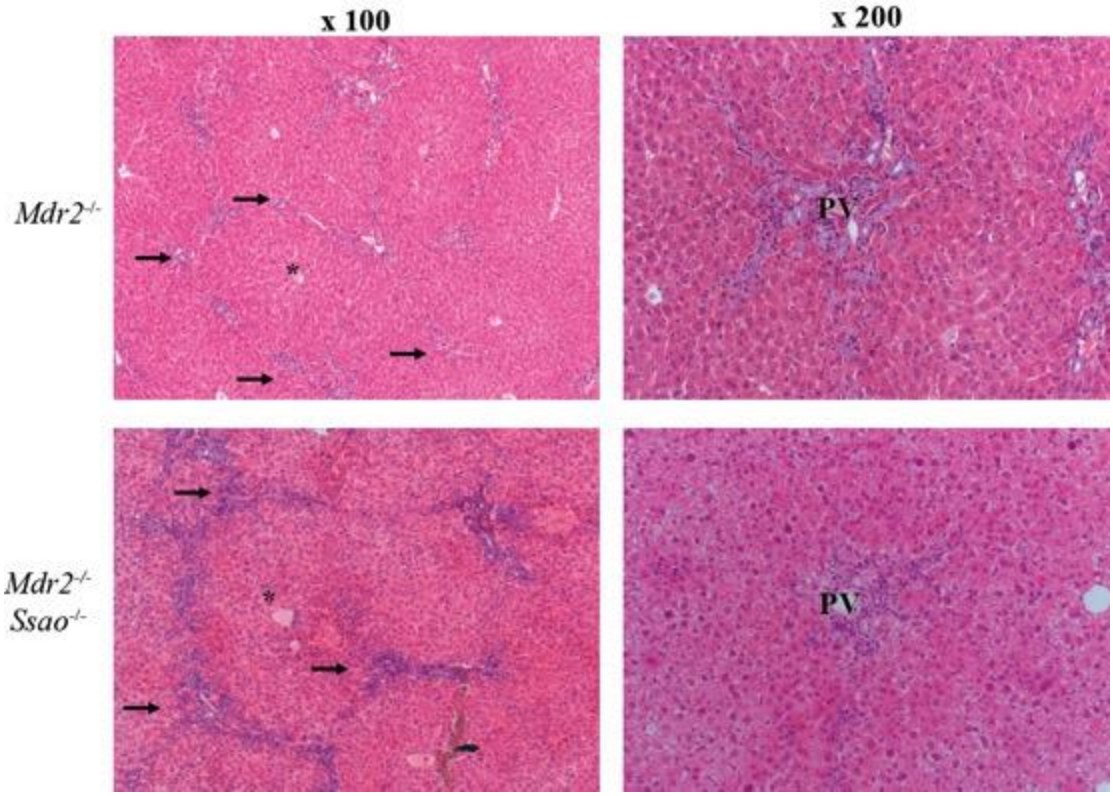

Figure 6.17: Inflammatory infiltrate in *Mdr2*$^{-/-}$ vs. *Mdr2*$^{-/-}$ *Ssao*$^{-/-}$ mice
H&E staining in single and double knockouts, illustrating relatively greater infiltration in the latter; particularly marked in the portal and septal areas. Central veins indicated by adjacent asterisks, portal tracts by arrows and portal vein as PV.

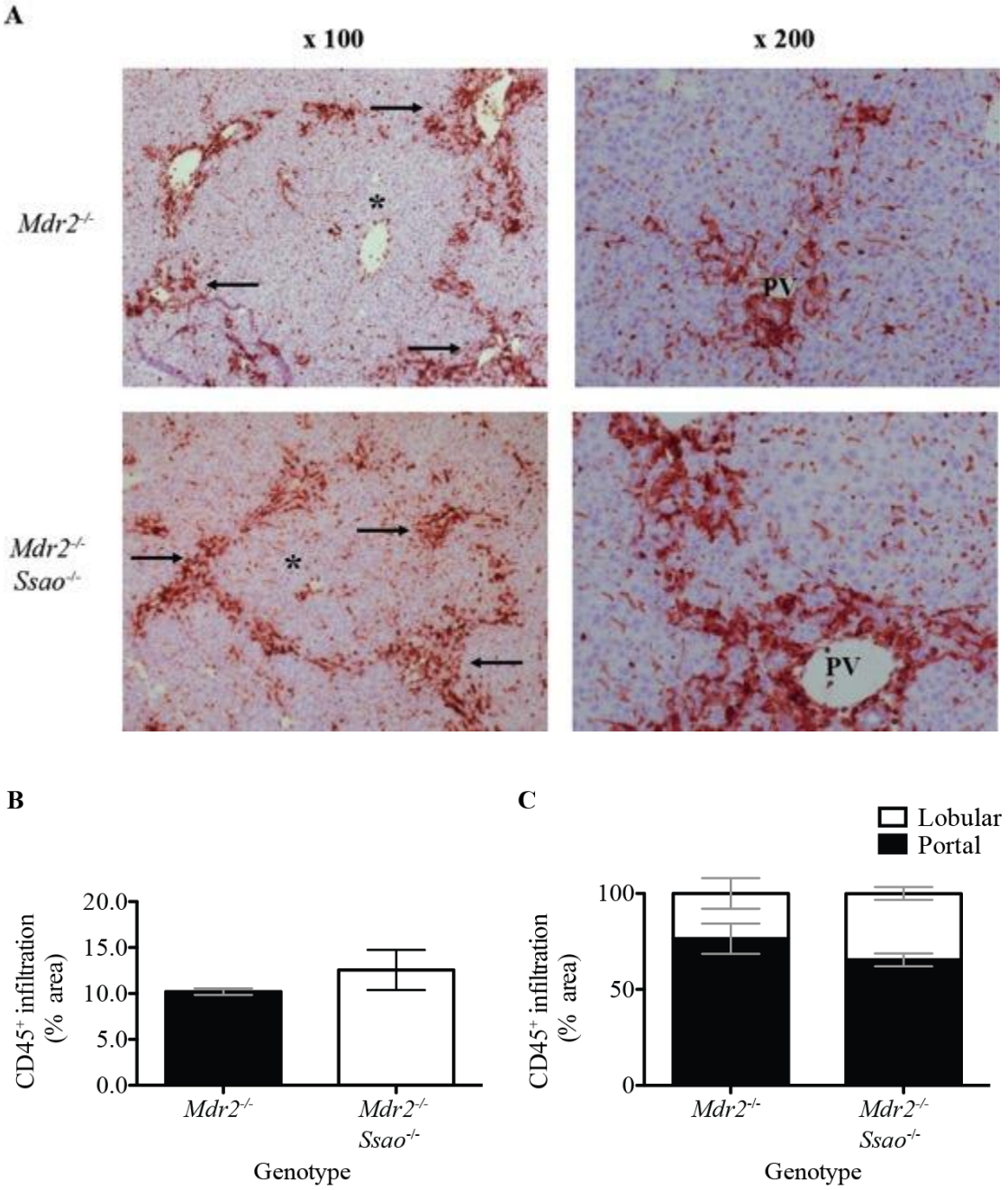

Figure 6.18: CD45$^+$ cell infiltration in *Mdr2*$^{-/-}$ vs. *Mdr2*$^{-/-}$ *Ssao*$^{-/-}$ mice

Representative CD45 immunostaining in single versus double knockouts. A greater Asterisks indicative of central veins (adjacent); arrows highlight portal triads; PV demonstrates portal veins (A). Quantitative assessment of positive staining provided by percentage surface area at x200 magnification (B) and x400 magnification specifically assessed in portal and lobular areas (C). 10 fields of view visualised per mouse; 4 mice in each group. Data presented as mean ± SD.

Flow cytometric analysis of the hepatic infiltrate revealed no statistically significant differences between *Mdr2*$^{-/-}$ and *Mdr2*$^{-/-}$ *Ssao*$^{-/-}$ animals albeit the total numbers were small (n=4, MW-test) (Figure 6.19). However, morphologically the severity of biliary injury appeared more pronounced in all double relative to single knockouts, with dense peri-ductal infiltrates associated with bile duct injury (Figure 6.20). Mice of both strains exhibited marked duct loss, with many portal tracts lacking an identifiable biliary structure.

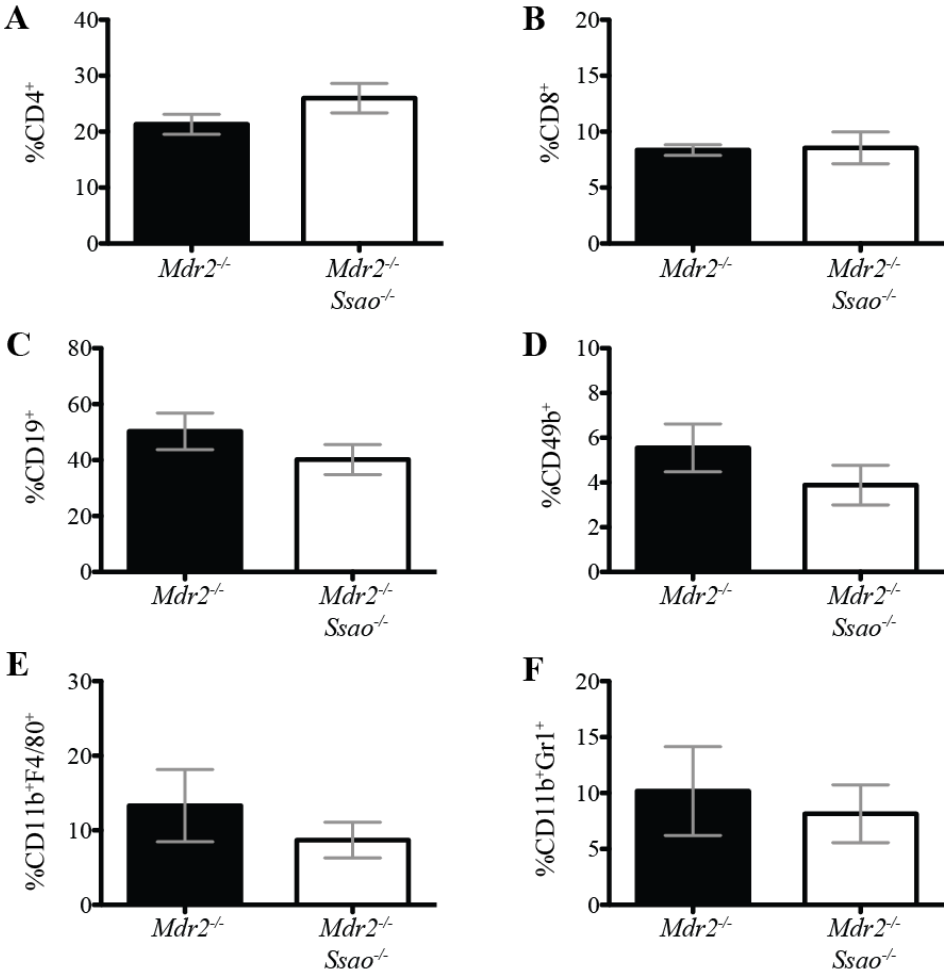

Figure 6.19: Phenotyping of infiltrating leucocyte populations
Liver infiltrating leucocytes were phenotyped by flow cytometry (n=4 in each group); specifically, expression of $CD3^+$ $CD4^+$ T-cells (A); $CD3^+$ $CD8^+$ T-cells (B); B-cells (C); NK-cells (D); $CD11b^+F4/80^+$ macrophages (E); putative myeloid-derived suppressor cells (F). Data represented by mean ± SD.

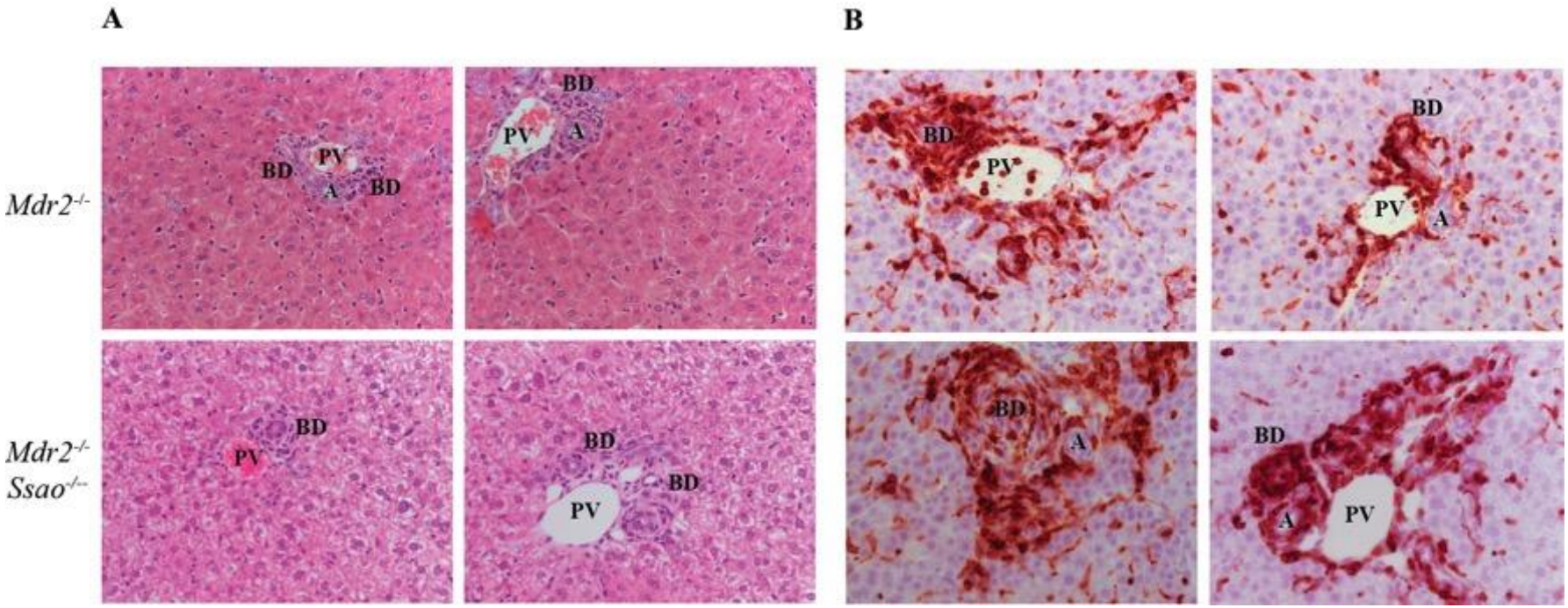

Figure 6.20: Biliary injury in *Mdr2*$^{-/-}$ vs. *Mdr2*$^{-/-}$*Ssao*$^{-/-}$ mice

H&E (A) and CD45 (B) immunostaining in single vs. double knockouts (x400 magnification). Marked periductal inflammatory injury was evident in all animals. Portal vein, PV; bile duct, BD; and hepatic arteriole, A.

Although no differences were seen with regard to inflammatory infiltrate or biliary injury between *Mdr2*$^{-/-}$ and *Mdr2*$^{-/-}$ Ssao$^{-/-}$ animals, it remained possible that fibrosis could be attenuated through an absence of SSAO generated aldehyde production. However, transcription of αSMA and Col1α1 were significantly up-regulated in double knockouts, possibly reflecting increased HSC activation and turnover of collagen in these mice (Figure 6.21).

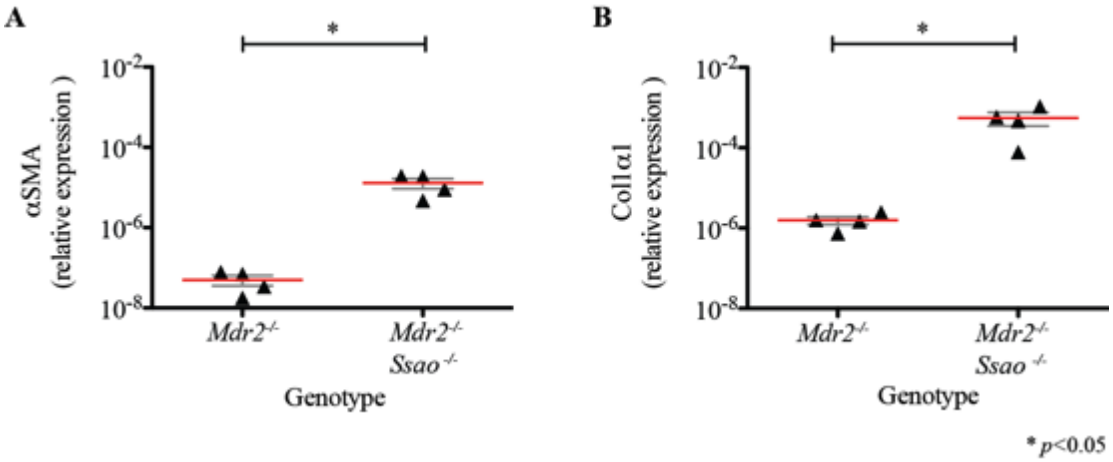

Figure 6.21: Transcription of fibrotic markers in the single vs. double knockouts
Expression of αSMA (A) and Col1α1 (B) at the mRNA level in *Mdr2*$^{-/-}$ vs. *Mdr2*$^{-/-}$*Ssao*$^{-/-}$ mice. Data represented by mean ± SD. Capped lines and asterisk indicate statistically significant differences (MW-test).

Sirius red staining of *Mdr2*$^{-/-}$ *Ssao*$^{-/-}$ mice indicated clear evidence of fibrotic liver disease, although nodule formation appeared somewhat incomplete relative to age and sex-matched *Mdr2*$^{-/-}$ counterparts (Figure 6.22). Quantitative differences in Sirius red surface area staining did not however reach statistical significance.

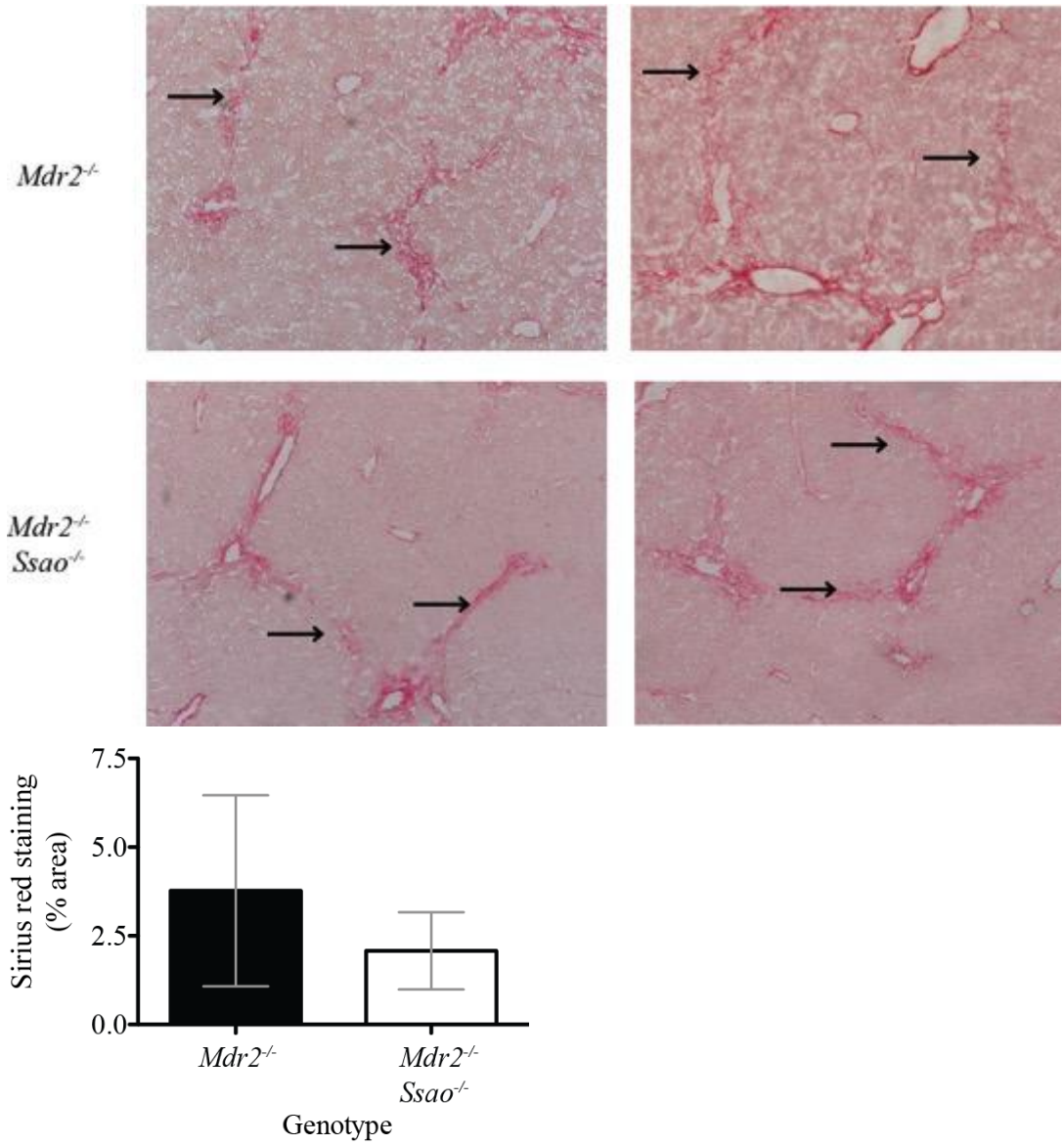

Figure 6.22: Sirius red staining in *Mdr2*$^{-/-}$ vs. *Mdr2*$^{-/-}$ *Ssao*$^{-/-}$ mice
Qualitative assessment of liver fibrosis between single and double knockouts was performed via Sirius red staining. Arrows indicate positively stained fibrous septae. Representative images (x100 magnification) of 4 mice per group. Quantification of staining area performed via ImageJ analysis, wherein 10 fields of view analysed at x200 magnification. Data presented as mean ± SD.

Further investigation of fibrotic indices was conducted using the hydroxyproline assay with all *Mdr2*$^{-/-}$ mouse liver specimens run at the same time as *Mdr2*$^{-/-}$ *Ssao*$^{-/-}$ animals to ensure comparability. These results were similar to that observed by Sirius red staining, wherein a trend toward fibrosis reduction could be observed in *Mdr2*$^{-/-}$ *Ssao*$^{-/-}$ mice (MW-test, p = 0.124; Figure 6.23).

.

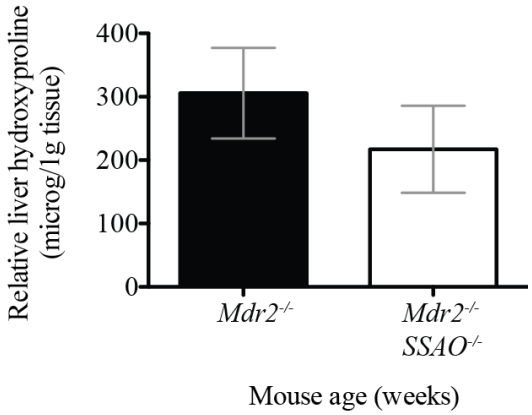

Figure 6.23: Hydroxyproline quantification in *Mdr2*$^{-/-}$ vs. *Mdr2*$^{-/-}$*Ssao*$^{-/-}$ mice
Validation of severity of liver fibrosis in single vs. double knockout mice with the liver hydroxyproline assay. Data represented as mean ± SD of 4 mice per group, each with 3 technical repeats (all female; aged 6 weeks).

6.3 Discussion

In the previous chapters, it was demonstrated that hepatic VAP-1 expression is increased in diseased human liver, with elevated enzyme activity particularly marked in end-stage PSC. Through effective substrate provision, VAP-1 modulated expression of downstream cell-adhesion molecules, promoting lymphocyte recruitment; a mechanism that could further contribute to pro-inflammatory pathways in immune-mediated hepatobiliary disease. sVAP-1 levels were elevated in PSC sera, possibly as a consequence of release by activated hepatic stellate cells and myofibroblasts, leading us to hypothesise that VAP-1 is a potential therapeutic target in PSC. To test the merit of targeted intervention in PSC, a murine model (*Mdr2*$^{-/-}$) mimicking several pathological features of the human condition was chosen and crossed with a strain harbouring specific mutation in the VAP-1 gene that renders the protein catalytically inactive whilst leaving the distribution and structural conformation of VAP-1 unaffected.

6.3.1 Choosing a PSC mouse model

The relatively low incidence of PSC (3 – 16/100,000 population; [258]), difficult accessibility of the human biliary tract for longitudinal studies, and variation in clinical course make it a difficult disease in study in humans. Therefore, well-defined and easily reproducible animal models for PSC would be invaluable research tools. The major attributes of an "ideal PSC model" have been recently been summarised by Marion Pollheimer and Peter Fickert [342,445,446]. Ideally, an immunogenetically predisposed animal would develop fibrous-obliterative cholangitis of the intra- and extrahepatic bile ducts in association with gastrointestinal inflammation (colitis).

Moreover, specific immunological phenotypes of inflammatory lymphocytes (e.g. $CD3^+$ $\alpha4\beta7^+$ $CCR9^+$) infiltrating portal tracts should exist associated with injury to the biliary epithelium. To date, however, no such animal model has been.

Perhaps the best studied is the *Mdr2*$^{-/-}$ mouse, which accurately recapitulates the obliterative fibro-sclerotic bile duct lesions seen within human PSC liver. Moreover, mutations in the human orthologue of *Mdr2* (*MDR3*) are associated with several intrahepatic cholestatic liver disorders [98]. For these reasons the *Mdr2*$^{-/-}$ mouse has been proposed as a model in which to test novel therapies *in vivo*. Several bile acid based treatments, nuclear acid receptor agonists as well as anti-fibrotic therapies have ameliorated hepatobiliary inflammation and fibrosis in the *Mdr2*$^{-/-}$ model [461,462]. We thus chose this model, and given the putative consequences of VAP-1 function in PSC hypothesised that an absence of amine oxidase activity would also provide protection.

6.3.2 Non-effect of SSAO ablation in the *Mdr2*$^{-/-}$ mouse

In our hands the hepatobiliary phenotype of *Mdr2*$^{-/-}$ on a C57BL/6 background was comparable to published findings using the FVB/N strain, with significant inflammation and fibrosis present in early life and progressing with age. The catalytic activity of VAP-1, which was detectable within diseased mouse liver, was ablated in *Mdr2*$^{-/-}$ *Ssao*$^{-/-}$ mice. However, we did not see a reduction in the hepatic infiltrate in *Mdr2*$^{-/-}$ *Ssao*$^{-/-}$ when compared to *Mdr2*$^{-/-}$ animals either by total $CD45^+$ cell staining or flow cytometry (Figures 6.16, 6.17, 6.18). This was unexpected given recently published data where absence of SSAO activity resulted in a significantly reduced $CD4^+$ and $NK1.1^+$ infiltrate in murine models of fatty liver injury [214]. Martilla-

Ichihara *et al*. demonstrated that small-molecule inhibitors of VAP-1 enzyme activity reduced the recruitment of intra-tumoural $CD11b^{+}$ $Gr1^{+}$ myeloid cells, which resemble myeloid-derived suppressor cells [463], in a murine xenograft model [311]. Murine Gr-1 is composed of two components – Ly6C and Ly6G, which are now more commonly adopted for defining myeloid subsets. Ly6G is exclusively expressed on neutrophils; whereas $Ly6C^{hi}$ defines an inflammatory monocyte subset, $Ly6C^{int}$ is associated with neutrophils and eosinophils, and $Ly6C^{lo}$ the patrolling (potentially immune-regulatory) population. The absence of further definition of the infiltrating myeloid populations represents a significant limitation to my studies, and future work will entail deeper immunophenotypic characterisation. It is possible however, that a lack of SSAO results in a failure to recruit of regulatory subsets leading to the inflammatory phenotype we saw in $Mdr2^{-/-}$ $Ssao^{-/-}$[193].

In contrast, while antibody blockade or deletion of the VAP-1 gene reduced injury in a ConA-induced model of hepatic injury in mice [213], the provision of an SSAO inhibitor to these animals had a minimal effect. Therefore a redundant role for VAP-1 in the $Mdr2^{-/-}$ model of liver injury cannot be discounted until the effects of anti-VAP-1 antibody have been investigated.

6.3.3 Remedial advantage of full VAP-1 deletion

Inhibition of enzyme activity or neutralising adhesion molecule properties of VAP-1 (without affecting amine oxidase function) have similarly inhibitory effects on leucocyte recruitment *in vitro*, with little to suggest enhanced inhibitory effect when applied in tandem [316]. VAP-1 has been shown to promote wound-healing responses and enhance expression of pro-fibrotic genes *COL1A1* and lysyl oxidase homolog

LOXL2 [214], suggesting that VAP-1 may have a direct effect on HSC. Göktürk et al. have illustrated overexpression of VAP-1 in arterial smooth muscle cells, which promotes elastin deposition [324]. However, the specific contribution of enzyme activity to such properties remains less clear as accelerated healing in scratch-assays appear independent of enzyme activity, and expression of pro-fibrotic genes unaffected by the transfection of a stellate cell line (LX2) with catalytically inactive VAP-1 [214].

Published studies of VAP-1 deletion in mice (*Aoc3*$^{-/-}$) clearly outnumber those assessing enzyme inhibition; and it appears that the former approach confers a greater degree of protection against liver injury *in vivo.* In the CCl_4 model of hepatitis, *Aoc3*$^{-/-}$ mice show a marked reduction in nearly all liver infiltrating mononuclear cell types and pro-inflammatory myeloid cells from as early as 2 weeks, [214]. The influence on leucocyte recruitment early in the disease course was paralleled by a reduction in hepatitis and reduced parenchymal and portal fibrosis. In a murine model of steatohepatitis (methionine choline deficient (MCD) diet), *Ssao*$^{-/-}$ mice showed a similar reduction in hepatic $CD4^+$ and $NK1.1^+$ T-cells assessed by flow cytometry to *Aoc3*$^{-/-}$ mice at 4 – 6 weeks of age, although biochemical indices of hepatobiliary inflammation (serum ALT) was no different to wild-type counterparts on the same chow [214]. This suggests that the absence of enzyme activity alone is not as protective as complete *Vap-1* deletion. Improvement in fibrotic liver injury has also been documented in *Aoc3*$^{-/-}$ mice exposed to a high-fat diet, despite no significant differences in any one particular immune-cell population [214]. This suggests that VAP-1/SSAO operates through effects on leucocyte adhesion, attenuation of

myofibroblast activity and reduced production of aldehydes to ameliorate the fibrotic response.

6.3.4 Congenital deletion vs. therapeutic manipulation

Aoc3 knockout animals develop normally, although they display mildly dysregulated leucocyte homing [320]. Absolute reduction in lymphocyte populations within the gut (Peyer's patches, PP) has been reported; and despite a relative increase in the numbers of PP $CD4^+$ and $CD8^+$ T-cells, these animals manifest attenuated T- and B-cell responses to oral vaccination and defective microbial handling [423]. These effects are not observed when administering antibody or enzyme inhibitors to fully developed wild-type animals leading Koskinen *et al* to propose that life-long absence of VAP-1 may give rise to compensatory mechanisms in development that alter components of anti-microbial defence.

The ability of enzymatically active VAP-1 in human PSC liver to induce expression of functional cell adhesion molecules on hepatic endothelium suggests novel therapeutic possibilities using enzyme inhibitors *or* neutralising antibodies against VAP-1.

As previously discussed cell-surface expression of VAP-1 although predominantly restricted to the liver, can be up-regulated on extra-hepatic sites such as synovium and gut under non-homeostatic conditions. LJP1207 is a potent inhibitor of both aspects of VAP-1 function; and in oxazolone induced colitis was shown to reduce mortality, improve body weight and improve colonic inflammation by inhibiting T_h2 immune cell responses [424]. Such reagents reduce other inflammatory responses including

peritonitis, arthritis, ischemia-reperfusion injury, lung inflammation, septic shock, hepatitis, colitis and fibrotic (kidney, liver) responses in several mouse models [212–214,309,312,407,424–429].

Anti-VAP-1 antibody-treated mice are protected from the development of liver fibrosis in response the MCD diet [214]. This is despite the antibody in question being free of enzyme-inhibition in vitro. A direct comparison of α4 versus VAP-1 inhibition in the concanavalin A model of hepatitis [213] reported thatVAP-1 reduced influx of $CD4^+$ (but not $CD8^+$) T-cells, attenuated early liver inflammation (lower serum ALT at 8 hours following injury) and lessened peri-portal inflammation. The anti-VAP-1 effects on lymphocyte recruitment were predominantly restricted to T-cells bearing a T_h2 cytokine profile; whereas α4-inhibition associated with significant exacerbation in hepatitic injury through increased production of IFNγ and reduced hepatic infiltration of protective myeloid-derived suppressor cells (MDSC). A modest (non-significant) improvement in serum ALT was observed with the enzyme inhibitor (BTT-2052) associated with a reduction of liver-infiltrating T_h2-cells [212,213]. There is little to suggest an additive effect through combining antibody and enzyme-abrogation.

My results suggest that loss of SSAO and the absence of VAP-1 in *Aoc3*$^{-/-}$ animals exacerbate liver injury in the *Mdr2* knockout mouse. The mechanisms of this effect are not clear but there are several possibilities. Defective microbial clearance has been associated with an absence of VAP-1. Recurrent episodes of ascending cholangitis are a feature of PSC that are associated with a worse clinical outcome (see chapter 5). Thus if lack of VAP-1/SSAO increases [423] hepatobiliary infection it could

exacerbate inflammatory responses; particularly in older female mice who develop choledocholithiasis [464]. These effects would not necessarily occur with pharmacological inhibition, and may prove conducive to further study. Secondly VAP-1/SSAO may be important for the recruitment of anti-inflammatory cells including MDSCs, T_{reg} or reparative macrophages; and their failure to be recruited to the injured liver could exacerbate PSC.

6.3.4.1 Is there a more appropriate model?

The *Mdr2*$^{-/-}$ mouse model may not be appropriate for examining the influence of VAP-1/SSAO activity however as unlike human PSC, *Mdr2*$^{-/-}$ mice neither exhibit features of colitis nor do they express MAdCAM-1 in the liver [342]. The absence of such features questions the rationale of targeting gut-liver homing in such mice. Several animal models have been proposed for studying certain aspects of disease pathogenesis although to date none allow a detailed study of the enterohepatic migration of T-cells. Seidel et al. have recently developed a strain expressing OVA on cholangiocytes, wherein OA-specific T-cells are primed in liver and draining lymph nodes, but despite acquiring effector function do not cause significant hepatobiliary inflammation [175]. However, when crossed with mice in which antigen-specific priming of T-cells is achieved in GALT, the investigators illustrate that gut-activated and not liver activated lymphocytes were responsible for the induction of immune-mediated cholangitis *in vivo*. Moreover, ~60% of LILs were $\alpha4\beta7^{+}$; and although the authors did not comment on VAP-1 and MAdCAM-1 within mouse liver, expression of ICAM-1, VCAM-1 and CCL25 were all up-regulated (assessed by qRT-PCR on whole liver). Furthermore, only gut-primed T-cells infiltrating the liver were shown to co-express CCR9 [173]. Using the same mice, Neumann et al. have shown that liver-

primed $\alpha4\beta7^{+}$ $CCR9^{-}$ T-cells are programmed with regulatory functions, in contrast to gut-primed $\alpha4\beta7$ $CCR9^{+}$ T-cells which were more in keeping with an effector phenotype [174]. It is plausible therefore, that such models may allow more rational targeting of immune pathways than based on the gut-liver homing hypothesis.

6.3.5 Summary

Despite findings of increased VAP-1 expression and enzyme activity on the livers of patients with PSC liver, absence of VAP-1 amine oxidase activity *in vivo* does not abrogate hepatobiliary injury in *Mdr2*$^{-/-}$ mice. Although a limited number of animals were examined, the data suggest worse inflammation in *Mdr2*$^{-/-}$ *Ssao*$^{-/-}$ mice suggesting a protective role for SSAO in this model. Whether this is due to defective microbial handling and recurrent ascending cholangitis or a failure to recruit anti-inflammatory cells to the liver or defective fibrosis is open to conjecture; and delineation of disease phenotype in older mice, as well as the *Mdr2*$^{-/-}$ x *Aoc3*$^{-/-}$ cross an area of on-going investigation.

The lack of supportive evidence to support a pathological enterohepatic circulation of gut-primed effector T-cells in this model of sclerosing cholangitis suggests that challenging the gut-liver homing hypothesis may require better, more suited mouse models, with well-defined lymphocyte recruitment pathways.

7 Conclusions and future work

Inflammatory bowel disease is frequently associated with concurrent skin, joint and eye inflammation. In contrast, autoimmune hepatobiliary diseases developing in the context of IBD usually run an independent course to that of gut inflammation. This clinical observation led to the proposal of a disease model wherein mucosal effector memory T-cells are recruited to the liver secondary to aberrantly expressed endothelial cell adhesion molecules and chemokines that are normally 'gut-restricted'. These cells reactivate in the liver to drive hepatobiliary damage following exposure to an as yet unidentified, shared antigenic trigger [2].

The well-established roles of CCL25–CCR9 and MAdCAM-1–α4β7 in lymphocyte recruitment to the gut are mirrored by their involvement in homing to the liver in PSC; however, a caveat exists because intestinal CCL25–CCR9 interactions have been reported to be restricted to small bowel whereas PSC is most commonly a complication of colonic inflammation. The putative contribution of VAP-1 in furthering mucosal lymphocyte recruitment to the inflamed liver has also recently been described [294].

The aims of this thesis were to investigate the contribution of CCL25–CCR9 interactions in colitis, and consequences of hepatic VAP-1 expression with regards to lymphocyte homing in PSC.

7.1 CCL25–CCR9 expression in colitis

I have shown for the first time that CCR9 is expressed at high frequencies on effector T cells in the inflamed human colon. I was also able to show that CCL25, the CCR9 ligand is increased in the inflamed colon and correlates with inflammatory activity providing further evidence that the CCL25–CCR9 axis is active in patients with colitis.

Unfortunately attempts at CCL25 localisation within tissue (immunohistochemistry) were unsuccessful. CCL25 is expressed by mucosal epithelium and plays a key role in leucocyte recruitment to the gut, and under specific pro-inflammatory conditions, the liver [132]. The presence of CCL25 on hepatic endothelium demonstrated in previous studies, and on mucosal endothelium in the gut illustrated by other peoples' work [127] may reflect secretion by the intestinal epithelium and subsequent capture and presentation by the endothelial glycocalyx. Constitutive CCL25 expression by small bowel epithelium (isolated cells and tissue sections) has been demonstrated by *in situ* hybridisation [142,375]; an avenue yet to be explored in the inflamed human colon. An alternative technique toward determining cellular source of colonic CCL25 could be evaluation of epithelial/endothelial cells by flow cytometry, although a lack of reliable and commercially available fluorescence-conjugated human antibody toward human CCL25 currently precludes such analysis. Along similar lines however, isolation of purified cell populations could facilitate qualitative and quantitative analysis of CCL25 transcription and protein expression via established techniques of qRT-PCR, western blotting and immunocytochemistry.

The factors mediating CCL25 expression within human intestinal tissue are largely unknown, in part due to chemokine transcription diminishing following cell culture [378]. In mice, members of the lymphotoxin (LT) / TNF family of cytokines can regulate constitutive expression of homeostatic and inflammatory chemokines in secondary lymphoid organs and small intestine. Rodents subject to intra-peritoneal TNFα injection exhibit diffuse CCL25 reactivity (immunohistochemistry) in almost the entire lamina propria contrasting with the relatively sparse distribution observed in uninjured mice [136]. However, Ericcson *et al*. report a similar degree of CCL25 mRNA expression in the small intestine of $LT\alpha^{-/-}$, $LT\beta^{-/-}$, and *TNF receptor (R1)* knockout mice, with levels remaining fairly constant despite intravenous LPS injection and in germ-free conditions [378]. Moreover, CCL25 transcription was unaltered in several intestinal epithelial cell lines (mouse small intestine: MODE-K, S1-H10 mICcl2; human small intestine: CCL-241; human colorectal adenocarcinoma: HT-29, Caco-2) following TNFα and IFNγ stimulation. Caudal-related homeobox (*Cdx*)-*1* and *Cdx-2*, transcription factors that are restricted to gut epithelium in adult mice, enhanced the activity of a murine CCL25 promoter in MODE-K small intestinal cell lines. The authors concluded that CCL25 expression is neither dependent on intestinal microfloral colonisation nor enriched by the effect of inflammatory cytokines. However MODE-K cells failed to express CCL25 mRNA at levels seen in freshly isolated murine small intestinal epithelial cells despite CDX transfection. Additional factors must therefore be required for maintaining constitutive expression in tissue.

Until now, the aberrant lymphocyte homing model of PSC/IBD, has been challenged by a lack of supportive evidence implicating the CCL25–CCR9 axis in colonic

lymphocyte recruitment [123,142,148,343]. Previous studies were largely restricted in their examination of large bowel under non-inflammatory conditions, and several lines of evidence implicate activity of this pathway in murine colitis [380,382]. Data presented in this thesis (Chapter 3) further illustrate involvement of the CCL25–CCR9 pathway in human colonic IBD, which correlates with severity of intestinal inflammation.

If CCL25 expression is driven by colitis activity, and colonic $CCR9^+$ T cells are responsible for driving hepatobiliary inflammation in PSC, then it should follow that the risk of PSC increases with intestinal activity; which clinically is not the case. However, pre-exposure of primed $CCR9^+$ T-cells to high CCL25 levels in the gut during the onset of active IBD, may be capable of modulating subsequent migratory responses [136] (Figure 7.1). In such a model, pro-inflammatory mucosal $CCR9^+$ T-cells would preferentially undergo local recruitment during the onset of active colonic disease, due to high levels of intestinal CCL25 expression [136]. Thereafter, mucosal T-cells down-regulate expression of active CCR9, favouring retention in the intestine for as long as inflammation persists. On achieving remission from a colitis flare, the colonic CCL25 gradient is attenuated, and primed mucosal $CCR9^+$ lymphocytes now become permissive to enterohepatic recirculation and are recruited to the liver sinusoids in response to aberrant hepatic endothelial CCL25 expression [127]. Support of this hypothesis is lent by Hosoe *et al*., who show that pre-exposure of $CCR9^+$ intraepithelial lymphocytes (IELs) or lamina propria lymphocytes (LPLs) to CCL25 drastically attenuates the migratory response *in vitro* ("chemokine desensitisation" [136]). A similar response can also been observed following pre-

incubation of $\alpha 4\beta 7^{+}$ lymphocytes to soluble recombinant MAdCAM-1 prior to HSEC flow adhesion assays (own data; unpublished).

To prove such a hypothesis in humans would require the study of liver biopsies from patients with IBD who do not have any clinical or biochemical evidence of liver disease (clearly unethical). Nevertheless, Bungay *et al*. report radiological features of sclerosing cholangitis in ~20% of individuals with asymptomatic colitis, despite the presence of normal liver biochemistry [465], suggested that subclinical hepatobiliary disease exists in a greater proportion of patients with IBD than currently recognised.

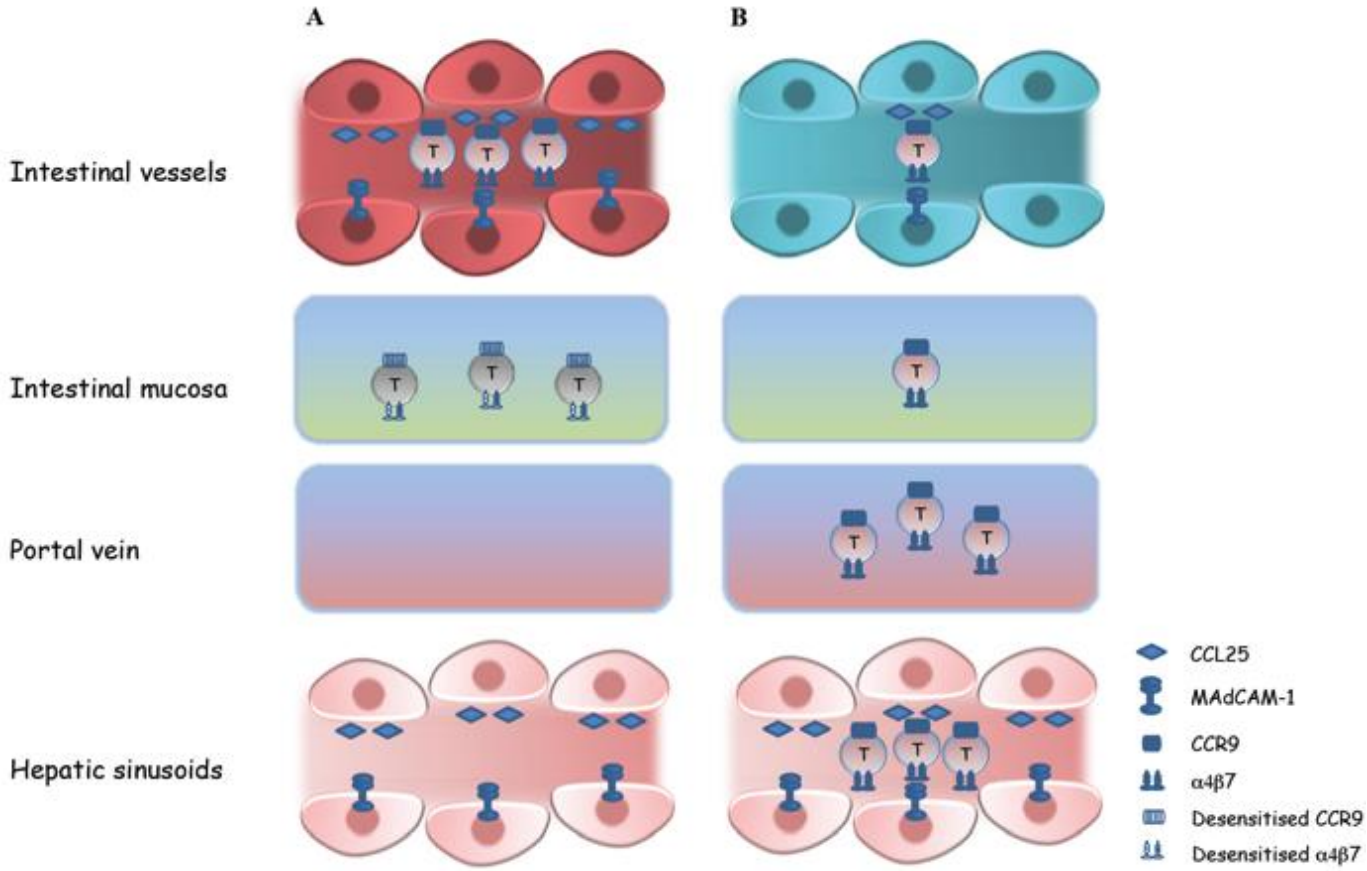

Figure 7.1: CCL25 desensitisation and the mucosal lymphocyte homing hypothesis in PSC/IBD
In patients with active colitis (A) overexpression of CCL25 and MAdCAM-1 in the gut microenvironment would desensitise CCR9-mediated lymphocyte recruitment to extraintestinal sites, resulting in preferential trafficking and retainment of mucosal T-cells within the colon. During periods of prolonged IBD remission (B), low-level colitic activity down-regulates CCL25 expression in the gut, allowing locally primed $CCR9^{+}$ lymphocytes to now migrate to the liver where CCL25 is aberrantly expressed by hepatic endothelial cells.

The capacity to imprint lymphocytes with gut-tropism is restricted to intestinal rather than liver DCs [296]. However recent studies in mice report that priming by HSEC induced α4β7-expression on naïve T-cells [174] dominated by regulatory, immunosuppressive properties [176]. This may in-turn account for the relatively mild IBD phenotype observed in PSC patients, as well as relatively increased colonic cancer risk posed by IBD alone. There is also emerging evidence to suggest that functional characteristics of tissue-infiltrating $\alpha4\beta7^{+}$ T-cells are distinct depending on site of priming [173], with liver-primed lymphocytes ($CCR9^{-}$) being

immunoregulatory and gut-primed lymphocytes ($CCR9^+$) bearing predominantly effector functions. If proven, this may have significant therapeutic implications in PSC wherein focussed antagonism of effector $CCR9^+$ T-cells would minimise off-target effects associated with pan-α4β7 inhibition. Detailing whether such concepts apply to the human setting is an avenue under on-going investigation.

7.2 Hepatic VAP-1 expression studies

In addition to CCL25–CCR9 interactions, enterohepatic mucosal lymphocyte recruitment involves the endothelial addressin MAdCAM-1 and its integrin receptor α4β7 [289]. The Birmingham group has implicated another endothelial molecule, VAP-1, in leucocyte recruitment to the human liver [67]; and shown that through its amine oxidase activity how VAP-1 can modulate expression of other cell adhesion molecules [67]. Using similar methodology, I was able to reproduce these findings wherein treatment of HSEC with VAP-1 substrates was shown to up-regulate MAdCAM-1 expression and increase adhesion of $\alpha4\beta7^+$ lymphocytes *in vitro* (Chapter 4); fuelling deeper investigation into the role of VAP-1 in PSC.

VAP-1 transcription in liver tissue was increased in end-stage PSC cirrhosis relative to non-diseased specimens and other inflammatory diseases, representing the first study to detail VAP-1 expression at the message level across different aetiologies. The significant differences between PSC and other diseases led me to investigate tissue localisation and enzyme activity. I found VAP-1 expressed by endothelium in normal human liver and showed marked increase by immunohistochemistry in fibrotic scar tissue in a range of autoimmune liver diseases, consistent with that reported by others [214]. I then went on to show for the first time that this was

reflected by elevated VAP-1 amine oxidase activity in PSC liver; whereas under non-inflammatory situations hepatic enzyme activity was significantly lower than that in the gut [409].

The high-level enzyme activity in colon may be secondary to an increased burden of dietary and microbe-derived amines that regularly enter the gut. Given links between enteric dysbiosis and an inflamed colon in PSC patients, it is perhaps unsurprising that the degree of amine oxidase activity is similar between afflicted disease sites, further strengthening associations between gut and liver inflammatory disease processes. As little is known about the physiological or pathophysiological substrates that active VAP-1 *in vivo*, I went on to study a range of potential amine substrates. In so doing, I found that the most efficient substrate was cysteamine, which was more efficient than methylamine at inducing functionally active MAdCAM-1 on HSEC. Cysteamine is produced by gut bacteria, as well as generated through intestinal epithelial vanin-1 activity. Moreover, when instilled into the colon in mice cysteamine induces colitis providing another theoretical link between gut and liver.

7.3 Soluble VAP-1 in PSC

The most notable limitation of the tissue studies was the restriction to end-stage liver disease. However because VAP-1 exists as a circulating soluble form in human serum I was able to study sVAP-1 levels in patients with all stages of disease and look for correlation with clinical characteristics or disease course. I prospectively collected serum samples from our autoimmune liver disease clinic and measured sVAP-1 levels across a range of genders, age groups, aetiologies and disease stages. In summary, sVAP-1 levels were significantly greater in patients with liver disease, particularly

those with PSC whether they were cirrhotic or non-cirrhotic. Moreover, sVAP-1 levels predicted clinical disease progression, underlining its worth as a putative biomarker in liver disease patients.

Previous studies have reported correlation between serum amine oxidase activity and serum sVAP-1 protein. I was unable to confirm this using the capture and immobilisation (Maxisorp plate) method but when I repeat a limited analysis in patients for with sVAP-1 levels below 400 ng/mL the correlation was demonstrated. Efforts to quantify methylamine in serum were also unsuccessful, probably due to the presence of extensive non-specific background signals and/or inherent volatility of the compound. This was confirmed when I used whole serum + addition of MAO-A and MAO-B inhibitors and was unable to detect SSAO activity, suggesting that endogenous VAP-1 substrates has either evaporated or been consumed prior to experimentation.

Thus, several unanswered questions remain with respect to serum amine oxidase activity and substrate quantification. Optimisation of both techniques would further our understanding of the role of serum VAP-1 in PSC as well as liver disease in general. In addition to optimising capture antibody levels for the enzyme assay, there is merit in a 'head-to-head' comparison of Amplex Red techniques, as well as an appraisal of exogenous substrate-free enzyme activity on freshly collected specimens. Quantification of substrates other than methylamine is not well described for human bodily fluids, although theoretically feasible provided the amine being assessed exhibits stability under ambient conditions. Another major hurdle in trying to determine specific amine concentrations stems from the difficulty in differentiating test subject from related biogenic compounds – specifically other amines. Zhang et al.

claim to have circumvented this problem as well as that of prolonged sample pre-treatment times, through prior distillation and micro-trapping of volatile aliphatic amines [466].

Based on my findings I have proposed a revised PSC pathogenesis model unifying pre-existing concepts of enteric dysbiosis, a leaky inflamed gut, and aberrant mucosal lymphocyte homing (Figure 7.2). In a genetically predisposed individual, immune dysregulation leads to a change in the microbiome with increased frequencies of bacteria that generate VAP-1 substrates including cysteamine. The increased intestinal derived amines enter the portal circulation through the weakened epithelial lining resulting form colitis and are delivered to hepatic sinusoids where they active VAP-1 on hepatic endothelial cells. The resulting increased amine oxidase activity drives an increase in chemokine and adhesion molecules including MAdCAM-1 that promote homing of mucosal lymphocytes. Elevated VAP-1 expression has direct effects on leucocyte recruitment, and through amine oxidase activity augments fibrogenesis tissue fibrosis. Increased release of sVAP-1 may further exacerbate inflammation by driving leucocyte chemotaxis and recruitment to afflicted sites.

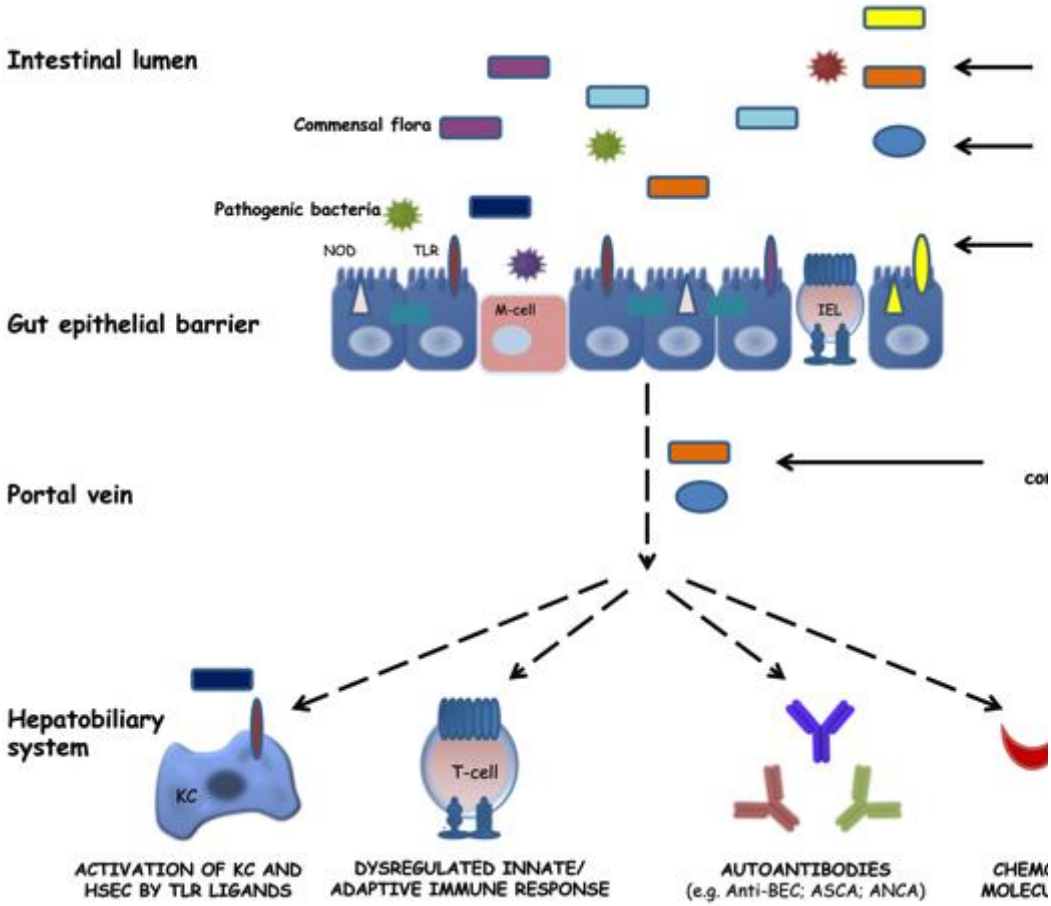

Figure 7.2: Putative aetiopathogenic pathways in PSC
Alterations in commensal flora (e.g. as a result of Fut2 variants) and defective microbial handling (e.g. a consequence of NOD2/CARD9 variants) can lead to the translocation of various bacterial components via an inflamed 'leaky' colon. In the liver, these products may behave as ligands for pattern recognition receptors (PRR) such as TLRs the activation of which triggers cytokine release from Kupffer cells (KC) and endothelial cells. Cytokine release is followed by the recruitment and activation of neutrophils, macrophages and lymphocytes to portal tracts through increased expression of chemokines and adhesion molecules. Bacterial derived amines, as well as those generated by intestinal epithelial inflammation (e.g. via vanin-1) can behave as substrates for VAP-1 enzyme activity resulting in upregulation of MAdCAM-1, ICAM-1 and VCAM-1 on HSEC. Soluble VAP-1 release into serum (not depicted) may exert local and distal chemotactic effects that potentiate recruitment of pro-inflammatory leucocyte subsets to the liver. Mutations in genes such as MST-1 and components of the IL-2 pathway may further affect innate and adaptive immune responses leading to chronic inflammation.

Bacterial components may also act as antigens (e.g. FtsZ) and stimulate production of antibodies that bind biliary epithelial cells leading to increased TLR4 and TLR9 expression and enhanced responses to bacterial products. Activation of these PRR perpetuates the secretion of pro-inflammatory cytokines and chemokines, the persistence of chronic inflammation and eventually biliary fibrosis, progressive cholestasis and secondary biliary cirrhosis [1].

7.4 Genetic inactivation of SSAO in murine sclerosing cholangitis

There are several lines of evidence to suggest that VAP-1 enzyme inhibition would lead to reduced leucocyte infiltration in PSC. The research group from Turku have illustrated that enzyme activity is crucial in mediating the rolling and transmigratory functions of VAP-1 [316,425], and that enzyme inhibition attenuates leucocyte extravasation. Provision of the archetypal substrate benzylamine also results in NFκB activation and increased chemokine and adhesion molecule expression as reported previously [321], enhancing the ability of HSEC to recruit leucocytes under flow (detailed in Chapter 6). VAP-1 can be found in the heart, lungs, spleen and blood vessels of mice; although in contrast to humans little can be detected on the hepatic endothelial surface under homeostatic conditions [67,212,213]. Nevertheless recent reports suggest an absence of VAP-1 enzyme activity confers protection against liver fibrosis and a reduction in the infiltration of $CD4^+$ T-cell subsets *in vivo* [213,214].

Extrapolating techniques applied to human tissue lysates, I was able to confirm that low levels of VAP-1 enzyme activity can be detected in the livers of *Mdr2*$^{-/-}$ mice, although due to current project license restrictions any comparisons with wild-type animals were precluded. *Mdr2*$^{-/-}$ mice were crossed onto *Ssao*$^{-/-}$ mice in which wild type VAP-1 was replaced by an enzyme dead mutant; but despite an absence of VAP-1 enzyme activity I was unable to detect a protective effect on hepatobiliary injury. Moreover, serum indices of hepatobiliary inflammation appeared more prominent in double knockout animals. Although, the number of animals studied was small and restricted to female mice, the findings suggest that a lack of enzymatic activity might exacerbate liver injury. The findings need to be confirmed in older mice and in models lacking all VAP-1 knockout functional properties, which, based on previously

published studies, I would expect to reduce the infiltration of pro-inflammatory cell populations [213,214]. Conversely, if the hypothesis proposed by Koskinen et al. holds true [316], then perhaps *Mdr2*$^{-/-}$ strains should only be challenged therapeutically with targeted antibodies and/or enzyme inhibitors, or through creation of a strain allowing targeted deletion after birth (e.g. a Cre-LoxP facilitated deletion).

The fact remains that hepatic VAP-1 expression in mice is relatively sparse, and there is no evidence to suggest the presence of MAdCAM-1 or CCL25 in the *Mdr2*$^{-/-}$ mouse liver suggesting it may not be a good model to test the mucosal lymphocyte homing hypothesis, and as proposed in previous chapters may require better-suited animal models [173,175].

7.5 Future work

The accepted doctrine in any realm of scientific research is that more questions will arise than answers generated. The existing series of studies suggest several aspects wherein future research efforts should be directed in order to better characterise contributions of mucosal lymphocyte homing in PSC disease pathogenesis. In this respect future studies should involve:

Determining CCL25 localisation and expression patterns in tissue

- Identifying the cell-types as well as factors responsible for CCL25 expression in the human colon are of critical importance. Isolation of human colonic epithelial and endothelial cell populations would allow analysis of CCL25 expression pre- and post-stimulation with inflammatory cytokines and bacterial products. Analysis of CCL25 expression could ostensibly be performed via flow-cytometry

should a suitable conjugated antibody become available, or through techniques performed on whole tissue described in Chapter 3.

- Given the emergence of data in mice illustrating ability of HSEC-primed T-cells to home to the gut, it is plausible that lymphocytes derived from human liver can adhere to isolated colonic endothelial cells. To investigate this hypothesis, liver-derived lymphocytes could be obtained via FAC-sorting, and a comparison between $\alpha4\beta7^+$ ($CCR9^+$ and $CCR9^-$) versus a collective $CD3^+$ population drawn in flow-based adhesion assays across colonic endothelial cells that express CCL25. As HSEC purportedly imprint $\alpha4\beta7^+$ expression onto T-cells together with a tolerogenic phenotype, targeting CCR9 *in vivo* (selectively gut-primed T-cells) may confer a therapeutic advantage – provided the hypothesis can be tested and confirmed in man.

Detailed phenotypic characterisation of $CCR9^+$ T-cells

- Having illustrated that the majority of colonic $CCR9^+$ T-cells are $CD127^+$ but $CD25^-$, studies confirming the cytokine expression profile are of utmost importance in order to validate the functional characteristics of this population.
- Validation of murine data [173,174], wherein HSEC were able to prime naïve T-cells with a gut-tropic phenotype are in need of translation to the human setting. An appraisal of antigen presentation by APC subtype across the gut and liver (e.g. DC, HSEC, HSC, B-cells, BEC, tissue macrophages) is envisaged in which HLA expression is determined by flow cytometry, subsequent to which RALDH activity would be assessed through previously

published techniques (ALDEFLUOR^{TM} assay). Comparisons between gut- versus liver-primed $\alpha4\beta7$ CCR9^{+} / CCR9^{-} T-cells would then be drawn through detailing immunoregulatory (e.g. CD39^{+}, TGFβ/IL-10 secreting) versus cytotoxic (e.g. IL23R^{+}, granzyme/perforin/IL-17/TNFα-secreting) phenotypes, and co-expression of other homing receptors determined (e.g. CCR10, CXCR3). Furthermore, qRT-PCR on cellular (as opposed to tissue-derived) genomic material would depict expression of key transcription factors (e.g. RORγ, STAT3) and ELISA/western blotting to substantiate downstream protein translation.

Given the pivotal influence of CD103^{+} DC in mediating human colitis, it is envisaged that $\alpha4\beta7^{+}$ CCR9^{+} T-cells are gut-primed, effector T-cells; whereas $\alpha4\beta7^{+}$ CCR9^{-} T-cells (liver-derived) are endowed with a more regulatory, immunotolerant phenotype. In this context, selective targeting of CCR9 *in vivo* may pose a distinct therapeutic advantage.

Quantification of VAP-1 protein in gut and liver

- Using western blots and tissue ELISA, tissue protein lysates from varying aetiologies can be used to quantify hepatic and colonic protein expression of VAP-1. Thus far, quantitative protein differences have only been demonstrated for gene expression and enzymatic activity. However, given the inherent variation in tissue sampling, normalisation of enzyme activity to a given quantity of VAP-1 protein would yield a more accurate determination of inherent differences.

- HSEC ELISA (Chapter 4) delineated the functional consequences of VAP-1 expression in terms of inducing downstream CAMs. However, further evaluation by flow-based adhesion assays are required to determine whether induction by VAP-1 amine substrates + TNFα are meaningful in terms of cell-recruitment to HSEC. Moreover, the development of newer, more potent antibodies and enzyme inhibitors directed toward VAP-1 warrants testing in a similar regard. Obtaining an anti-MAdCAM-1 and/or and anti-α4β7 inhibitor for parallel experimentation would also be of benefit. Nevertheless, the data presented in this thesis suggests that VAP-1 inhibition would likely mitigate the degree of α4β7-dependent adhesion to HSEC *in vivo* irrespective of the amine substrate used.

Substantiate the effects of soluble VAP-1

- Assessment of enzyme activity in human serum clearly requires further optimisation. A setup wherein escalating recombinant VAP-1 amounts are contrasted with increasing capture antibody concentrations represents the most 'straight-forward' approach, and would require validation in serum samples bearing low, intermediate and high sVAP-1 levels prior to widespread application.
- The chemotactic effect of purified human sVAP-1 has been recently described for $CD4^+$ T-cells in Boyden chamber assays [214]. Given the diverse range of sVAP-1 levelss observed in patients, it would be of interest to see whether serum samples from varying aetiologies harbour different chemotactic potential. As the identity of the VAP-1 ligand is not yet known, this series of

experiments would require parallel investigation with highly specific anti-VAP-1 antibodies and/or enzyme inhibitors.

Evaluate consequences of targeting VAP-1 across different cholangitis models

- The preliminary results presented in Chapter 6 suggest an absence of VAP-1 enzyme activity is not protective against murine sclerosing cholangitis – at least in young, female *Mdr2*$^{-/-}$ mice. The *Mdr2*$^{-/-}$ *Ssao*$^{-/-}$ model necessitates further evaluation at older age groups and in a larger numbers of animals (from different litters). Phenotypic characterisation of *Mdr2*$^{-/-}$ mice crossed with animals having a full VAP-1 knockout (*Aoc3*$^{-/-}$) requires investigation in a similar regard; with detailed assessment of infiltrating leucocytic populations that are potentially protective (e.g. MDSC, T_{reg}).
- Given the described harmful consequences with regard to defective microbial handling in *Aoc3*$^{-/-}$ animals and a potentially increased risk of biliary sepsis in sclerosing cholangitis, a parallel appraisal of anti–VAP-1 antibodies and enzyme inhibitors in fully developed *Mdr2*$^{-/-}$ mice may be in order.
- SSAO substrate specificity may also differ between species, and detailing the variation in enzymatic efficiency through varying amine provision may provide additional insights into current findings.
- The availability of cholangiopathy models that exhibit intestinal inflammation, and with better-characterised gut and liver homing pathways is attractive, and Ova-Bil x Ova-iFABP mice would theoretically be more conducive to therapeutic exploration of VAP-1 neutralisation, α4β7-inhibitors and CCR9 blocking antibodies. Evaluation of VAP-1 expression in the gut and liver of these mice represents another avenue of intended exploration.

List of References

1 Trivedi PJ, Adams DH. Mucosal immunity in liver autoimmunity: A comprehensive review. *J Autoimmun* 2013;**46**:97–111. doi:10.1016/j.jaut.2013.06.013

2 Adams DH, Eksteen B. Aberrant homing of mucosal T cells and extra-intestinal manifestations of inflammatory bowel disease. *Nat Rev Immunol* 2006;**6**:244–51. doi:10.1038/nri1784

3 Ueno H, Weissman IL. The origin and fate of yolk sac hematopoiesis: application of chimera analyses to developmental studies. *Int J Dev Biol* 2010;**54**:1019–31. doi:10.1387/ijdb.093039hu

4 Oh JE, Lee HK. Pattern Recognition Receptors and Autophagy. *Front Immunol* 2014;**5**:doi: 10.3389/fimmu.2014.00300.

5 Delves PJ, Roitt IM. The immune system. Second of two parts. *N Engl J Med* 2000;**343**:108–17. doi:10.1056/NEJM200007133430207

6 Mauri C, Bosma A. Immune regulatory function of B cells. *Annu Rev Immunol* 2012;**30**:221–41. doi:10.1146/annurev-immunol-020711-074934

7 Trivedi PJ, Jones ND. The Immune System in Liver Transplantation: Rejection vs. Tolerance. In: Neuberger JM, Ferguson J, Newsome PN, eds. *Liver Transplantation*. John Wiley & Sons, Ltd 2013. 160–83.

8 Collins A, Littman DR, Taniuchi I. RUNX proteins in transcription factor networks that regulate T-cell lineage choice. *Nat Rev Immunol* 2009;**9**:106–15. doi:10.1038/nri2489

9 Smith-Garvin JE, Koretzky GA, Jordan MS. T cell activation. *Annu Rev Immunol* 2009;**27**:591–619. doi:10.1146/annurev.immunol.021908.132706

10 Liao W, Lin J-X, Leonard WJ. IL-2 family cytokines: new insights into the complex roles of IL-2 as a broad regulator of T helper cell differentiation. *Curr Opin Immunol* 2011;**23**:598–604. doi:10.1016/j.coi.2011.08.003

11 Swain SL, McKinstry KK, Strutt TM. Expanding roles for CD4+ T cells in immunity to viruses. *Nat Rev Immunol* 2012;**12**:136–48. doi:10.1038/nri3152

12 Zhu J, Paul WE. CD4 T cells: fates, functions, and faults. *Blood* 2008;**112**:1557–69. doi:10.1182/blood-2008-05-078154

13 Nurieva RI, Chung Y. Understanding the development and function of T follicular helper cells. *Cell Mol Immunol* 2010;**7**:190–7. doi:10.1038/cmi.2010.24

14 Williams MA, Tyznik AJ, Bevan MJ. Interleukin-2 signals during priming are required for secondary expansion of CD8+ memory T cells. *Nature* 2006;**441**:890–3. doi:10.1038/nature04790

15 Moore KW, de Waal Malefyt R, Coffman RL, *et al.* Interleukin-10 and the interleukin-10 receptor. *Annu Rev Immunol* 2001;**19**:683–765. doi:10.1146/annurev.immunol.19.1.683

16 Katt J, Schwinge D, Schoknecht T, *et al.* increased Th17 response to pathogen stimulation in patients with primary sclerosing cholangitis. *Hepatology* Published Online First: 8 April 2013. doi:10.1002/hep.26447

17 Weaver CT, Harrington LE, Mangan PR, *et al.* Th17: an effector CD4 T cell lineage with regulatory T cell ties. *Immunity* 2006;**24**:677–88. doi:10.1016/j.immuni.2006.06.002

18 Sakaguchi S. Naturally arising CD4+ regulatory t cells for immunologic self-tolerance and negative control of immune responses. *Annu Rev Immunol* 2004;**22**:531–62.

19 Li MO, Wan YY, Flavell RA. T cell-produced transforming growth factor-beta1 controls T cell tolerance and regulates Th1- and Th17-cell differentiation. *Immunity* 2007;**26**:579–91. doi:10.1016/j.immuni.2007.03.014

20 Li MO, Sanjabi S, Flavell RA. Transforming growth factor-beta controls development, homeostasis, and tolerance of T cells by regulatory T cell-dependent and -independent mechanisms. *Immunity* 2006;**25**:455–71. doi:10.1016/j.immuni.2006.07.011

21 Marson A, Kretschmer K, Frampton GM, *et al.* Foxp3 occupancy and regulation of key target genes during T-cell stimulation. *Nature* 2007;**445**:931–5. doi:10.1038/nature05478

22 Esplugues E, Huber S, Gagliani N, *et al.* Control of TH17 cells occurs in the small intestine. *Nature* 2011;**475**:514–8. doi:10.1038/nature10228

23 Geginat J, Paroni M, Facciotti F, *et al.* The CD4-centered universe of human T cell subsets. *Semin Immunol* 2013;**25**:252–62. doi:10.1016/j.smim.2013.10.012

24 Huber M, Heink S, Grothe H, *et al.* A Th17-like developmental process leads to CD8(+) Tc17 cells with reduced cytotoxic activity. *Eur J Immunol* 2009;**39**:1716–25. doi:10.1002/eji.200939412

25 Bernuzzi F, Fenoglio D, Battaglia F, *et al.* Phenotypical and functional alterations of CD8 regulatory T cells in primary biliary cirrhosis. *J Autoimmun* 2010;**35**:176–80. doi:10.1016/j.jaut.2010.06.004

26 Cosmi L, De Palma R, Santarlasci V, *et al.* Human interleukin 17-producing cells originate from a CD161+CD4+ T cell precursor. *J Exp Med* 2008;**205**:1903–16. doi:10.1084/jem.20080397

27 Fergusson JR, Smith KE, Fleming VM, *et al.* CD161 Defines a Transcriptional and Functional Phenotype across Distinct Human T Cell Lineages. *Cell Rep* 2014;**9**:1075–88. doi:10.1016/j.celrep.2014.09.045

28 Groh V, Steinle A, Bauer S, *et al.* Recognition of stress-induced MHC molecules by intestinal epithelial gammadelta T cells. *Science* 1998;**279**:1737–40.

29 Spada FM, Grant EP, Peters PJ, *et al.* Self-recognition of CD1 by gamma/delta T cells: implications for innate immunity. *J Exp Med* 2000;**191**:937–48.

30 Rajoriya N, Fergusson JR, Leithead JA, *et al.* Gamma Delta T-lymphocytes in Hepatitis C and Chronic Liver Disease. *Front Immunol* 2014;**5**:doi: 10.3389/fimmu.2014.00400.

31 Mackay CR, Marston WL, Dudler L. Naive and memory T cells show distinct pathways of lymphocyte recirculation. *J Exp Med* 1990;**171**:801–17.

32 Butcher EC, Williams M, Youngman K, *et al.* Lymphocyte trafficking and regional immunity. *Adv Immunol* 1999;**72**:209–53.

33 Sallusto F, Mackay CR, Lanzavecchia A. The role of chemokine receptors in primary, effector, and memory immune responses. *Annu Rev Immunol* 2000;**18**:593–620. doi:10.1146/annurev.immunol.18.1.593

34 Sallusto F, Lenig D, Förster R, *et al.* Two subsets of memory T lymphocytes with distinct homing potentials and effector functions. *Nature* 1999;**401**:708–12. doi:10.1038/44385

35 Medzhitov R. Origin and physiological roles of inflammation. *Nature* 2008;**454**:428–35. doi:10.1038/nature07201

36 Grant AJ, Goddard S, Ahmed-Choudhury J, *et al.* Hepatic Expression of Secondary Lymphoid Chemokine (CCL21) Promotes the Development of Portal-Associated Lymphoid Tissue in Chronic Inflammatory Liver Disease. *Am J Pathol* 2002;**160**:1445–55. doi:10.1016/S0002-9440(10)62570-9

37 Ley K, Laudanna C, Cybulsky MI, *et al.* Getting to the site of inflammation: the leukocyte adhesion cascade updated. *Nat Rev Immunol* 2007;**7**:678–89. doi:10.1038/nri2156

38 Eriksson EE, Xie X, Werr J, *et al.* Importance of primary capture and L-selectin-dependent secondary capture in leukocyte accumulation in inflammation and atherosclerosis in vivo. *J Exp Med* 2001;**194**:205–18.

39 Sperandio M, Smith ML, Forlow SB, *et al.* P-selectin glycoprotein ligand-1 mediates L-selectin-dependent leukocyte rolling in venules. *J Exp Med* 2003;**197**:1355–63. doi:10.1084/jem.20021854

40 Malý P, Thall A, Petryniak B, *et al.* The alpha(1,3)fucosyltransferase Fuc-TVII controls leukocyte trafficking through an essential role in L-, E-, and P-selectin ligand biosynthesis. *Cell* 1996;**86**:643–53.

41 Hidalgo A, Peired AJ, Wild MK, *et al.* Complete identification of E-selectin ligands on neutrophils reveals distinct functions of PSGL-1, ESL-1, and CD44. *Immunity* 2007;**26**:477–89. doi:10.1016/j.immuni.2007.03.011

42 Wong J, Johnston B, Lee SS, *et al.* A minimal role for selectins in the recruitment of leukocytes into the inflamed liver microvasculature. *J Clin Invest* 1997;**99**:2782–90. doi:10.1172/JCI119468

43 Adams DH, Hubscher SG, Fisher NC, *et al.* Expression of E-selectin and E-selectin ligands in human liver inflammation. *Hepatology* 1996;**24**:533–8. doi:10.1002/hep.510240311

44 Kadono T, Venturi GM, Steeber DA, *et al.* Leukocyte rolling velocities and migration are optimized by cooperative L-selectin and intercellular adhesion molecule-1 functions. *J Immunol* 2002;**169**:4542–50.

45 Oo YH, Adams DH. The role of chemokines in the recruitment of lymphocytes to the liver. *J Autoimmun* 2010;**34**:45–54. doi:10.1016/j.jaut.2009.07.011

46 Baltus T, Weber KSC, Johnson Z, *et al.* Oligomerization of RANTES is required for CCR1-mediated arrest but not CCR5-mediated transmigration of leukocytes on inflamed endothelium. *Blood* 2003;**102**:1985–8. doi:10.1182/blood-2003-04-1175

47 Andrian UH von, Mackay CR. T-cell function and migration. Two sides of the same coin. *N Engl J Med* 2000;**343**:1020–34. doi:10.1056/NEJM200010053431407

48 Verkaar F, van Offenbeek J, van der Lee MMC, *et al.* Chemokine cooperativity is caused by competitive glycosaminoglycan binding. *J Immunol* 2014;**192**:3908–14. doi:10.4049/jimmunol.1302159

49 Mellado M, Rodríguez-Frade JM, Mañes S, *et al.* Chemokine signaling and functional responses: the role of receptor dimerization and TK pathway activation. *Annu Rev Immunol* 2001;**19**:397–421. doi:10.1146/annurev.immunol.19.1.397

50 Hynes RO. Integrins: bidirectional, allosteric signaling machines. *Cell* 2002;**110**:673–87.

51 Arnaout MA, Mahalingam B, Xiong J-P. Integrin structure, allostery, and bidirectional signaling. *Annu Rev Cell Dev Biol* 2005;**21**:381–410. doi:10.1146/annurev.cellbio.21.090704.151217

52 Laudanna C, Kim JY, Constantin G, *et al.* Rapid leukocyte integrin activation by chemokines. *Immunol Rev* 2002;**186**:37–46.

53 Shamri R, Grabovsky V, Gauguet J-M, *et al.* Lymphocyte arrest requires instantaneous induction of an extended LFA-1 conformation mediated by endothelium-bound chemokines. *Nat Immunol* 2005;**6**:497–506. doi:10.1038/ni1194

54 Constantin G, Majeed M, Giagulli C, *et al.* Chemokines trigger immediate beta2 integrin affinity and mobility changes: differential regulation and roles in lymphocyte arrest under flow. *Immunity* 2000;**13**:759–69.

55 Giagulli C, Scarpini E, Ottoboni L, *et al.* RhoA and zeta PKC control distinct modalities of LFA-1 activation by chemokines: critical role of LFA-1 affinity triggering in lymphocyte in vivo homing. *Immunity* 2004;**20**:25–35.

56 Kinashi T. Intracellular signalling controlling integrin activation in lymphocytes. *Nat Rev Immunol* 2005;**5**:546–59. doi:10.1038/nri1646

57 Stagg AJ, Kamm MA, Knight SC. Intestinal dendritic cells increase T cell expression of alpha4beta7 integrin. *Eur J Immunol* 2002;**32**:1445–54. doi:10.1002/1521-4141(200205)32:5<1445::AID-IMMU1445>3.0.CO;2-E

58 Ambrosio D D', Albanesi C, Lang R, *et al.* Quantitative differences in chemokine receptor engagement generate diversity in integrin-dependent lymphocyte adhesion. *J Immunol* 2002;**169**:2303–12.

59 Nourshargh S, Alon R. Leukocyte Migration into Inflamed Tissues. *Immunity* 2014;**41**:694–707. doi:10.1016/j.immuni.2014.10.008

60 Barreiro O, Yanez-Mo M, Serrador JM, *et al.* Dynamic interaction of VCAM-1 and ICAM-1 with moesin and ezrin in a novel endothelial docking structure for adherent leukocytes. *J Cell Biol* 2002;**157**:1233–45. doi:10.1083/jcb.200112126

61 Carman CV, Springer TA. A transmigratory cup in leukocyte diapedesis both through individual vascular endothelial cells and between them. *J Cell Biol* 2004;**167**:377–88. doi:10.1083/jcb.200404129

62 Turowski P, Martinelli R, Crawford R, *et al.* Phosphorylation of vascular endothelial cadherin controls lymphocyte emigration. *J Cell Sci* 2008;**121**:29–37. doi:10.1242/jcs.022681

63 Muller WA. How endothelial cells regulate transmigration of leukocytes in the inflammatory response. *Am J Pathol* 2014;**184**:886–96. doi:10.1016/j.ajpath.2013.12.033

64 Nourshargh S, Krombach F, Dejana E. The role of JAM-A and PECAM-1 in modulating leukocyte infiltration in inflamed and ischemic tissues. *J Leukoc Biol* 2006;**80**:714–8. doi:10.1189/jlb.1105645

65 Wegmann F, Petri B, Khandoga AG, *et al.* ESAM supports neutrophil extravasation, activation of Rho, and VEGF-induced vascular permeability. *J Exp Med* 2006;**203**:1671–7. doi:10.1084/jem.20060565

66 Shetty S, Weston CJ, Oo YH, *et al.* Common lymphatic endothelial and vascular endothelial receptor-1 mediates the transmigration of regulatory T cells across human hepatic sinusoidal endothelium. *J Immunol* 2011;**186**:4147–55.

67 Weston CJ, Adams DH. Hepatic consequences of vascular adhesion protein-1 expression. *J Neural Transm* 2011;**118**:1055–64. doi:10.1007/s00702-011-0647-0

68 Tek-en G. Layers of the Alimentary Canal. 2014. http://commons.wikimedia.org/wiki/File:Layers_of_the_GI_Tract_english.svg (accessed 22 Mar2015).

69 Robinson CJ, Bohannan BJM, Young VB. From structure to function: the ecology of host-associated microbial communities. *Microbiol Mol Biol Rev MMBR* 2010;**74**:453–76. doi:10.1128/MMBR.00014-10

70 Mueller C, Macpherson AJ. Layers of mutualism with commensal bacteria protect us from intestinal inflammation. *Gut* 2006;**55**:276–84. doi:10.1136/gut.2004.054098

71 Akira S, Takeda K, Kaisho T. Toll-like receptors: critical proteins linking innate and acquired immunity. *Nat Immunol* 2001;**2**:675–80. doi:10.1038/90609

72 Strober W, Murray PJ, Kitani A, *et al.* Signalling pathways and molecular interactions of NOD1 and NOD2. *Nat Rev Immunol* 2006;**6**:9–20. doi:10.1038/nri1747

73 Swamy M, Jamora C, Havran W, *et al.* Epithelial decision makers: in search of the "epimmunome." *Nat Immunol* 2010;**11**:656–65. doi:10.1038/ni.1905

74 Hershberg RM, Cho DH, Youakim A, *et al.* Highly polarized HLA class II antigen processing and presentation by human intestinal epithelial cells. *J Clin Invest* 1998;**102**:792–803. doi:10.1172/JCI3201

75 Owyang AM, Zaph C, Wilson EH, *et al.* Interleukin 25 regulates type 2 cytokine-dependent immunity and limits chronic inflammation in the gastrointestinal tract. *J Exp Med* 2006;**203**:843–9. doi:10.1084/jem.20051496

76 Walker LJ, Kang Y-H, Smith MO, *et al.* Human MAIT and CD8αα cells develop from a pool of type-17 precommitted CD8+ T cells. *Blood* 2012;**119**:422–33. doi:10.1182/blood-2011-05-353789

77 Gapin L, Cheroutre H, Kronenberg M. Cutting edge: TCR alpha beta+ CD8 alpha alpha+ T cells are found in intestinal intraepithelial lymphocytes of mice that lack classical MHC class I molecules. *J Immunol* 1999;**163**:4100–4.

78 Macdonald TT, Monteleone G. Immunity, inflammation, and allergy in the gut. *Science* 2005;**307**:1920–5. doi:10.1126/science.1106442

79 Stenstad H, Svensson M, Cucak H, *et al.* Differential homing mechanisms regulate regionalized effector CD8alphabeta+ T cell accumulation within the small intestine. *Proc Natl Acad Sci U S A* 2007;**104**:10122–7. doi:10.1073/pnas.0700269104

80 Niess JH, Brand S, Gu X, *et al.* CX3CR1-mediated dendritic cell access to the intestinal lumen and bacterial clearance. *Science* 2005;**307**:254–8. doi:10.1126/science.1102901

81 Rescigno M, Urbano M, Valzasina B, *et al.* Dendritic cells express tight junction proteins and penetrate gut epithelial monolayers to sample bacteria. *Nat Immunol* 2001;**2**:361–7. doi:10.1038/86373

82 Johansson-Lindbom B, Svensson M, Pabst O, *et al.* Functional specialization of gut CD103+ dendritic cells in the regulation of tissue-selective T cell homing. *J Exp Med* 2005;**202**:1063–73. doi:10.1084/jem.20051100

83 Huang FP, Platt N, Wykes M, *et al.* A discrete subpopulation of dendritic cells transports apoptotic intestinal epithelial cells to T cell areas of mesenteric lymph nodes. *J Exp Med* 2000;**191**:435–44.

84 Reis e Sousa C. Dendritic cells in a mature age. *Nat Rev Immunol* 2006;**6**:476–83. doi:10.1038/nri1845

85 Yrlid U, Milling SWF, Miller JL, *et al.* Regulation of intestinal dendritic cell migration and activation by plasmacytoid dendritic cells, TNF-alpha and type 1 IFNs after feeding a TLR7/8 ligand. *J Immunol* 2006;**176**:5205–12.

86 Moseman EA, Liang X, Dawson AJ, *et al.* Human plasmacytoid dendritic cells activated by CpG oligodeoxynucleotides induce the generation of CD4+CD25+ regulatory T cells. *J Immunol* 2004;**173**:4433–42.

87 Makita S, Kanai T, Nemoto Y, *et al.* Intestinal lamina propria retaining CD4+CD25+ regulatory T cells is a suppressive site of intestinal inflammation. *J Immunol* 2007;**178**:4937–46.

88 Yuan X, Dee MJ, Altman NH, *et al.* IL-2Rβ-Dependent Signaling and CD103 Functionally Cooperate To Maintain Tolerance in the Gut Mucosa. *J Immunol* Published Online First: 19 December 2014. doi:10.4049/jimmunol.1400955

89 Macpherson AJ, Smith K. Mesenteric lymph nodes at the center of immune anatomy. *J Exp Med* 2006;**203**:497–500. doi:10.1084/jem.20060227

90 Corbett AJ, Eckle SBG, Birkinshaw RW, *et al.* T-cell activation by transitory neo-antigens derived from distinct microbial pathways. *Nature* 2014;**509**:361–5. doi:10.1038/nature13160

91 Reantragoon R, Corbett AJ, Sakala IG, *et al.* Antigen-loaded MR1 tetramers define T cell receptor heterogeneity in mucosal-associated invariant T cells. *J Exp Med* 2013;**210**:2305–20. doi:10.1084/jem.20130958

92 Dusseaux M, Martin E, Serriari N, *et al.* Human MAIT cells are xenobiotic-resistant, tissue-targeted, CD161hi IL-17-secreting T cells. *Blood* 2011;**117**:1250–9. doi:10.1182/blood-2010-08-303339

93 Ussher JE, Klenerman P, Willberg CB. Mucosal-associated invariant T-cells: new players in anti-bacterial immunity. *Front Immunol* 2014;**5**:450. doi:10.3389/fimmu.2014.00450

94 Le Bourhis L, Martin E, Péguillet I, *et al.* Antimicrobial activity of mucosal-associated invariant T cells. *Nat Immunol* 2010;**11**:701–8. doi:10.1038/ni.1890

95 Gold MC, Cerri S, Smyk-Pearson S, *et al.* Human mucosal associated invariant T cells detect bacterially infected cells. *PLoS Biol* 2010;**8**:e1000407. doi:10.1371/journal.pbio.1000407

96 Kjer-Nielsen L, Patel O, Corbett AJ, *et al.* MR1 presents microbial vitamin B metabolites to MAIT cells. *Nature* 2012;**491**:717–23. doi:10.1038/nature11605

97 Le Bourhis L, Guerri L, Dusseaux M, *et al.* Mucosal-associated invariant T cells: unconventional development and function. *Trends Immunol* 2011;**32**:212–8. doi:10.1016/j.it.2011.02.005

98 Hirschfield GM, Chapman RW, Karlsen TH, *et al.* The genetics of complex cholestatic disorders. *Gastroenterology* 2013;**144**:1357–74. doi:10.1053/j.gastro.2013.03.053

99 Powell N, Walker AW, Stolarczyk E, *et al.* The transcription factor T-bet regulates intestinal inflammation mediated by interleukin-7 receptor+ innate lymphoid cells. *Immunity* 2012;**37**:674–84. doi:10.1016/j.immuni.2012.09.008

100 Mazmanian SK, Liu CH, Tzianabos AO, *et al.* An immunomodulatory molecule of symbiotic bacteria directs maturation of the host immune system. *Cell* 2005;**122**:107–18. doi:10.1016/j.cell.2005.05.007

101 Flint HJ, Scott KP, Louis P, *et al.* The role of the gut microbiota in nutrition and health. *Nat Rev Gastroenterol Hepatol* 2012;**9**:577–89. doi:10.1038/nrgastro.2012.156

102 Hrncir T, Stepankova R, Kozakova H, *et al.* Gut microbiota and lipopolysaccharide content of the diet influence development of regulatory T cells: studies in germ-free mice. *BMC Immunol* 2008;**9**:65. doi:10.1186/1471-2172-9-65

103 Frantz AL, Rogier EW, Weber CR, *et al.* Targeted deletion of MyD88 in intestinal epithelial cells results in compromised antibacterial immunity associated with downregulation of polymeric immunoglobulin receptor, mucin-2, and antibacterial peptides. *Mucosal Immunol* 2012;**5**:501–12. doi:10.1038/mi.2012.23

104 Madsen K, Cornish A, Soper P, *et al.* Probiotic bacteria enhance murine and human intestinal epithelial barrier function. *Gastroenterology* 2001;**121**:580–91.

105 Lodes MJ, Cong Y, Elson CO, *et al.* Bacterial flagellin is a dominant antigen in Crohn disease. *J Clin Invest* 2004;**113**:1296–306. doi:10.1172/JCI20295

106 Hampe J, Franke A, Rosenstiel P, *et al.* A genome-wide association scan of nonsynonymous SNPs identifies a susceptibility variant for Crohn disease in ATG16L1. *Nat Genet* 2007;**39**:207–11. doi:10.1038/ng1954

107 Nischalke HD, Berger C, Aldenhoff K, *et al.* Toll-like receptor (TLR) 2 promoter and intron 2 polymorphisms are associated with increased risk for spontaneous bacterial peritonitis in liver cirrhosis. *J Hepatol* 2011;**55**:1010–6. doi:10.1016/j.jhep.2011.02.022

108 Bruns T, Reuken PA, Fischer J, *et al.* Further evidence for the relevance of TLR2 gene variants in spontaneous bacterial peritonitis. *J Hepatol* 2012;**56**:1207–8; author reply 1208–9. doi:10.1016/j.jhep.2011.09.010

109 Watanabe T, Kitani A, Murray PJ, *et al.* NOD2 is a negative regulator of Toll-like receptor 2-mediated T helper type 1 responses. *Nat Immunol* 2004;**5**:800–8. doi:10.1038/ni1092

110 Maeda S, Hsu L-C, Liu H, *et al.* Nod2 mutation in Crohn's disease potentiates NF-kappaB activity and IL-1beta processing. *Science* 2005;**307**:734–8. doi:10.1126/science.1103685

111 Hisamatsu T, Suzuki M, Reinecker H-C, *et al.* CARD15/NOD2 functions as an antibacterial factor in human intestinal epithelial cells. *Gastroenterology* 2003;**124**:993–1000. doi:10.1053/gast.2003.50153

112 Kobayashi KS, Chamaillard M, Ogura Y, *et al.* Nod2-dependent regulation of innate and adaptive immunity in the intestinal tract. *Science* 2005;**307**:731–4. doi:10.1126/science.1104911

113 Sellon RK, Tonkonogy S, Schultz M, *et al.* Resident enteric bacteria are necessary for development of spontaneous colitis and immune system activation in interleukin-10-deficient mice. *Infect Immun* 1998;**66**:5224–31.

114 Hart AL, Hassi HO Al-, Rigby RJ, *et al.* Characteristics of intestinal dendritic cells in inflammatory bowel diseases. *Gastroenterology* 2005;**129**:50–65.

115 Ng SC, Benjamin JL, McCarthy NE, *et al.* Relationship between human intestinal dendritic cells, gut microbiota, and disease activity in Crohn's disease. *Inflamm Bowel Dis* 2011;**17**:2027–37. doi:10.1002/ibd.21590

116 Duboc H, Rajca S, Rainteau D, *et al.* Connecting dysbiosis, bile-acid dysmetabolism and gut inflammation in inflammatory bowel diseases. *Gut* 2013;**62**:531–9. doi:10.1136/gutjnl-2012-302578

117 Kaur N, Chen C-C, Luther J, *et al.* Intestinal dysbiosis in inflammatory bowel disease. *Gut Microbes* 2011;**2**:211–6. doi:10.4161/gmic.2.4.17863

118 Manichanh C, Borruel N, Casellas F, *et al.* The gut microbiota in IBD. *Nat Rev Gastroenterol Hepatol* 2012;**9**:599–608. doi:10.1038/nrgastro.2012.152

119 Henao-Mejia J, Elinav E, Jin C, *et al.* Inflammasome-mediated dysbiosis regulates progression of NAFLD and obesity. *Nature* 2012;**482**:179–85. doi:10.1038/nature10809

120 Spruss A, Kanuri G, Wagnerberger S, *et al.* Toll-like receptor 4 is involved in the development of fructose-induced hepatic steatosis in mice. *Hepatology* 2009;**50**:1094–104. doi:10.1002/hep.23122

121 Erridge C. Diet, commensals and the intestine as sources of pathogen-associated molecular patterns in atherosclerosis, type 2 diabetes and non-alcoholic fatty liver disease. *Atherosclerosis* 2011;**216**:1–6. doi:10.1016/j.atherosclerosis.2011.02.043

122 Ye D, Li FYL, Lam KSL, *et al.* Toll-like receptor-4 mediates obesity-induced non-alcoholic steatohepatitis through activation of X-box binding protein-1 in mice. *Gut* 2012;**61**:1058–67. doi:10.1136/gutjnl-2011-300269

123 Papadakis KA, Prehn J, Nelson V, *et al.* The role of thymus-expressed chemokine and its receptor CCR9 on lymphocytes in the regional specialization of the mucosal immune system. *J Immunol* 2000;**165**:5069–76.

124 Briskin M, Winsor-Hines D, Shyjan A, *et al.* Human mucosal addressin cell adhesion molecule-1 is preferentially expressed in intestinal tract and associated lymphoid tissue. *Am J Pathol* 1997;**151**:97–110.

125 Cimbro R, Vassena L, Arthos J, *et al.* IL-7 induces expression and activation of integrin α4β7 promoting naive T-cell homing to the intestinal mucosa. *Blood* 2012;**120**:2610–9. doi:10.1182/blood-2012-06-434779

126 Jaensson-Gyllenbäck E, Kotarsky K, Zapata F, *et al.* Bile retinoids imprint intestinal CD103+ dendritic cells with the ability to generate gut-tropic T cells. *Mucosal Immunol* 2011;**4**:438–47. doi:10.1038/mi.2010.91

127 Eksteen B, Grant AJ, Miles A, *et al.* Hepatic endothelial CCL25 mediates the recruitment of CCR9+ gut-homing lymphocytes to the liver in primary sclerosing cholangitis. *J Exp Med* 2004;**200**:1511–7. doi:10.1084/jem.20041035

128 Annacker O, Coombes JL, Malmstrom V, *et al.* Essential role for CD103 in the T cell-mediated regulation of experimental colitis. *J Exp Med* 2005;**202**:1051–61. doi:10.1084/jem.20040662

129 Mora JR, Iwata M, Eksteen B, *et al.* Generation of gut-homing IgA-secreting B cells by intestinal dendritic cells. *Science* 2006;**314**:1157–60. doi:10.1126/science.1132742

130 Coombes JL, Siddiqui KRR, Arancibia-Cárcamo CV, *et al.* A functionally specialized population of mucosal CD103+ DCs induces Foxp3+ regulatory T cells via a TGF-beta and retinoic acid-dependent mechanism. *J Exp Med* 2007;**204**:1757–64. doi:10.1084/jem.20070590

131 Feng N, Jaimes MC, Lazarus NH, *et al.* Redundant role of chemokines CCL25/TECK and CCL28/MEC in IgA+ plasmablast recruitment to the intestinal lamina propria after rotavirus infection. *J Immunol* 2006;**176**:5749–59.

132 Eksteen B, Liaskou E, Adams DH. Lymphocyte homing and its role in the pathogenesis of IBD. *Inflamm Bowel Dis* 2008;**14**:1298–312. doi:10.1002/ibd.20453

133 Bell SJ, Rigby R, English N, *et al.* Migration and maturation of human colonic dendritic cells. *J Immunol* 2001;**166**:4958–67.

134 Mora JR, Cheng G, Picarella D, *et al.* Reciprocal and dynamic control of CD8 T cell homing by dendritic cells from skin- and gut-associated lymphoid tissues. *J Exp Med* 2005;**201**:303–16. doi:10.1084/jem.20041645

135 Wurbel M-A, Malissen B, Campbell JJ. Complex regulation of CCR9 at multiple discrete stages of T cell development. *Eur J Immunol* 2006;**36**:73–81. doi:10.1002/eji.200535203

136 Hosoe N, Miura S, Watanabe C, *et al.* Demonstration of functional role of TECK/CCL25 in T lymphocyte-endothelium interaction in inflamed and uninflamed intestinal mucosa. *Am J Physiol Gastrointest Liver Physiol* 2004;**286**:G458–66. doi:10.1152/ajpgi.00167.2003

137 Stenstad H, Ericsson A, Johansson-Lindbom B, *et al.* Gut-associated lymphoid tissue–primed CD4+ T cells display CCR9-dependent and -independent homing to the small intestine. *Blood* 2006;**107**:3447–54. doi:10.1182/blood-2005-07-2860

138 Mora JR, Andrian UH von. T-cell homing specificity and plasticity: new concepts and future challenges. *Trends Immunol* 2006;**27**:235–43. doi:10.1016/j.it.2006.03.007

139 Wagner N, Löhler J, Kunkel EJ, *et al.* Critical role for beta7 integrins in formation of the gut-associated lymphoid tissue. *Nature* 1996;**382**:366–70. doi:10.1038/382366a0

140 Chu P-S, Nakamoto N, Ebinuma H, *et al.* C-C motif chemokine receptor 9 positive macrophages activate hepatic stellate cells and promote liver fibrosis in mice. *Hepatology* 2013;**58**:337–50. doi:10.1002/hep.26351

141 Gupta P, Sharma PK, Mir H, *et al.* CCR9/CCL25 expression in non-small cell lung cancer correlates with aggressive disease and mediates key steps of metastasis. *Oncotarget* 2014;**5**:10170–9.

142 Kunkel EJ, Campbell JJ, Haraldsen G, *et al.* Lymphocyte CC chemokine receptor 9 and epithelial thymus-expressed chemokine (TECK) expression distinguish the small intestinal immune compartment: Epithelial expression of tissue-specific chemokines as an organizing principle in regional immunity. *J Exp Med* 2000;**192**:761–8.

143 Papadakis KA, Prehn J, Moreno ST, *et al.* CCR9-positive lymphocytes and thymus-expressed chemokine distinguish small bowel from colonic Crohn's disease. *Gastroenterology* 2001;**121**:246–54.

144 Saruta M, Yu QT, Avanesyan A, *et al.* Phenotype and Effector Function of CC Chemokine Receptor 9-Expressing Lymphocytes in Small Intestinal Crohn's Disease. *J Immunol* 2007;**178**:3293–300. doi:10.4049/jimmunol.178.5.3293

145 Rivera–Nieves J, Ho J, Bamias G, *et al.* Antibody Blockade of CCL25/CCR9 Ameliorates Early but not Late Chronic Murine Ileitis. *Gastroenterology* 2006;**131**:1518–29. doi:10.1053/j.gastro.2006.08.031

146 Wermers JD, McNamee EN, Wurbel M-A, *et al.* The chemokine receptor CCR9 is required for the T-cell-mediated regulation of chronic ileitis in mice. *Gastroenterology* 2011;**140**:1526–35.e3. doi:10.1053/j.gastro.2011.01.044

147 Mizuno S, Kanai T, Mikami Y, *et al.* CCR9+ plasmacytoid dendritic cells in the small intestine suppress development of intestinal inflammation in mice. *Immunol Lett* 2012;**146**:64–9. doi:10.1016/j.imlet.2012.05.001

148 Apostolaki M, Manoloukos M, Roulis M, *et al.* Role of β7 Integrin and the Chemokine/Chemokine Receptor Pair CCL25/CCR9 in Modeled TNF-Dependent Crohn's Disease. *Gastroenterology* 2008;**134**:2025–35. doi:10.1053/j.gastro.2008.02.085

149 Hadley GA, Bartlett ST, Via CS, *et al.* The epithelial cell-specific integrin, CD103 (alpha E integrin), defines a novel subset of alloreactive CD8+ CTL. *J Immunol* 1997;**159**:3748–56.

150 Hadeiba H, Lahl K, Edalati A, *et al.* Plasmacytoid dendritic cells transport peripheral antigens to the thymus to promote central tolerance. *Immunity* 2012;**36**:438–50. doi:10.1016/j.immuni.2012.01.017

151 Keshav S, Vaňásek T, Niv Y, *et al.* A Randomized Controlled Trial of the Efficacy and Safety of CCX282-B, an Orally-Administered Blocker of Chemokine Receptor CCR9, for Patients with Crohn's Disease. *PLoS ONE* 2013;**8**:e60094.

152 Trivedi PJ, Hirschfield GM. Treatment of autoimmune liver disease: current and future therapeutic options. *Ther Adv Chronic Dis* 2013;**4**:119–41. doi:10.1177/2040622313478646

153 Nemeth E, Baird AW, O'Farrelly C. Microanatomy of the liver immune system. *Semin Immunopathol* 2009;**31**:333–43. doi:10.1007/s00281-009-0173-4

154 Pellicoro A, Ramachandran P, Iredale JP, *et al.* Liver fibrosis and repair: immune regulation of wound healing in a solid organ. *Nat Rev Immunol* 2014;**14**:181–94. doi:10.1038/nri3623

155 Yona S, Kim K-W, Wolf Y, *et al.* Fate mapping reveals origins and dynamics of monocytes and tissue macrophages under homeostasis. *Immunity* 2013;**38**:79–91. doi:10.1016/j.immuni.2012.12.001

156 Holt AP, Haughton EL, Lalor PF, *et al.* Liver myofibroblasts regulate infiltration and positioning of lymphocytes in human liver. *Gastroenterology* 2009;**136**:705–14. doi:10.1053/j.gastro.2008.10.020

157 Ramachandran P, Pellicoro A, Vernon MA, *et al.* Differential Ly-6C expression identifies the recruited macrophage phenotype, which orchestrates the regression of murine liver fibrosis. *Proc Natl Acad Sci U S A* 2012;**109**:E3186–95. doi:10.1073/pnas.1119964109

158 Seki E, Brenner DA. Toll-like receptors and adaptor molecules in liver disease: update. *Hepatology* 2008;**48**:322–35. doi:10.1002/hep.22306

159 Shimoda S, Harada K, Niiro H, *et al.* CX3CL1 (fractalkine): a signpost for biliary inflammation in primary biliary cirrhosis. *Hepatol Baltim Md* 2010;**51**:567–75. doi:10.1002/hep.23318

160 Isse K, Harada K, Zen Y, *et al.* Fractalkine and CX3CR1 are involved in the recruitment of intraepithelial lymphocytes of intrahepatic bile ducts. *Hepatology* 2005;**41**:506–16. doi:10.1002/hep.20582

161 Terada R, Yamamoto K, Hakoda T, *et al.* Stromal cell-derived factor-1 from biliary epithelial cells recruits CXCR4-positive cells: implications for inflammatory liver diseases. *Lab Investig J Tech Methods Pathol* 2003;**83**:665–72.

162 Heydtmann M, Lalor PF, Eksteen JA, *et al.* CXC chemokine ligand 16 promotes integrin-mediated adhesion of liver-infiltrating lymphocytes to cholangiocytes and hepatocytes within the inflamed human liver. *J Immunol* 2005;**174**:1055–62.

163 Afford SC, Humphreys EH, Reid DT, *et al.* Vascular cell adhesion molecule 1 expression by biliary epithelium promotes persistence of inflammation by inhibiting effector T-cell apoptosis. *Hepatology* 2014;**59**:1932–43. doi:10.1002/hep.26965

164 Trivedi PJ, Cullen S. Etiopathogenesis of primary biliary cirrhosis: an overview of recent developments. *Hepatol Int* 2013;**7**:28–47. doi:10.1007/s12072-012-9362-7

165 Eksteen B, Miles A, Curbishley SM, *et al.* Epithelial inflammation is associated with CCL28 production and the recruitment of regulatory T cells expressing CCR10. *J Immunol* 2006;**177**:593–603.

166 Crispe IN. The liver as a lymphoid organ. *Annu Rev Immunol* 2009;**27**:147–63. doi:10.1146/annurev.immunol.021908.132629

167 Benseler V, Warren A, Vo M, *et al.* Hepatocyte entry leads to degradation of autoreactive CD8 T cells. *Proc Natl Acad Sci U S A* 2011;**108**:16735–40. doi:10.1073/pnas.1112251108

168 Limmer A, Ohl J, Kurts C, *et al.* Efficient presentation of exogenous antigen by liver endothelial cells to CD8+ T cells results in antigen-specific T-cell tolerance. *Nat Med* 2000;**6**:1348–54. doi:10.1038/82161

169 Limmer A, Ohl J, Wingender G, *et al.* Cross-presentation of oral antigens by liver sinusoidal endothelial cells leads to CD8 T cell tolerance. *Eur J Immunol* 2005;**35**:2970–81. doi:10.1002/eji.200526034

170 Bowen DG, Zen M, Holz L, *et al.* The site of primary T cell activation is a determinant of the balance between intrahepatic tolerance and immunity. *J Clin Invest* 2004;**114**:701–12. doi:10.1172/JCI21593

171 Katz SC, Pillarisetty VG, Bleier JI, *et al.* Liver sinusoidal endothelial cells are insufficient to activate T cells. *J Immunol* 2004;**173**:230–5.

172 Knolle PA, Schmitt E, Jin S, *et al.* Induction of cytokine production in naive CD4(+) T cells by antigen-presenting murine liver sinusoidal endothelial cells but failure to induce differentiation toward Th1 cells. *Gastroenterology* 1999;**116**:1428–40.

173 Eickmeier I, Seidel D, Grün JR, *et al.* Influence of CD8 T cell priming in liver and gut on the enterohepatic circulation. *J Hepatol* 2014;**60**:1143–50. doi:10.1016/j.jhep.2014.02.011

174 Neumann K, Kruse N, Szilagyi B, *et al.* Connecting liver and gut: murine liver sinusoidal endothelium induces gut tropism of CD4+ T cells via retinoic acid. *Hepatology* 2012;**55**:1976–84. doi:10.1002/hep.24816

175 Seidel D, Eickmeier I, Kühl AA, *et al.* CD8 T cells primed in the gut-associated lymphoid tissue induce immune-mediated cholangitis in mice. *Hepatology* Published Online First: 26 August 2013. doi:10.1002/hep.26702

176 Kruse N, Neumann K, Schrage A, *et al.* Priming of CD4+ T cells by liver sinusoidal endothelial cells induces CD25low forkhead box protein 3- regulatory T cells suppressing autoimmune hepatitis. *Hepatology* 2009;**50**:1904–13. doi:10.1002/hep.23191

177 Goddard S, Youster J, Morgan E, *et al.* Interleukin-10 secretion differentiates dendritic cells from human liver and skin. *Am J Pathol* 2004;**164**:511–9. doi:10.1016/S0002-9440(10)63141-0

178 Cabillic F, Rougier N, Basset C, *et al.* Hepatic environment elicits monocyte differentiation into a dendritic cell subset directing Th2 response. *J Hepatol* 2006;**44**:552–9. doi:10.1016/j.jhep.2005.08.010

179 Thomson AW, Knolle PA. Antigen-presenting cell function in the tolerogenic liver environment. *Nat Rev Immunol* 2010;**10**:753–66. doi:10.1038/nri2858

180 Holz LE, Benseler V, Vo M, *et al.* Naïve CD8 T cell activation by liver bone marrow-derived cells leads to a “neglected” IL-2low Bimhigh phenotype, poor CTL function and cell death. *J Hepatol* 2012;**57**:830–6. doi:10.1016/j.jhep.2012.05.015

181 Sawa Y, Arima Y, Ogura H, *et al.* Hepatic interleukin-7 expression regulates T cell responses. *Immunity* 2009;**30**:447–57. doi:10.1016/j.immuni.2009.01.007

182 Douglas DB, Beiting DP, Loftus JP, *et al.* Combinatorial effects of interleukin 10 and interleukin 4 determine the progression of hepatic inflammation following murine enteric parasitic infection. *Hepatology* 2010;**51**:2162–71. doi:10.1002/hep.23576

183 Lunz JG 3rd, Specht SM, Murase N, *et al.* Gut-derived commensal bacterial products inhibit liver dendritic cell maturation by stimulating hepatic interleukin-6/signal transducer and activator of transcription 3 activity. *Hepatology* 2007;**46**:1946–59. doi:10.1002/hep.21906

184 Uhrig A, Banafsche R, Kremer M, *et al.* Development and functional consequences of LPS tolerance in sinusoidal endothelial cells of the liver. *J Leukoc Biol* 2005;**77**:626–33. doi:10.1189/jlb.0604332

185 Goubier A, Dubois B, Gheit H, *et al.* Plasmacytoid dendritic cells mediate oral tolerance. *Immunity* 2008;**29**:464–75. doi:10.1016/j.immuni.2008.06.017

186 Huang L-R, Wohlleber D, Reisinger F, *et al.* Intrahepatic myeloid-cell aggregates enable local proliferation of CD8+ T cells and successful immunotherapy against chronic viral liver infection. *Nat Immunol* 2013;**14**:574–83. doi:10.1038/ni.2573

187 Trivedi PJ, Hirschfield GM. Review article: overlap syndromes and autoimmune liver disease. *Aliment Pharmacol Ther* 2012;**36**:517–33. doi:10.1111/j.1365-2036.2012.05223.x

188 Mieli-Vergani G, Vergani D. Autoimmune hepatitis. *Nat Rev Gastroenterol Hepatol* 2011;**8**:320–9. doi:10.1038/nrgastro.2011.69

189 Gupta A, Bowlus CL. Primary sclerosing cholangitis: etiopathogenesis and clinical management. *Front Biosci Elite Ed* 2012;**4**:1683–705.

190 Longhi MS, Hussain MJ, Mitry RR, *et al.* Functional study of CD4+CD25+ regulatory T cells in health and autoimmune hepatitis. *J Immunol* 2006;**176**:4484–91.

191 Rong G, Zhou Y, Xiong Y, *et al.* Imbalance between T helper type 17 and T regulatory cells in patients with primary biliary cirrhosis: the serum cytokine profile and peripheral cell population. *Clin Exp Immunol* 2009;**156**:217–25. doi:10.1111/j.1365-2249.2009.03898.x

192 Peiseler M, Sebode M, Franke B, *et al.* FOXP3+ regulatory T cells in autoimmune hepatitis are fully functional and not reduced in frequency. *J Hepatol* 2012;**57**:125–32. doi:10.1016/j.jhep.2012.02.029

193 Sebode M, Peiseler M, Franke B, *et al.* Reduced FOXP3(+) regulatory T cells in patients with primary sclerosing cholangitis are associated with IL2RA gene polymorphisms. *J Hepatol* 2014;**60**:1010–6. doi:10.1016/j.jhep.2013.12.027

194 Harada K, Shimoda S, Sato Y, *et al.* Periductal interleukin-17 production in association with biliary innate immunity contributes to the pathogenesis of cholangiopathy in primary biliary cirrhosis. *Clin Exp Immunol* 2009;**157**:261–70. doi:10.1111/j.1365-2249.2009.03947.x

195 Zhao L, Tang Y, You Z, *et al.* Interleukin-17 contributes to the pathogenesis of autoimmune hepatitis through inducing hepatic interleukin-6 expression. *PloS One* 2011;**6**:e18909. doi:10.1371/journal.pone.0018909

196 Atarashi K, Nishimura J, Shima T, *et al.* ATP drives lamina propria T(H)17 cell differentiation. *Nature* 2008;**455**:808–12. doi:10.1038/nature07240

197 Puel A, Döffinger R, Natividad A, *et al.* Autoantibodies against IL-17A, IL-17F, and IL-22 in patients with chronic mucocutaneous candidiasis and autoimmune polyendocrine syndrome type I. *J Exp Med* 2010;**207**:291–7. doi:10.1084/jem.20091983

198 Oo YH, Banz V, Kavanagh D, *et al.* CXCR3-dependent recruitment and CCR6-mediated positioning of Th-17 cells in the inflamed liver. *J Hepatol* 2012;**57**:1044–51. doi:10.1016/j.jhep.2012.07.008

199 Maggi L, Santarlasci V, Capone M, *et al.* CD161 is a marker of all human IL-17-producing T-cell subsets and is induced by RORC. *Eur J Immunol* 2010;**40**:2174–81. doi:10.1002/eji.200940257

200 Becker C, Wirtz S, Blessing M, *et al.* Constitutive p40 promoter activation and IL-23 production in the terminal ileum mediated by dendritic cells. *J Clin Invest* 2003;**112**:693–706. doi:10.1172/JCI17464

201 Ivanov II, Atarashi K, Manel N, *et al.* Induction of intestinal Th17 cells by segmented filamentous bacteria. *Cell* 2009;**139**:485–98. doi:10.1016/j.cell.2009.09.033

202 Cua DJ, Sherlock JP. Autoimmunity's collateral damage: Gut microbiota strikes "back." *Nat Med* 2011;**17**:1055–6. doi:10.1038/nm0911-1055

203 Mielants H, Veys EM, Cuvelier C, *et al.* The evolution of spondyloarthropathies in relation to gut histology. II. Histological aspects. *J Rheumatol* 1995;**22**:2273–8.

204 Marzo AL, Vezys V, Williams K, *et al.* Tissue-level regulation of Th1 and Th2 primary and memory CD4 T cells in response to Listeria infection. *J Immunol* 2002;**168**:4504–10.

205 Klonowski KD, Williams KJ, Marzo AL, *et al.* Dynamics of blood-borne CD8 memory T cell migration in vivo. *Immunity* 2004;**20**:551–62.

206 Lee W-Y, Kubes P. Leukocyte adhesion in the liver: distinct adhesion paradigm from other organs. *J Hepatol* 2008;**48**:504–12. doi:10.1016/j.jhep.2007.12.005

207 Shetty S, Lalor PF, Adams DH. Lymphocyte recruitment to the liver; molecular insights into the pathogenesis of liver injury and hepatitis. *Toxicology* 2008;**254**:136–46. doi:10.1016/j.tox.2008.08.003

208 Borchers AT, Shimoda S, Bowlus C, *et al.* Lymphocyte recruitment and homing to the liver in primary biliary cirrhosis and primary sclerosing cholangitis. *Semin Immunopathol* 2009;**31**:309–22. doi:10.1007/s00281-009-0167-2

209 Kawasuji A, Hasegawa M, Horikawa M, *et al.* L-selectin and intercellular adhesion molecule-1 regulate the development of Concanavalin A-induced liver injury. *J Leukoc Biol* 2006;**79**:696–705. doi:10.1189/jlb.0905527

210 March S, Garcia-Pagán J-C, Massaguer A, *et al.* P-selectin mediates leukocyte rolling in concanavalin-A-induced hepatitis. *Liver Int* 2005;**25**:1053–60. doi:10.1111/j.1478-3231.2005.01137.x

211 Jaruga B, Hong F, Kim W-H, *et al.* IFN-gamma/STAT1 acts as a proinflammatory signal in T cell-mediated hepatitis via induction of multiple chemokines and adhesion molecules: a critical role of IRF-1. *Am J Physiol Gastrointest Liver Physiol* 2004;**287**:G1044–52. doi:10.1152/ajpgi.00184.2004

212 Bonder CS, Norman MU, Swain MG, *et al.* Rules of recruitment for Th1 and Th2 lymphocytes in inflamed liver: a role for alpha-4 integrin and vascular adhesion protein-1. *Immunity* 2005;**23**:153–63. doi:10.1016/j.immuni.2005.06.007

213 Lee W-Y, Salmi M, Kelly MM, *et al.* Therapeutic advantage of anti-VAP-1 over anti-α4 integrin antibody in concanavalin a-induced hepatitis. *Hepatology* 2013;**58**:1413–23. doi:10.1002/hep.26469

214 Weston CJ, Shepherd EL, Claridge LC, *et al.* Vascular adhesion protein-1 promotes liver inflammation and drives hepatic fibrosis. *J Clin Invest* Published Online First: 22 December 2014. doi:10.1172/JCI73722

215 Chuang Y-H, Lian Z-X, Cheng C-M, *et al.* Increased levels of chemokine receptor CXCR3 and chemokines IP-10 and MIG in patients with primary biliary cirrhosis and their first degree relatives. *J Autoimmun* 2005;**25**:126–32. doi:10.1016/j.jaut.2005.08.009

216 Nishioji K, Okanoue T, Itoh Y, *et al.* Increase of chemokine interferon-inducible protein-10 (IP-10) in the serum of patients with autoimmune liver diseases and

increase of its mRNA expression in hepatocytes. *Clin Exp Immunol* 2001;**123**:271–9.

217 Manousou P, Kolios G, Drygiannakis I, *et al.* CXCR3 axis in patients with primary biliary cirrhosis: a possible novel mechanism of the effect of ursodeoxycholic acid. *Clin Exp Immunol* 2013;**172**:9–15. doi:10.1111/cei.12032

218 Oo YH, Weston CJ, Lalor PF, *et al.* Distinct roles for CCR4 and CXCR3 in the recruitment and positioning of regulatory T cells in the inflamed human liver. *J Immunol* 2010;**184**:2886–98. doi:10.4049/jimmunol.0901216

219 Hynes RO. The Extracellular Matrix: Not Just Pretty Fibrils. *Science* 2009;**326**:1216–9. doi:10.1126/science.1176009

220 Dranoff JA, Wells RG. Portal fibroblasts: Underappreciated mediators of biliary fibrosis. *Hepatology* 2010;**51**:1438–44. doi:10.1002/hep.23405

221 Henderson NC, Arnold TD, Katamura Y, *et al.* Targeting of αv integrin identifies a core molecular pathway that regulates fibrosis in several organs. *Nat Med* 2013;**19**:1617–24. doi:10.1038/nm.3282

222 Popov Y, Patsenker E, Stickel F, *et al.* Integrin alphavbeta6 is a marker of the progression of biliary and portal liver fibrosis and a novel target for antifibrotic therapies. *J Hepatol* 2008;**48**:453–64. doi:10.1016/j.jhep.2007.11.021

223 Bonner JC. Regulation of PDGF and its receptors in fibrotic diseases. *Cytokine Growth Factor Rev* 2004;**15**:255–73. doi:10.1016/j.cytogfr.2004.03.006

224 Oakley F, Teoh V, Ching-A-Sue G, *et al.* Angiotensin II activates I kappaB kinase phosphorylation of RelA at Ser 536 to promote myofibroblast survival and liver fibrosis. *Gastroenterology* 2009;**136**:2334–44.e1. doi:10.1053/j.gastro.2009.02.081

225 Huang X, Wu J, Spong S, *et al.* The integrin alphavbeta6 is critical for keratinocyte migration on both its known ligand, fibronectin, and on vitronectin. *J Cell Sci* 1998;**111 (Pt 15)**:2189–95.

226 Patsenker E, Popov Y, Stickel F, *et al.* Inhibition of Integrin Alphavbeta6 on Cholangiocytes Blocks Tgfbeta Activation and Retards Biliary Fibrosis Progression. *Gastroenterology* 2008;**135**:660–70. doi:10.1053/j.gastro. 2008.04.009

227 Viñas O, Bataller R, Sancho-Bru P, *et al.* Human hepatic stellate cells show features of antigen-presenting cells and stimulate lymphocyte proliferation. *Hepatology* 2003;**38**:919–29. doi:10.1053/jhep.2003.50392

228 Duffield JS, Forbes SJ, Constandinou CM, *et al.* Selective depletion of macrophages reveals distinct, opposing roles during liver injury and repair. *J Clin Invest* 2005;**115**:56–65. doi:10.1172/JCI22675

229 Fallowfield JA, Mizuno M, Kendall TJ, *et al.* Scar-associated macrophages are a major source of hepatic matrix metalloproteinase-13 and facilitate the resolution of murine hepatic fibrosis. *J Immunol* 2007;**178**:5288–95.

230 Ide M, Kuwamura M, Kotani T, *et al.* Effects of gadolinium chloride (GdCl(3)) on the appearance of macrophage populations and fibrogenesis in thioacetamide-

induced rat hepatic lesions. *J Comp Pathol* 2005;**133**:92–102. doi:10.1016/j.jcpa.2005.01.011

231 Pradere J-P, Kluwe J, De Minicis S, *et al.* Hepatic macrophages but not dendritic cells contribute to liver fibrosis by promoting the survival of activated hepatic stellate cells in mice. *Hepatology* 2013;**58**:1461–73. doi:10.1002/hep.26429

232 Sunami Y, Leithäuser F, Gul S, *et al.* Hepatic activation of IKK/NFκB signaling induces liver fibrosis via macrophage-mediated chronic inflammation. *Hepatology* 2012;**56**:1117–28. doi:10.1002/hep.25711

233 Karlmark KR, Weiskirchen R, Zimmermann HW, *et al.* Hepatic recruitment of the inflammatory Gr1+ monocyte subset upon liver injury promotes hepatic fibrosis. *Hepatology* 2009;**50**:261–74. doi:10.1002/hep.22950

234 Aspinall AI, Curbishley SM, Lalor PF, *et al.* CX(3)CR1 and vascular adhesion protein-1-dependent recruitment of CD16(+) monocytes across human liver sinusoidal endothelium. *Hepatology* 2010;**51**:2030–9. doi:10.1002/hep.23591

235 Imamura M, Ogawa T, Sasaguri Y, *et al.* Suppression of macrophage infiltration inhibits activation of hepatic stellate cells and liver fibrogenesis in rats. *Gastroenterology* 2005;**128**:138–46.

236 Mitchell C, Couton D, Couty J-P, *et al.* Dual role of CCR2 in the constitution and the resolution of liver fibrosis in mice. *Am J Pathol* 2009;**174**:1766–75. doi:10.2353/ajpath.2009.080632

237 Pellicoro A, Aucott RL, Ramachandran P, *et al.* Elastin accumulation is regulated at the level of degradation by macrophage metalloelastase (MMP-12)

during experimental liver fibrosis. *Hepatology* 2012;**55**:1965–75. doi:10.1002/hep.25567

238 Popov Y, Sverdlov DY, Bhaskar KR, *et al.* Macrophage-mediated phagocytosis of apoptotic cholangiocytes contributes to reversal of experimental biliary fibrosis. *Am J Physiol Gastrointest Liver Physiol* 2010;**298**:G323–34. doi:10.1152/ajpgi.00394.2009

239 Liaskou E, Zimmermann HW, Li K-K, *et al.* Monocyte subsets in human liver disease show distinct phenotypic and functional characteristics. *Hepatology* 2013;**57**:385–98. doi:10.1002/hep.26016

240 Zimmermann HW, Seidler S, Nattermann J, *et al.* Functional contribution of elevated circulating and hepatic non-classical CD14CD16 monocytes to inflammation and human liver fibrosis. *PloS One* 2010;**5**:e11049. doi:10.1371/journal.pone.0011049

241 Wynn TA. Fibrotic disease and the TH1/TH2 paradigm. *Nat Rev Immunol* 2004;**4**:583–94. doi:10.1038/nri1412

242 Chiaramonte MG, Donaldson DD, Cheever AW, *et al.* An IL-13 inhibitor blocks the development of hepatic fibrosis during a T-helper type 2-dominated inflammatory response. *J Clin Invest* 1999;**104**:777–85. doi:10.1172/JCI7325

243 Muhanna N, Doron S, Wald O, *et al.* Activation of hepatic stellate cells after phagocytosis of lymphocytes: A novel pathway of fibrogenesis. *Hepatology* 2008;**48**:963–77. doi:10.1002/hep.22413

244 Meng F, Wang K, Aoyama T, *et al.* Interleukin-17 signaling in inflammatory, Kupffer cells, and hepatic stellate cells exacerbates liver fibrosis in mice. *Gastroenterology* 2012;**143**:765–76.e1–3. doi:10.1053/j.gastro.2012.05.049

245 Safadi R, Ohta M, Alvarez CE, *et al.* Immune stimulation of hepatic fibrogenesis by CD8 cells and attenuation by transgenic interleukin-10 from hepatocytes. *Gastroenterology* 2004;**127**:870–82.

246 Novobrantseva TI, Majeau GR, Amatucci A, *et al.* Attenuated liver fibrosis in the absence of B cells. *J Clin Invest* 2005;**115**:3072–82. doi:10.1172/JCI24798

247 Wehr A, Baeck C, Heymann F, *et al.* Chemokine receptor CXCR6-dependent hepatic NK T Cell accumulation promotes inflammation and liver fibrosis. *J Immunol* 2013;**190**:5226–36. doi:10.4049/jimmunol.1202909

248 Desmoulière A, Darby I, Costa AM, *et al.* Extracellular matrix deposition, lysyl oxidase expression, and myofibroblastic differentiation during the initial stages of cholestatic fibrosis in the rat. *Lab Investig J Tech Methods Pathol* 1997;**76**:765–78.

249 Lorena D, Darby IA, Reinhardt DP, *et al.* Fibrillin-1 expression in normal and fibrotic rat liver and in cultured hepatic fibroblastic cells: modulation by mechanical stress and role in cell adhesion. *Lab Investig J Tech Methods Pathol* 2004;**84**:203–12. doi:10.1038/labinvest.3700023

250 Perepelyuk M, Terajima M, Wang AY, *et al.* Hepatic stellate cells and portal fibroblasts are the major cellular sources of collagens and lysyl oxidases in normal liver and early after injury. *Am J Physiol Gastrointest Liver Physiol* 2013;**304**:G605–14. doi:10.1152/ajpgi.00222.2012

251 Tang L, Tanaka Y, Marumo F, *et al.* Phenotypic change in portal fibroblasts in biliary fibrosis. *Liver* 1994;**14**:76–82.

252 Wells RG. Portal Fibroblasts in Biliary Fibrosis. *Curr Pathobiol Rep* 2014;**2**:185–90. doi:10.1007/s40139-014-0054-y

253 Mederacke I, Hsu CC, Troeger JS, *et al.* Fate-tracing reveals hepatic stellate cells as dominant contributors to liver fibrosis independent of its etiology. *Nat Commun* 2013;**4**:2823. doi:10.1038/ncomms3823

254 Trivedi PJ, Chapman RW. PSC, AIH and overlap syndrome in inflammatory bowel disease. *Clin Res Hepatol Gastroenterol* 2012;**36**:420–36. doi:10.1016/j.clinre.2011.10.007

255 Broomé U, Löfberg R, Veress B, *et al.* Primary sclerosing cholangitis and ulcerative colitis: evidence for increased neoplastic potential. *Hepatology* 1995;**22**:1404–8.

256 Braden B, Halliday J, Aryasingha S, *et al.* Risk for colorectal neoplasia in patients with colonic Crohn's disease and concomitant primary sclerosing cholangitis. *Clin Gastroenterol Hepatol* 2012;**10**:303–8. doi:10.1016/j.cgh.2011.10.020

257 Imam MH, Thackeray EW, Lindor KD. Colonic neoplasia in young patients with inflammatory bowel disease and primary sclerosing cholangitis. *Colorectal Dis* 2013;**15**:198–203. doi:10.1111/j.1463-1318.2012.03133.x

258 Hirschfield GM, Karlsen TH, Lindor KD, *et al.* Primary sclerosing cholangitis. *Lancet* Published Online First: 27 June 2013. doi:10.1016/S0140-6736(13)60096-3

259 Ngu JH, Gearry RB, Wright AJ, *et al.* Inflammatory bowel disease is associated with poor outcomes of patients with primary sclerosing cholangitis. *Clin Gastroenterol Hepatol* 2011;**9**:1092–7. doi:10.1016/j.cgh.2011.08.027

260 Boberg KM, Bergquist A, Mitchell S, *et al.* Cholangiocarcinoma in primary sclerosing cholangitis: risk factors and clinical presentation. *Scand J Gastroenterol* 2002;**37**:1205–11.

261 Rudolph G, Gotthardt D, Kloeters-Plachky P, *et al.* In PSC with dominant bile duct stenosis, IBD is associated with an increase of carcinomas and reduced survival. *J Hepatol* 2010;**53**:313–7. doi:10.1016/j.jhep.2010.02.030

262 Jørgensen KK, Lindström L, Cvancarova M, *et al.* Immunosuppression after liver transplantation for primary sclerosing cholangitis influences activity of inflammatory bowel disease. *Clin Gastroenterol Hepatol* 2013;**11**:517–23. doi:10.1016/j.cgh.2012.12.027

263 Bergquist A, Montgomery SM, Bahmanyar S, *et al.* Increased risk of primary sclerosing cholangitis and ulcerative colitis in first-degree relatives of patients with primary sclerosing cholangitis. *Clin Gastroenterol Hepatol* 2008;**6**:939–43. doi:10.1016/j.cgh.2008.03.016

264 Karlsen TH, Franke A, Melum E, *et al.* Genome-wide association analysis in primary sclerosing cholangitis. *Gastroenterology* 2010;**138**:1102–11. doi:10.1053/j.gastro.2009.11.046

265 Melum E, Franke A, Schramm C, *et al.* Genome-wide association analysis in primary sclerosing cholangitis identifies two non-HLA susceptibility loci. *Nat Genet* 2011;**43**:17–9. doi:10.1038/ng.728

266 Bergquist A, Lindberg G, Saarinen S, *et al.* Increased prevalence of primary sclerosing cholangitis among first-degree relatives. *J Hepatol* 2005;**42**:252–6. doi:10.1016/j.jhep.2004.10.011

267 Folseraas T, Melum E, Franke A, *et al.* Genetics in primary sclerosing cholangitis. *Best Pract Res Clin Gastroenterol* 2011;**25**:713–26. doi:10.1016/j.bpg.2011.09.010

268 Wakabayashi K, Lian Z-X, Moritoki Y, *et al.* IL-2 receptor alpha(-/-) mice and the development of primary biliary cirrhosis. *Hepatology* 2006;**44**:1240–9. doi:10.1002/hep.21385

269 Bo X, Broome U, Remberger M, *et al.* Tumour necrosis factor alpha impairs function of liver derived T lymphocytes and natural killer cells in patients with primary sclerosing cholangitis. *Gut* 2001;**49**:131–41.

270 Hara H, Saito T. CARD9 versus CARMA1 in innate and adaptive immunity. *Trends Immunol* 2009;**30**:234–42. doi:10.1016/j.it.2009.03.002

271 Raab M, Wang H, Lu Y, *et al.* T cell receptor "inside-out" pathway via signaling module SKAP1-RapL regulates T cell motility and interactions in lymph nodes. *Immunity* 2010;**32**:541–56. doi:10.1016/j.immuni.2010.03.007

272 Katagiri K, Katakai T, Ebisuno Y, *et al.* Mst1 controls lymphocyte trafficking and interstitial motility within lymph nodes. *EMBO J* 2009;**28**:1319–31. doi:10.1038/emboj.2009.82

273 Häuser F, Deyle C, Berard D, *et al.* Macrophage-stimulating protein polymorphism rs3197999 is associated with a gain of function: implications for

inflammatory bowel disease. *Genes Immun* 2012;**13**:321–7. doi:10.1038/gene.2011.88

274 Lee D-H, Esworthy RS, Chu C, *et al.* Mutation accumulation in the intestine and colon of mice deficient in two intracellular glutathione peroxidases. *Cancer Res* 2006;**66**:9845–51. doi:10.1158/0008-5472.CAN-06-0732

275 Goto Y, Obata T, Kunisawa J, *et al.* Innate lymphoid cells regulate intestinal epithelial cell glycosylation. *Science* 2014;**345**:1254009. doi:10.1126/science.1254009

276 Rausch P, Rehman A, Künzel S, *et al.* Colonic mucosa-associated microbiota is influenced by an interaction of Crohn disease and FUT2 (Secretor) genotype. *Proc Natl Acad Sci U S A* 2011;**108**:19030–5. doi:10.1073/pnas.1106408108

277 Folseraas T, Melum E, Rausch P, *et al.* Extended analysis of a genome-wide association study in primary sclerosing cholangitis detects multiple novel risk loci. *J Hepatol* 2012;**57**:366–75. doi:10.1016/j.jhep.2012.03.031

278 Liu JZ, Hov JR, Folseraas T, *et al.* Dense genotyping of immune-related disease regions identifies nine new risk loci for primary sclerosing cholangitis. *Nat Genet* Published Online First: 21 April 2013. doi:10.1038/ng.2616

279 Moran CJ, Walters TD, Guo C-H, *et al.* IL-10R polymorphisms are associated with very-early-onset ulcerative colitis. *Inflamm Bowel Dis* 2013;**19**:115–23. doi:10.1002/ibd.22974

280 Devkota S, Wang Y, Musch MW, *et al.* Dietary-fat-induced taurocholic acid promotes pathobiont expansion and colitis in Il10-/- mice. *Nature* 2012;**487**:104–8. doi:10.1038/nature11225

281 Papp M, Norman GL, Vitalis Z, *et al.* Presence of anti-microbial antibodies in liver cirrhosis--a tell-tale sign of compromised immunity? *PloS One* 2010;**5**:e12957. doi:10.1371/journal.pone.0012957

282 Terjung B, Söhne J, Lechtenberg B, *et al.* p-ANCAs in autoimmune liver disorders recognise human beta-tubulin isotype 5 and cross-react with microbial protein FtsZ. *Gut* 2010;**59**:808–16. doi:10.1136/gut.2008.157818

283 Karrar A, Broomé U, Södergren T, *et al.* Biliary epithelial cell antibodies link adaptive and innate immune responses in primary sclerosing cholangitis. *Gastroenterology* 2007;**132**:1504–14. doi:10.1053/j.gastro.2007.01.039

284 Xu B, Broome U, Ericzon B-G, *et al.* High frequency of autoantibodies in patients with primary sclerosing cholangitis that bind biliary epithelial cells and induce expression of CD44 and production of interleukin 6. *Gut* 2002;**51**:120–7.

285 Tabibian JH, Weeding E, Jorgensen RA, *et al.* Randomised clinical trial: vancomycin or metronidazole in patients with primary sclerosing cholangitis - a pilot study. *Aliment Pharmacol Ther* 2013;**37**:604–12. doi:10.1111/apt.12232

286 Quraishi, Mohammed Nabil, Sergeant, Martin, Kay, Gemma L, *et al.* Probing the microbiota in PSC: the gut adherent micro-biota of PSC-IBD is distinct to that of IBD and controls. *Hepatology* 2014;**60**:267A. doi:10.1002/hep.27470

287 Fickert P, Fuchsbichler A, Wagner M, *et al.* Regurgitation of bile acids from leaky bile ducts causes sclerosing cholangitis in Mdr2 (Abcb4) knockout mice. *Gastroenterology* 2004;**127**:261–74.

288 Jahnel J, Fickert P, Langner C, *et al.* Impact of experimental colitis on hepatobiliary transporter expression and bile duct injury in mice. *Liver Int* 2009;**29**:1316–25. doi:10.1111/j.1478-3231.2009.02044.x

289 Grant AJ, Lalor PF, Hübscher SG, *et al.* MAdCAM-1 expressed in chronic inflammatory liver disease supports mucosal lymphocyte adhesion to hepatic endothelium (MAdCAM-1 in chronic inflammatory liver disease). *Hepatology* 2001;**33**:1065–72. doi:10.1053/jhep.2001.24231

290 Miles A, Liaskou E, Eksteen B, *et al.* CCL25 and CCL28 promote alpha4 beta7-integrin-dependent adhesion of lymphocytes to MAdCAM-1 under shear flow. *Am J Physiol Gastrointest Liver Physiol* 2008;**294**:G1257–67. doi:10.1152/ajpgi.00266.2007

291 Wright N, Hidalgo A, Rodríguez-Frade JM, *et al.* The chemokine stromal cell-derived factor-1 alpha modulates alpha 4 beta 7 integrin-mediated lymphocyte adhesion to mucosal addressin cell adhesion molecule-1 and fibronectin. *J Immunol* 2002;**168**:5268–77.

292 Salmi M, Kalimo K, Jalkanen S. Induction and function of vascular adhesion protein-1 at sites of inflammation. *J Exp Med* 1993;**178**:2255–60.

293 Grant AJ, Lalor PF, Salmi M, *et al.* Homing of mucosal lymphocytes to the liver in the pathogenesis of hepatic complications of inflammatory bowel disease. *Lancet* 2002;**359**:150–7. doi:10.1016/S0140-6736(02)07374-9

294 Liaskou E, Karikoski M, Reynolds GM, *et al.* Regulation of mucosal addressin cell adhesion molecule 1 expression in human and mice by vascular adhesion

protein 1 amine oxidase activity. *Hepatology* 2011;**53**:661–72. doi:10.1002/hep.24085

295 Shen SH, Wertz DL, Klinman JP. Implication for functions of the ectopic adipocyte copper amine oxidase (AOC3) from purified enzyme and cell-based kinetic studies. *PloS One* 2012;**7**:e29270. doi:10.1371/journal.pone.0029270

296 Eksteen B, Mora JR, Haughton EL, *et al.* Gut homing receptors on CD8 T cells are retinoic acid dependent and not maintained by liver dendritic or stellate cells. *Gastroenterology* 2009;**137**:320–9. doi:10.1053/j.gastro.2009.02.046

297 Ciccia F, Bombardieri M, Principato A, *et al.* Overexpression of interleukin-23, but not interleukin-17, as an immunologic signature of subclinical intestinal inflammation in ankylosing spondylitis. *Arthritis Rheum* 2009;**60**:955–65. doi:10.1002/art.24389

298 Sherlock JP, Joyce-Shaikh B, Turner SP, *et al.* IL-23 induces spondyloarthropathy by acting on ROR-γt+ CD3+CD4-CD8- entheseal resident T cells. *Nat Med* 2012;**18**:1069–76. doi:10.1038/nm.2817

299 Poussier P, Ning T, Banerjee D, *et al.* A unique subset of self-specific intraintestinal T cells maintains gut integrity. *J Exp Med* 2002;**195**:1491–7.

300 Salmi M, Jalkanen S. A 90-kilodalton endothelial cell molecule mediating lymphocyte binding in humans. *Science* 1992;**257**:1407–9.

301 Smith DJ, Salmi M, Bono P, *et al.* Cloning of vascular adhesion protein 1 reveals a novel multifunctional adhesion molecule. *J Exp Med* 1998;**188**:17–27.

302 Schwelberger HG. The origin of mammalian plasma amine oxidases. *J Neural Transm Vienna Austria 1996* 2007;**114**:757–62. doi:10.1007/s00702-007-0684-x

303 Jalkanen S, Salmi M. Cell surface monoamine oxidases: enzymes in search of a function. *EMBO J* 2001;**20**:3893–901. doi:10.1093/emboj/20.15.3893

304 Souza SE D', Ginsberg MH, Plow EF. Arginyl-glycyl-aspartic acid (RGD): a cell adhesion motif. *Trends Biochem Sci* 1991;**16**:246–50.

305 Salminen TA, Smith DJ, Jalkanen S, *et al.* Structural model of the catalytic domain of an enzyme with cell adhesion activity: human vascular adhesion protein-1 (HVAP-1) D4 domain is an amine oxidase. *Protein Eng* 1998;**11**:1195–204.

306 Airenne TT, Nymalm Y, Kidron H, *et al.* Crystal structure of the human vascular adhesion protein-1: Unique structural features with functional implications. *Protein Sci Publ Protein Soc* 2005;**14**:1964–74. doi:10.1110/ps.051438105

307 Salmi M, Jalkanen S. VAP-1: an adhesin and an enzyme. *Trends Immunol* 2001;**22**:211–6.

308 Maula S-M, Salminen T, Kaitaniemi S, *et al.* Carbohydrates located on the top of the "cap" contribute to the adhesive and enzymatic functions of vascular adhesion protein-1. *Eur J Immunol* 2005;**35**:2718–27. doi:10.1002/eji.200526351

309 Salmi M, Jalkanen S. Human vascular adhesion protein 1 (VAP-1) is a unique sialoglycoprotein that mediates carbohydrate-dependent binding of lymphocytes to endothelial cells. *J Exp Med* 1996;**183**:569–79.

310 Ferjančič Š, Gil-Bernabé AM, Hill SA, *et al.* VCAM-1 and VAP-1 recruit myeloid cells that promote pulmonary metastasis in mice. *Blood* 2013;**121**:3289–97. doi:10.1182/blood-2012-08-449819

311 Marttila-Ichihara F, Castermans K, Auvinen K, *et al.* Small-molecule inhibitors of vascular adhesion protein-1 reduce the accumulation of myeloid cells into tumors and attenuate tumor growth in mice. *J Immunol* 2010;**184**:3164–73. doi:10.4049/jimmunol.0901794

312 Lalor PF, Edwards S, McNab G, *et al.* Vascular adhesion protein-1 mediates adhesion and transmigration of lymphocytes on human hepatic endothelial cells. *J Immunol* 2002;**169**:983–92.

313 McNab G, Reeves JL, Salmi M, *et al.* Vascular adhesion protein 1 mediates binding of T cells to human hepatic endothelium. *Gastroenterology* 1996;**110**:522–8.

314 Kivi E, Elima K, Aalto K, *et al.* Human Siglec-10 can bind to vascular adhesion protein-1 and serves as its substrate. *Blood* 2009;**114**:5385–92. doi:10.1182/blood-2009-04-219253

315 Aalto K, Autio A, Kiss EA, *et al.* Siglec-9 is a novel leukocyte ligand for Vascular Adhesion Protein-1 and can be utilized in PET-imaging of inflammation and cancer. *Blood* 2011;**118**:3725–33.

316 Koskinen K, Vainio PJ, Smith DJ, *et al.* Granulocyte transmigration through the endothelium is regulated by the oxidase activity of vascular adhesion protein-1 (VAP-1). *Blood* 2004;**103**:3388–95. doi:10.1182/blood-2003-09-3275

317 Bono P, Jalkanen S, Salmi M. Mouse vascular adhesion protein 1 is a sialoglycoprotein with enzymatic activity and is induced in diabetic insulitis. *Am J Pathol* 1999;**155**:1613–24. doi:10.1016/S0002-9440(10)65477-6

318 Bono P, Salmi M, Smith DJ, *et al.* Cloning and characterization of mouse vascular adhesion protein-1 reveals a novel molecule with enzymatic activity. *J Immunol* 1998;**160**:5563–71.

319 Abella A, García-Vicente S, Viguerie N, *et al.* Adipocytes release a soluble form of VAP-1/SSAO by a metalloprotease-dependent process and in a regulated manner. *Diabetologia* 2004;**47**:429–38. doi:10.1007/s00125-004-1346-2

320 Stolen CM, Marttila-Ichihara F, Koskinen K, *et al.* Absence of the endothelial oxidase AOC3 leads to abnormal leukocyte traffic in vivo. *Immunity* 2005;**22**:105–15. doi:10.1016/j.immuni.2004.12.006

321 Lalor PF, Sun PJ, Weston CJ, *et al.* Activation of vascular adhesion protein-1 on liver endothelium results in an NF-kappaB-dependent increase in lymphocyte adhesion. *Hepatology* 2007;**45**:465–74. doi:10.1002/hep.21497

322 Gubisne-Haberle D, Hill W, Kazachkov M, *et al.* Protein cross-linkage induced by formaldehyde derived from semicarbazide-sensitive amine oxidase-mediated deamination of methylamine. *J Pharmacol Exp Ther* 2004;**310**:1125–32. doi:10.1124/jpet.104.068601

323 Mercier N, Kakou A, Challande P, *et al.* Comparison of the effects of semicarbazide and beta-aminopropionitrile on the arterial extracellular matrix in the Brown Norway rat. *Toxicol Appl Pharmacol* 2009;**239**:258–67. doi:10.1016/j.taap.2009.06.005

324 Göktürk C, Nilsson J, Nordquist J, *et al.* Overexpression of semicarbazide-sensitive amine oxidase in smooth muscle cells leads to an abnormal structure of the aortic elastic laminas. *Am J Pathol* 2003;**163**:1921–8. doi:10.1016/S0002-9440(10)63550-X

325 Dranoff JA, Feld JJ, Lavoie ÉG, *et al.* How does coffee prevent liver fibrosis? biological plausibility for recent epidemiological observations. *Hepatology* 2014;**60**:464–7. doi:10.1002/hep.27032

326 Lammert C, Juran BD, Schlicht E, *et al.* Reduced Coffee Consumption Among Individuals With Primary Sclerosing Cholangitis but Not Primary Biliary Cirrhosis. *Clin Gastroenterol Hepatol* Published Online First: 16 January 2014. doi:10.1016/j.cgh.2013.12.036

327 Olivieri A, Tipton K. Inhibition of bovine plasma semicarbazide-sensitive amine oxidase by caffeine. *J Biochem Mol Toxicol* 2011;**25**:26–7. doi:10.1002/jbt.20356

328 Stolen CM, Yegutkin GG, Kurkijärvi R, *et al.* Origins of serum semicarbazide-sensitive amine oxidase. *Circ Res* 2004;**95**:50–7. doi:10.1161/01.RES.0000134630.68877.2F

329 García-Vicente S, Abella A, Viguerie N, *et al.* The release of soluble VAP-1/SSAO by 3T3-L1 adipocytes is stimulated by isoproterenol and low concentrations of TNFalpha. *J Physiol Biochem* 2005;**61**:395–401.

330 Kurkijärvi R, Adams DH, Leino R, *et al.* Circulating form of human vascular adhesion protein-1 (VAP-1): increased serum levels in inflammatory liver diseases. *J Immunol* 1998;**161**:1549–57.

331 Aalto K, Havulinna AS, Jalkanen S, *et al.* Soluble vascular adhesion protein-1 predicts incident major adverse cardiovascular events and improves reclassification in a Finnish prospective cohort study. *Circ Cardiovasc Genet* 2014;**7**:529–35.

332 Ludvigsson JF, Bergquist A, Montgomery SM, *et al.* Risk of diabetes and cardiovascular disease in patients with primary sclerosing cholangitis. *J Hepatol* 2014;**60**:802–8. doi:10.1016/j.jhep.2013.11.017

333 Karim S, Liaskou E, Fear J, *et al.* Dysregulated hepatic expression of glucose transporters in chronic disease: contribution of semicarbazide-sensitive amine oxidase to hepatic glucose uptake. *Am J Physiol Gastrointest Liver Physiol* 2014;**307**:G1180–90. doi:10.1152/ajpgi.00377.2013

334 Enrique-Tarancón G, Marti L, Morin N, *et al.* Role of semicarbazide-sensitive amine oxidase on glucose transport and GLUT4 recruitment to the cell surface in adipose cells. *J Biol Chem* 1998;**273**:8025–32.

335 Morin N, Lizcano JM, Fontana E, *et al.* Semicarbazide-sensitive amine oxidase substrates stimulate glucose transport and inhibit lipolysis in human adipocytes. *J Pharmacol Exp Ther* 2001;**297**:563–72.

336 Chan BM, Elices MJ, Murphy E, *et al.* Adhesion to vascular cell adhesion molecule 1 and fibronectin. Comparison of alpha 4 beta 1 (VLA-4) and alpha 4 beta 7 on the human B cell line JY. *J Biol Chem* 1992;**267**:8366–70.

337 Boujedidi H, Bouchet-Delbos L, Cassard-Doulcier A-M, *et al.* Housekeeping gene variability in the liver of alcoholic patients. *Alcohol Clin Exp Res* 2012;**36**:258–66. doi:10.1111/j.1530-0277.2011.01627.x

338 Congiu M, Slavin JL, Desmond PV. Expression of common housekeeping genes is affected by disease in human hepatitis C virus-infected liver. *Liver Int* 2011;**31**:386–90. doi:10.1111/j.1478-3231.2010.02374.x

339 Weise JB, Goeroegh T, Meyer JE, *et al.* A comparative study of chemokine rantes detection using ELISA and Western blot. *Res Commun Mol Pathol Pharmacol* 2001;**110**:139–42.

340 Xiao S, Yu PH. A fluorometric high-performance liquid chromatography procedure for simultaneous determination of methylamine and aminoacetone in blood and tissues. *Anal Biochem* 2009;**384**:20–6. doi:10.1016/j.ab.2008.09.029

341 Shetty S, Weston CJ, Adams DH, *et al.* A Flow Adhesion Assay to Study Leucocyte Recruitment to Human Hepatic Sinusoidal Endothelium Under Conditions of Shear Stress. *J Vis Exp JoVE* Published Online First: 2014. doi:10.3791/51330

342 Fickert P, Pollheimer MJ, Beuers U, *et al.* Characterization of Animal Models for Primary Sclerosing Cholangitis (PSC). *J Hepatol* Published Online First: 19 February 2014. doi:10.1016/j.jhep.2014.02.006

343 Papadakis KA, Prehn J, Moreno ST, *et al.* CCR9–Positive lymphocytes and thymus-expressed chemokine distinguish small bowel from colonic Crohn's disease. *Gastroenterology* 2001;**121**:246–54. doi:10.1053/gast.2001.27154

344 Campbell DJ, Butcher EC. Rapid acquisition of tissue-specific homing phenotypes by CD4(+) T cells activated in cutaneous or mucosal lymphoid tissues. *J Exp Med* 2002;**195**:135–41.

345 Svensson M, Marsal J, Ericsson A, *et al.* CCL25 mediates the localization of recently activated CD8alphabeta(+) lymphocytes to the small-intestinal mucosa. *J Clin Invest* 2002;**110**:1113–21. doi:10.1172/JCI15988

346 Danese S, Fiocchi C. Ulcerative Colitis. *N Engl J Med* 2011;**365**:1713–25. doi:10.1056/NEJMra1102942

347 Baumgart DC, Sandborn WJ. Crohn's disease. *Lancet* 2012;**380**:1590–605. doi:10.1016/S0140-6736(12)60026-9

348 Bustin SA, Benes V, Garson JA, *et al.* The MIQE Guidelines: Minimum Information for Publication of Quantitative Real-Time PCR Experiments. *Clin Chem* 2009;**55**:611–22. doi:10.1373/clinchem.2008.112797

349 Ward ST, Li KK, Hepburn E, *et al.* The effects of CCR5 inhibition on regulatory T-cell recruitment to colorectal cancer. *Br J Cancer* Published Online First: 18 November 2014. doi:10.1038/bjc.2014.572

350 Watanabe T, Kobunai T, Yamamoto Y, *et al.* Predicting Ulcerative Colitis-Associated Colorectal Cancer Using Reverse-Transcription Polymerase Chain Reaction Analysis. *Clin Colorectal Cancer* 2011;**10**:134–41. doi:10.1016/j.clcc.2011.03.011

351 Günaltay, Kumawat AK, Nyhlin N, *et al.* Enhanced Levels of Chemokines and Their Receptors in the Colon of Microscopic Colitis Patients Indicate Mixed Immune Cell Recruitment. *Mediators Inflamm* 2015.

352 Cooney RM, Warren BF, Altman DG, *et al.* Outcome measurement in clinical trials for Ulcerative Colitis: towards standardisation. *Trials* 2007;**8**:17. doi:10.1186/1745-6215-8-17

353 Rutgeerts P, Sandborn WJ, Feagan BG, *et al.* Infliximab for induction and maintenance therapy for ulcerative colitis. *N Engl J Med* 2005;**353**:2462–76. doi:10.1056/NEJMoa050516

354 Manginot C, Baumann C, Peyrin-Biroulet L. An endoscopic Mayo score of 0 is associated with a lower risk of colectomy than a score of 1 in ulcerative colitis. *Gut* 2014;:gutjnl – 2014–308839. doi:10.1136/gutjnl-2014-308839

355 Toedter G, Li K, Marano C, *et al.* Gene Expression Profiling and Response Signatures Associated With Differential Responses to Infliximab Treatment in Ulcerative Colitis. *Am J Gastroenterol* 2011;**106**:1272–80. doi:10.1038/ajg.2011.83

356 Hart AL, Kamm MA, Knight SC, *et al.* Prospective Evaluation of Intestinal Homing Memory T Cells in Ulcerative Colitis: *Inflamm Bowel Dis* 2004;**10**:496–503. doi:10.1097/00054725-200409000-00002

357 Weiss W, Görg A. Sample solublization buffers for two-dimensional electrophoresis. *Methods Mol Biol Clifton NJ* 2008;**424**:35–42. doi:10.1007/978-1-60327-064-9_3

358 Feng B-S, Chen X, Li P, *et al.* Expression of integrin alphavbeta6 in the intestinal epithelial cells of patients with inflammatory bowel disease. *North Am J Med Sci* 2009;**1**:200–4. doi:10.4297/najms.2009.4200

359 Qiu W, Wu B, Wang X, *et al.* PUMA-mediated intestinal epithelial apoptosis contributes to ulcerative colitis in humans and mice. *J Clin Invest* 2011;**121**:1722–32. doi:10.1172/JCI42917

360 Ng SC, Kamm MA, Stagg AJ, *et al.* Intestinal dendritic cells: Their role in bacterial recognition, lymphocyte homing, and intestinal inflammation. *Inflamm Bowel Dis* 2010;**16**:1787–807. doi:10.1002/ibd.21247

361 Zabel BA, Agace WW, Campbell JJ, *et al.* Human G Protein–Coupled Receptor Gpr-9-6/Cc Chemokine Receptor 9 Is Selectively Expressed on Intestinal Homing T Lymphocytes, Mucosal Lymphocytes, and Thymocytes and Is Required for Thymus-Expressed Chemokine–Mediated Chemotaxis. *J Exp Med* 1999;**190**:1241–56. doi:10.1084/jem.190.9.1241

362 Mora JR, Bono MR, Manjunath N, *et al.* Selective imprinting of gut-homing T cells by Peyer's patch dendritic cells. *Nature* 2003;**424**:88–93. doi:10.1038/nature01726

363 Linton L, Karlsson M, Grundström J, *et al.* HLA-DR(hi) and CCR9 Define a Pro-Inflammatory Monocyte Subset in IBD. *Clin Transl Gastroenterol* 2012;**3**:e29. doi:10.1038/ctg.2012.23

364 Eberhardson M, Marits P, Jones M, *et al.* Treatment of inflammatory bowel disease by chemokine receptor-targeted leukapheresis. *Clin Immunol Orlando Fla* 2013;**149**:73–82. doi:10.1016/j.clim.2013.05.021

365 Costa MFS, Bornstein VU, Candéa AL, *et al.* CCL25 induces α4β7 integrin-dependent migration of IL-17+γδ T lymphocytes during an allergic reaction. *Eur J Immunol* 2012;**42**:1250–60. doi:10.1002/eji.201142021

366 Mann ER, McCarthy NE, Peake STC, *et al.* Skin- and gut-homing molecules on human circulating γδ T cells and their dysregulation in inflammatory bowel

disease. *Clin Exp Immunol* 2012;**170**:122–30. doi:10.1111/j.1365-2249.2012.04649.x

367 Autschbach F, Funke B, Katzenmeier M, *et al.* Expression of chemokine receptors in normal and inflamed human intestine, tonsil, and liver—An immunohistochemical analysis with new monoclonal antibodies from the 8th international workshop and conference on human leucocyte differentiation antigens. *Cell Immunol* 2005;**236**:110–4. doi:10.1016/j.cellimm.2005.08.016

368 Iwata M, Hirakiyama A, Eshima Y, *et al.* Retinoic acid imprints gut-homing specificity on T cells. *Immunity* 2004;**21**:527–38. doi:10.1016/j.immuni.2004.08.011

369 Mann ER, Bernardo D, Hassi HO Al-, *et al.* Human Gut-Specific Homeostatic Dendritic Cells Are Generated from Blood Precursors by the Gut Microenvironment: *Inflamm Bowel Dis* 2012;**18**:1275–86. doi:10.1002/ibd.21893

370 Ericsson A, Svensson M, Arya A, *et al.* CCL25/CCR9 promotes the induction and function of CD103 on intestinal intraepithelial lymphocytes. *Eur J Immunol* 2004;**34**:2720–9. doi:10.1002/eji.200425125

371 Jaensson E, Uronen-Hansson H, Pabst O, *et al.* Small intestinal CD103+ dendritic cells display unique functional properties that are conserved between mice and humans. *J Exp Med* 2008;**205**:2139–49. doi:10.1084/jem.20080414

372 Welty NE, Staley C, Ghilardi N, *et al.* Intestinal lamina propria dendritic cells maintain T cell homeostasis but do not affect commensalism. *J Exp Med* 2013;**210**:2011–24. doi:10.1084/jem.20130728

373 Mann ER, Bernardo D, Ng SC, *et al.* Human gut dendritic cells drive aberrant gut-specific t-cell responses in ulcerative colitis, characterized by increased IL-4 production and loss of IL-22 and IFNγ. *Inflamm Bowel Dis* 2014;**20**:2299–307. doi:10.1097/MIB.0000000000000223

374 Sanders TJ, McCarthy NE, Giles EM, *et al.* Increased Production of Retinoic Acid by Intestinal Macrophages Contributes to Their Inflammatory Phenotype in Patients With Crohn's Disease. *Gastroenterology* 2014;**146**:1278–88.e2. doi:10.1053/j.gastro.2014.01.057

375 Wurbel MA, Philippe JM, Nguyen C, *et al.* The chemokine TECK is expressed by thymic and intestinal epithelial cells and attracts double- and single-positive thymocytes expressing the TECK receptor CCR9. *Eur J Immunol* 2000;**30**:262–71. doi:10.1002/1521-4141(200001)30:1<262::AID-IMMU262>3.0.CO;2-0

376 Middleton J, Neil S, Wintle J, *et al.* Transcytosis and surface presentation of IL-8 by venular endothelial cells. *Cell* 1997;**91**:385–95.

377 Vicari AP, Figueroa DJ, Hedrick JA, *et al.* TECK: a novel CC chemokine specifically expressed by thymic dendritic cells and potentially involved in T cell development. *Immunity* 1997;**7**:291–301.

378 Ericsson A, Kotarsky K, Svensson M, *et al.* Functional Characterization of the CCL25 Promoter in Small Intestinal Epithelial Cells Suggests a Regulatory Role for Caudal-Related Homeobox (Cdx) Transcription Factors. *J Immunol* 2006;**176**:3642–51. doi:10.4049/jimmunol.176.6.3642

379 Meurens F, Berri M, Siggers RH, *et al.* Commensal bacteria and expression of two major intestinal chemokines, TECK/CCL25 and MEC/CCL28, and their receptors. *PloS One* 2007;**2**:e677. doi:10.1371/journal.pone.0000677

380 Wurbel M-A, McIntire MG, Dwyer P, *et al.* CCL25/CCR9 interactions regulate large intestinal inflammation in a murine model of acute colitis. *PloS One* 2011;**6**:e16442. doi:10.1371/journal.pone.0016442

381 Wurbel M-A, Le Bras S, Ibourk M, *et al.* CCL25/CCR9 interactions are not essential for colitis development but are required for innate immune cell protection from chronic experimental murine colitis. *Inflamm Bowel Dis* 2014;**20**:1165–76. doi:10.1097/MIB.0000000000000059

382 Zhu S, Bing Y, Wang X, *et al.* CCL25/CCR9 interactions regulate the function of iNKT cells in oxazolone-induced colitis in mice. *PloS One* 2014;**9**:e100167. doi:10.1371/journal.pone.0100167

383 Chen HJ, Edwards R, Tucci S, *et al.* Chemokine 25-induced signaling suppresses colon cancer invasion and metastasis. *J Clin Invest* 2012;**122**:3184–96. doi:10.1172/JCI62110

384 Feng L-Y, Ou Z-L, Wu F-Y, *et al.* Involvement of a Novel Chemokine Decoy Receptor CCX-CKR in Breast Cancer Growth, Metastasis and Patient Survival. *Clin Cancer Res* 2009;**15**:2962–70. doi:10.1158/1078-0432.CCR-08-2495

385 Parmo-Cabañas M, García-Bernal D, García-Verdugo R, *et al.* Intracellular signaling required for CCL25-stimulated T cell adhesion mediated by the integrin alpha4beta1. *J Leukoc Biol* 2007;**82**:380–91. doi:10.1189/jlb.1206726

386 Miles A, Liaskou E, Eksteen B, *et al.* CCL25 and CCL28 promote alpha4 beta7-integrin-dependent adhesion of lymphocytes to MAdCAM-1 under shear flow. *Am J Physiol Gastrointest Liver Physiol* 2008;**294**:G1257–67. doi:10.1152/ajpgi.00266.2007

387 Wurbel M-A, Malissen M, Guy-Grand D, *et al.* Impaired accumulation of antigen-specific CD8 lymphocytes in chemokine CCL25-deficient intestinal epithelium and lamina propria. *J Immunol* 2007;**178**:7598–606.

388 Wendland M, Czeloth N, Mach N, *et al.* CCR9 is a homing receptor for plasmacytoid dendritic cells to the small intestine. *Proc Natl Acad Sci U S A* 2007;**104**:6347–52. doi:10.1073/pnas.0609180104

389 Hadeiba H, Sato T, Habtezion A, *et al.* CCR9 expression defines tolerogenic plasmacytoid dendritic cells capable of suppressing acute graft-versus-host disease. *Nat Immunol* 2008;**9**:1253–60. doi:10.1038/ni.1658

390 Atif SM, Uematsu S, Akira S, *et al.* CD103-CD11b+ dendritic cells regulate the sensitivity of CD4 T-cell responses to bacterial flagellin. *Mucosal Immunol* 2014;**7**:68–77. doi:10.1038/mi.2013.25

391 Walters MJ, Wang Y, Lai N, *et al.* Characterization of CCX282-B, an orally bioavailable antagonist of the CCR9 chemokine receptor, for treatment of inflammatory bowel disease. *J Pharmacol Exp Ther* 2010;**335**:61–9. doi:10.1124/jpet.110.169714

392 Tamoutounour S, Henri S, Lelouard H, *et al.* CD64 distinguishes macrophages from dendritic cells in the gut and reveals the Th1-inducing role of mesenteric

lymph node macrophages during colitis. *Eur J Immunol* 2012;**42**:3150–66. doi:10.1002/eji.201242847

393 Nakamoto N, Ebinuma H, Kanai T, *et al.* CCR9+ macrophages are required for acute liver inflammation in mouse models of hepatitis. *Gastroenterology* 2012;**142**:366–76. doi:10.1053/j.gastro.2011.10.039

394 Kim S, Kim T. Selection of optimal internal controls for gene expression profiling of liver disease. *BioTechniques* 2003;**35**:456–8, 460.

395 Noonan T, Lukas S, Peet GW, *et al.* The oxidase activity of vascular adhesion protein-1 (VAP-1) is essential for function. *Am J Clin Exp Immunol* 2013;**2**:172–85.

396 Weston CJ, Shepherd EL, Adams DH. Cellular localization and trafficking of vascular adhesion protein-1 as revealed by an N-terminal GFP fusion protein. *J Neural Transm* Published Online First: 9 March 2013. doi:10.1007/s00702-013-1003-3

397 Jeitner TM, Lawrence DA. Mechanisms for the Cytotoxicity of Cysteamine. *Toxicol Sci* 2001;**63**:57–64. doi:10.1093/toxsci/63.1.57

398 Sikiric P, Seiwerth S, Grabarevic Z, *et al.* Cysteamine-colon and cysteamine-duodenum lesions in rats. Attenuation by gastric pentadecapeptide BPC 157, cimetidine, ranitidine, atropine, omeprazole, sulphasalazine and methylprednisolone. *J Physiol Paris* 2001;**95**:261–70.

399 Pitari G, Malergue F, Martin F, *et al.* Pantetheinase activity of membrane-bound Vanin-1: lack of free cysteamine in tissues of Vanin-1 deficient mice. *FEBS Lett* 2000;**483**:149–54.

400 Klicek R, Kolenc D, Suran J, *et al.* Stable gastric pentadecapeptide BPC 157 heals cysteamine-colitis and colon-colon-anastomosis and counteracts cuprizone brain injuries and motor disability. *J Physiol Pharmacol* 2013;**64**:597–612.

401 Martin F, Penet M-F, Malergue F, *et al.* Vanin-1–/– mice show decreased NSAID- and Schistosoma-induced intestinal inflammation associated with higher glutathione stores. *J Clin Invest* 2004;**113**:591–7. doi:10.1172/JCI19557

402 Berruyer C, Pouyet L, Millet V, *et al.* Vanin-1 licenses inflammatory mediator production by gut epithelial cells and controls colitis by antagonizing peroxisome proliferator-activated receptor gamma activity. *J Exp Med* 2006;**203**:2817–27. doi:10.1084/jem.20061640

403 Gensollen T, Bourges C, Rihet P, *et al.* Functional polymorphisms in the regulatory regions of the VNN1 gene are associated with susceptibility to inflammatory bowel diseases. *Inflamm Bowel Dis* 2013;**19**:2315–25. doi:10.1097/MIB.0b013e3182a32b03

404 Yu DPH. Deamination of methylamine and angiopathy; toxicity of formaldehyde, oxidative stress and relevance to protein glycoxidation in diabetes. In: Finberg PDJPM, Youdim PDMBH, Riederer PDP, *et al.*, eds. *MAO — The Mother of all Amine Oxidases*. Springer Vienna 1998. 201–16.

405 Yu PH, Zuo DM. Oxidative deamination of methylamine by semicarbazide-sensitive amine oxidase leads to cytotoxic damage in endothelial cells. Possible consequences for diabetes. *Diabetes* 1993;**42**:594–603.

406 Tirziu D, Jaba IM, Yu P, *et al.* Endothelial nuclear factor-κB-dependent regulation of arteriogenesis and branching. *Circulation* 2012;**126**:2589–600. doi:10.1161/CIRCULATIONAHA.112.119321

407 Wong M, Saad S, Zhang J, *et al.* Semicarbazide-sensitive amine oxidase (SSAO) inhibition ameliorates kidney fibrosis in a unilateral ureteral obstruction murine model. *Am J Physiol Renal Physiol* 2014;**307**:F908–16. doi:10.1152/ajprenal.00698.2013

408 Shackel NA, McGuinness PH, Abbott CA, *et al.* Identification of novel molecules and pathogenic pathways in primary biliary cirrhosis: cDNA array analysis of intrahepatic differential gene expression. *Gut* 2001;**49**:565–76. doi:10.1136/gut.49.4.565

409 Boomsma F, van Dijk J, Bhaggoe UM, *et al.* Variation in semicarbazide-sensitive amine oxidase activity in plasma and tissues of mammals. *Comp Biochem Physiol C Pharmacol Toxicol Endocrinol* 2000;**126**:69–78. doi:10.1016/S0742-8413(00)00101-8

410 Kaitaniemi S, Grön K, Elovaara H, *et al.* Functional Modulation of Vascular Adhesion Protein-1 by a Novel Splice Variant. *PLoS ONE* 2013;**8**:e54151. doi:10.1371/journal.pone.0054151

411 Mouzaki M, Comelli EM, Arendt BM, *et al.* Intestinal microbiota in patients with nonalcoholic fatty liver disease. *Hepatology* 2013;**58**:120–7. doi:10.1002/hep.26319

412 Raman M, Ahmed I, Gillevet PM, *et al.* Fecal microbiome and volatile organic compound metabolome in obese humans with nonalcoholic fatty liver disease.

Clin Gastroenterol Hepatol 2013;**11**:868–75.e1–3. doi:10.1016/j.cgh.2013.02.015

413 Armstrong MJ, Adams LA, Canbay A, *et al.* Extrahepatic complications of nonalcoholic fatty liver disease. *Hepatology* 2014;**59**:1174–97. doi:10.1002/hep.26717

414 Kurkijärvi R, Yegutkin GG, Gunson BK, *et al.* Circulating soluble vascular adhesion protein 1 accounts for the increased serum monoamine oxidase activity in chronic liver disease. *Gastroenterology* 2000;**119**:1096–103.

415 Holt A, Degenhardt OS, Berry PD, *et al.* The effects of buffer cations on interactions between mammalian copper-containing amine oxidases and their substrates. *J Neural Transm Vienna Austria 1996* 2007;**114**:733–41. doi:10.1007/s00702-007-0680-1

416 Pouyet L, Roisin-Bouffay C, Clément A, *et al.* Epithelial vanin-1 controls inflammation-driven carcinogenesis in the colitis-associated colon cancer model. *Inflamm Bowel Dis* 2010;**16**:96–104. doi:10.1002/ibd.21031

417 Dai Z-L, Wu G, Zhu W-Y. Amino acid metabolism in intestinal bacteria: links between gut ecology and host health. *Front Biosci Landmark Ed* 2011;**16**:1768–86.

418 Smith EA, Macfarlane GT. Studies on Amine Production in the Human Colon: Enumeration of Amine forming Bacteria and Physiological Effects of Carbohydrate and pH. *Anaerobe* 1996;**2**:285–97. doi:10.1006/anae.1996.0037

419 Povero D, Eguchi A, Niesman IR, *et al.* Lipid-induced toxicity stimulates hepatocytes to release angiogenic microparticles that require Vanin-1 for uptake by endothelial cells. *Sci Signal* 2013;**6**:ra88. doi:10.1126/scisignal.2004512

420 Schneider YJ, Trouet A. Effect of chloroquine and methylamine on endocytosis of fluorescein-labelled controlled IgG and of anti-(plasma membrane) IgG by cultured fibroblasts. *Eur J Biochem FEBS* 1981;**118**:33–8.

421 Nguyen DH, Hurtado-Ziola N, Gagneux P, *et al.* Loss of Siglec expression on T lymphocytes during human evolution. *Proc Natl Acad Sci* 2006;**103**:7765–70. doi:10.1073/pnas.0510484103

422 Johnson-Léger C, Aurrand-Lions M, Imhof BA. The parting of the endothelium: miracle, or simply a junctional affair? *J Cell Sci* 2000;**113 (Pt 6)**:921–33.

423 Koskinen K, Nevalainen S, Karikoski M, *et al.* VAP-1-Deficient Mice Display Defects in Mucosal Immunity and Antimicrobial Responses: Implications for Antiadhesive Applications. *J Immunol* 2007;**179**:6160–8. doi:10.4049/jimmunol.179.9.6160

424 Salter-Cid LM, Wang E, O'Rourke AM, *et al.* Anti-inflammatory effects of inhibiting the amine oxidase activity of semicarbazide-sensitive amine oxidase. *J Pharmacol Exp Ther* 2005;**315**:553–62. doi:10.1124/jpet.105.089649

425 Salmi M, Yegutkin GG, Lehvonen R, *et al.* A cell surface amine oxidase directly controls lymphocyte migration. *Immunity* 2001;**14**:265–76.

426 Tohka S, Laukkanen M, Jalkanen S, *et al.* Vascular adhesion protein 1 (VAP-1) functions as a molecular brake during granulocyte rolling and mediates recruitment in vivo. *FASEB J* 2001;**15**:373–82. doi:10.1096/fj.00-0240com

427 Merinen M, Irjala H, Salmi M, *et al.* Vascular adhesion protein-1 is involved in both acute and chronic inflammation in the mouse. *Am J Pathol* 2005;**166**:793–800. doi:10.1016/S0002-9440(10)62300-0

428 Martelius T, Salaspuro V, Salmi M, *et al.* Blockade of vascular adhesion protein-1 inhibits lymphocyte infiltration in rat liver allograft rejection. *Am J Pathol* 2004;**165**:1993–2001. doi:10.1016/S0002-9440(10)63250-6

429 Foot JS, Yow TT, Schilter H, *et al.* PXS-4681A, a potent and selective mechanism-based inhibitor of SSAO/VAP-1 with anti-inflammatory effects in vivo. *J Pharmacol Exp Ther* 2013;**347**:365–74. doi:10.1124/jpet.113.207613

430 Boonstra K, Weersma RK, van Erpecum KJ, *et al.* Population-based epidemiology, malignancy risk, and outcome of primary sclerosing cholangitis. *Hepatology* 2013;**58**:2045–55. doi:10.1002/hep.26565

431 Trivedi PJ, Bruns T, Cheung A, *et al.* Optimising risk stratification in primary biliary cirrhosis: AST/platelet ratio index predicts outcome independent of ursodeoxycholic acid response. *J Hepatol* 2014;**60**:1249–58. doi:10.1016/j.jhep.2014.01.029

432 Trivedi PJ, Lammers WJ, van Buuren HR, *et al.* Stratification of hepatocellular carcinoma risk in primary biliary cirrhosis: a multicentre international study. *Gut* Published Online First: 7 January 2015. doi:10.1136/gutjnl-2014-308351

433 Dyson JK, Webb G, Hirschfield GM, *et al.* Unmet clinical need in autoimmune liver diseases. *J Hepatol* 2015;**62**:208–18. doi:10.1016/j.jhep.2014.09.010

434 Lammers WJ, van Buuren HR, Hirschfield GM, *et al.* Levels of Alkaline Phosphatase and Bilirubin are Surrogate Endpoints of Outcomes of Patients with

Primary Biliary Cirrhosis – an International Follow-up Study. *Gastroenterology* doi:10.1053/j.gastro.2014.08.029

435 Maple P, Jones C, Andrews N. Time resolved fluorometric immunoassay, using europium labelled antihuman IgG, for the detection of human tetanus antitoxin in serum. *J Clin Pathol* 2001;**54**:812–5.

436 Koutroubakis IE, Petinaki E, Vardas E, *et al.* Circulating soluble vascular adhesion protein 1 in patients with inflammatory bowel disease. *Eur J Gastroenterol Hepatol* 2002;**14**:405–8.

437 Toiyama Y, Miki C, Inoue Y, *et al.* Circulating form of human vascular adhesion protein-1 (VAP-1): decreased serum levels in progression of colorectal cancer and predictive marker of lymphatic and hepatic metastasis. *J Surg Oncol* 2009;**99**:368–72. doi:10.1002/jso.21246

438 Bloom S, Fleming K, Chapman R. Adhesion molecule expression in primary sclerosing cholangitis and primary biliary cirrhosis. *Gut* 1995;**36**:604–9.

439 Adams DH, Mainolfi E, Burra P, *et al.* Detection of circulating intercellular adhesion molecule-1 in chronic liver diseases. *Hepatology* 1992;**16**:810–4.

440 Lim AG, Jazrawi RP, Levy JH, *et al.* Soluble E-selectin and vascular cell adhesion molecule-1 (VCAM-1) in primary biliary cirrhosis. *J Hepatol* 1995;**22**:416–22.

441 Armstrong MJ, Hazlehurst JM, Parker R, *et al.* Severe asymptomatic non-alcoholic fatty liver disease in routine diabetes care; a multi-disciplinary team approach to diagnosis and management. *QJM Mon J Assoc Physicians* 2014;**107**:33–41. doi:10.1093/qjmed/hct198

442 Armstrong MJ, Houlihan DD, Bentham L, *et al.* Presence and severity of non-alcoholic fatty liver disease in a large prospective primary care cohort. *J Hepatol* 2012;**56**:234–40. doi:10.1016/j.jhep.2011.03.020

443 Corpechot C, Gaouar F, Naggar A El, *et al.* Baseline values and changes in liver stiffness measured by transient elastography are associated with severity of fibrosis and outcomes of patients with primary sclerosing cholangitis. *Gastroenterology* 2014;**146**:970–9. doi:10.1053/j.gastro.2013.12.030

444 Soriano BD, Tam L-TT, Lu HS, *et al.* A fluorescent-based HPLC assay for quantification of cysteine and cysteamine adducts in Escherichia coli-derived proteins. *J Chromatogr B* 2012;**880**:27–33. doi:10.1016/j.jchromb.2011.11.011

445 Pollheimer MJ, Trauner M, Fickert P. Will we ever model PSC? – "It's hard to be a PSC model!" *Clin Res Hepatol Gastroenterol* 2011;**35**:792–804. doi:10.1016/j.clinre.2011.04.014

446 Pollheimer MJ, Fickert P. Animal Models in Primary Biliary Cirrhosis and Primary Sclerosing Cholangitis. *Clin Rev Allergy Immunol* Published Online First: 30 August 2014. doi:10.1007/s12016-014-8442-y

447 Smit JJ, Schinkel AH, Oude Elferink RP, *et al.* Homozygous disruption of the murine mdr2 P-glycoprotein gene leads to a complete absence of phospholipid from bile and to liver disease. *Cell* 1993;**75**:451–62.

448 Krones E, Erwa W, Trauner M, *et al.* Serum alkaline phosphatase levels accurately reflect cholestasis in mice. *Hepatology* 2014;:n/a – n/a. doi:10.1002/hep.27622

449 Mamari S Al, Djordjevic J, Halliday JS, *et al.* Improvement of serum alkaline phosphatase to <1.5 upper limit of normal predicts better outcome and reduced risk of cholangiocarcinoma in primary sclerosing cholangitis. *J Hepatol* 2013;**58**:329–34. doi:10.1016/j.jhep.2012.10.013

450 Halling Linder C, Englund UH, Narisawa S, *et al.* Isozyme profile and tissue-origin of alkaline phosphatases in mouse serum. *Bone* 2013;**53**:399–408. doi:10.1016/j.bone.2012.12.048

451 Trivedi PJ, Weston CJ, Webb GJ, *et al.* Serum alkaline phosphatase in Mdr2(-/-) mice is strain-specific. *Hepatology* Published Online First: 30 April 2015. doi:10.1002/hep.27874

452 Baghdasaryan A, Claudel T, Kosters A, *et al.* Curcumin improves sclerosing cholangitis in Mdr2−/− mice by inhibition of cholangiocyte inflammatory response and portal myofibroblast proliferation. *Gut* 2010;**59**:521–30. doi:10.1136/gut.2009.186528

453 Connolly MK, Bedrosian AS, Mallen-St. Clair J, *et al.* In liver fibrosis, dendritic cells govern hepatic inflammation in mice via TNF-α. *J Clin Invest* Published Online First: 12 October 2009. doi:10.1172/JCI37581

454 Yang G-X, Lian Z-X, Chuang Y-H, *et al.* Adoptive transfer of CD8(+) T cells from transforming growth factor beta receptor type II (dominant negative form) induces autoimmune cholangitis in mice. *Hepatology* 2008;**47**:1974–82. doi:10.1002/hep.22226

455 Arase H, Saito T, Phillips JH, *et al.* Cutting edge: the mouse NK cell-associated antigen recognized by DX5 monoclonal antibody is CD49b (alpha 2 integrin, very late antigen-2). *J Immunol* 2001;**167**:1141–4.

456 van Nieuwerk CM, Groen AK, Ottenhoff R, *et al.* The role of bile salt composition in liver pathology of mdr2 (-/-) mice: differences between males and females. *J Hepatol* 1997;**26**:138–45.

457 Barashi N, Weiss ID, Wald O, *et al.* Inflammation-induced hepatocellular carcinoma is dependent on CCR5 in mice. *Hepatology* 2013;**58**:1021–30. doi:10.1002/hep.26403

458 Halilbasic E, Fiorotto R, Fickert P, *et al.* Side Chain Structure Determines Unique Physiologic and Therapeutic Properties of norUrsodeoxycholic Acid in Mdr2−/− Mice. *Hepatology* 2009;**49**:1972–81. doi:10.1002/hep.22891

459 Huang Y, de Boer WB, Adams LA, *et al.* Image analysis of liver collagen using sirius red is more accurate and correlates better with serum fibrosis markers than trichrome. *Liver Int* 2013;**33**:1249–56. doi:10.1111/liv.12184

460 Salmi M, Jalkanen S. Homing-associated molecules CD73 and VAP-1 as targets to prevent harmful inflammations and cancer spread. *FEBS Lett* 2011;**585**:1543–50. doi:10.1016/j.febslet.2011.04.033

461 Fickert P, Wagner M, Marschall H, *et al.* 24-norUrsodeoxycholic Acid Is Superior to Ursodeoxycholic Acid in the Treatment of Sclerosing Cholangitis in Mdr2 (Abcb4) Knockout Mice. *Gastroenterology* 2006;**130**:465–81. doi:10.1053/j.gastro.2005.10.018

462 Schuppan D, Kim YO. Evolving therapies for liver fibrosis. *J Clin Invest* 2013;**123**:1887–901. doi:10.1172/JCI66028

463 Gabrilovich DI, Bronte V, Chen S-H, *et al.* The Terminology Issue for Myeloid-Derived Suppressor Cells. *Cancer Res* 2007;**67**:425–425. doi:10.1158/0008-5472.CAN-06-3037

464 Lammert F, Wang DQ-H, Hillebrandt S, *et al.* Spontaneous cholecysto- and hepatolithiasis in Mdr2-/- mice: a model for low phospholipid-associated cholelithiasis. *Hepatology* 2004;**39**:117–28. doi:10.1002/hep.20022

465 Bungay, Helen, Buchel O, Cummings F, *et al.* Prevalence and determinants of PSC in a cohort of patients with inflammatory bowel disease and normal liver function tests. *Gut* 2008;**57**:A41.

466 Zhang Y, Mao J, Yu PH, *et al.* A micro trapping system coupled with a high performance liquid chromatography procedure for methylamine determination in both tissue and cigarette smoke. *Anal Chim Acta* 2012;**752**:106–11. doi:10.1016/j.aca.2012.09.027